Role of Survivin as a Resistor against Nanotoxicity in Cancer Cells

Autophagy as a Key Mechanism

Dissertation
zur Erlangung des Grades
Doktor der Naturwissenschaften

am Fachbereich Biologie

JOHANNES GUTENBERG-UNIVERSITÄT MAINZ

Vorgelegt von
Christina Breder-Bonk
Geb. Breder
geboren am 15.03.1991 in Saryagatsch, Kasachstan

Mainz, 2024

Dekan:	Prof. Dr. Eckhard Thines
Erster Berichterstatter:	Prof. Dr. Bernhard Lieb
Zweiter Berichterstatter:	Prof. Dr. Oliver Krämer
Tag der mündlichen Prüfung:	20.06.2024

Je mehr ich weiß, um so mehr weiß ich,
dass ich nicht(s) weiß.

Aristoteles

TABLE OF CONTENTS

Summary 1

1 Introduction 2

1.1 Cancer 2

1.2 Cell Death Mechanisms: Necrosis and Apoptosis 4

1.3 Autophagy 6

1.4 Autophagy related alternative Cell Death Mechanisms 9

1.5 Survivin 10

1.5.1 Molecular Functions of Survivin 10

1.5.2 Survivin in non-cancerous Diseases 12

1.5.3 Survivin in Cancer 13

1.6 Nanomaterials 15

1.7 Silica Nanoparticles 16

1.7.1 Silica Nanoparticle-based Technology in Cancer Therapy 17

1.8 Aim of the Study 19

2 Results and Discussion 25

2.1 Amorphous Silica Nanoparticles 25

2.1.1 Characterization of Amorphous Silica Nanoparticles 25

2.1.2 Amorphous Silica Nanoparticles impair the Cell Viability 25

2.2 Characterization of Survivin-mediated Resistance against SiNP-mediated Toxicity 26

2.2.1 Survivin Overexpression can rescue Cells from SiNP-mediated Cell Toxicity 26

2.2.2 Exposure Time in Serum-free Medium determines SiNP Toxicity 27

2.2.3 Summary 30

2.3 Role of Autophagy in SiNP-mediated Toxicity and Survivin-mediated Resistance 30

2.3.1 SiNP induce a Lysosomal Shift related to Autophagy Initiation 30

2.3.2 Survivin suppresses Silica Nanoparticle-induced Autophagy 32

2.3.3 Survivin as Autophagy Modulator 35

2.3.4 Summary 39

2.4 Role of the Cytoskeleton Stability in Survivin-mediated Resistance against SiNP Toxicity ... 39

2.4.1 Summary 42

2.5 Role of ROS in SiNP-dependent Toxicity and Survivin-mediated Resistance 42

2.5.1 SiNP-dependent ROS Generation 42

2.5.2 Mitochondrial ROS Generation and Mitophagy 43

2.5.3 Survivin affects the SiNP-mediated ROS Generation 46
2.5.4 Lysosome-dependent ROS Generation 49
2.5.5 Survivin regulates Galectin-1 Translocation in Response to SiNP 52
2.5.6 Summary 53
2.6 Relationship between Survivin and ROS-dependent Signaling Pathways 54
2.6.1 SiNP-mediated Stress Signaling Pathways 54
2.6.2 Stress-induced Kinase p38 and related Pathways 55
2.6.3 FoxO Signaling in the Context of SiNP-dependent ROS Generation and Survivin Overexpression 58
2.6.4 Summary 61
2.7 Autophagy Modulators 61
2.7.1 Influence of AMPK Inhibitor Compound C on the Nanoparticle Toxicity 61
2.7.2 Influence of PI3K Inhibitor LY294002 and Wortmannin on Nanoparticle Toxicity 64
2.7.3 Influence of Autophagy Late-Stage Inhibitor Chloroquine on the Nanoparticle Toxicity 66
2.7.4 Summary 67
3 Conclusion and Outlook 68
3.1 Lineup of the Thesis 68
3.2 SiNP-mediated Toxicity 68
3.3 Survivins Defense Mechanisms against SiNP Toxicity 69
3.3.1 Survivin-dependent Galectin-1 Regulation as a Defense Mechanism against SiNP Toxicity 69
3.4 Survivin influences Starvation and SiNP induced Signaling Pathways 71
3.4.1 Influence of Survivin on the Akt/mTOR and Akt/FoxO Pathway 71
3.4.2 Relationship between p38 and Akt 73
3.4.3 Relationship between Survivin, p38 and SiNP-generated ROS 74
3.4.4 SiNP induce EGFR-mediated extracellular Signaling 75
3.5 Autophagy Modulators 76
3.5.1 AMPK-dependent Autophagy Initiation 76
3.5.2 PI3K/Akt/mTOR dependent Autophagy Regulation 77
4 Materials and Methods 78
4.1 Materials 78
4.1.1 Appliances 78
4.1.2 Consumables 80
4.1.3 Enzymes 82
4.1.4 Buffers and Solutions 82
4.1.5 Commercial Kits and Staining 83

4.1.6 Cell Lines 84
4.1.7 Antibodies 85
4.1.8 Nanoparticles 87
4.1.9 Software 88
4.2 Methods 89
4.2.1 Cell biological Methods 89
4.2.2 Treatments 91
4.2.3 Protein Analysis 92
4.2.4 Transfection 95
4.2.5 Fixation and Staining of Cells for Microscopy 96
4.2.6 Microscopy 97
4.2.7 Fluorescence-activated Cell Sorting (FACS) via Flow Cytometry 98
4.2.8 High-Content-Analysis via Array Scan 98
4.2.9 Biochemical Assays 98
5 References 100
6 Appendix 119
6.1 Abbreviations 119
6.2 Content of Figures 123
6.3 Content of Tables 124
6.4 Supplementary Figures 125
6.5 Supplementary Tables 133
7 Own Publication 134
8 Danksagung 156
9 Eidesstattliche Erklärung 157
10 Curriculum Vitae 158

SUMMARY

The tumor biomarker Survivin belongs to the family of inhibitors of apoptosis proteins and is associated with malignant tumor progression and poor treatment outcomes. The reasons are manifold because Survivin impacts apoptosis and several other essential cellular processes like autophagy, thereby promoting therapy resistance. Nanotechnology is a promising tool that can be used to target Survivin-related pathways and overcome tumor resistance.

In the context of chemotherapy, nanoparticles are commonly used as carriers of chemotherapeutic drugs. However, nanoparticles can function as a strengthening adjuvant, since nanoparticulate material has cellular effects. Therefore, pristine, amorphous silica nanoparticles (SiNP) were used as model particles to test their influence on Survivin-expressing cancer cell models.

Biochemical methods were applied to reveal a Survivin-based protective mechanism against nanotoxicity. The cell-based analyses were complemented by qualitative and quantitative microscopy techniques, including organelle-specific immunofluorescent staining and automated high-content cell analysis.

Overall, the toxicity of SiNP was characterized as a rapid process, which depended on the concentration and the exposure time in a serum-free environment. The toxicity of SiNP was manifested through apoptotic and necrotic phenotypes and exhibited increased autophagic characteristics. Mechanistically, SiNP induced the generation of ROS and activated stress kinase p38, while pro-survival kinases Akt and MAPK 44/42 (ERK) were downregulated. Mitochondrial stress was identified as the main ROS source, while lysosomal leakage could be excluded. The initiation of SiNP-dependent autophagy was confirmed through immunoblot analysis and microscopic tracking of autophagy-related organelles, further suggesting a PI3K/Akt/mTOR independent initiation pathway. SiNP destabilized the cytoskeleton, leading to cytoskeleton collapse, and thereby triggering autophagy. Unexpectedly, the results also suggested that SiNP may impair autophagy in the late stage, leading to the accumulation of autophagy-related organelles and autophagy-dependent cell death. Remarkably, Survivin overexpression delayed those SiNP-dependent effects and suppressed autophagy. Overall, an elevated Survivin level suppressed all autophagy characteristics and stabilized the cytoskeleton structure. In response to the SiNP-generated ROS stress, Survivin altered the mitochondrial phenotype and suppressed the activation of p38. Moreover, p38 inhibition increased the viability of Survivin overexpressing cells but not wild-type cells, indicating a Survivin-specific mechanism.

To prove the detailed role of autophagy in SiNP-induced toxicity, SiNP treatment was combined with different autophagy modulators. Taken together, impairing the late stage of autophagy leads to enhanced nanotoxicity compared to the initiation or inhibition of initial autophagy.

In summary, this work supports the hypothesis that autophagy plays a crucial role in Survivin-induced resistance. Therefore, novel cancer treatments targeting Survivin should consider its role in autophagy as a potential target for combined therapies.

1 INTRODUCTION

1.1 CANCER

In recent decades, cancer has been the subject of intensive research analyzing the causes, development, and disease itself. Nevertheless, cancer is still one of the top ten causes of death worldwide. According to the International Agency for Research on Cancer (IARS), powered by the World Health Organization (WHO), the breast, lung, prostate, and digestive tract are the tissues most commonly affected by cancer, with lung cancer causing the most deaths worldwide in 2020 (IARC, 2024).

In general cancer cells can originate from epithelial cells, endothelial cells, and blood or immune cells, categorizing the malignant cancer types into Carcinomas, Sarcomas, and Leukemias/Lymphomas (Cooper, 2000). The development of cancer is a multistep process and a consequence of acquired mutations initiated by environmental factors such as ultraviolet radiation, viral diseases, or dietary issues such as obesity, and abusive use of alcohol and tobacco. Genetic predisposition, age-related hormone disbalances, and others can act as tumor promotors by stimulating the outgrowth of cells in early tumor development (Blackadar, 2016). Even though intensive research has helped to successfully identify cancer-inducing factors such as substances in tobacco or different types of viruses, cancer-related diseases are on the rise. The reasons for the high number of cancer-related deaths today are manifold. The more than 200 types of cancer are categorized into several subtypes with varying genetic and molecular expression patterns leading to different tumor behaviors. The diversity of cancer cell types in malignant tumors increases further by acquiring several genetic mutations during tumor growth. However, as large as the variety of cancer types and subtypes is, a single cancerous tissue can consist of different variations of cancer cells, each of which may respond differently to standardized cancer therapy (Ma et al., 2019). This tumor cell inconsistency has the consequence that one cancer drug might not be enough to address all tumor cells and instead promotes cancer cell progression and resistance of nonresponding tumor cells (Shi et al., 2023).

The classical standard procedure involves surgical resection of the tumor tissue followed by a combination of radiation and chemotherapy. The accessibility of the tumor and the tumor stadium limits the application of surgical resections (Arruebo et al., 2011). On the other hand, radiation and chemotherapy are often accompanied by side effects since healthy tissue is affected by both treatment approaches (Moses et al., 2003). In recent decades, non-invasive ablation techniques extended the surgical resection by applying radiofrequency, microwave, or ultrasound to create hyperthermia or by use of cryoablation as a hypothermic application to reach the tumor side (Chu & Dupuy, 2014; Yakkala et al., 2019).

New cancer-specific treatment approaches include hormones, stem cells, genes, and immunotherapy. Another cancer treatment approach, covered by the umbrella term targeted drug therapy, uses cancer-specific motilities for targeted drug delivery and drug design (Debela et al., 2021).

A prerequisite for cancer-targeted therapy is the molecular characterization of the tumor, including the genetic clarification of the tumor cells, necessary for the development of a precise drug design. The targeted drug therapy aims for an improved treatment outcome while minimizing side effects. A specific drug design combined with cancer-targeting moieties, such as antibodies and peptides, should reduce the drug load, increase the bioavailability of the drug, avoid fast clearance from the blood, and improve the drug release and application and the tumor side while avoiding healthy cells at best (Min & Lee, 2022).

The past decades turned out that targeted therapy has a problem with drug resistance. Hence, most cancer cells have a high mutation rate, and tumor cells adapt fast to chemotherapeutic drugs, avoiding cell death through various mechanisms (Sabnis & Bivona, 2019): Targeted cancer cells can increase the DNA repair capacity, suppressing cell death pathways while promoting pro-survival factors and tumor reorganization, also known as tumor plasticity. Furthermore, cancer cells can modulate the tumor microenvironment (TME) to protect the tumor tissue from immune cells. In addition, tumor cells might neutralize, export, or simply not take up the drug (Lei et al., 2023).

The challenges for targeted drug therapies are immense, considering the highly diverse complexity of tumors and their inclination for resistance mechanisms. However, for this very reason, it is of great interest to intensify cancer research efforts to achieve a precise and successful treatment application for malignant cancer diseases.

In this context, cancer cell markers are important for the characterization of tumor tissue and, in addition, serve as specific target structures for optimal cancer therapy. The anti-apoptotic protein Survivin is abnormally expressed in various cancer types among other diseases and rarely expressed in healthy adult tissue, making Survivin an attractive therapy target (Albadari & Li, 2023). However, Survivin-expressing tumor cells evade cell death and promote cancer progression, dysregulating the essential cell processes, apoptosis, and autophagy (Lin et al., 2019). Regarding this influence, understanding these mechanisms is of great importance for the development of effective cancer drugs. Therefore, the essential cell processes are presented first, followed by further details on Survivin as a modulator of the described processes, the nanotechnological treatment approach, and the aim of the work.

1.2 Cell Death Mechanisms: Necrosis and Apoptosis

Cell death signals are often suppressed in malignant tumor cells through enhanced expression of inhibitor of apoptosis (IAP) proteins such as Survivin. In general, cell death occurs in two categories: energy-independent necrosis and energy-dependent apoptosis.

The energy-independent cell death mechanism, necrosis, is triggered by toxic stimuli and occurs as secondary cell death after apoptosis or in parallel to the apoptotic process, depending on the initiation signal and level of stimulus. In contrast to apoptotic cell death, necrosis is not limited to single cells and rather affects a whole area of cells in a tissue. Cell swelling, membrane rupture, and the fragmentation of the nucleus, known as karyorrhexis, characterize necrotic cell death (Figure 3). Moreover, the energy metabolism and the morphology of cell organelles are affected. However, a controlled form of necrosis has been described, referred to as necroptosis, mediated by receptor interaction protein kinases 1 (RIPK1) and 3 (RIPK3) and is associated with inflammatory processes (Cui et al., 2016; Kawahara et al., 1998).

Apoptosis, referred to as programmed cell death, involves the controlled activation of caspases. Apoptosis exhibits a specific time-dependent phenotype: First, cell shrinkage and chromatin condensation, also known as pyknosis, occur. Then, apoptotic bodies form, enclosing the cell content in intact plasma membranes. Macrophages digest the apoptotic bodies to prevent inflammation from release of cell contents. Under cell culture conditions, this clearance pathway is unavailable, leading to secondary cell death, which ascribes to necrosis. Apoptosis can be triggered extrinsically by cell death receptor activation or through intrinsic stimuli via mitochondria (Figure 1).

The extrinsic pathway begins with the activation of transmembrane receptors through ligand binding: The ligand-receptor couples include the tumor necrosis factor (TNF)/ type 1 TNF receptor (TNFR1), the Fas-Ligand (Fas-L)/ Fas receptor (CD95/Apo-1) and TNF-related apoptosis-inducing ligand (TRAIL)/TRAIL receptor. Then, adaptor proteins are recruited and bind to the receptor's cytosolic death domain, inducing an activation cascade forming the death-inducing signaling complex (DISC). Then DISC activates the initiation caspases caspase-2, -8, -9, and -10, which consequently activate effector caspases triggering apoptosis (Jan & Chaudhry, 2019).

A wide range of stress stimuli, such as growth factor depletion, oxidative stress, toxins, hypoxia, viral infection, and others, can trigger the intrinsic cell death pathway. The stress signals can change the mitochondrial membrane, initiating the opening of the mitochondrial permeability transition pore. As a result, the mitochondrial membrane potential collapses, and mitochondrial proteins promote an apoptosis outflow into the cytosol. The release of mitochondrial cytochrome C into the cytosol initiates the formation of the cell death complex,

called apoptosome. The apoptosome is a heptameric structure with repeating units consisting of apoptotic protease activating factor 1 (Apaf-1) and cytochrome C, which recruits and activates the apoptotic initiator caspase-9. In addition, the released mitochondrial proteins HtrA2/Omi and Smac/DIABLO increase the apoptotic stimulus by neutralizing inhibitors of apoptosis (IAP) family members such as Survivin, Bcl-2, and BcL-XL, among others.

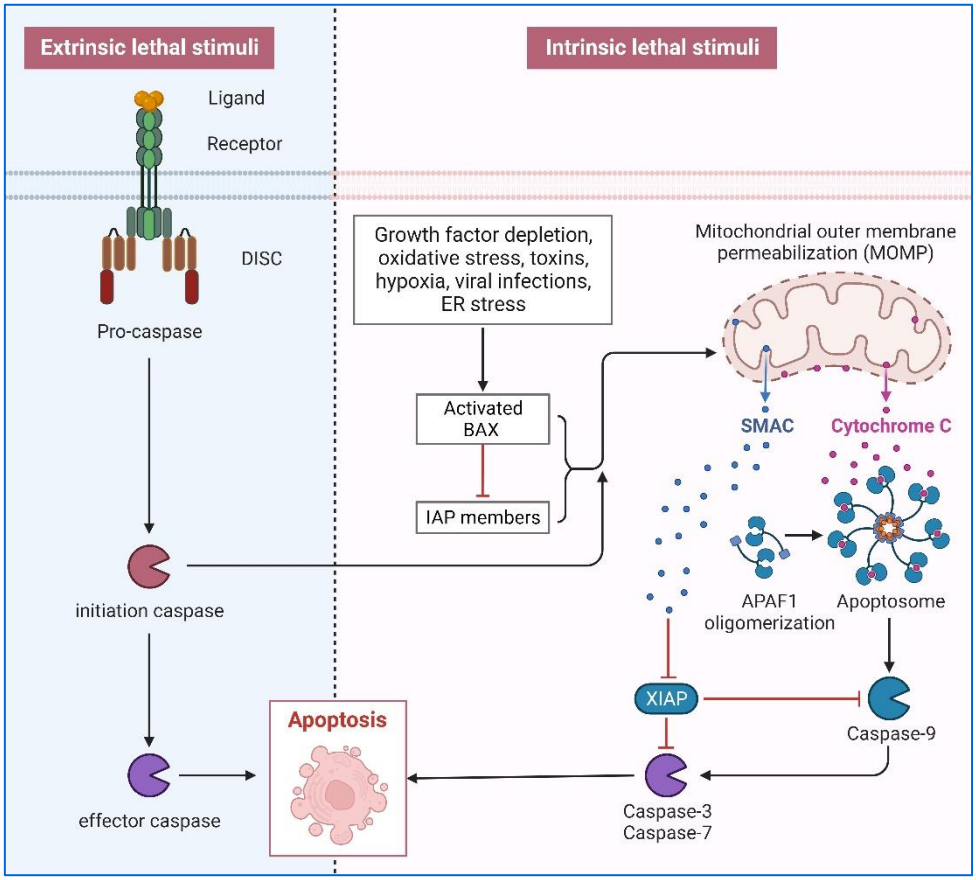

Figure 1. Illustration of the extrinsic and intrinsic apoptotic pathway. The extrinsic cell death pathway is triggered by ligand-receptor interactions, promoting the assimilation of the DIS complex (DISC), activating initiation caspases, which activate effector caspases and the intrinsic cell death pathway, leading to apoptosis. The intrinsic cell death pathway is triggered by several cell stress stimuli and is associated with the release of mitochondrial proteins. The mitochondrial proteins activate initiation caspase-9 and inactivate anti-apoptotic proteins such as XIAP and other IAP family members. The image was adapted from Micheau et al. (2018) (Micheau, 2018), using the BioRender.com template "Apoptosis Extrinsic and Intrinsic Pathways" (https://app.biorender.com/biorender-templates, accessed on 05 January, 2024).

Furthermore, unfolded, and accumulated proteins can trigger the so-called unfolded protein response (UPR) of the endoplasmic reticulum (ER), inducing apoptosis. The unfolded protein response is a cellular stress response that activates three proteins: inositol-requiring protein-1α (IRE1α), PERK protein kinase RNA (PKR)-like ER kinase (PERK) and activating transcription factor 6 (ATF6). Their role is to restore protein homeostasis by increasing the expression of ER chaperones, reducing mRNA translation to alleviate ER stress, and exporting unfolded proteins into the cytosol for degradation through either the ubiquitin pathway or the

ER-assisted degradation (ERAD). When ER stress is not relieved, it triggers apoptosis through stress kinases p38 and (c-Jun-N-terminal kinase) JNK, as well as pro-apoptotic transcription factor CHOP. In turn, Bax activation and Bcl-2 inhibition promote mitochondrial protein release and initiate the apoptotic pathway (Sano & Reed, 2013).
However, as soon as an initiation caspase activates effector caspase-3, -6, or -7, apoptosis progresses irreversibly regardless of the apoptosis pathway. The most effective caspase, the caspase-3, is targeted by both cell death pathways. Active caspase-3 cleaves and releases the caspase-activated DNase (CAD) from CAD inhibitor ICAD. In turn, CAD degrades chromosomal DNA and induces pyknosis. Gelsolin is the nucleation base for actin fibers and represents an important target of caspase-3 cleavage. The degradation of gelsolin leads to cytoskeleton reorganization, which impairs intracellular transport and signal transduction and further promotes the formation of apoptotic bodies (Elmore, 2007).

1.3 AUTOPHAGY

Autophagy is an umbrella term for several kinds of autophagy pathways, including chaperone-mediated autophagy (CMA), microautophagy, and macroautophagy. Generally, it is a highly regulated process conserved across species. Canonical autophagy is an essential process balancing cell homeostasis and obtaining cell survival. It acts as recycling machinery, removes damaged organelles like mitochondria, and degrades obsolete proteins and RNA to usable building blocks fed back into the metabolic cycle. Thereby, canonical autophagy regulates the supply of amino and nucleic acids under nutrition-deprived conditions (Kocot & Wroblewska, 2022; Mizushima & Komatsu, 2011). The CMA and microautophagy direct cargo straight to lysosomes for degradation. Macroautophagy involves the formation of autophagosomes, which then fuse with lysosomes, resulting in the degradation of the autophagosomal content (Parzych & Klionsky, 2014). Other autophagy types involve the degradation of targeted organelles: Mitophagy degrades damaged mitochondria, while lysophagy describes a process that renews old lysosomes (Yao et al., 2021).

The protein of interest, Survivin, was recently described as a switch between autophagy and apoptosis (Lin et al., 2019). Cancer cells either activate autophagy to avoid apoptosis or suppress it to promote tumor progression, which is linked to cancer-related characteristics such as modified metabolism and immunomodulation (X. Chen et al., 2016; Xi et al., 2022). Additionally, autophagy encourages the development of cancer stem cells and the epithelial-to-mesenchymal transition (EMT) (Alvarez-Meythaler et al., 2020). Cancer stem cells describe a subpopulation of cancer cells that are immortal, highly resistant, and self-renewing and further possess a differentiation potential. As a result, cancer stem cells can increase the tumor drug resistance (Nazio et al., 2019). In addition, EMT increases the invasive nature of cancer

cells, and consequently, metastasis, increasing the mortality of the cancer diseases in the long term (Gundamaraju et al., 2022). However, cancer cells can disrupt autophagy, highlighting the role of autophagy as a crucial target for cancer therapy (Abulikemu et al., 2022).

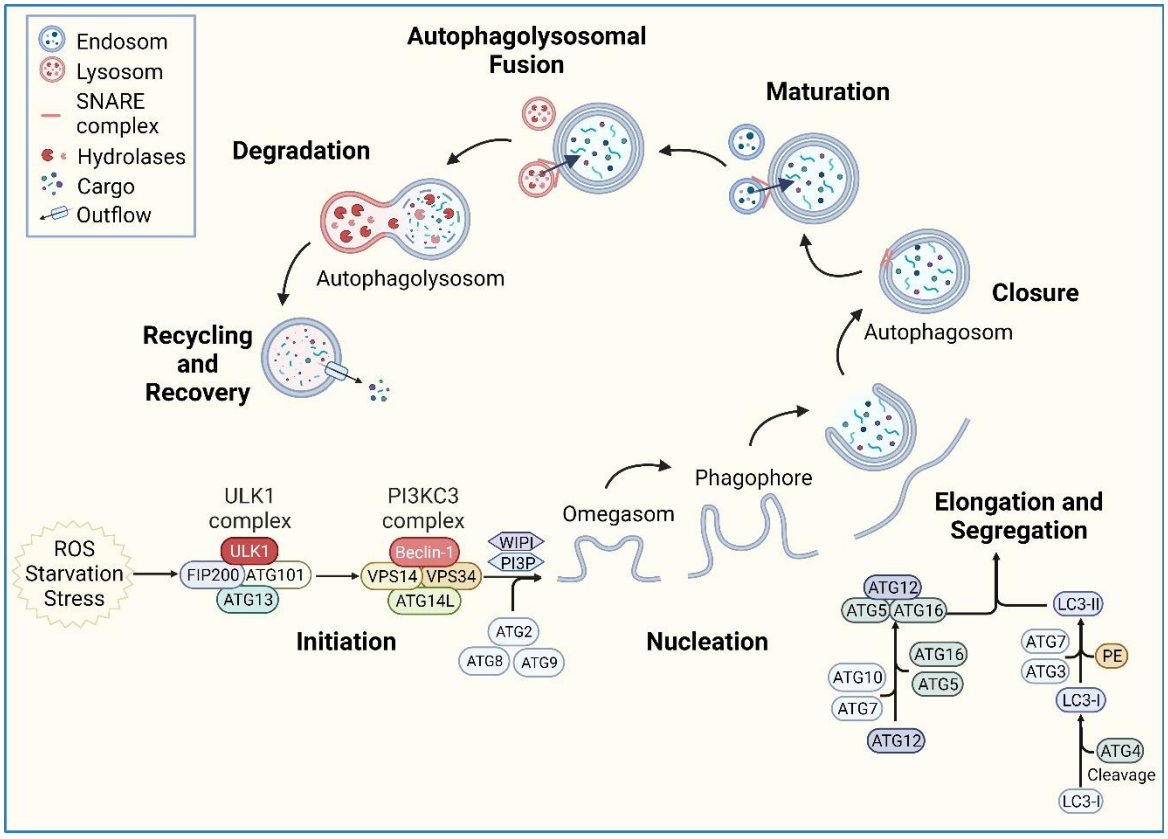

Figure 2. Canonical autophagy. Stress stimuli from different sources activate the ULK1 and PI3KC3 complex, initiating the autophagy process. Autophagosome nucleation starts with an omegasom-shaped membrane, which extends in the elongation process to a phagophore. The enlarged phagophore membrane encloses cargo. Then, the phagophore is sealed and released from the donor membrane in the segregation process, generating an autophagosome. The autophagosome is further maturing on the way to the perinuclear region through the fusion of endosomes. The fusion with lysosomes creates autophagolysosomes. Lysosomal hydrolysis degrades the autophagolysosomal content. In the final step, the degraded components flow into the cytosol, and lysosomes recover. Created with biorender.com

The autophagy process splits into eight steps, beginning with the initiation and nucleation and followed by the elongation, segregation, closure, and maturation of the autophagosomal membrane and finishes with the autophagosomal fusion, degradation and the recycling and recovery step (Figure 2). Autophagy is initiated by several stimuli of chemical or mechanical nature, promoting the formation of the ULK-1 complex consisting of ULK, FIP200, ATG101, and ATG13 and further activation of the PI3KC3 complex (Beclin1, VPS14, VPS34, ATG 14L). Because of the PI3KC3 complex activation, phosphatidylinositol-3-phosphate (PI(3)P) forms that initiate a recruiting cascade via WD-repeat protein interacting with phosphoinositides (WIPI), resulting in the recruitment and lipidation of ATG8, ATG2, and ATG9. Autophagy-

related genes (ATG) and their proteins are essential for lipidation and formation of autophagosome membranes. The recruited ATGs (ATG8, ATG2, and ATG9) promote the membrane bending of an organelle donor membrane to an omegasome and further to a phagophore, referred to as a nucleation step of autophagosomes (Figure 2). ATGs such as ATG3, AG7, ATG5, ATG12, and ATG 16L1 mediate the elongation and the segregation of the phagophore membrane from the cytosolic organelle donor membrane. ATG7 activates ATG12 and promotes with ATG3 the lipidation of LC3. ATG10 mediates the conjugation of ATG12 with ATG5. The conjugate can promote LC3 lipidation and is a conjugation partner for the complexation of ATG16L1, essential for the formation of autophagosomes. During the elongation, cytosolic LC3-Iconjugate to phosphatidylethanolamine (PE) on the curved phagophore membrane to generate LC3-II, which is incorporated into the elongated autophagosomal membrane. LC3-II is a specific autophagosomal marker, responsible for selecting and loading of certain cargos and for the further progression of the autophagy process (Birgisdottir et al., 2013). When the early autophagosomes are fully loaded, PI(3)P and ATGs are cleared from the membrane surface, initiating the membrane fusion via SNARE, and generating a double-membraned autophagosomal vesicle. The SNARE-mediated fusion with endosomes further maturates autophagosomes. Parallel to the maturation process, autophagosomes, and lysosomes move to the perinuclear region via dynein on microtubules. In the final step, mature autophagosomes fuse with lysosomes forming autophagolysosomes (Figure 3). On the lysosomal surface, the tethering of those vesicular organelles is mainly facilitated by the homotypic fusion and vacuole protein sorting (HOPS) complex. The HOPS complex interacts with LC3-II and STX17 on autophagosomes, inducing the complexation of STX17, SNAP29, and VAMP8 to the SNARE complex. Finally, the SNARE complex mediates the fusion to autophagolysosomes.

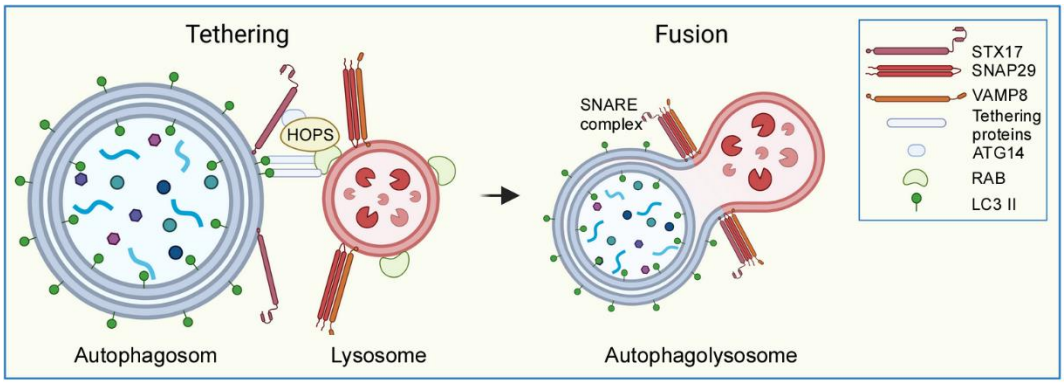

Figure 3. Tethering and fusion of autophagosomes with lysosomes. Tethering facilitated by the HOPS complex consisting of vacuolar protein sorting proteins VPS11, VPS16, VPS18, Vps33A, VPS39, and VPS41 recruiting STX17 and binding to Ras-like GTPase (RAB) on lysosomes and LC3 on autophagosomes. Then, the SNARE complex forms, promoting the fusion of the vacuolar vesicles to an autophagolysosome. Created with biorender.com

After the lysosomal degradation of the autophagolysosomal content, including the inner membrane of the autophagosome, autophagy is completed. In the recovery process of lysosomes, the degraded soluble content is ejected through the membrane that is accompanied by a water outflow, resulting in the shrinkage of the organelle. Then, assisted by actin fiber constructs the vesicular membrane bents to tubular structures. The tubular shape facilitates the constriction of newly recovered lysosomal vesicles. A new autophagic cycle can start. (Hernandez-Caceres et al., 2021; Mizushima, 2020; Yu et al., 2018).

1.4 AUTOPHAGY RELATED ALTERNATIVE CELL DEATH MECHANISMS

The intensity and duration of stress signals determines the outcome of autophagy consequences. Sublethal stress signals trigger protective autophagy through JNK-mediated Bcl-2 phosphorylation and release of Beclin-1, an initiator of autophagy (Liu et al., 2017; Wei, Pattingre, et al., 2008). Stress signals with a high intensity or prolonged duration induce apoptosis by activating JNK-dependent Bcl-2 multiphosphorylation that results in Bax activation and mitochondrial release of mitochondrial proapoptotic proteins cytochrome C and Smac/DIABLO into the cytosol (Wei, Sinha, et al., 2008). Autophagy regulates intracellular reactive oxygen species (ROS) levels by increasing mitophagy through HIF-1α/BNIP3 pathway activation, avoiding ROS-dependent apoptosis induction (Zhang et al., 2019). However, several autophagy-related proteins can induce apoptosis: ATG5 and ATG12 can interact with IAP family members like Bcl-2 and Mcl-1. They can also promote the release of mitochondrial cytochrome C (Rubinstein et al., 2011; Yousefi et al., 2006). On the other hand, apoptosis-related caspases regulate autophagy by cleaving and degrading ATGs, controlling the autophagy activation level (Tsapras & Nezis, 2017).

Various alternate cell death mechanisms have been described in the past few decades, sharing certain features with apoptosis and necrosis, while others function entirely differently. They classify into entosis, ferroptosis, methuosis, necroptosis, NETosis, parthanatos, pyronecrosis, pyroptosis, lysosome-dependent cell death, autophagy-associated cell death (autosis) and autophagic cell death (Nirmala & Lopus, 2020). The last three mechanisms, which are the most relevant for this work, will be described in more detail.

The lysosome-dependent cell death is induced by the permeabilization or rupture of lysosome membranes, releasing lysosomal proteases like cathepsins and increasing the acidic level in the cytoplasm (Serrano-Puebla & Boya, 2018; Uchimoto et al., 1999). Cytosolic proteases, lysosome-penetrating compounds, and elevated ROS levels can induce this type of cell death. Consequently, pro-apoptotic proteins such as Bid and Bax activate the cell death cascade via mitochondrial cytochrome C release (Aits & Jaattela, 2013).

Jung et al. (2020) differentiated the terms of autophagy-involving cell death mechanisms: Authentic autophagy cell death can be prevented by autophagy inhibitors and does not involve

apoptotic or necrotic phenotypes. In contrast, autophagy-mediated cell death (autosis) is associated with an increased autophagy flux but involves other apoptotic and necrotic characteristics necessary for an efficient cell death process (Jung et al., 2020). Autosis has several indicators, such as chromatin condensation, increased formation of autophagosomes and autophagolysosomes, enlarged mitochondria, fragmented ER, and membrane destabilization or rupture (Nirmala & Lopus, 2020). Autosis depends on Na+, and K+-ATPases triggered by the viral transactivator of transcription (Tat) peptide, through interaction with autophagy-inducing factor Beclin-1, or starvation (Bai et al., 2023).

In summary, autophagy can directly mediate cell death or appear as part of an orchestrated cell death together with other cell death pathways: Autophagy and apoptosis form a highly dynamic system that responds quickly to various stimuli of different origins and intensities, regulating numerous cell processes. The complex crosstalk complicates the development of specific and efficient anti-cancer drugs cause the experimental differentiation between those processes is difficult and the evaluation of the specific drug effects challenging.

1.5 SURVIVIN

The anti-apoptotic protein Survivin is abnormally expressed in various cancer types. Hence, Survivin is promoting the cancer progression by regulating both apoptosis and autophagy, and further is acting as a switch between the two processes, Survivin will be described in detail.

1.5.1 MOLECULAR FUNCTIONS OF SURVIVIN

Survivin has a size of 16.5 kDa and is the smallest member of the inhibitor of apoptosis (IAP) family and can act as a monomer or dimer, as well as homo- and heterodimer, increasing the functionality of the smallest IAP member. All IAP members bear at least one highly conserved N-terminal baculovirus inhibitor of apoptosis repeat (BIR) domain with a Zn2+ finger formation, which is responsible for the integrity of the α-helical BIR domain (Figure 4) (Deveraux & Reed, 1999). Survivin has only one BIR domain, contributing to its small size and function, and lacks a C-terminal RING finger domain, unlike other IAP members like XIAP, c-IAP-1, c-IAP-2, NAIP, and BRUCE (Deveraux & Reed, 1999). The N-terminal BIR domain and the C-terminal α-helix enable the dimeric Survivin to interact with both helices with various interaction partners. Survivin can appear in seven splice variants, while the ex2 isoform is the most common splice variant, referred to as the wild-type (wt) form. (Pavlyukov et al., 2011; Wheatley & Altieri, 2019; Wolanin & Piwocka, 2007).

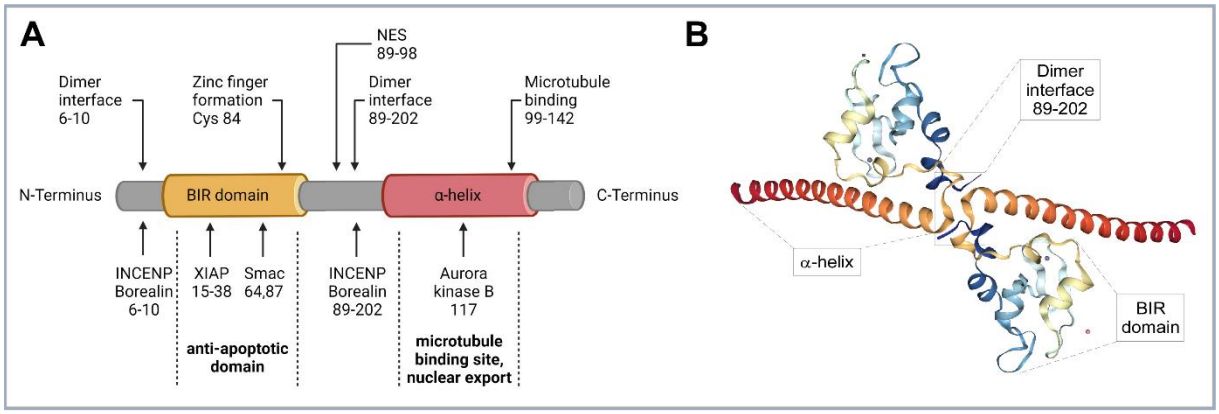

Figure 4. Molecular structure of Survivin. A) Graphical illustration of Survivins functional domains adapted from Hu et al. (2017), (Hu et al., 2017) and created with Biorender.com. B) Adapted crystal structure of a Survivin dimer, created by Chantalat et al. (2000) (Chantalat et al., 2000).

A central linker region positioned between aa 90-120 modulates the dimerization and further the molecular functions of Survivin (Verdecia et al., 2000). Stauber et al. (2006) showed that Survivin bears a nuclear export signal (NES) that is located in the dimerization region (89-98), resulting in nuclear accumulation of the Survivin dimer (Stauber et al., 2006), while monomeric Survivin mainly stays in the cytoplasm (Engelsma et al., 2007). Several studies proposed a balanced regulatory process between the monomeric and dimeric forms of Survivin: Wang et al. (2010) showed that CREB-binding protein (CBP) mediated acetylation of Lys129 promotes the dimeric form of Survivin. The free deacetylated Survivin monomers can interact with the CRM1 export receptor and translocate to the cytoplasm (Wang et al., 2010). Pavlyukov et al. (2011) analyzed the role of monomeric Survivin in apoptotic processes by mutating the linker region and further showed that Survivin monomers interact with Smac/DIABLO and XIAP more efficiently than Survivin dimers (Pavlyukov et al., 2011). Another group showed that the monomeric but not the dimeric form is part of the chromosomal passenger complex (Delacour-Larose et al., 2007). The chromosomal passenger complex is formed during mitosis to separate the chromosome pairs and distribute them to the two daughter cells (Carmena et al., 2012). In more detail, the chromosomal passenger complex assembles by monomeric Survivin binding to INCENP and borealin. Simultaneously, Survivin detaches from the kinetochore binding microtubules and destabilizes the microtubule network, while dimeric Survivin enhances the microtubule stability (Cheung et al., 2009; Delacour-Larose et al., 2007; Jeyaprakash et al., 2007; Pavlyukov et al., 2011). In addition, Survivin carries a mitochondrial targeting sequence (MTS) responsible for the mitochondrial localization of Survivin (Dunajova et al., 2016). The different signal sequences, Survivin can localize in the nucleus, mitochondria, or the cytoplasm (Dunajova et al., 2016; Engels et al., 2007; Stauber et al., 2007). The localization of Survivin is a key element for its function as an apoptosis inhibitor. In normal non-transformed cells, Survivin controls the mitotic cell division as a member of the chromosomal

passenger complex and as part of the mitotic spindle assembly checkpoint, guiding the transition from metaphase to anaphase (Knauer et al., 2006). Therefore, non-malignant cells have a limited cytosolic and nuclear expression of Survivin, while mitochondrial Survivin correlates with cancerous malignancy. Mitochondrial Survivin suppresses several mitochondrial proteins through direct binding and results in a suppressed apoptosis (Ceballos-Cancino et al., 2007; Dohi et al., 2004; Townley & Wheatley, 2020).

1.5.2 SURVIVIN IN NON-CANCEROUS DISEASES

Abnormal levels of Survivin are associated with several diseases such as hyperplasia, different autoimmune disorders, and cancer (Li et al., 2021). Survivin is expressed in hepatocytes of patients with chronic hepatitis and during cirrhotic phases of the infection, correlating with the development of hepatocellular carcinoma (HCC) (Akpinar et al., 2020). Typically, phosphorylation of Survivin is increased in peripheral blood mononuclear cells (PBMCs), while patients with Behecet`s Disease (BD) show a decreased Survivin phosphorylation level in the plasma (Pahlavan et al., 2020). Hence, Survivin is a critical player in hematopoiesis, the depletion of Survivin leads to bone marrow loss associated with high patient mortality (Leung et al., 2007). Inflammatory processes can trigger the Survivin expression in macrophages and granulocytes complying with metabolic demands and further increasing the lifespan as IAP protein, which plays an important role in autoimmune and allergic reactions (Liu & Cao, 2016; Navegantes et al., 2017). In addition, Survivin controls the antigen presentation of dendritic cells and the autoantibody production, promoting autoimmune diseases such as rheumatic arthritis (Andersson et al., 2012; Svensson et al., 2010). Elevated Survivin levels were also documented for smoking patients with autoimmune disorders (Perricone et al., 2016). Smoking is under suspicion to promote the secretion of Survivin, resulting in a decrease of Survivin targeting cytotoxic T-cells associated with arthritis (Wasen et al., 2017). An increased number of leukocytes is an indicator of inflammatory processes. However, in addition, it is associated with an increased Survivin expression level determined in several diseases such as inflammatory bowel diseases, lichen planus, multiple sclerosis, myasthenia gravis, psoriasis, pulmonary arterial hypertension, rheumatic arthritis, and systemic sclerosis (Gravina et al., 2017). In addition to the immunological role of Survivin, Survivin is a critical resistor against oxidative stress and apoptosis in neuronal cells, ensuring the early development of the brain and promoting repair mechanisms. A depletion of Survivin resulted in reduced brain mass and apoptosis and was associated with neurodegenerative diseases such as Alzheimer's (Baratchi et al., 2011; Jiang et al., 2005; Sriramoju et al., 2015). Decreased Survivin levels are also critical for liver regeneration (Hagemann et al., 2013). However, elevated Survivin levels in fibroblasts led to hyperplasia, vasculopathy, and organ failure (Brunasso & Massone, 2016).

In sum, elevated Survivin levels are related to inflammatory diseases and increase autoimmune reactivity. However, Survivin can also act as a resistor against neurodegenerative processes, and inflammation and further promotes regeneration and homeostasis.

1.5.3 SURVIVIN IN CANCER

The Survivin coding mRNA is one of the top five elevated mRNAs in cancer and is handled as a promising treatment target for various tumor types (Velculescu et al., 1999).
Splicing variants, posttranslational modification, the formation of dimers and subcellular compartmentalization determine the regulatory functions of Survivin, complicating the cancer treatment. Nuclear Survivin regulates pro-survival genes or initiates DNA repair mechanisms (Vequaud et al., 2016). The accumulation of nuclear Survivin can promote the survival of senescent cancer cells (Wang et al., 2011). Further, nuclear Survivin suppresses the miRNA transcription (Andersson et al., 2017). Du et al. (2012) demonstrated that several tumor cells exhibit a reduced miRNA expression level, especially chemo-resistant tumor cells that envelope a miRNA deficiency (Du & Pertsemlidis, 2012).

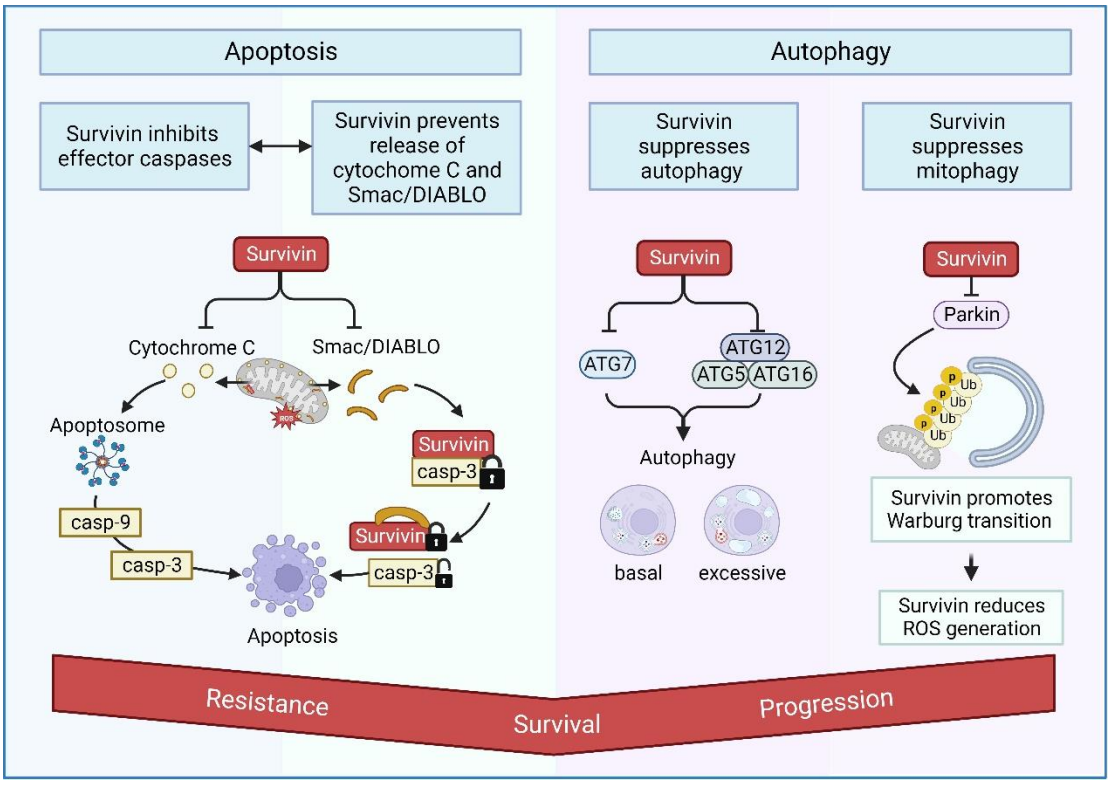

Figure 5. Survivin in apoptosis and autophagy. Survivin inhibits apoptotic and autophagy-related processes, favoring cancer cell resistance, survival, and progression. Created with biorender.com

Survivin is a protein that can contribute to the progression of cancer cells by inhibiting apoptosis and promoting proliferation (Figure 5). When it accumulates in mitochondria, it can prevent the activation of intrinsic apoptotic stimuli. Therefore, mitochondrial Survivin is a

specific indicator for many types of cancer cells (Dohi et al., 2004). Survivin can bind mitochondrial pro-apoptotic molecules such as Smac/DIABLO and prevent their release into the cytosol. Several studies have analyzed the direct interaction between Survivin and Smac/DIABLO. However, when mitochondria release Smac/DIABLO into the cytosol, it can neutralize IAP proteins and restore caspase activity. (Ceballos-Cancino et al., 2007). In consequence, IAP proteins cannot inhibit pro-apoptotic effector caspases, and the apoptotic pathway is triggered. Due to the binding of Survivin to Smac/DIABLO in mitochondria, the release of Smac/DIABLO can be suppressed or delayed. Additionally, the complex is stabilized in the cytosol, preventing Smac/DIABLO from binding, and activating pro-apoptotic proteins in the cytoplasm. In the end, Survivin is accumulated in mitochondria and neutralizes Smac/DIABLO on the spot, preventing or delaying apoptosis (Ceballos-Cancino et al., 2007).
Furthermore, Survivin decreases the mitophagy flux by inhibiting the ubiquitination of depolarized mitochondria mediated by E3 ligase parkin (Figure 5) (Townley & Wheatley, 2020). In turn, defective mitochondria accumulate in cancer cells, and the metabolic pathway switches from oxidative phosphorylation to glycolysis, also known as the Warburg effect. The altered metabolism produces less ROS, in exchange for a reduced ATP level, thereby protecting cells from high oxidative stress (Lu et al., 2015). In addition, Survivin can prevent FoxO3-mediated ROS generation (Hagenbuchner et al., 2013). As a consequence of the alternate metabolism, cancer cells produce more lactate and enhance the expression of hyaluronic acid and its receptor CD44, causing decreased adherence of the cells, promoting migration phased in metastasis (Stern et al., 2002). However, anaerobic glycolysis leads to an acidified extracellular tumor microenvironment, preventing macrophage-selected phagocytosis of tumor cells. Moreover, acidification can impair the T-cell metabolism and function, protecting tumors against immunological clearance (Chen et al., 2020; Kornberg, 2020).
Ausserlechner and Hagenbuchner (2016) defined a Survivin complex that is generated after the recruitment of dynamic-like-protein 1 (Drp1) by Survivin-inducing mitochondrial fission, the survivosome (Hagenbuchner et al., 2016). The complex contains autophagy-inducing protein beclin-1, PTEN-induced-kinase-1 (PINK-1), and ubiquitin ligase PARK2, also known as parkin. This complex is responsible for morphological changes in the mitochondrial network, leading to aberrant metabolism, increasing glycolysis, and reduced ROS production due to the downregulation of respiratory complexes (Hagenbuchner et al., 2013). Through this pathway, Survivin can decrease the sensitivity of cancer cells against ROS-depending cancer therapeutics. In contrast, glycolysis inhibitors like lonidamine (LND) or 2-deoxy-D-glucose (2DG) interrupt the formation of the survivosome and induce the degradation of Survivin, mediated by parkin and beclin-1, which is culminating in apoptosis (Ausserlechner & Hagenbuchner, 2016). In a recent publication, Hagenbuchner et al. (2019) showed that the disruption of the XIAP-Survivin complex is responsible for the morphological transformation of

mitochondria. Survivin is released from XIAP and recruits Drp1 to translocate from the cytoplasm to the mitochondria, accompanied by the downregulation of respiratory complexes I and IV (Hagenbuchner et al., 2019). Furthermore, Chen et al. 2018 investigated that Notch signaling increases by Drp-related mitochondrial fission, which promotes enhanced expression of Notch1 in a positive feedback loop (Chen et al., 2018). Active Notch1, also known as Notch1 intracellular domain (NICD1), facilitates RBP-Jκ binding to the Survivin promotor for transcriptional activation (Chen et al., 2011).

Survivin has a regulatory function in the autophagy process by decreasing the basal activity level of autophagy (Lin et al., 2019). Survivin might protect the cancer cells by limiting autophagy on the basal level since the cell-protective autophagy can switch into autophagy-dependent cell death when autophagy is in an excessive mode (Humphry & Wheatley, 2018). Regarding cancer therapy, this adaptive mechanism would be of great importance for the strategic design of combinatorial cancer treatments, targeting autophagy in Survivin overexpressing cancer cells. Most common treatment strategies involve Survivin-specific inhibitors, which directly address the Survivin protein expression or indirectly suppress the Survivin upstream promotors. The most common Survivin inhibitor is the small molecule sepantronium bromide (YM155) that directly attenuates the transcription of Survivin. LY2181308, a short hairpin shRNA, was used against Survivin in acute lymphoblastic leukemia, a prostate cancer (Raetz et al., 2014; Wiechno et al., 2014). Interrupting the PI3K/Akt, Wnt/β-catenin or JAK/STAT3 signaling pathway, as well as the endothelial receptor pathway, or triggering p53 activity attenuates Survivin expression and protein level (Gravina et al., 2017).

However, a single point of attack is usually not sufficient to overcome tumor resistance, which is why the combination of Survivin inhibitors with other treatment strategies and targets is of great interest. The autophagy process was identified as a promising target pathway for a combination treatment with amorphous silica nanoparticles (SiNP). Nanomaterials and SiNP, used in cancer treatments, will be presented in the following sections.

1.6 NANOMATERIALS

Nanomaterials possess many favorable physical and chemical properties and are therefore on the rise as main products or supplements for different applications in various fields such as the food-, drug-, cosmetic- and electronic industries, among others.

In general, nanomaterials are categorized as one- to three-dimensional materials based on the number of dimensions that exceed 100 nm in size. One-dimensional nanomaterials include nanotubes, nanorods, or nanowires that exhibit one dimension outside the 100 nm scale. Nanofilms, -layers, or -coatings are classified into two-dimensional nanomaterials due to their plate-like structure. Nanomaterials with no confined 100 nm scale, like powders, dispersions

of nanoparticles, bundles of nanowires, or tubes are classified as three-dimensional nanomaterials. Single particles in a size range of < 100 nm have been defined as zero-dimensional nanomaterials (Joudeh & Linke, 2022). In addition, nanomaterials, especially nanoparticles, can be produced with hollows, mesopores, or in a dense state (Figure 6A).
Nanomaterials are highly attractive for diverse applications in different industry branches due to their high surface-to-volume ratio on the nanometer scale, shape diversity, and modifiable surface chemistry. Especially nanoparticles are easy to produce in a bulk range that increases the production amount every year (Vance et al., 2015). They can be prepared from different materials such as carbon, metal, metal oxide, polymers, lipids, semiconductors, and others. The properties of nanomaterials can differ dramatically in their physical, chemical, and biological reactivity from their bulk material properties and consequently must be evaluated separately for their hazardous potential (Ji et al., 2021).

1.7 Silica Nanoparticles

The fields for possible silica nanoparticle (SiNP) applications increase every year due to the benefits of easy, low-cost production methods and simple surface modification chemistry. The following section presents the advantages and current application fields of silica nanoparticle-based technologies.
In general, SiNP are categorized into crystalline and amorphous SiNP while the first type is highly cell- and genotoxic, the FDA approved the latter type as a food supplement (Diab et al., 2017; Mebert et al., 2017; Murugadoss et al., 2017).
The fields for SiNP applications include SiNP as carriers for pesticides in the agriculture sector. Other fields use SiNP in the desalination of ocean water, as an absorbent for metallic contaminations, or as a supplement for refrigerants and many others (Liu & Sayes, 2022). In addition, solid particles such as SiNP can stabilize oil-water mixtures, also known as Pickering emulsions (Tikekar et al., 2013). This ability makes SiNP a popular supplement in the food industry as an anticaking agent E551 (Brand et al., 2021). In the biomedical field, SiNP improve contrast and imaging quality, either used as drug delivery vehicles or for diagnostics purposes, (Blechinger et al., 2010; Darwish et al., 2020). For medical formulations, drugs can be conjugated to the surface via Si-OH groups, absorbed into porous SiNP, or enclosed into hollow SiNP (Figure 6) (Gao et al., 2020; Takai-Yamashita & Fuji, 2020).

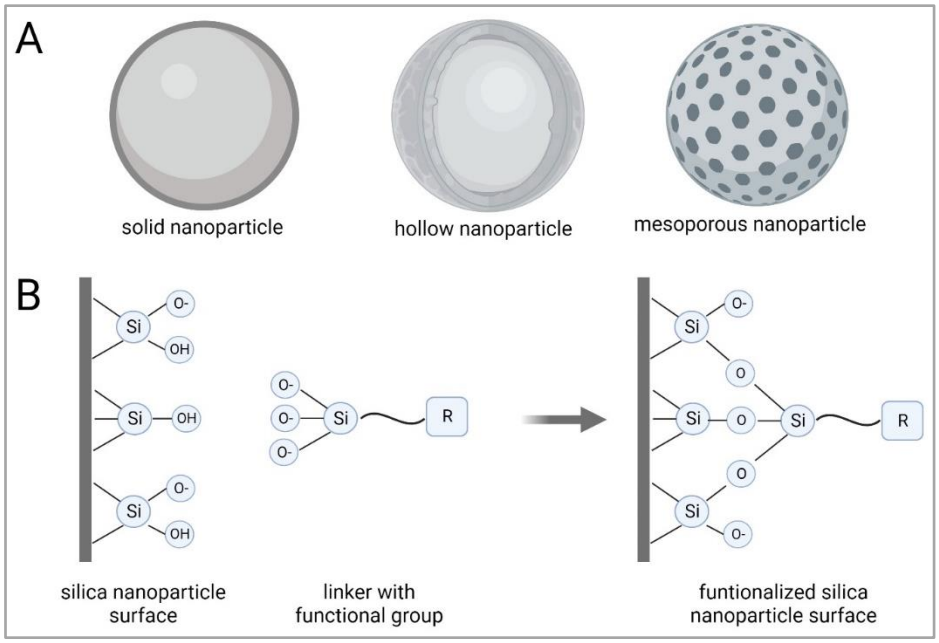

Figure 6. Silica nanoparticle types and functionalization. A) Different morphologies of silica nanoparticles. B) Modification of the silica nanoparticle surface. A linker group conjugates different residues (R) such as drugs or other functional groups to the silanol groups on the silica nanoparticle surface. Illustration adapted from da Cruz Schneider (2022), (da Cruz Schneid, 2022).

In general, the toxicity or rather safety of SiNP depends on the concentration and application form. Besides the safe production and application of SiNP, natural sources as well as industrial waste and the release of SiNP as pollutants are bearing the risk of being inhaled, and causing harmful effects in the distal airways and further in the alveolar or other tissues after the absorption into the bloodstream (Greenberg et al., 2007; Leung et al., 2012). Outside the mining industry, the most likely sources for SiNP are food products, drugs, or cosmetics absorbed by the gastrointestinal tract and the skin (Liu & Sayes, 2022). After the intravenous absorption of SiNP, or nanoparticles in general, most of the nanoparticles accumulate in the liver and spleen for clearance (Duan & Li, 2013). On the cellular level, especially SiNP are more often detected in lysosomes than in the cytoplasm, initiating autophagy and potentially impairing late-stage autophagy due to the accumulation in lysosomes (Abulikemu et al., 2022; Chu et al., 2011). Further, ER stress, inflammation, genotoxicity, apoptosis, and necrosis occur due to exposure to SiNP under specific conditions (Liu & Sayes, 2022).
However, nanomaterials, especially SiNP can enhance the efficacy of traditional chemotherapy drugs due to their unique physical and chemical properties.

1.7.1 Silica Nanoparticle-based Technology in Cancer Therapy

The cell diversity of a tumor is responsible for the inadequate effectiveness of chemotherapeutic drugs, promoting multidrug resistances and tumor recurrences (J. Wang et

al., 2017). In addition, classical chemotherapeutics such as cisplatin or doxorubicin have major side effects that can burden the patient's quality of life (L. Dai et al., 2016; Ongnok et al., 2020). The development of novel nanomaterials, functionalized with anti-cancer drugs, is ongoing in hopes of reducing the side effects of chemotherapeutic drugs. Drug delivery vehicles in the form of nanoparticles address these problems by encapsulating the active components into the nanoparticle's inner voids or absorbing them to the surface. In addition, coupling the drug to a protective carrier can improve the drug solubility, enhance the bioavailability, and increase the number of additional targeting moieties while diminishing the necessary drug load and related adverse side effects (Mu et al., 2020). The combination of silica-based nanoparticles showed great potential to potentiate the treatment efficiency used as a carrier or as an adjuvant for the combination with different anti-cancer drugs. In general, most anti-cancer drugs have a hydrophobic character that favors rapid excretion, resulting in a low body distribution and consequently limiting the tumor treatment efficiency (Gao et al., 2020).

Hence SiNP can be easily produced and modified cost-effectively. SiNP provide great opportunities to improve drug formulations and the therapy efficiency of the anti-cancer drug.

Several groups tested mesoporous silica nanoparticles (MSN) as drug delivery vehicles (Gao et al., 2020): Fang et al. (2019) loaded MSN with the common chemotherapeutic drug doxorubicin, and a photoreactive component. The activation of the photoactive component in combination with doxorubicin showed synergistic effects, improving the treatment efficiency (Fang et al., 2017). Hyperthermia therapy presents another technique to increase the efficiency of common chemotherapeutic drugs through a temperature increase induced by coupled photothermal agents (Chu et al., 2011; Tian et al., 2018). Besides the classical drugs, new approaches were pursued based on tumor-specific genetic mutations using siRNA, miRNA, shRNA, and plasmids or DNA fragments. Those nucleic acids are incorporated into modified MSN with cationic polymers to prevent early degradation (L. Chen et al., 2016; Dilnawaz & Sahoo, 2018; Lin et al., 2017; Liu et al., 2018; Tsai et al., 2019). Silicon-based mesoporous nanoparticles are further used as sonosensitizers: MSN stimulation in the cell with therapeutic ultrasound irradiation, triggers the diffusion of molecules through the MSN pores, catalyzing the formation ROS, inducing ROS-dependent cell stress (Y. W. Chen et al., 2016; Osminkina et al., 2015).

In sum, nanomaterials, especially silica-based nanoparticles, possess various application possibilities for cancer treatments. SiNP can be easily synthesized and modified specifically for the intended purpose. These advantages may increase the likelihood of developing a SiNP-based cancer drug that increases the treatment efficacy and minimizes side effects of the used anti-cancer compound.

1.8 AIM OF THE STUDY

The specific expression of Survivin in various tumor types makes Survivin and its coding gene BIRC5 a promising target for cancer-specific therapies (Kondapuram et al., 2023). An enhanced Survivin expression level in cancer cells promotes cancer cell progression through the suppressive modulation of apoptosis and autophagy (Figure 7). However, Survivin inhibitors of different types have not fulfilled expectations since they showed insufficient anti-tumor effects and high cell toxicity against noncancerous cells, due to the essential role of Survivin in mitosis (Li et al., 2019).

In this regard, nanoparticles are a promising tool to increase the efficacy of cancer drugs and to reduce therapeutic stress combined with increased patient well-being (Haleem et al., 2023). Nanoparticles such as SiNP have been shown to induce cell death under specific conditions addressing apoptosis, autophagy, or necrosis (Figure 7). However, the inhibitor of apoptosis protein Survivin suppressed or prevented apoptosis mediated by SiNP (Breder-Bonk et al., 2023; Liu & Sayes, 2022).

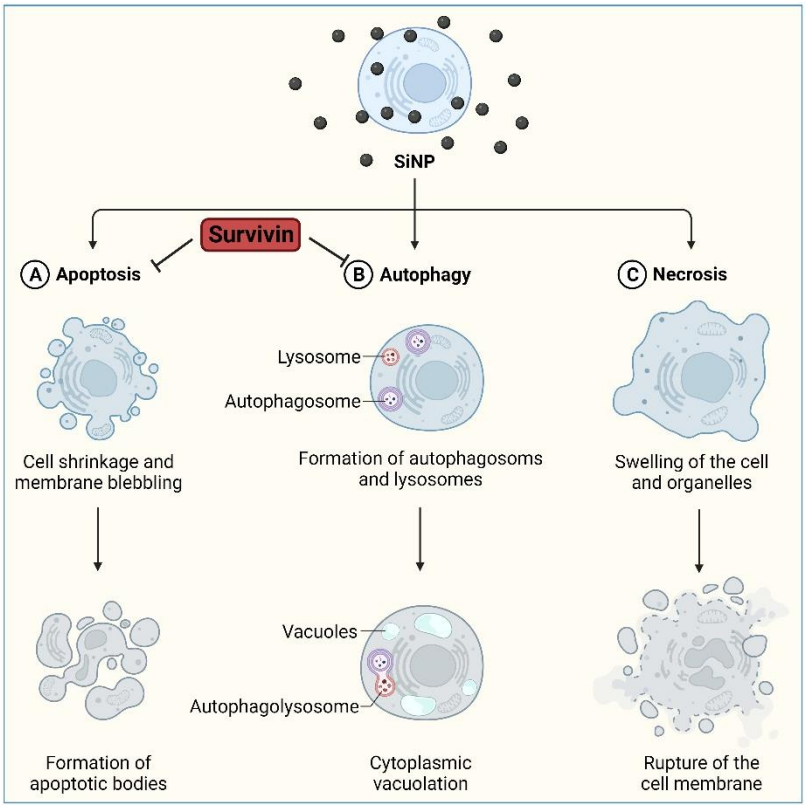

Figure 7. Types of cell death triggered by SiNP. SiNP trigger (A) apoptosis, (B) autophagy, and (C) necrosis. On the other hand, the tumor biomarker Survivin suppresses apoptosis and autophagy initiation. Created with biorender.com

Thus, the aim of the thesis was to reveal the detailed underlying mechanism of Survivin's protective function against SiNP-induced toxicity. Cell toxicity effects, especially considering autophagy-associated cell death were studied by use of pristine SiNP model particles of type NexSil20/AmSil20. Taken together, the main scientific objectives of this thesis are:

- Investigation of nanotoxicity-associated cellular effects and pathways, such as formation of ROS, initiation of autophagy, and biomechanical effects.

- Probing cellular resistance mechanisms against nanotoxicity in epithelial cancer cell models differing in their expression of Survivin.

- Evaluation of potential synergistic effects of combined treatments of SiNP treatments with different autophagy modulators.

Survivin as an anti-apoptotic protein has been extensively studied in the last few decades (Wheatley & Altieri, 2019). The molecular understanding of Survivin as a molecular switch between autophagy and apoptosis, promoting cancer resistance and progression, remains unclear and therefore will be elucidated in this work. The extended knowledge of Survivin-dependent mechanisms in autophagy-related processes might help develop customized silica nanoparticle-based drug formulations, and to improve the cancer treatment efficiency by facilitating the rational design of conjugated or encapsulated drugs.

2 RESULTS AND DISCUSSION

2.1 AMORPHOUS SILICA NANOPARTICLES

2.1.1 CHARACTERIZATION OF AMORPHOUS SILICA NANOPARTICLES

Nanosized materials have several chemical and physical advantages responsible for their popularity in diverse fields, including the food, cosmetic, and drug industries. Amorphous silica nanoparticles are widely considered harmless and approved by the FDA as a food additive. However, due to the wide distribution of nanoparticles the risk for an unintentional nanoparticle uptake increases, which makes it necessary to monitor potential harmful effects on human health.

Amorphous silica nanoparticles used in this study were commercially purchased as NexSil™ 20 (Nyacol® Nano Technologies, Ashland, USA) and further referred to as AmSil20 or SiNP. The AmSil20 were previously characterized as exhibiting a radius of 15.7 ± 1.9 nm and a negative zeta potential (-51 mV in water) resulting in a negative surface charge (Supplementary Table 1) (Breder-Bonk et al., 2023). The nanoparticle surface was not functionalized and therefore nanoparticles were categorized as naked/ plain. To visualize the interaction with the cell membrane as well as the cellular uptake a second comparable nanoparticle system was used. Kisker nanoparticles are plain SiNP with a diameter of 50 nm, bearing green or red fluorophores (Kisker® red/green, Kisker Biotech GmbH & Co. KG, Steinfurt).

2.1.2 AMORPHOUS SILICA NANOPARTICLES IMPAIR THE CELL VIABILITY

Due to the surface properties of plain AmSil20 nanoparticles, cell exposure was performed in a medium without serum; otherwise, serum proteins might form a protein corona around the nanoparticles, reducing the likelihood of interaction with cells and thus masking potential toxic effects (Docter et al., 2014).

The treatment of confluent A431 wild-type (wt) cells with the model particles (AmSil20) in a serum-free medium revealed a decrease in cell viability in a time and concentration-dependent manner (Figure 8). First toxic effects were detected after incubation with high nanoparticle concentrations (300, 600 µg/mL). In addition, nanoparticle concentrations of 60 µg/mL exhibit a significant impact on the cell viability after a prolonged incubation (24 h).

Hence, the results confirm that SiNP exhibited a time- and concentration-dependent toxicity under defined serum-free conditions, SiNP should be considered as potentially harmful material despite FDA approval.

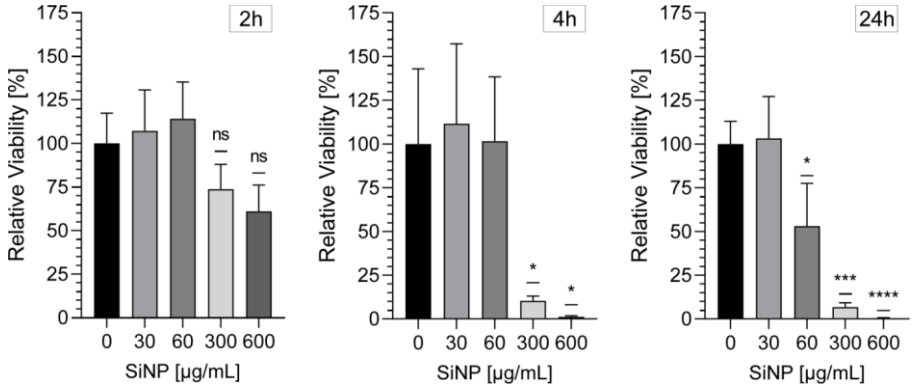

Figure 8. Time and concentration dependent SiNP cell toxicity. A431 wt cells incubated with increasing concentration of SiNP (AmSil20) in serum-deprived medium for 2, 4, and 24 h (4.2.2.1). Alamar Blue viability assay was performed for each time point and data was normalized to control groups that were incubated in serum-deprived medium without SiNP (black). The experiment was repeated three times and Anova two-way test was performed for each time point with p*<0.05, p***<0.001, p****<0.0001, ns= not significant.

2.2 Characterization of Survivin-mediated Resistance against SiNP-mediated Toxicity

2.2.1 Survivin Overexpression can rescue Cells from SiNP-mediated Cell Toxicity

It is well known that elevated Survivin levels correlate with increasing tumor resistance against chemo- and radiation- therapy, and further cancer progression. Therefore, Survivin is used as a common biomarker for the cancer prognosis (Huang et al., 2016; Tirro et al., 2006). The wide use of SiNP as drug carriers for chemotherapeutic drugs increases the interest for the inhibitor of apoptosis protein Survivin (Fytianos et al., 2020; Go et al., 2017; Janjua et al., 2023). Besides the nanoparticle-dependent cell toxicity mechanism of the model particles (AmSil20), the cell protective mechanism of Survivin were examined in the following sections.

To investigate if Survivin acts as a resistor against SiNP toxicity the epithelial cell line A431 with an artificially elevated Survivin expression level (A431 Survivin-GFP) was compared to A431 wt cells with an endogenous level of Survivin (en. Survivin). Therefore, the workgroup established a stably transfected A431 cell line bearing a Survivin-GFP plasmid. The transfected cell line was sorted for different expression levels of Survivin-GFP via fluorescence-activated cell sorting (FACS, 4.2.7). The cells were sorted by low, moderate, and high Survivin-GFP intensities. Cells with a relatively low intensity of Survivin-GFP were used for all following experiments and referred to as A431 Survivin-GFP or Surv.-GFP (Figure 9A). Then, A431 wt and A431 Surv.-GFP expressing cells were challenged with increasing SiNP concentrations. Both cell types exhibited a concentration-dependent decrease in cell viability.

However, the elevated expression of Survivin enhanced the resistance against SiNP-mediated toxicity (Figure 9).

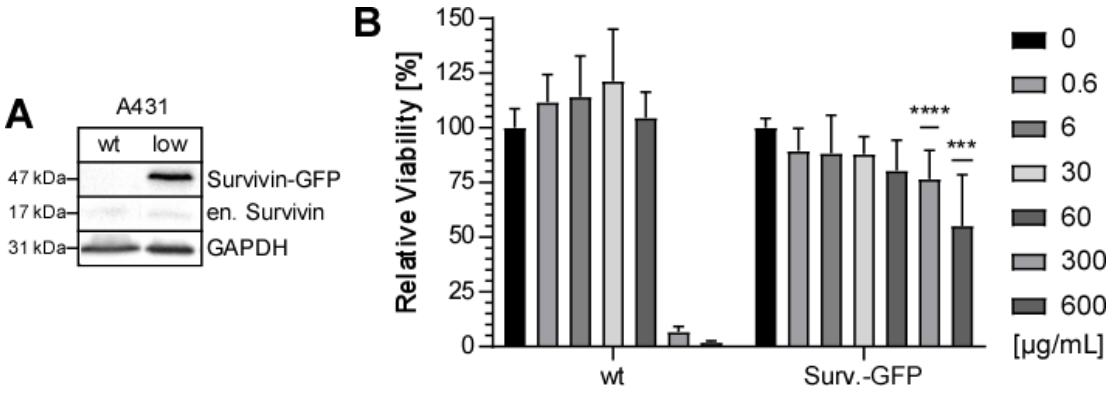

Figure 9. Survivin enhances resistance against SiNP. A) Confirmation of Survivin-GFP expression in stable transfected A431 cells in comparison to non-transfected A431 wt cells via immunoblot analysis. B) Concentration-dependent SiNP toxicity in A431 wt and Survivin-GFP expressing cells. Cells were treated for 4 h in serum serum-deprived medium with increasing SiNP concentrations (µg/mL). Cell viability was determined by the use of Alamar Blue reagent and data normalized to untreated control groups. An experiment was performed in triplicates and statistical analysis was performed with Anova two-way test with p***<0.001, p****<0.0001.

2.2.2 Exposure Time in Serum-free Medium determines SiNP Toxicity

To clarify the exact sequence of SiNP-mediated toxicity, time kinetics with fluorescence-labeled SiNP (Kisker, red) were performed. Experiments with A431 Survivin-GFP expressing cells showed that SiNP of type Kisker (red) attached immediately to the outer cell surface (
Figure 10,
Supplementary Figure 5).
Exposure to SiNP leads to cell contraction and loss of cell-cell contacts. After 90 min, the first strangulated vesicles become visible, also referred to as apoptotic bodies, indicating initiated apoptosis. After 115 min, necrotic processes were observed, resulting in membrane rupture and cell bursting, leading to the release of cytoplasmic content into the extracellular space until an end was reached at 150 min. The same set of experiments was performed with A431 GFP expressing and A431 wt cells. Those cell types showed a significantly forward-shifted apoptotic process; A431 wt cells exhibited apoptotic vesicles shortly after incubation with SiNP (exposed less than 1 min), while GFP-expressing cells showed the same effects after approximately 20 min (Supplementary Figure 2).
Hence, SiNP potentially accumulate in lysosomes, autophagosomes, or related vacuolar structures, late-stage autophagy inhibitor Chloroquine (CQ) was used to increase the size of these organelles. Clear dots of Kisker red nanoparticles (Kisker NP) were detected by use of CQ (

Figure 10) while no clear puncta were observed without CQ incubation (Supplementary Figure 1). However, with prolonged incubation in a serum-free medium Kisker NP aggregated over time and settled to the bottom. In addition, adhered Kisker NP form small aggregates, which became visible as demarcated spots after 1 min to 10 min on the cell membrane. These aggregates disappeared after 30 min, while the cytoplasm exhibited a stronger staining, indicating an uptake of the particles by endocytosis. Necrotic cell death was promoted by prolonged incubation with Kisker NP, characterized by cell bursting. Subsequently, the Kisker NP fluorescence disappeared from the cytoplasmic region. Another explanation for the disappearance of the fluorescence would be the rupture and shrinkage of the cell membrane to which the Kisker NP were attached.

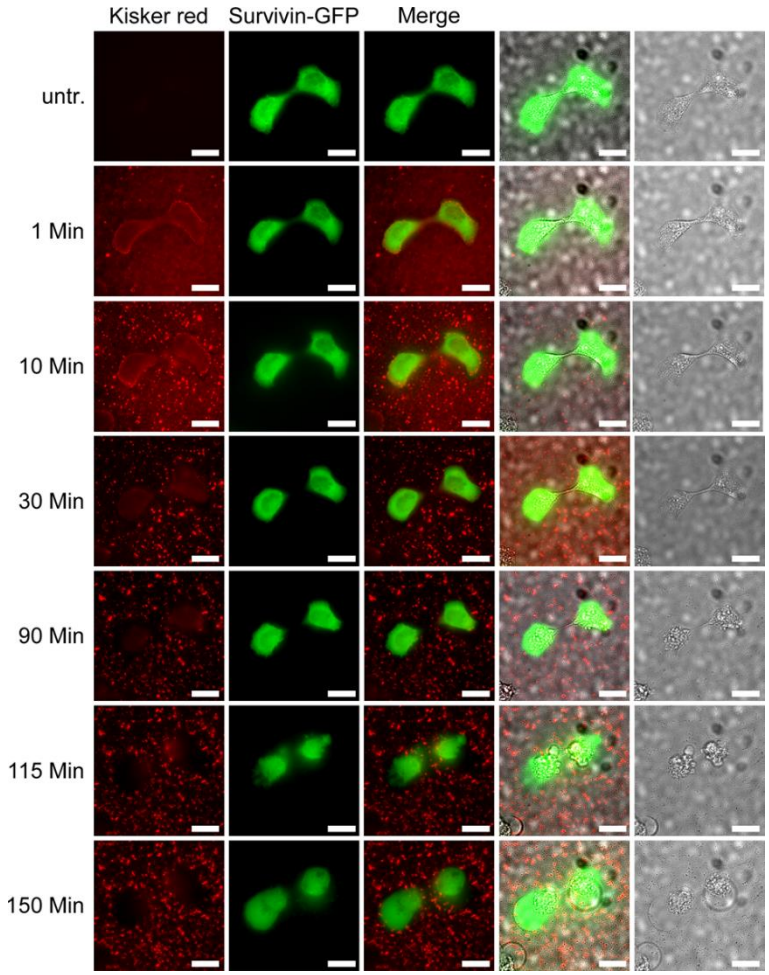

Figure 10. Time-dependent uptake of Kisker (red) NPs. A431 Survivin-GFP expressing cells incubated for 24 h with 20 µM CQ before treatment with 60 µg/mL Kisker red particles in serum-free medium for up to 150 min. Nanoparticle uptake and morphological changes were continuously examined with a Carl Zeiss fluorescence microscope and selected time points presented. The scale bar indicates for 25 µm.

Based on the above-described findings (2.2.1 and 2.2.2), the incubation time for SiNP in serum-free medium was shortened; A431 wt cells were treated with SiNP for 10 min and cultivated for two additional hours in a serum-containing medium. The shortened treatment was compared to the previous treatment with SiNP in a serum-free medium for 2 h. Different approaches were designed to provide information on whether autophagy-related cell death is initiated by SiNP or forced by the serum-free medium conditions alone (Figure 11).

The first treatment approach (A) corresponds to the previous experimental setup, in which cells remained in a serum-free medium for the entire treatment period with SiNP. In B, C, and D, cells were treated with SiNP in a serum-free medium for 10 min. The SiNP-containing medium was removed (C) or left in place (B) and an additional serum-containing medium was added to (B) and (C). In the treatment approach (D), cells were additionally washed three times with serum-free medium after treatment with SiNP, before FCS-containing medium was added. Subsequently, all approaches were incubated for 2 h 10 min. For time point 24 h, cells were washed three times, and a medium with FCS was added for further cultivation. Then the impact of the different treatment approaches on the cell viability was analyzed via Alamar Blue reagent assay (Figure 11).

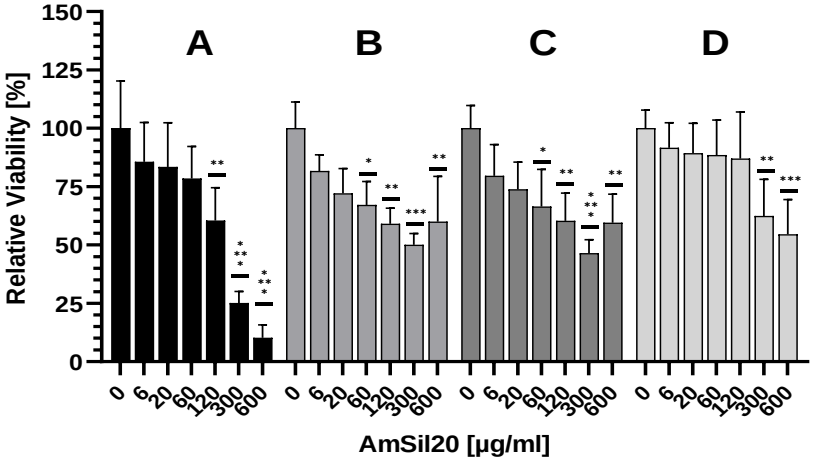

Figure 11. Contact and time dependent SiNP toxicity. A431 wt cells treated with rising SiNP concentrations starting from 0 µg/mL up to 600 µg/mL. Different treatment strategies were applied to investigate SiNP toxicity-related factors. For all approaches, cells were washed before the treatment to remove serum proteins. Then, cells were treated for 10 min with 100 µL serum-free medium containing different SiNP concentrations. After the 10 min incubation cells were treated as follows; A) Cells left in serum-free medium containing SiNP. B) 100 µL of serum-containing medium added to the remaining SiNP-containing medium C) Treatment medium discarded and 100 µL of serum-containing medium added. D) The treatment medium was removed, and cells were washed three times with serum-free medium and substituted with 100 µL of serum-containing medium. A-D) Cells were incubated for 2 h at 37°C, 5% CO_2. Cell viability was measured via Alamar Blue reagent assay after 2 h 10 min incubation (see section 4.2.9.1). The experiment was performed in three independent approaches and data were compared with a two-way ANOVA test to the intern control (0 µg/mL) for each experimental set (A-D). Significant differences to the control were defined as p*<0.05, p**<0.005, p***<0.001, p****<0.0001.

This experimental setting uncovered that adding a serum-containing medium can reduce the toxicity of high SiNP concentrations (Figure 11B, C, D) compared to complete treatment in a serum-free medium. This effect was independent of whether the SiNP-containing medium was exchanged completely (C) 21.3% ± 5.8% (300 µg/mL), 49.3% ± 12.3% (600 µg/mL), or serum-containing medium was added in addition to the treatment medium on top (B) 24.9% ± 4.9% (300 µg/mL), 49.8% ± 19.4% (600 µg/mL). Furthermore, washing before adding serum-containing medium decreased the toxicity of SiNP additionally, when 300 µg/mL were used D)

37.2% ± 15.7% (300 µg/mL), but not with 600 µg/mL (44.4% ± 14.8%). For all four approaches, the cell viability decreased with prolonged cultivation (24 h), (Supplementary Figure 3). These results indicate that the contact and uptake in the first 10 min of SiNP exposure is sufficient to damage cells as they progress. Specifically, cells that were washed after SiNP exposure (D) showed an additional decrease in cell viability at 24 h compared to 2 h. However, this loss of viability was overall lower than in approaches without washing steps (Figure 11A, B, C).

In addition, the results suggest that the number of particles adhering to the cell surface plays a crucial role in the toxicity induced by SiNP. Treatment (A) prevents the formation of a protein corona, which may otherwise weaken or prevent physical interaction with the cell membrane (Docter et al., 2014). Furthermore, the absence of serum in the treatment triggers autophagy. These two conditions result in increased toxicity of SiNP. Comparing treatments in which the serum-containing medium was added after exposure in serum-free medium B (SiNP remained in the medium) and C (medium with SiNP removed), it is striking that the cell viability did not differ after 2 h (0.5-4.4%) and after 24 h (0.9-11.0%). These results support the assumption that the SiNP toxicity is determined on the one hand by the fast adherence of uncoated SiNP and on the other hand by the protein corona formation in the presence of a serum-containing medium. Furthermore, the comparison between approaches B and C showed that the protein corona formation can almost eliminate the concentration-dependent toxicity of SiNP.

2.2.3 Summary

The uptake and the toxicity of SiNP depend on serum-free conditions. Under optimized test conditions, the used SiNP caused a fast decline of the cell viability in a time and concentration-dependent manner. Morphological changes indicate the participation of apoptotic and necrotic cell death processes in SiNP-mediated toxicity. However, the artificially enhanced expression of the inhibitor of apoptosis protein Survivin increased the resistance against SiNP.

2.3 Role of Autophagy in SiNP-mediated Toxicity and Survivin-mediated Resistance

2.3.1 SiNP induce a Lysosomal Shift related to Autophagy Initiation

The canonical autophagy is triggered by serum starvation to deal with the lack of growth factors and nutrition (Kocot & Wroblewska, 2022). Starving cells induce the generation of autophagosomes, which provide cellular content for lysosomal degradation. Since serum-free conditions are required for the application of SiNP, autophagy must be considered as a reaction process. Chloroquine (CQ), a late-stage autophagy inhibitor, prevents the degradation

of autophagosomes by impairing their fusion with lysosomes, resulting in the accumulation of autophagosomes and lysosomes. In addition, CQ causes osmotic imbalances, which lead to the swelling of acidic organelles (Mauthe et al., 2018). The CQ-related effects enable the observation of the autophagy process, especially the autophagy initiation level, via Lysotracker dyes and immunoblot analysis. Lysotracker dyes are cell-permeable weak bases coupled to fluorophores that intercalate into acidic lumens of lysosomes, late endosomes, or autophagolysosomes in living cells (Zhitomirsky et al., 2018).

The staining of acidic bodies with Lysotracker red dye revealed an enhanced generation of acidic puncta as a response to SiNP and a shift of acidic puncta from a peripheral localization in the cytoplasm to accumulated puncta in the perinuclear region, as depicted in Figure 12.

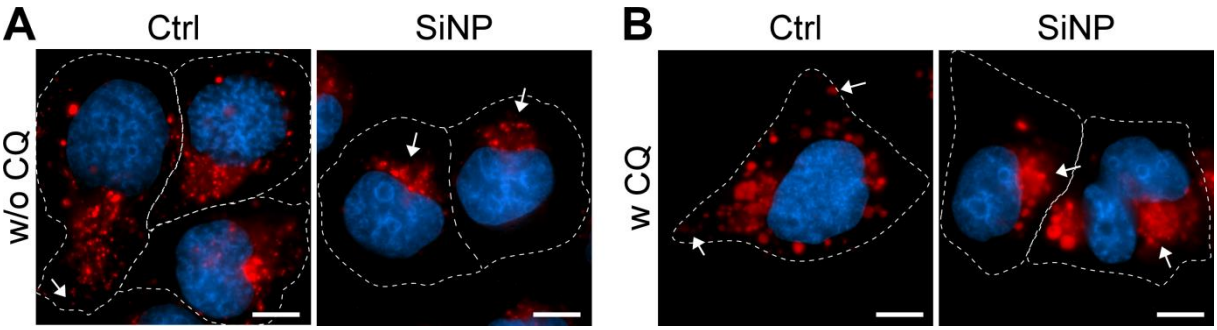

Figure 12. Autophagy-related lysosomal shift. A431 wt cells were cultivated for 24 h in the absence (A) or presence (B) of 20 µM CQ and then treated with 60 µg/mL SiNP for 4 h. Cells were stained alive with 2 µg/mL Hoechst 33342 for 10 min and with 50 µM Lysotracker red (Invitrogen) for 30 min and imaged immediately after (4.2.5.5). Arrows point to acidic bodies localized in the peripheral or perinuclear region. The scale bar is equal to 25 µm.

To determine if SiNP address autophagy through lysosome or autophagosome manipulation both organelle types were stained parallel with LAMP-1 (FITC, green) as a marker for lysosomes and LC3 (Cy3, red) for autophagosomes, in the presence (Figure 13A) or absence (Figure 13B) of late-stage autophagy inhibitor CQ. In the presence of CQ, separated LAMP-1 and LC3 puncta were evenly distributed in the cytoplasm of control cells (Figure 13A), while LAMP-1 and LC3 double positive puncta (orange) were absent. Orange dots indicate autophagolysosomes, which appeared prominently in cells without CQ treatment, supporting CQ as a suitable late-stage autophagy inhibitor (Figure 13B). However, a characteristic of autophagy initiation is the shift of autophagosomes and lysosomes from the peripheral cytoplasm to the perinuclear region. The achieved proximity of lysosomes and autophagosomes is essential for autophagolysosomal fusion (Heuser, 1989; Jahreiss et al., 2008). The translocation of LAMP-1 and LC3 positive puncta was observed in starving cells and was enhanced due to SiNP treatment. In more detail, treatment with SiNP in the presence of CQ, translocated LAMP-1 and LC3 positive puncta near the nucleus, forming a dense, but non-overlapping accumulation of LAMP-1 and LC3 puncta, which was less pronounced in control cells. In addition, SiNP promoted the generation of more lysosomes compared to

control cells indicated by the increased number of green puncta in Figure 13B. This issue is further elaborated in the following sections. However, this first experiment gives evidence that SiNP affected the autophagy process.

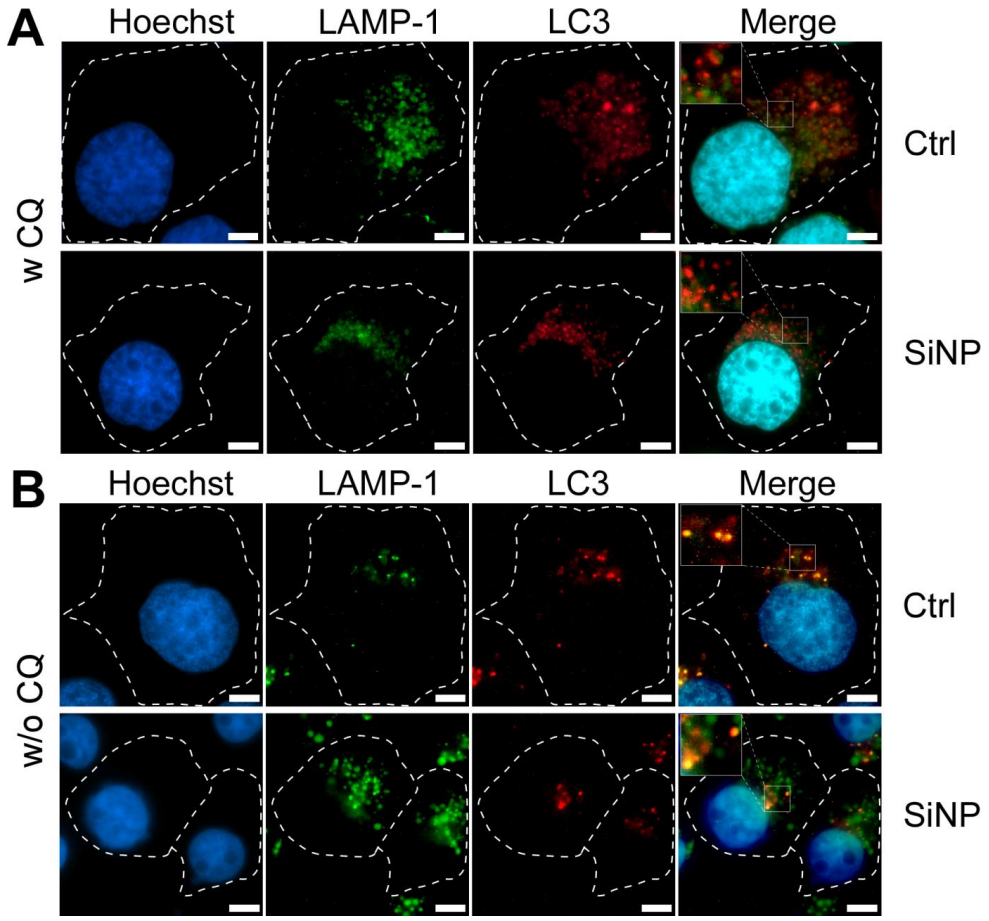

Figure 13. Localization of lysosomes and autophagosomes. A431 wt cells incubated for 2 h in serum-deprived medium (Ctrl) or treated with 60 µg/mL SiNP (A, B) in the presence (A) or absence (B) of 20 µM CQ. Samples were fixed and permeabilized, then stained with LAMP-1 (FITC, green) to mark lysosomes and with LC3 (Texas red) to tag autophagosomes. Nuclei stained with Hoechst 33342 (4.2.5.2). Overlapping yellow fluorescence indicates autophagolysosomes. A squared area of 50 pixels was magnified by a factor of 2.2x for a better observation of the co-localization of LC3 and LAMP-1 positive puncta. The scale bar indicates 10 µm.

2.3.2 Survivin suppresses Silica Nanoparticle-induced Autophagy

Considering that SiNP affected autophagy in A431 wt cells (2.3.1), the autophagy-inducing effect of SiNP on Survivin-overexpressing cells (A431 Surv.-GFP) was investigated with the use of CQ with different techniques (Figure 13, Figure 15,

Figure 17). Autophagy is a dynamic process where LC3-Iis converted to the autophagy active form LC3-II to elongate the autophagosomal membrane (Figure 14A). In the late stage of autophagy, autophagosomal LC3-II is degraded due to the fusion with lysosomes. CQ stops the autophagolysosomal degradation without affecting the autophagy initiation (Mauthe et al.,

2018). Considering CQ-treated and untreated samples it is possible to make conclusions on the entire autophagy flux based on the LC3-I to LC3-II ratio in these samples (Figure 14B).

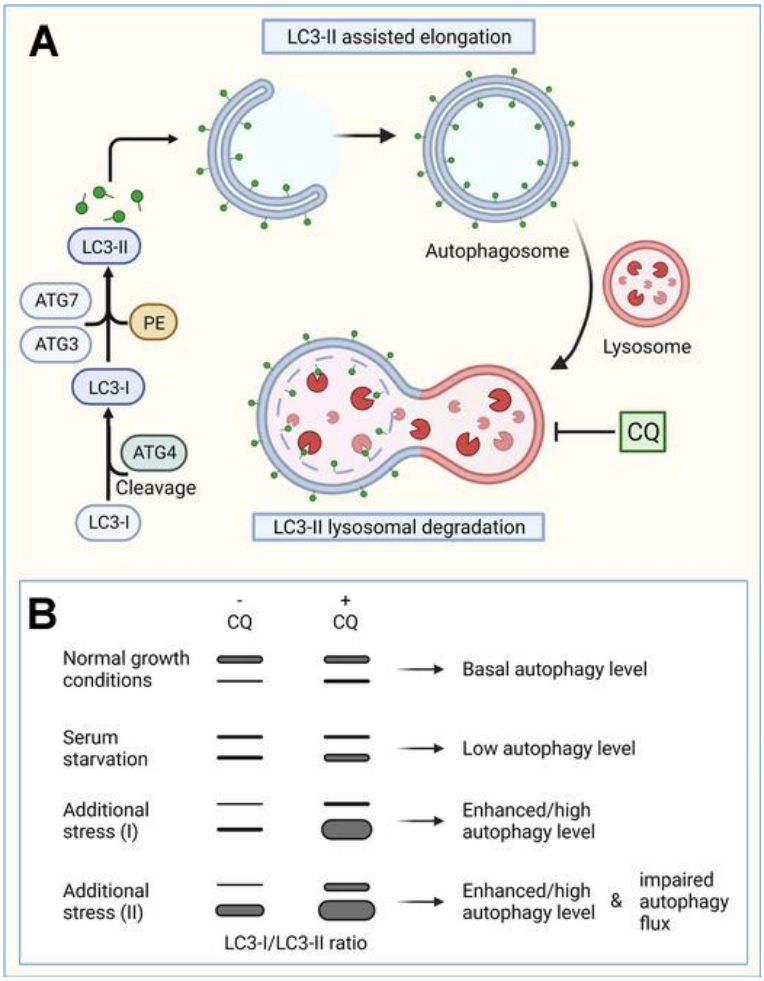

Figure 14. LC3 conversion in response to different stimuli. A) LC3 conversion and degradation in the autophagy process. When autophagy is initiated LC3-I is cleaved and then conjugated to phosphatidyl-ethanolamine (PE) to generate the autophagy-active form LC3-II, which is incorporated into the inner and outer autophagosomal membrane. In the late autophagy process, LC3-II is degraded after fusion with lysosomes. B) Theoretical LC3 conversion assay output via immunoblot analysis for different conditions and stress stimuli levels.

In this regard, serum deprivation, as well as SiNP, initiated the conversion of LC3 proteins, shifting the ratio from LC3-I to the LC3-II form in A431 wt and Survivin-GFP expressing cells, indicating autophagy (Figure 14, Figure 15). A sharp increase of LC3-II in A431 wt cells was induced in response to SiNP in comparison to control treatments (without CQ: 8.1x higher; with CQ: 3.0x time higher). Interestingly, A431 Survivin-GFP expressing cells exhibited to the same stimuli a comparable LC3 conversion pattern in response, but overall generated less LC3-I and LC3-II: In the absence of serum, A431 Survivin-GFP cells generated 3.0x less LC3-I and 3.5x less LC3-II in samples without CQ, and 1.5x less LC-I and 3.5x less LC3-II in samples with CQ than A431 wt cells. In response to SiNP, A431 Survivin-GFP expressing cells generated in comparison to A431 wt cells without CQ 1.4x less LC3-I and 7.3x less LC3-II, and with CQ 1.1x less LC3-I and 4.5x less LC3-II. The experiment showed that SiNP increased the LC3 conversion and consequently the autophagy flux in addition to serum starvation. Furthermore, the results indicated that an elevated Survivin level does not prevent the SiNP-dependent autophagy initiation; it rather suppressed the overall reaction to autophagy-triggering stimuli in the cells.

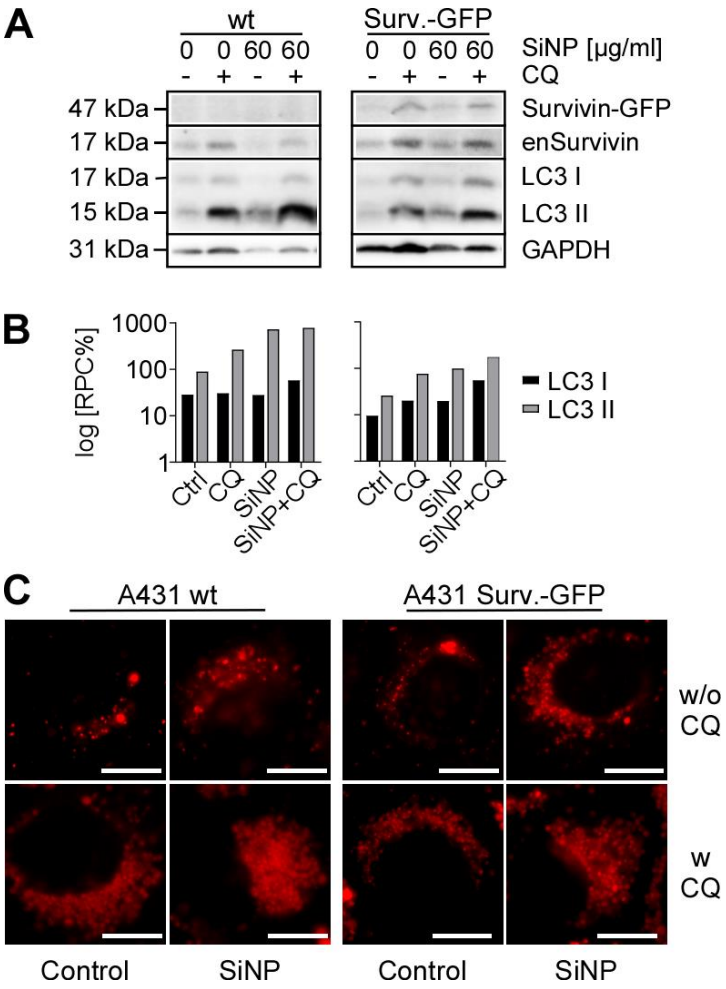

Figure 15. Autophagy is triggered by serum deprivation and SiNP. A431 wt and Survivin-GFP expressing cells were treated with 60 µg/mL SiNP for 4h with (w) or without (w/o) CQ-treatment. A) Immunoblot analysis. B) LC3-I and LC3-II protein content quantified via ImageJ analysis. Data normalized to GAPDH bands and plotted as relative protein content (RPC) on a logarithmic scale (log10). C) Acidic bodies stained with Lysotracker red (4.2.5.5). Scale bar indicates 25 µm.

Under the same treatment, conditions as used in the LC3 conversion immunoblot assay (Figure 15A, B) the staining with Lysotracker red exhibited supporting results (Figure 15C). The treatment with serum-deprived medium or SiNP induced the characteristic autophagy-related organelle shift to the perinuclear region in A431 wt and Survivin-GFP expressing cells. Serum-deprived medium induced canonical autophagy to keep cellular homeostasis balanced as indicated by the shift of acidic bodies (1st and 3rd column, Figure 15). The treatment with SiNP promoted the additional generation and accumulation of acidic puncta in the perinuclear region, indicating enhanced autophagy initiation and flux (2nd and 4th column, Figure 15). These observations were valid for A431 wt and Survivin-GFP expressing cells. However, by use of CQ in the experimental settings A431 wt cells showed significantly more and bigger acidic puncta than Survivin-GFP expressing cells, especially when treated with SiNP (lower row, Figure 15). Nonetheless, the treatment with SiNP led to dense accumulations of acidic bodies in the perinuclear region in A431 wt cells, again less pronounced in Survivin-GFP expressing cells. In summary, the SiNP triggered the translocation of acidic bodies to the perinuclear region, indicating autophagy. Furthermore, elevated Survivin levels show the potential to suppress the translocation and the generation of acidic bodies in response to serum deprivation, especially in response to SiNP.

2.3.3 Survivin as Autophagy Modulator

After it was shown that an increased Survivin level attenuates autophagy in response to various stress stimuli, the role of Survivin in autophagy was further investigated by switching off Survivin using siRNA technology. Different Survivin expression levels were achieved by transient transfection of Survivin silencing siRNA BIRC5. Furthermore, cells with an enhanced Survivin level (A431 Surv.-GFP) and cells with an endogenous Survivin level (A431 GFP) were transfected to compare various Survivin ranges. The Survivin-specific knockout was confirmed by the loss of the GFP fluorescence in A431 Survivin-GFP expressing cells (Figure 16 A, Supplementary Figure 4).

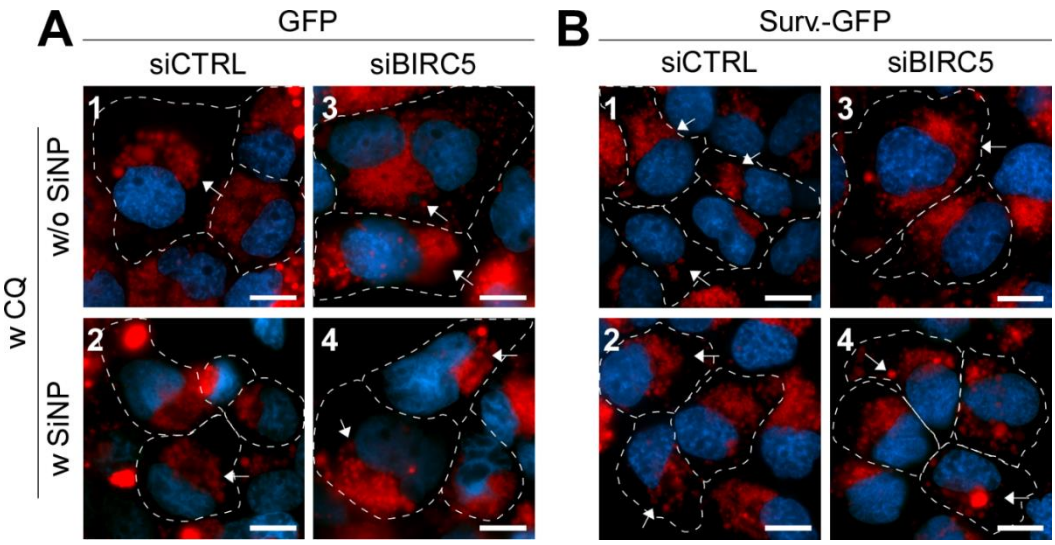

Figure 16. Tracing of the acidic body generation via Lysotracker staining. A431 Survivin-GFP or GFP expressing cells transiently transfected with siBIRC5 or with siCTRL. Transiently transfected cells were incubated for 2 h in a serum-deprived medium in the absence or presence of 60 µg/mL SiNP. Samples stained with 50 nM Lysotracker red dye for 30 min and imaged immediately. The successful Survivin knockdown was confirmed by a vanished GFP fluorescence (

Supplementary Figure 5). The scale bar is equal to 25 µm.

Survivin takes part in the mitotic process as a member of the spindle-forming complex (Kallio et al., 2001 305) hence, Survivin knockdown results in an impaired cell division, recognizable by multinuclear cells and large misshaped nuclei. This phenomenon is prominent in siBIRC5 transiently transfected A431 GFP expressing cells and rarely seen in siBIRC5 transiently transfected A431 Survivin-GFP expressing cells (Figure 16 B3), indicating a remaining Survivin expression level attributed to the stably transfected Survivin-GFP bearing plasmid (Supplementary Figure 6 B3). Again, the SiNP treatment led to the perinuclear accumulation of acidic puncta compared to cells incubated in a serum-deprived medium in all cell types. Focusing on the impact of different Survivin expression levels on the formation of acidic bodies there was no distinct difference between siBIRC5 and siCTRL transiently transfected A431

Survivin-GFP or GFP cells (Supplementary Figure 6). To elaborate on the overall generation of acidic puncta, the transiently transfected cells were incubated with CQ before being treated with aSiNPs. The inhibition of the autophagy turnover via CQ revealed that siBIRC5 transient transfected cells (Figure 16 A3, B3) increased the number of acidic puncta after serum deprivation when compared to siCTRL transfected cells (Figure 16 A1, B1). In response to SiNP, the cells induced the autophagy characteristic translocation of acidic bodies to the perinuclear region, independent from the Survivin level. However, with a decreasing Survivin level (Figure 16 A4, B4), the accumulations of acidic puncta got denser than in cells with a higher Survivin level (Figure 16 A2, B2). In addition, the Survivin knockdown in A431 GFP (Figure 16 B4) led to dense accumulations as observed in similar treated A431 Survivin-GFP cells (Figure 16 A4), but due to the impaired mitosis the siBIRC5 transiently transfected A431 GFP cells exhibited more acidic puncta (Figure 16 B4).

The results so far indicate a suppressive effect of enhanced Survivin levels on the generation of acidic bodies. How different Survivin levels might influence the localization of LAMP-1 positive lysosomes, LC3 positive autophagosomes, and double positive autophagolysosomes was pursued via immunofluorescence microscopy in A431 wt cells transiently transfected with siBIRC5 or siCTRL in the presence of 20 µM CQ (

Figure 17).

The distribution and localization of autophagosomes and lysosomes were used to conclude the autophagy progression (Heuser, 1989; Jahreiss et al., 2008). Under normal conditions, lysosomes localize at the outer membrane region. During autophagy lysosomes and autophagosomes translocate to the perinuclear region to facilitate the fusion of autophagolysosomes.

The experiment showed that under normal growth conditions (w FCS), LC3 puncta (Cy3, red) were observed throughout the cell, but when compared to control cells (A), Survivin-suppressed cells exhibited an increased number of LC3 puncta (

Figure 17B). Similar observations were made for LAMP-1 puncta (FITC, green). In contrast, serum deprivation (w/o FCS) led to a dense accumulation of LC3 and LAMP-1 puncta at the perinuclear region in siBIRC5 transiently transfected cells and less pronounced in control cells with intact Survivin protein expression (

Figure 17A).

To review SiNP as an autophagy inducer next to serum deprivation, the SiNP exposure time was shortened to 10 min and compared to the standard incubation time (2 h), (

Figure 17). The typical shift of autophagy-related LC3 and LAMP-1 puncta to the perinuclear region, as observed after 2 h in siCTRL transiently transfected cells, was also seen after a shortened treatment time (

Figure 17A). In contrast, Survivin suppression via siBIRC5 resulted in an alternate circle-like phenotype of the organelles, when treated for 10 min or 2 h with SiNP. In addition, siBIRC5 transiently transfected cells reacted with a distinct accumulation in response to serum deprivation compared to control cells (
Figure 17B).

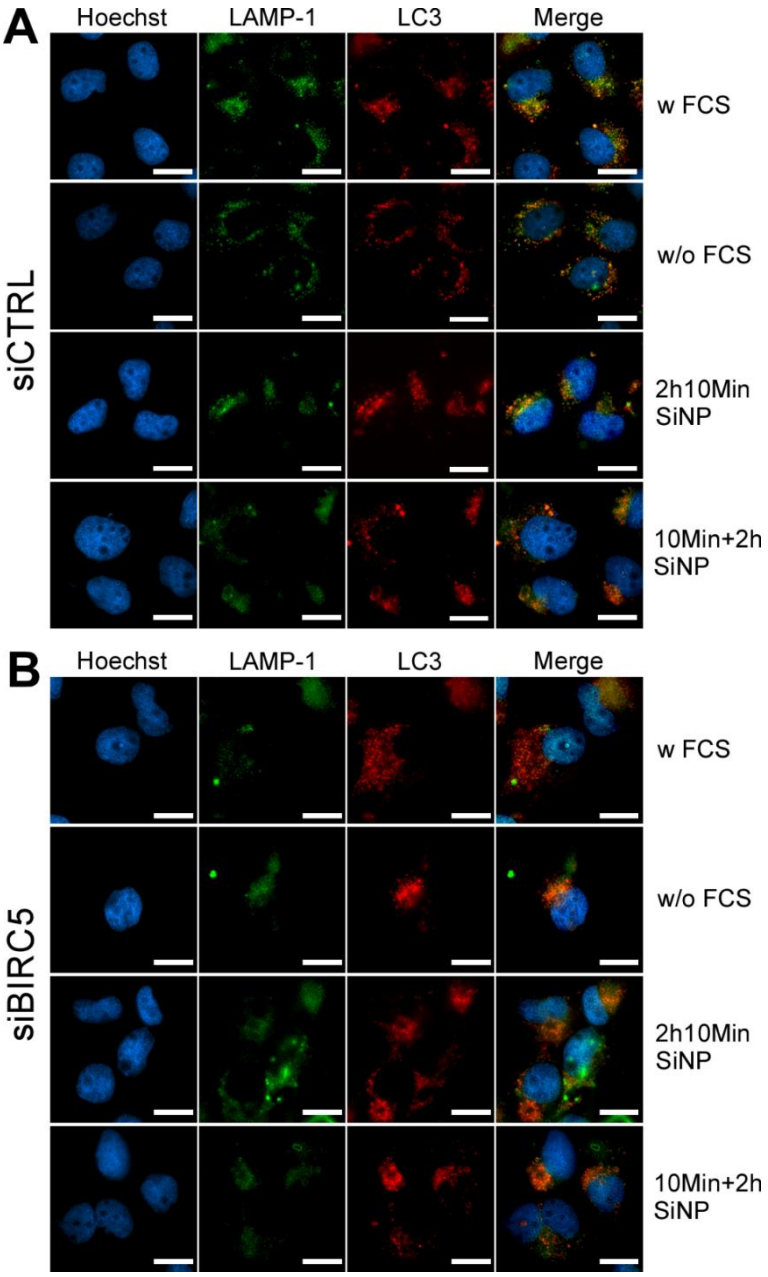

Figure 17. Influence of Survivin knockdown on the localization of autophagy-related organelles. A431 wt cells transiently transfected with siBIRC5 (A) siCTRL (B). Cells were fixed without treatment in a serum-containing medium (first row) or after incubation in a serum-free medium (second row). Cells treated with 60 µg/mL SiNP for 2 h 10 min (third row) or for 10 min (fourth row). After the 10 min treatment supernatant was removed, and serum-containing medium was added for an additional 2 h. All samples were fixed and permeabilized before staining with Hoechst 33342 (nuclei), LAMP-1 (FITC), and LC3 (Cy3) was performed (4.2.5). Scale bar indicates 25 µm.

In sum, Survivin knockdown resulted in the enhanced generation of autophagy-related organelles and increased the sensitivity to serum-starvation-induced autophagy, indicated by LC3 and LAMP-1 puncta shifting to the perinuclear region. In addition, the SiNP-stimulated autophagy initiation is delayed or reduced rather than prevented by enhanced Survivin levels, which was indicated by a less pronounced perinuclear shift of acidic bodies compared to cells with a Survivin knockdown. The results support Survivin as a main regulator of autophagy-related organelle cellular organization and transport during the autophagy process.

However, Survivin knockdown cells showed increased autophagy characteristics such as an enhanced generation of acidic bodies and their accumulation in the perinuclear region. Therefore, the effects of the Survivin knockdown were further investigated by an LC3 conversion assay performed as immunoblot analysis (

Figure 18).

A431 wt cells were transiently transfected with siBIRC5 or siCTRL and challenged with SiNP in the presence or absence of 20 µM CQ. Hence, ROS might play a role in the SiNP-mediated cell toxicity the ROS scavenger N-acetylcysteine (NAC) was examined in addition.

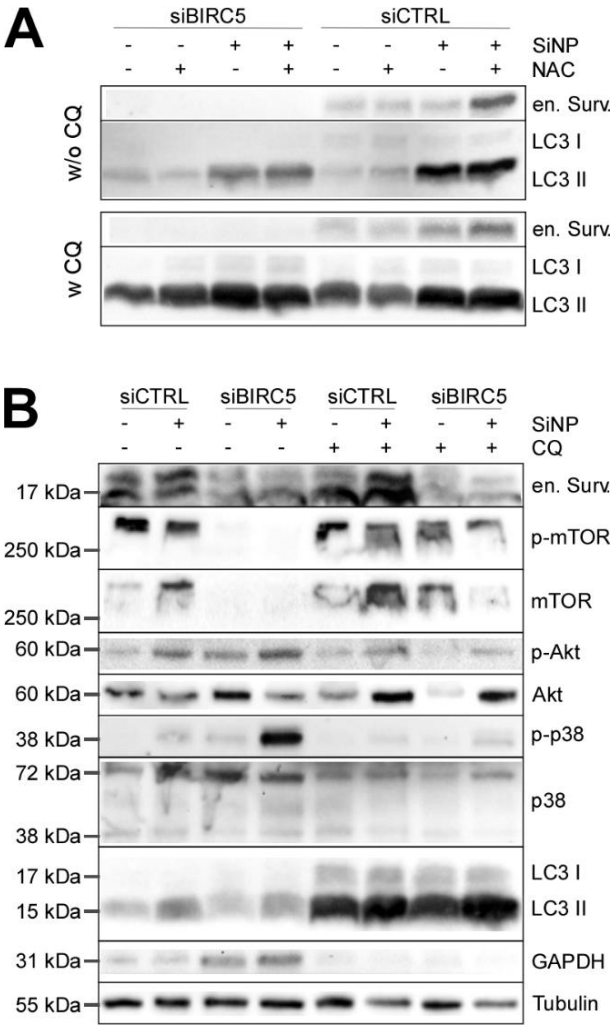

Figure 18. Influence of Survivin on the autophagy flux. A) LC3 conversion assay analyzed by immunoblot analysis. A431 wt cells transiently transfected with siBIRC5 or with control siRNA (siCTRL). Cells were treated with or without 20 µM CQ before being challenged with SiNP (60 µg/mL) for 2 h. Then, Survivin protein expression and LC3 conversion were examined via western blot analysis (4.2.3). B) Similar treated A431 wt cells transiently transfected with siBIRC5 or siCTRL were analyzed for autophagy and stress-related proteins examined via western blot analysis.

The use of NAC did not affect LC3 protein expression or autophagy dependent LC3 conversion, but increased Survivin expression in control transfected cells

Figure 18A). As seen in Supplementary Figure 4 Survivin was successfully depleted by siBIRC5. The Survivin knockdown resulted in a complete conversion of LC3-I into the autophagy active form LC3-II while Survivin-expressing cells maintained LC3-I bands. Furthermore, siCTRL transfected cells exhibited a significantly higher amount of LC3-II after treatment with SiNP than Survivin-silenced cells (

Figure 18). However, CQ treatment revealed comparable amounts of LC3-II in siBIRC5 and siCTRL transiently transfected cells. Taken together, the Survivin knockdown accelerates the conversion of LC3-I to the autophagy-active form LC3-II (

Figure 18A) and the autophagy-dependent LC3-II degradation (

Figure 18B). In sum, the Survivin knockdown increased the autophagy flux. The experiment showed that Survivin does not affect LC3 protein expression, as seen by the constant amount of LC3-II in the presence of CQ (
Figure 18B), but rather controls the LC3 conversion and the autophagy turnover.
Hence the autophagy flux is affected by the Survivin knockdown, related cell signaling pathways were examined via immunoblot analysis (
Figure 18B). Concurrent with a decreased Survivin expression, mTOR disappeared after treatment in a serum-free medium without and with SiNP, whereas GAPDH protein levels slightly increased compared to siCTRL transiently transfected cells. Hence, autophagy was initiated by mTOR suppression, it fits that the activated autophagy process was correlating with a decreased mTOR activation and expression (Jung et al., 2010). However, the Survivin suppression had no significant impact on the activation of the pro-survival kinase Akt, which promotes the mTOR activation (Glaviano et al., 2023). In contrast, stress kinase p38 was activated in Survivin-suppressed cells after serum deprivation and after treatment with SiNP, while siCTRL transiently transfected cells did not activate p38 after serum deprivation. On the contrary, SiNP-dependent activation of p38 was significantly lower in control cells than in Survivin-suppressed cells.
In general, inhibitors, as well as specific inhibitors often affect more than one target. Here, the late-stage autophagy inhibitor affected the glycolytic housekeeping gene GAPDH, decreased p38 activation, and overall p38 protein expression. Interestingly, CQ-dependent inhibition of the autophagy turnover led to p-mTOR/ mTOR stabilization. Therefore, the CQ-specific effects have to be considered, when used in combination with other autophagy-targeting drugs (2.7).

2.3.4 Summary

SiNP induced autophagy and increased the autophagy turnover (Figure 12, Figure 13, Figure 15,

Figure 17 B). Survivin decelerates the autophagy turnover rather than downregulating the LC3 protein expression by suppressing the perinuclear translocation of autophagy-related organelles. However, the late stage of autophagy might be impaired by SiNP, which is supported by several studies (Abulikemu et al., 2022; Guo et al., 2016). Furthermore, SiNP activated the stress kinase MAPK p38, while pro-survival kinase Akt was downregulated (Figure 16B). In addition, Survivin suppressed p38 and might represent a resistance mechanism against the SiNP toxicity.

2.4 Role of the Cytoskeleton Stability in Survivin-mediated Resistance against SiNP Toxicity

In section 2.3.3 it was proposed that Survivin has an impact on the localization of lysosomes and autophagosomes thereby regulating the autophagy turnover rate. Further, in section 2.2.2 the direct interaction of SiNP with the cell membrane was shown. Hence mechanical stress can potentially induce autophagy, SiNP were examined as a mechanical stressor (Hernandez-Caceres et al., 2021). Hence, autophagosome maturation is accompanied by actin, and cause the autophagy-related lysosomal movement is microtubule-dependent (Aumuller et al., 1997) the effect of SiNP on the cytoskeletal structure was examined considering β-actin and β-tubulin.

Treatment with SiNP in the presence of serum (FCS) showed no obvious influence on the actin distribution and structure, pointing out that serum-coated SiNP have a minimized potential to interact with cell membranes (Figure 19). This assumption is further supported by viability assays in Figure 11. However, over time serum deprivation led to distinct staining in the perinuclear region attributable to actin's role in the formation of autophagosomes and autophagolysosomes, which was summarized by Hernandez-Caceres (2021) (Hernandez-Caceres et al., 2021). In addition to the distinct perinuclear accumulation of actin, the exposure to SiNP led to actin puncta in the outer membrane region, while serum deprivation alone showed none. Hence, actin is essential for endocytosis-related deformation of the cell membrane; these actin puncta might mark endocytic vesicles (Akamatsu et al., 2020). However, such prominent actin puncta in the outer membrane region appeared less often in Survivin-GFP-expressing cells.

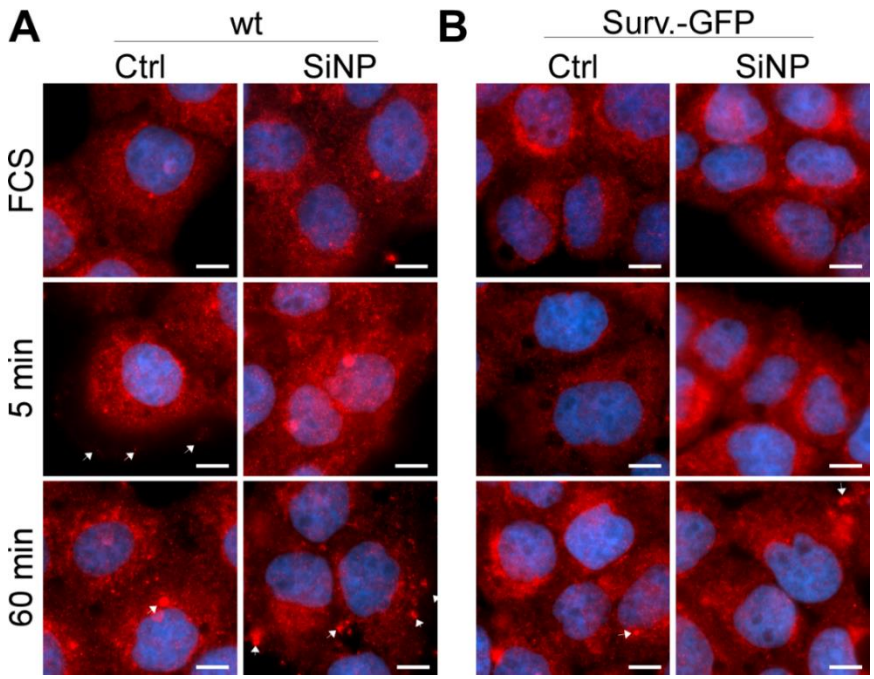

Figure 19. Impact of SiNP on the actin network. A431 wt and Survivin-GFP expressing cells were incubated either in medium with serum (FCS) +/- 60 µg/mL SiNP, or in serum-deprived medium +/- 60 µg/mL SiNP for 5, 30, or 60

minutes. Cells stained with Hoechst (blue) and β-actin (red) (4.2.5). Arrows point on actin accumulations, related to autophagy or endocytosis. Scale bar indicates for 50 µm.

The transport of autophagosomes, lysosomes, and autolysosomes is accomplished by motor proteins dynein and kinesis, using microtubule as the anchor and directional guide (Geeraert et al., 2010; Nakamura & Yoshimori, 2017). Hence microtubule-dependent transport is a highly dynamic system, switching between microtubule polymerization and depolymerization (Kimura et al., 2008; Yang et al., 2011), the impact of SiNP and Survivin was examined on the base of β-tubulin by immunofluorescence staining (Figure 20).

A full growth medium, containing serum, was used as control for the normal state of microtubule structure (first row). Here, β-tubulin shows long filaments starting from centrosomes in the perinuclear region reaching the outer membrane. Full growth medium supplemented with SiNP showed no anomalies in comparison to the FCS control (second row). Serum deprivation for 1 h decreased cytoplasmic microtubule formations (third row), while additional exposure to SiNP induced shrinkage of the cytoplasmic microtubule network and a denser microtubule formation around nuclei (fourth row). The altered phenotype correlated with a shape indicating early events of detachment. Hence Survivin was shown to stabilize microtubules (Giodini et al., 2002; Rosa et al., 2006), it was speculated that Survivin may protect cancer cells against SiNP-induced cell death by promoting microtubule polymerization. Indeed, Survivin overexpression stabilized the microtubule network against the SiNP-induced shrinkage (fourth row).

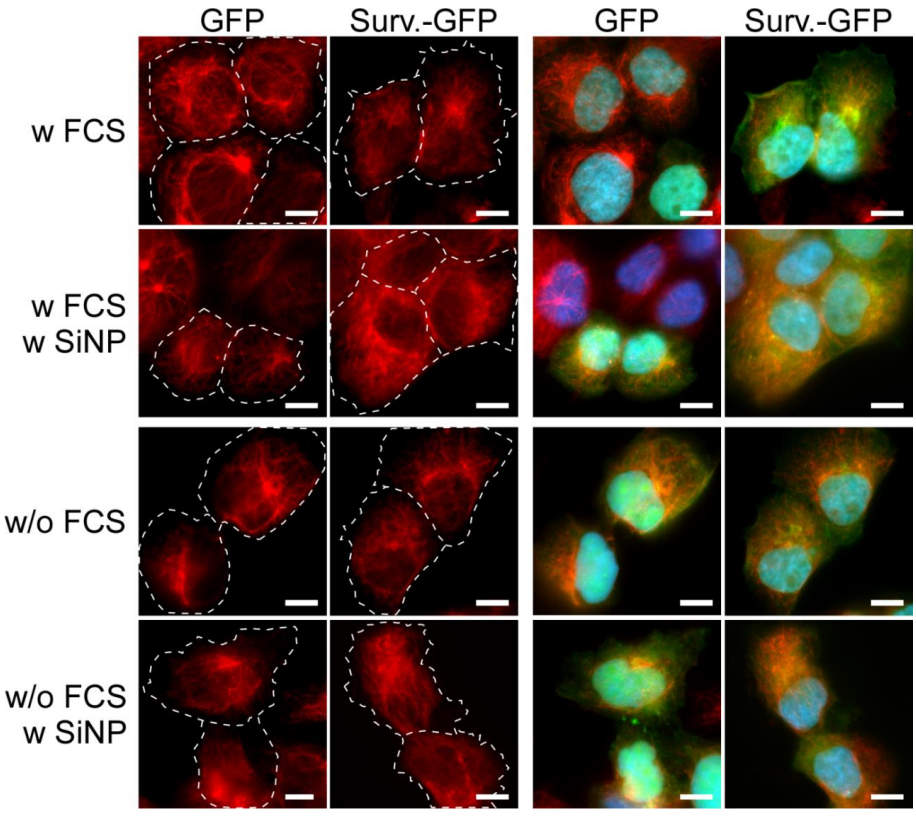

Figure 20. Impact of SiNP onto microtubule dynamics of β-tubulin. A431 GFP and Survivin-GFP expressing cells incubated in FCS or without FCS in combination with 60 µg/mL SiNP for 1 h. Cells were stained with Hoechst (blue) and β-tubulin (red) (4.2.5) to visualize the microtubule network. Scale bar indicates 25 µm.

2.4.1 SUMMARY

Amorphous SiNP are taken up by endocytosis and induce the generation of autophagosomes and/or autolysosomes (Figure 19). Survivin-GFP overexpressing cells showed less SiNP-generated actin puncta in the outer membrane region than wild-type cells, indicating a reduced endocytosis. Further, SiNP caused a decline of β-tubulin fibers (Figure 20), which might be responsible for the collapse of the lysosomal cellular organization observed before (see section 2.3) (Kimura et al., 2008; Yang et al., 2011). Survivin in turn stabilized the microtubule network, which may be related to the suppression of lysosome translocation and reduced autophagy turnover.

2.5 ROLE OF ROS IN SINP-DEPENDENT TOXICITY AND SURVIVIN-MEDIATED RESISTANCE

2.5.1 SINP-DEPENDENT ROS GENERATION

Reactive oxygen species (ROS) are not only stressors but also signal transducers that can activate pro-apoptotic or anti-apoptotic signaling pathways. Among other things, serum deficiency can increase ROS levels, activating signaling pathways that help to adapt to temporary nutrient deficiency and thereby preventing apoptosis induction (Lee et al., 2010). In the following experiments, SiNP of type AmSil20 will be examined for their ROS-inducing properties and how Survivin expressing cells counteract ROS stress.

To compare the ROS generation between A431 wt and Survivin-GFP expressing cells CellROX orange live staining was used for the experiments to ensure fluorophore compatibility (Figure 21). First, cells were treated with 50 µM Menadione for 1 h in a serum-containing medium to induce the generation of ROS. For further measurements, the exposure time for CellROX orange was set to the Menadione-treated control sample for each cell type. A431 Survivin-GFP expressing cells showed a significantly higher basal ROS level than A431 wt cells incubated in a serum-containing medium (w FCS). Survivin-GFP expressing cells showed no difference in the CellROX orange intensity between the ROS positive control (Menadione) and the basal ROS intensity (w FCS). On the contrary, A431 wt cells showed a clear increase in the CellROX orange intensity after treatment with Menadione (Figure 21A). However, as expected serum deprivation-induced a ROS increase in A431 wt cells when compared to

control samples (w FCS). The addition of 60 µg/mL SiNP did not lead to a further increase of ROS but to single ROS accumulations of high intensity (Figure 21B).
Survivin-GFP expressing cells behaved differently, hence short serum deprivation as well as the addition of SiNP led to a ROS burst after a 30-minute incubation (Figure 21D). Prolonged serum deprivation decreased the ROS level to an undetectable level when the exposure time was fixed to the corresponding positive control. Incubation with SiNP for 60 min decreased the ROS level in A431 Survivin-GFP expressing cells significantly and was not detectable after 120 min.

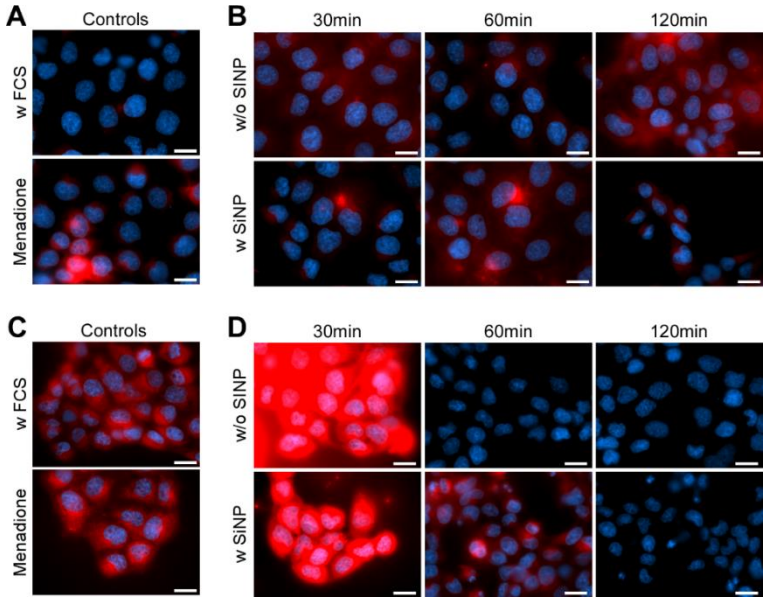

Figure 21. Time-dependent ROS regulation. A431 wt (A, B) and Survivin-GFP expressing cells (C, D) were incubated without (Ctrl) or with 60 µg/mL SiNP in a serum-deprived medium for 30, 60, and 120 min. Nuclei stained with Hoechst 33342 (4.2.5.2) and ROS with CellROX orange reagent (4.2.5.6). The exposure time for CellROX orange was set to the positive control (50 µM Menadione, 1 h in serum-containing medium, A, B) for all samples of each cell type. The scale bar indicates 50 µm.

This experiment showed that Survivin overexpression increased the basal ROS level significantly. In addition, Survivin-GFP-expressing cells increased the ROS level rapidly (ROS burst) with a subsequent rapid elimination of ROS, which did not occur in A431 wt cells. These results might indicate Survival-dependent activation of ROS scavenging processes as described by Zorocv et al. (2014) , which will be further examined in the next sections (Zorov et al., 2014).

2.5.2 Mitochondrial ROS Generation and Mitophagy

Mitochondria represent the main source of cellular ROS, releasing ROS periodically into the cytoplasm. An elevated ROS level, not compensated by ROS scavengers can initiate and activate mitochondrial fission and mitophagy to remove damaged mitochondria thereby

reducing the ROS generation (Zorov et al., 2014). In the next section mitochondria and mitophagy will be examined on the one hand considering SiNP-mediated stress and on the other hand considering the role of elevated Survivin levels for mitochondria-related stress.

Ahmad et al. (2013) proposed a model to predict cellular stress based on the shape of mitochondria. The group identified three different shapes of mitochondria corresponding to different stress levels mediated by mitochondrial ROS levels. Tubular mitochondria indicate healthy cells while “donut” formed mitochondria indicate a low stress/ROS level. Mitochondria with a “blub” punctual form correlate with increased ROS levels and cell toxicity (Ahmad et al., 2013).

Mitotracker deep red FM dye (Invitrogen) was used to stain mitochondria of A431 wt and Survivin-GFP expressing cells. For the validation the Mitotracker deep red staining was visualized in a yellow panel to generate a better contrast (Figure 22).

A431 wt cells showed overall tubular structures in untreated control cells incubated in a serum-containing medium (w FCS, Figure 22A). Survivin-GFP expressing cells showed tubular-like structures but shorter and clumsier (w FCS, Figure 22C). Serum deprivation induced the formation of “donut” and “blub” shaped mitochondria in wild-type and Survivin-GFP expressing cells, while this mitochondria phenotype was more prominent in Survivin-GFP expressing cells than in the wild-type (Figure 22 B, D). Treatment with 60 µg/mL SiNP led to a mixed phenotype with predominantly blub-shaped mitochondria in both cell types. However, those “blub” formed mitochondria differed between A431 wt and A431 Survivin-GFP expressing cells; A431 wt cells showed a more homogenous mitochondrial mass with single “blubs” (Figure 22 B). In contrast, Survivin-GFP expressing cells exhibited more clearly separated mitochondria “blubs” (Figure 22D).

Menadione-treated cells were used as positive control for ROS-related effects. The treatment resulted in shrinkage of the mitochondrial mass or accumulation of the mitochondrial mass in the perinuclear region in both cell types. Furthermore, Menadione led to the loss of the mitochondrial tubular structure in A431 wt cells, which were maintained in Survivin-GFP expressing cells. The mitochondrial changes caused by Menadione showed phenotypical similarities to SiNP-induced effects. These results may indicate mitochondria-mediated apoptosis induced by SiNP-dependent ROS generation, since “blub” shaped mitochondria were shown to be related to enhanced cytotoxicity (Ahmad et al., 2013).

In addition, the altered mitochondrial phenotype of Survivin-GFP expressing cells in untreated (w FCS) and treated cells (SiNP) might indicate mitochondrial fission. This specific phenotype is related to the Warburg effect, which shifts the metabolic function of mitochondria from oxidative phosphorylation to glycolysis, resulting in high glucose consumption, lower ATP levels, and lower ROS production, relative to the oxidative phosphorylation metabolism. (Ausserlechner & Hagenbuchner, 2016). Survivin was determined as a critical factor for

mitochondrial fragmentation and fission and the implementation of the Warburg effect. In detail, Survivin suppresses the mitochondria-targeted autophagy, also known as mitophagy leading to the accumulation of transformed mitochondria (Hagenbuchner et al., 2019).

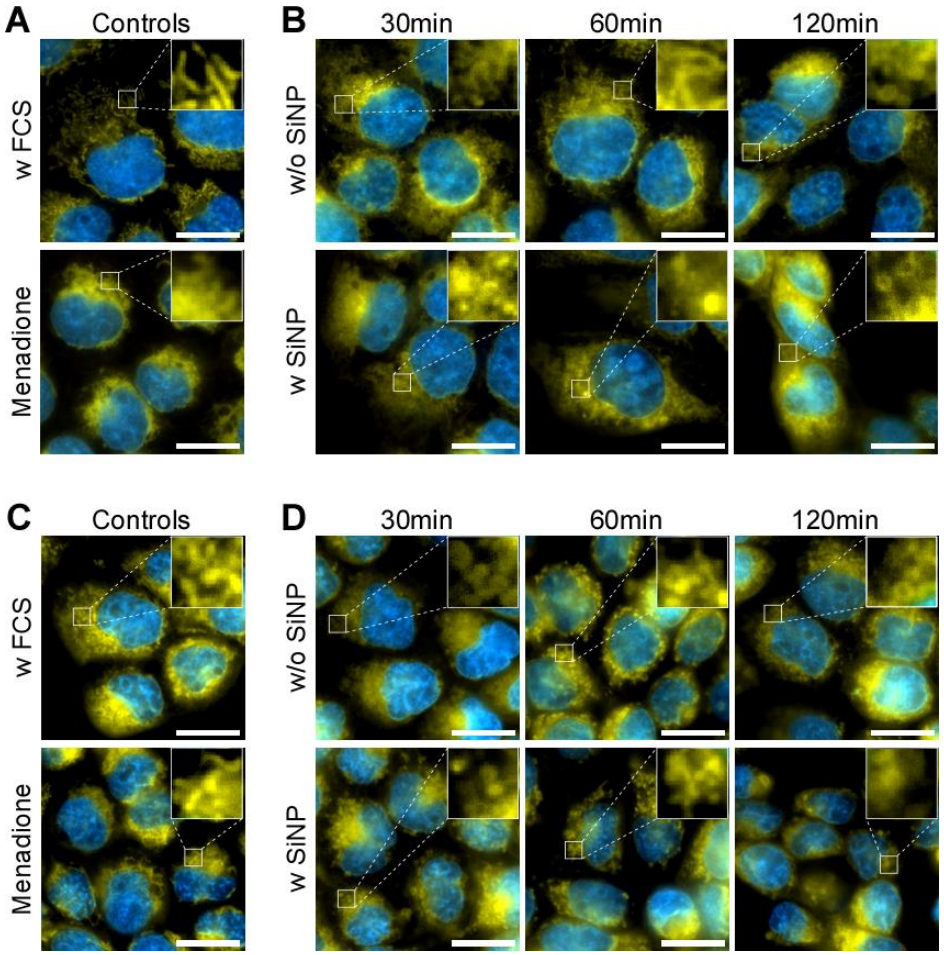

Figure 22. Mitochondrial fusion and fission. A431 wt (A, B) and Survivin-GFP expressing cells (C, D) were treated in a serum-deprived medium without (Ctrl) or with 60 µg/mL SiNP for 2 h. ROS-inducing agent Menadione (50 µM) incubated for 1 h was used as positive control. Mitochondria were stained with 50 nM Mitotracker deep red staining solution for 30 minutes (4.2.5.4). For better contrast and visualization, the color panel was changed from red to yellow. Additionally, the mitochondrial structure was enlarged by a factor of 4,164x. Nuclei stained with Hoechst 33342 (4.2.5.2). Scale bars indicate 50 µm.

The impact of SiNP and Survivin on the mitophagy induction was examined by double staining of mitochondria and acidic bodies (Figure *23*). A431 wt cells were treated with serum-deprived medium or with SiNP in the absence (A) or presence (B) of autophagy late-stage inhibitor CQ. Mitophagy active organelles were identified by double positive staining (Lysotracker green+/ Mitotracker deep red+).

In this context, mitophagy was observed in serum-starved cells and was further enhanced after incubation with SiNP. Yet, SiNP increased the amount and the size of acidic bodies stained by Lysotracker green dye in the perinuclear region, when compared to serum-starved cells, indicating enhanced autophagy levels. In sum, this experiment gives evidence that

mitochondria degrade through either macroautophagy or chaperone-mediated mitophagy in response to ROS-related stress stimuli generated by SiNP.

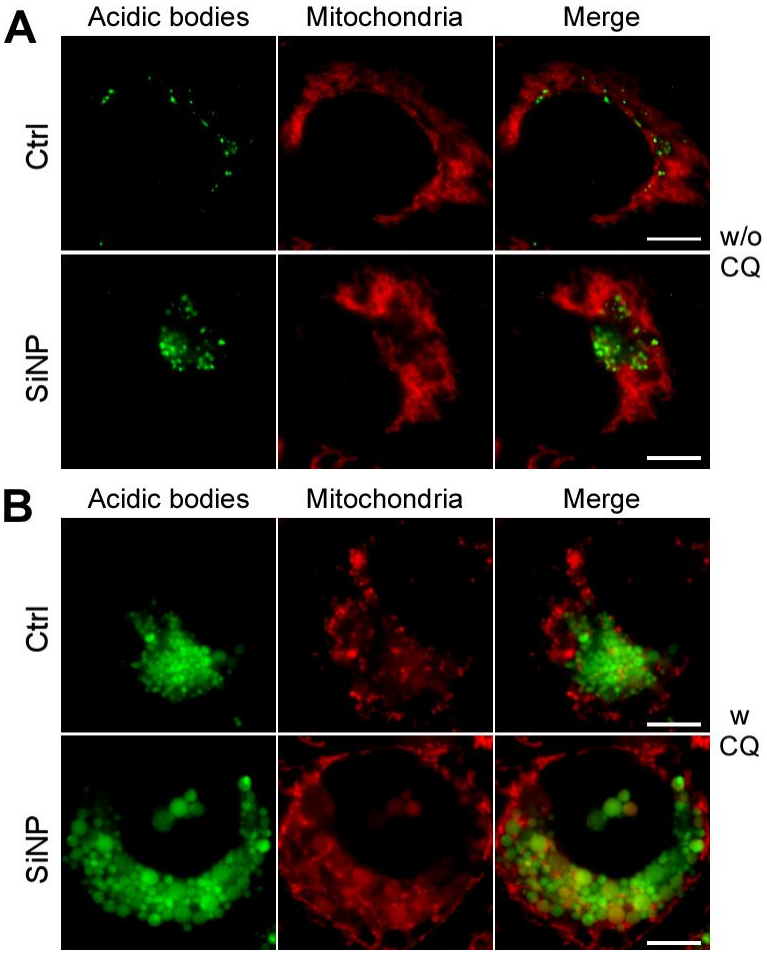

Figure 23. Mitophagy induction as a survival strategy or gate to cell death. A431 wt cells treated with 60 µg/mL SiNP in the absence (A) or presence (B) of 20 µM CQ. Live cell staining was performed with 50 nM Lysotracker green (acidic bodies, 4.2.5.5) and 50 nM Mito-tracker deep red (mitochondria, 4.2.5.4) for 30 min before images were taken and examined immediately. The scale bar indicates 20 µm.

2.5.3 Survivin affects the SiNP-mediated ROS Generation

Serum starvation and SiNP increase the generation of ROS (2.5.1), which can in turn stimulate the structural transformation of mitochondria (2.5.2). In this regard, the role of different Survivin levels on the generation of ROS was examined in the following section. Therefore, ROS were marked with CellROX stainings and observed microscopically or quantified by an automated array scan read-out.

The live cell staining reagent CellROX orange, was applied to enable the comparison of fluorescent green Survivin-GFP expressing cells and A431 wt cells (Figure 24).

Optimized image processing showed that Survivin-GFP expressing cells shifted ROS accumulations to the perinuclear region, especially after treatment with SiNP. In contrast, Survivin normal expressing cells (wt) showed a ring-like ROS staining in the cytoplasmic region (Figure 24A). Survivin-GFP expressing cells incubated with increasing SiNP concentrations correlated with an increasing ROS level (Figure 24B). The wild-type cells did not elevate the ROS level after SiNP incubation compared to serum-starved control cells. In addition, CellROX

orange staining revealed that Survivin-GFP expressing cells handled SiNP-mediated generation of ROS differently from wild-type cells due to different cellular CellROX orange signal localization (Figure 24A). Hence, mitochondria are the main resource of cellular ROS CellROX orange is mainly oxidized at the side of mitochondria. This observation of different cellular CellROX orange localizations supports the assumption that enhanced Survivin levels control the cellular ROS level through influencing mitochondria (2.5.3).

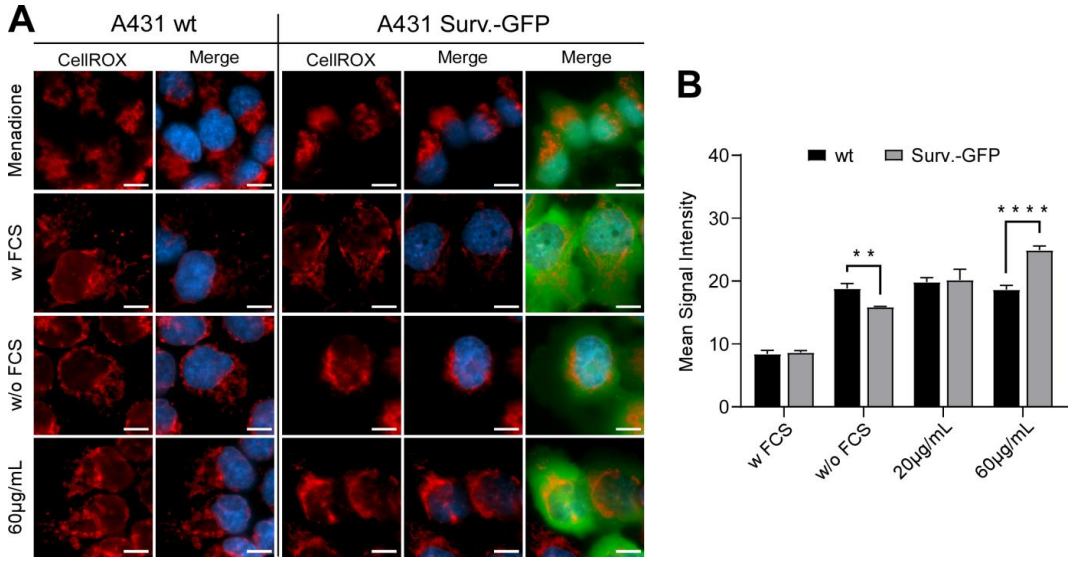

Figure 24. ROS measurement via CellROX orange. A431 wt and Survivin-GFP overexpressing cells incubated in medium with FCS (w FCS) or without FCS (w/o FCS) with 20 or 60 µg/mL SiNP in serum-free medium for 2 h. Staining was performed as described in section 4.2.5.6. A) Fluorescence microscopy. Images are presented in an optimized manner to clarify the distribution of CellROX orange fluorescence in the cell. Accordingly, this plot does not reflect the actual intensity (w FCS as lowest, Menadione as highest). Scale bars indicate 10 µm. B) CellROX orange quantification via array scan. Read-out was performed immediately after staining. The algorithm “Target Activation” was used to set the mask around nuclei with a ring distance of three pixels to define the area to measure CellROX orange fluorescence in the cytoplasm. Data was collected from three samples with 5000 measured cells. Anova two-way test was performed with p** <0.001, p**** <0.0001.

Complementing the investigations of Survivin`s impact on the cellular ROS level, siBIRC5 was used to knock down Survivin in A431 wt cells and stained with fixable CellROX green staining (Figure 25). The oxidized CellROX green dye intercalates into DNA resulting in a predominant nuclear localization. The specific localization and fixation simplify the measurement settings for array scan analysis and further avoid inaccuracies that occur with CellROX orange staining (Figure 24A).

Two-time points were selected to track possible time-dependent changes in the ROS level during incubation with SiNP in Survivin-knock down control groups. CellROX green staining requires an incubation period of 30 minutes, setting the earliest time point for observation to this timepoint. The second time point was set to 2 h since SiNP-mediated toxicity can be monitored, while enough adherent cells remain for analysis.

Microscopy and array scan analysis showed a SiNP concentration-dependent increase of ROS independent of the Survivin level (Figure 25, Supplementary Figure 7). However, cells with a decreased Survivin level exhibited an increased CellROX fluorescence intensity in comparison to control cells (Figure 25 A, C). In a serum-free medium, distinct CellROX green dots appeared in cell nuclei, comparable to those in control cells. After treatment for 30 min or 2 h with SiNP, the CellROX green signal increased. Compared to control cells, Survivin deficient cells showed a strong CellROX green intensity in nuclei as well as in the cytoplasm, which was minor in control cells (Figure 25 A, C).

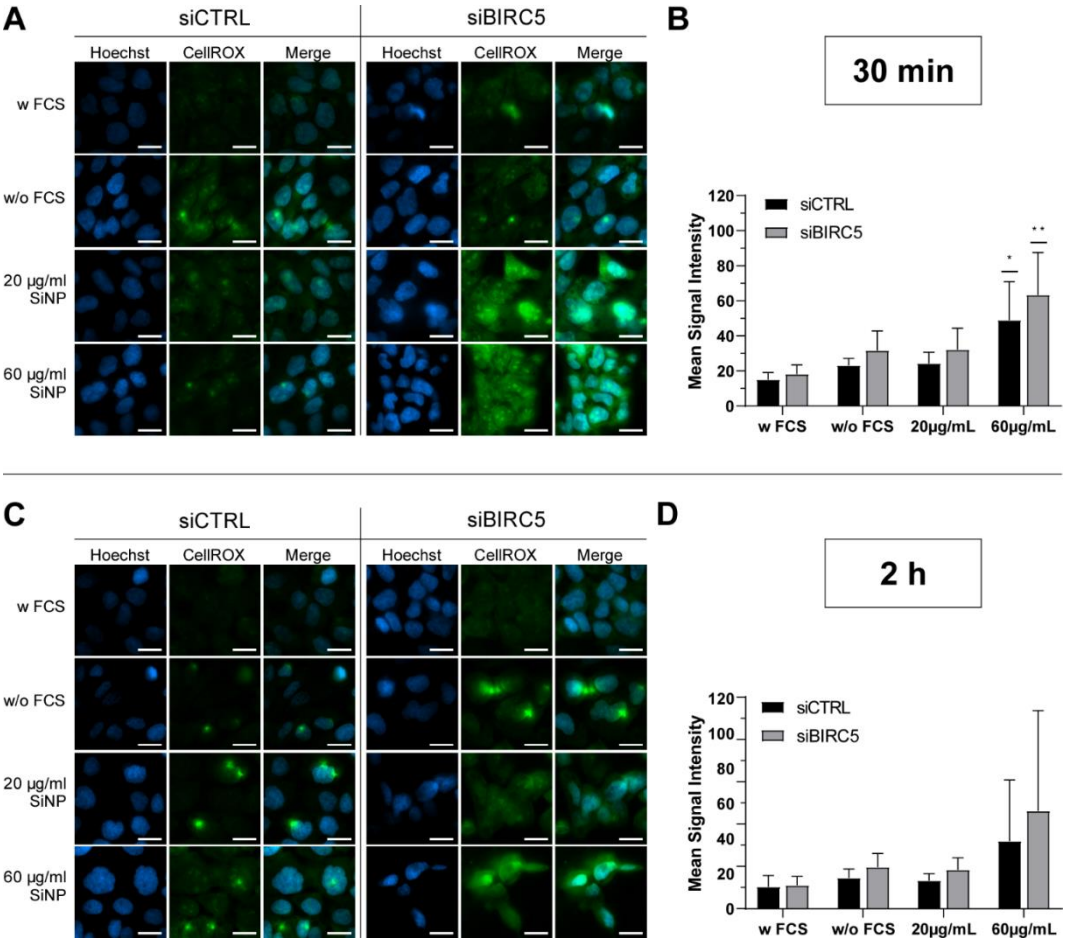

Figure 25. Influence of Survivin knockdown on ROS generation upon SiNP exposure. A431 wt cells were transiently transfected with siBIRC5 or siCTRL (4.2.4.1). CellROX green (2.5 nM) incubated with serum-containing medium (w FCS), serum-free medium (w/o FCS), or with 20 or 60 µg/mL SiNP in serum-free medium for 30 min. Nuclei stained alive with 2 µg/mL Hoechst 34222. CellROX green assay was performed after 30 min (A, B) or 2 h (C, D) exposure to SiNP. A, C) CellROX green assay evaluated via fluorescence microscopy with fixed exposure time for CellROX (green) to control groups (w/o FCS). Scale bar indicates 10 µm. B, D) Array scan quantitative analysis. The "Molecular translocation" algorithm was used for mask settings. The mean signal intensity measured in nuclei (B, D): The data were normalized to serum-free medium (w/o FCS) to visualize the effect of SiNP on ROS level in Survivin normal (siCTRL) or deficient cells (siBIRC5). The data set was compiled from four independent experiments with triplicates. Anova two-way test was performed comparing control groups (w/o FCS) to SiNP-treated samples with p*<0.05 and p** <0.01.

However, in both experiments, Survivin silenced cells (siBIRC5) showed a higher ROS level applying for SiNP treated samples and control groups (w FCS, w/o FCS) than Survivin normal expressing cells (siCTRL). When the data were normalized by subtraction of the cell-dependent ROS level baseline (w FCS), the data revealed that the amount of SiNP-generated ROS does not differ between control and Survivin-deficient cells (Supplementary Figure 7). In sum, the experiments revealed that SiNP induced ROS in a time and concentration-dependent manner. Furthermore, the results showed that the Survivin level influenced the basal cellular ROS level and is less potent to counteract the SiNP-induced ROS generation.

In sum, array scan analysis revealed that ROS is significantly increasing due to serum deprivation and additionally due to SiNP treatment. Thereby the ROS level changed significantly within 30 min and was elevated in a concentration-dependent manner. However, the array scan analysis revealed that Survivin-GFP expressing cells exhibit a higher ROS baseline level than A431 wt cells, also supported by previous findings in Figure 21, but does not differ from A431 wt cells in the amount of produced ROS by serum deprivation or SiNP treatment.

2.5.4 Lysosome-dependent ROS Generation

Reactive oxygen species are part of the normal cellular metabolisms and can also act as signaling molecules in pro- or anti-apoptotic signaling pathways (Lee et al., 2010; White et al., 2020; Wu et al., 2013). Several groups showed that silica nanoparticles can catalyze the generation of ROS depending on the accumulation in the acidic environment of lysosomes (Decan et al., 2016, Guo, 2016 #74). To verify this assumption SiNP were intracellularly localized by use of fluorescent SiNP of type Kisker green in combination with Lysotracker red staining to tag acidic bodies (

Figure 26A).

This experiment revealed that fluorescent green Kisker NP accumulated in Lysotracker red-dyed acidic bodies, giving evidence that SiNP interacted with the autophagy process.

To obtain more information about the interaction between SiNP and autophagy-related organelles, Kisker NP (green) treated cells were separately stained with specific antibodies against lysosome marker LAMP-1 (Cy3) or autophagosome marker LC3 (Cy3) in the presence or absence of late-stage inhibitor CQ (

Figure 26B, C).

Figure 26B showed that LAMP-1 positive puncta co-localized with Kisker NP in the presence and absence of CQ. This undermines the assumption that SiNP predominantly accumulated in lysosomes on the first side. In the later process of autophagy, nanoparticles were also found in autophagolysosomes.

Figure 26C reveals that SiNP co-localize with LC3 puncta in the absence of late-stage inhibitor CQ. In the presence of CQ, the fusion of autophagosomes with lysosomes should be interrupted, and indeed green Kisker NP no longer co-localize with LC3 positive puncta, indicating that lysosomes are the main carriers of SiNP (
Figure 26C).
These results are consistent with recent literature showing that SiNP explicitly accumulate in lysosomes, impairing lysosomal function and preventing autophagy flux in the long term (Abulikemu et al., 2022; Schutz et al., 2016).

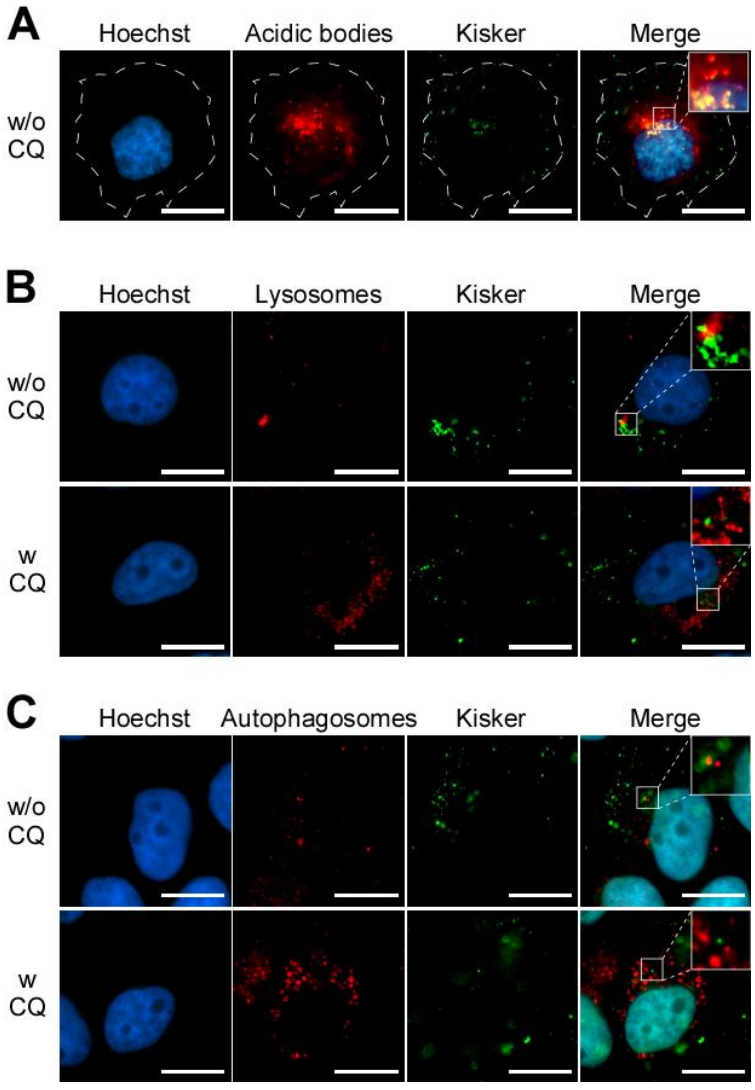

Figure 26. Localization of SiNP in autophagy-related compartments. A) Co-localization of Kisker NP (green) with Lysotracker red stained acidic bodies after treatment with 60 µg/mL for 2 h (4.2.5.5). B, C) A431 wt cells treated with 60 µg/mL Kisker green NP for 2 h in the absence (w/o) or presence (w) of CQ in a serum-deprived medium. Samples were fixed, stained with Hoechst 33342, and with antibodies against lysosome-specific LAMP-1 (Cy3) and autophagosome-specific LC3 (Cy3), (4.2.5).

Hence SiNP might catalyze ROS in the acidic environment of lysosomes (Decan et al., 2016, Guo, 2016 #74) and recent publications proposed lysosomal rupture as an additional ROS source, this issue was examined for the thesis work (Abulikemu et al., 2022; Schutz et al., 2016). Aits et. al (2015) proposed a galectin-1/3-assay for the precise detection of leaky lysosomes (Aits et al., 2015). Galectin-1 and 3 are recruited to leaky lysosomes, promoting

lysosomal recovery (Figure 27A). In consequence, galectin-1 and 3 puncta accumulate in the cytoplasmic area, which can be observed microscopically (Figure 27B).

Incubation with 2 mM LLMOe for 1 h in a serum-containing medium induced distinct galectin-1 puncta, while DMSO-treated controls showed no accumulations of galectin-1. Incubation with 60 µg/mL SiNP for 1 h showed few small galectin-1 accumulations, while cells incubated in serum-deprived medium showed few, but significantly bigger galectin-puncta (Figure 27B). Furthermore, a detailed time kinetic experiment was performed to evaluate early galectin puncta formations in response to SiNP (Figure 28). No galectin puncta occurred in A431 wt nor Survivin-GFP expressing cells considering several time points in between a 45-minute time range.

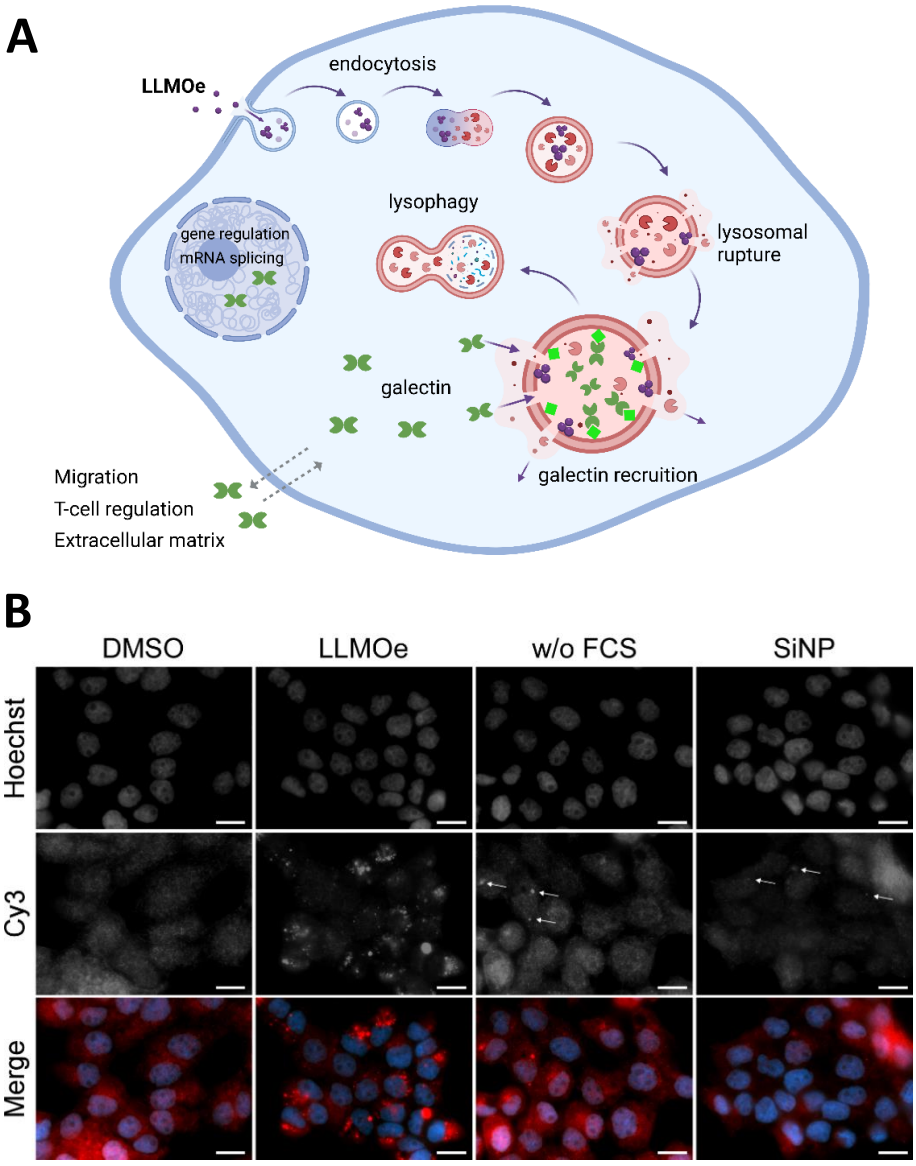

Figure 27. Galectin-1-assay. A) Theoretical illustration of a galectin-1-assay. The functionality of the galectin-1 assay is presented for L-Leucyl-L-Leucine methyl ester (hydrochloride) (LLMOe) which leads to lysosomal rupture. Cells take up the chemical compound by endocytosis. After fusion with lysosomes, the lysosomal membrane is ruptured by complex formations of the LLMOe. Galectins, such as galectin-1 and 3 recognize the glycosylated

proteins on the inside of lysosomal membranes to initiate repair mechanisms (Aits et al., 2015; Papadopoulos et al., 2020). The lysosomal accumulations of galectin-1 or 3 can be used to identify leaky lysosomes via fluorescence microscopy. Created with Biorender.com. B) A431 wt cells incubated with LLMOe (2 mM for 1 h) to trigger lysosomal rupture and galectin-1 accumulation in damaged lysosomes. Hence, LLMOe is dissolved in DMSO, and DMSO is examined as an additional control of the assay system. Further A431 wt cells were incubated for 1 h in a serum-deprived medium with or without SiNP (60 µg/mL). Arrows point on galectin puncta. Scale bar indicates 50 µm.

In summary, SiNP predominantly localized in lysosomes and autophagolysosomes but less in autophagosomes, indicating that lysosomal localization of SiNP might be critical for SiNP-mediated toxicity. Furthermore, SiNP-dependent lysosomal rupture can be excluded as a critical ROS source in early events of SiNP toxicity, due to the lack of galectin puncta. Efficient Lysotracker staining after SiNP treatments also supports this assumption, hence the staining reagent only intercalates into lysosomes with an intact acidic lumen (Figure 15).

2.5.5 Survivin regulates Galectin-1 Translocation in Response to SiNP

Notwithstanding that no galectin puncta formed, an interesting observation was made, nevertheless. Galectin-1 translocated into the nucleus with proceeding incubation time in serum-deprived medium and with the addition of SiNP in wild-type cells, while Survivin-GFP expressing cells showed the opposite effect.

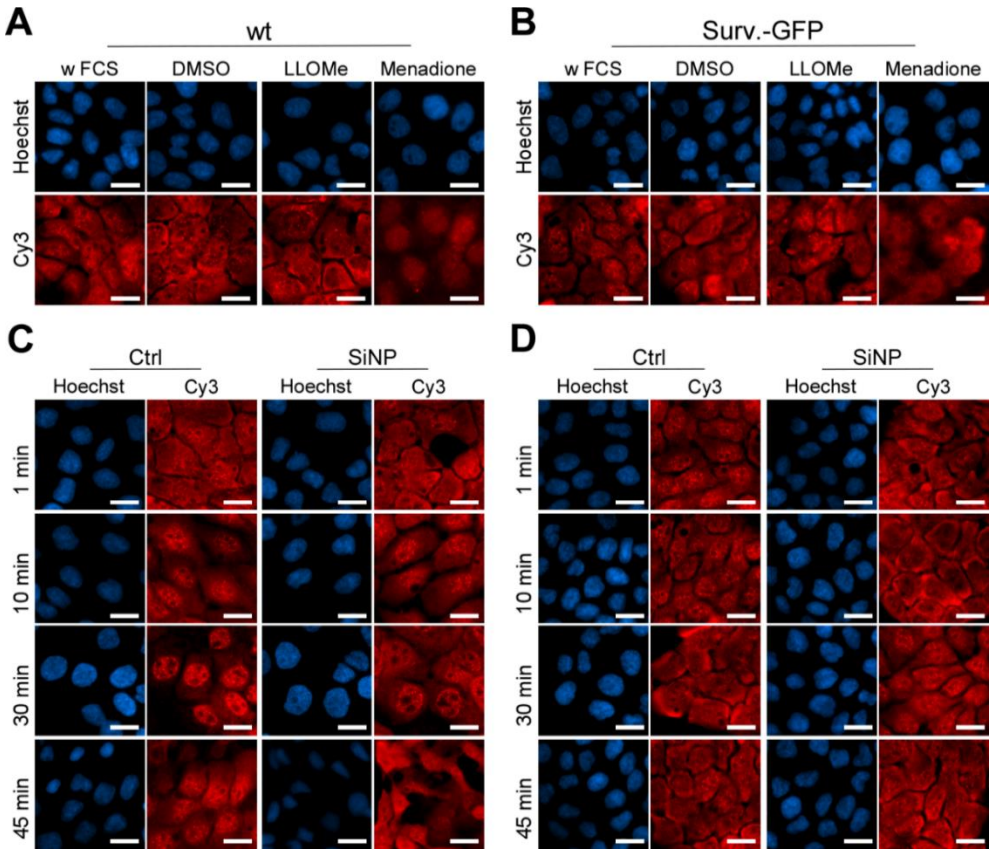

Figure 28. Time-related galectin-1 puncta assay. A, B) A431 wt and Survivin-GFP expressing cells treated with lysosome permeabilizing agent LLMOe (2 mM, 1 h) as a positive control for leaky lysosomes. Menadione (50 nM, 1 h) was used as a control for ROS-related effects. DMSO treatment was used as a control for LLMOe and Menadione's unspecific effects. Incubation in serum-containing medium (w FCS) was used as a negative control for normal galectin-1 distribution. A431 wt (C) and Survivin-GFP expressing cells (D) incubated in serum-deprived medium (Ctrl) or additionally in the presence of 60 µg/mL SiNP. Treatment finished after 1, 10, 30, and 45 min. Cells fixed, then stained with Hoechst 33342 (blue) and galectin-1 (Cy3), (4.2.5). Scale bars indicate 10 µm.

Translocation of galectin-1 into the cytoplasm correlated with morphological stability, while nuclear translocation emerged with cell shrinkage (Figure 28). However, a time-dependent burst of ROS was observed in previous experiments (Figure 21, Figure 25). Therefore, an additional control, menadione, was introduced to investigate whether ROS themselves could induce lysosomal damage and galectin puncta independent of SiNP (Figure 28). Control cells showed few clear galectin-1 puncta after treatment with menadione (Figure 28A). In addition, predominantly nuclear localization of galectin-1 was observed, while Survivin-GFP expressing cells showed a more distributed galectin-1 phenotype leaning to a cytoplasmic localization (Figure 28B).

In sum, ROS-inducing agent menadione had a marginal effect on the lysosomal rupture but might had an impact on the localization of galectin-1, since ROS-inducing agent menadione and serum deprivation-induced the nuclear translocation of galectin-1 in A431 wt cells. Altogether, enhanced Survivin expression levels seem to suppress the galectin-1 nuclear translocation in response to stress stimuli like ROS, which might contribute to Survivin’s resistance mechanisms.

2.5.6 SUMMARY

The presented results showed that SiNP induced the generation of ROS in addition to serum deprivation. Survivin negatively controlled the basal level of cellular ROS in response to mild stress and under normal growth conditions but could not prevent SiNP-dependent ROS generation. However, the treatment with SiNP reduced and deformed the mitochondrial mass. Survivin-GFP overexpressing cells in turn exhibited a significantly different mitochondrial phenotype than wild-type cells, indicating the fission and fusion of mitochondria, which might be related to the Warburg effect (Hagenbuchner et al., 2019). In this context, mitophagy was identified as a clearing mechanism induced in response to SiNP to eliminate mitochondrial ROS (2.5.2). However, SiNP predominantly accumulated in lysosomes, but lysosomal leakage as an additional ROS source was refuted via galectin-1 assays (Figure 27, Figure 28). Nevertheless, the galectin-1 assays revealed that Survivin-GFP expressing cells regulate galectin-1 in response to SiNP and ROS-inducing agent menadione by galectin-1 nuclear exclusion (Figure 28). If the Survivin-dependent regulation of galectin-1 plays a key role in the

defense against SiNP-mediated toxicity remains to be clarified. In sum, Survivin might modulate the basal ROS level through the transformation of mitochondria or mitophagy to switch between signaling pathways such as autophagy and apoptosis (Humphry & Wheatley, 2018).

2.6 Relationship between Survivin and ROS-dependent Signaling Pathways

2.6.1 SiNP-mediated Stress Signaling Pathways

Stress-induced signal transduction activates or deactivates multiple signaling pathways simultaneously. The complex interactions induced by SiNP-mediated stress were investigated by immunoblot analysis and complemented with viability tests. In particular, the possible involvement of signal transducing MAPKs p38 and p44/42 were analyzed in association with the ROS generation and the autophagy process (Figure 29).

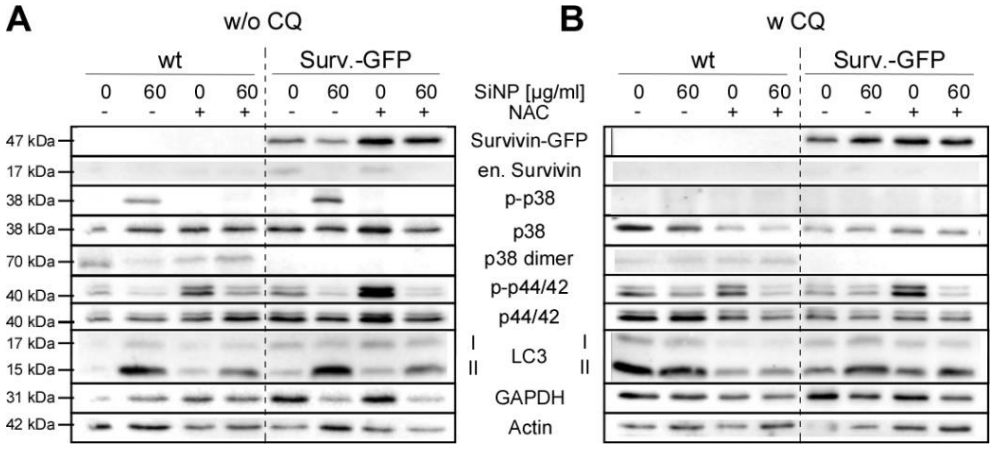

Figure 29. Relationship between p38 activation and Survivin downregulation in the context of elevated ROS levels. A431 wt and Survivin-GFP expressing cells treated without (A) or with (B) late-stage autophagy inhibitor Chloroquine (CQ) 24 h before SiNP treatment. Additionally, 5 µM NAC (+/-) was incubated for 2 h before SiNP were added. Cells incubated in the absence (-) or presence (+) of NAC and/ or CQ in serum-free medium with (+) or without (-) SiNP for 4 h. Western blot analysis was performed for inhibitor of apoptosis protein Survivin, autophagy-related protein LC3, survival pathways MAPK p38, p44/42, and housekeeping genes GAPDH and Actin.

The presented results showed so far that serum deprivation and SiNP treatment enhanced the ROS level (see section 2.5). In this context, redox-sensitive proteins GAPDH and p38 were identified as targets of SiNP-mediated toxicity (Figure 29, Figure 31A).

The housekeeping gene GAPDH, important for oxidative phosphorylation metabolism, was suppressed on the protein level after incubation with SiNP (Figure 29, Figure 31 A). However, GAPDH plays an important role in mitophagy as well. Mitochondrial GAPDH directs mitochondria to lysosomes for degradation (Yogalingam et al., 2013). In this regard, SiNP-

induced autophagy correlated with a decreased GAPDH expression. Townley et al. (2020) showed that mitochondrial Survivin can prevent mitophagy (Townley & Wheatley, 2020). Here, a Survivin knockdown in A431 wt cells correlated with an increased GAPDH expression (Figure 16). However, SiNP decreased the Survivin and GAPDH expression in A431 wt and Survivin-GFP expressing cells, but stayed stable in the presence of CQ, indicating the interrupted mitophagy-dependent degradation of GAPDH (Figure 29, Figure 31A). These findings support the assumption that mitophagy is activated due to ROS-mediated stress generated by serum deprivation and SiNP treatment. In turn, mitophagy is highlighted as a possible resistance mechanism of Survivin overexpressing cells in section 2.5.2.

SiNP treatment activates the stress kinase p38 and further leads to the formation of ROS-induced heterodimers in A431 wt cells (Figure 29, Figure 30). Introducing ROS scavenger NAC to the SiNP treatment suppressed the p38 activation, but not the formation of heterodimers in A431 wt cells (Figure 29 A, B). The p38 suppression by NAC was consistent in most but not all experiments. Those deviations might be associated with minor changes, regarding cell confluence, cell viability, or cell culture passage/age. However, supplementation with ROS scavenger NAC did not rescue cells from SiNP toxicity (Supplementary Figure 9, Supplementary Figure 10). This observation might indicate non-compensable ROS levels, or other ROS-independent stress transducing pathways as proposed by Lee et al. (2019), (Lee et al., 2019).

2.6.2 Stress-induced Kinase p38 and related Pathways

However, several studies pointed out that the activation ratio of the MAPKs p38 and Erk (p44/42) is a key decision point for tumor cells to decide to go under dormancy or promote tumor growth: A higher p38/Erk ratio leads to dormancy while a higher Erk/p38 ratios support tumor progression (Aguirre-Ghiso et al., 2003). Parallel to p38 activation MAPK p44/42 was deactivated in response to SiNP-induced stress. The ROS scavenger NAC increased p44/42 activity in serum-deprived cells but could not protect the cells from SiNP-induced MAPK p44/42 deactivation. However, ROS scavenger NAC could significantly reduce the LC3 conversion, indicated by slighter LC3-II bands in comparison to SiNP-treated cells without NAC (Figure 29 A, B). Inhibition of the autophagy turnover via CQ treatment revealed that NAC reduced the overall generation of LC3-I and II proteins, but with a higher impact in wild-type cells than in Survivin-GFP expressing cells (Figure 29 B). However, other signaling pathways were addressed by SiNP such as JNK and Nf-κB (Supplementary Figure 8), but not further examined in the thesis work.

Since autophagy is a highly dynamic process, autophagy in response to serum deprivation and SiNP treatment was examined as time kinetic and evaluated in an immunoblot (Figure 30).

The main autophagy negative regulator, mTOR is actively suppressing autophagy under normal growth conditions. Deprivation of serum activates AMP-activated protein kinase (AMPK) leading to mTOR inhibition and autophagy initiation (He & Klionsky, 2009; Wang & Levine, 2010). In A431 wt cells, p-mTOR vanished after incubation for 30 min in a serum-deprived medium, while autophagy active LC3-II increased, indicating for mTOR dependent autophagy initiation (Figure 30). Prolonged incubation in serum-free medium reactivates mTOR activity (120 min), caused by autophagy-mediated recovery of essential building blocks (Wang & Levine, 2010). Further incubation (4 h) without serum inactivates mTOR again, suggesting that the nutritional status is low again, and autophagy is reactivated as a survival pathway under starvation conditions (Deleyto-Seldas & Efeyan, 2021). In the presence of glutamine deficiency, cancer cells use this pathway to escape from apoptosis by promoting Akt/mTOR activation (Khan et al., 2018; Villar et al., 2017).

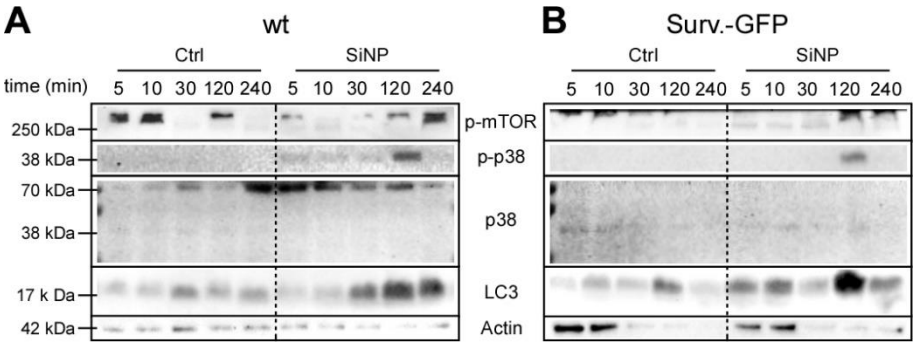

Figure 30. Dynamic autophagy regulation. Time course of autophagy and apoptosis relevant mechanisms in A431 wt (A) and Survivin-GFP expressing cells (B) upon treatment with 60 µg/mL SiNP or serum-free medium (Ctrl) for 5, 10, 30, 120, and 240 min, respectively. Western blot analysis was performed for autophagy-related actors mTOR, LC3 I/ II, and stress kinase p38. The housekeeping gene Actin was used as a loading control. For acceleration of the analysis, membranes were cut to specific heights before specific antibodies were applied, resulting in bans appearing close to the edge.

The SiNP rapidly decreased p-mTOR expression after treatment for 5 min to 30 min, while p-mTOR reappeared after 120 min, and remained active in the observation period (4 h). LC3 conversion was higher with than without SiNP and remained high after mTOR reactivation, indicating mTOR-independent autophagy initiation triggered by SiNP. Interestingly, SiNP activated stress kinase p38 time-dependently, reaching a peak after 2 h. The phosphorylated/ active form of p38 is a marker for cell stress, which in turn can induce apoptosis, depending on the duration and intensity of the stress signal (Jia et al., 2007). The activation level of p38 correlated with decreasing p-mTOR levels. After treatment for 4 h, p-mTOR reappeared, while p-p38 vanished completely (Figure 30).

However, using a polyclonal antibody against p38 led to the discovery of p38 bands with a size of about 70 kDa in A431 wt cells, in addition to the 38 kDa band of the normal p38 protein (Figure 29, Figure 30). Bassi et al. (2017), described heterodimers of p38 and MKK3 with a

similar size, promoted by high ROS levels (Bassi et al., 2017). These dimers appeared exclusively in A431 wt cells and never in Survivin-GFP expressing cells. The dimers band increased with incubation in a serum-deprived medium (Figure 30), indicating a starvation-induced ROS production (White et al., 2020). Additional treatment with SiNP generated a similar amount of p38 dimers after a short incubation period (5 min). Interestingly the dimers band decreased in SiNP-treated cells steadily with time, with a parallel increase in the LC3 proteins. In comparison to control cells, Survivin-GFP expressing cells showed no redox-sensitive p38 heterodimers. Further, Survivin overexpression delayed p38 activation in response to SiNP. Activation of p38 increased the conversion of LC3-I to the autophagy active form LC3-II, independent of the mTOR activity. Therefore, autophagy suppression in Survivin overexpressing cells may result in an mTOR-independent manner, which is supported by recent publications (Lin et al., 2019).

However, the epidermal growth factor receptor (EGFR) plays an important role in extracellular signal transduction and participates in tumor progression (Stauber et al., 2012). Several stress signals can lead to the endocytic uptake of EGFR followed by the degradation of the receptor in a ligand-independent manner (Tomas et al., 2017). The endocytosis of inactive EGFR can stimulate the autophagy initiation and EGFR degradation (Tan et al., 2016).
Hence, A431 cells had an increased EGFR expression level, the EGFR expression was analyzed via immunoblotting (Figure 31A). Samples that were treated with SiNP exhibited two additional bands with a lighter molecular weight of around 60 kDa and 40 kDa (Figure 31A). Those bands might indicate the soluble isoform of the EGFR and/ or fragments of the receptor (Albitar et al., 2010; Kohda et al., 1993). However, cells additionally incubated with NAC showed no suppression of the light-molecular-weight-EGFR fragments compared to the control treatment (Figure 31A).

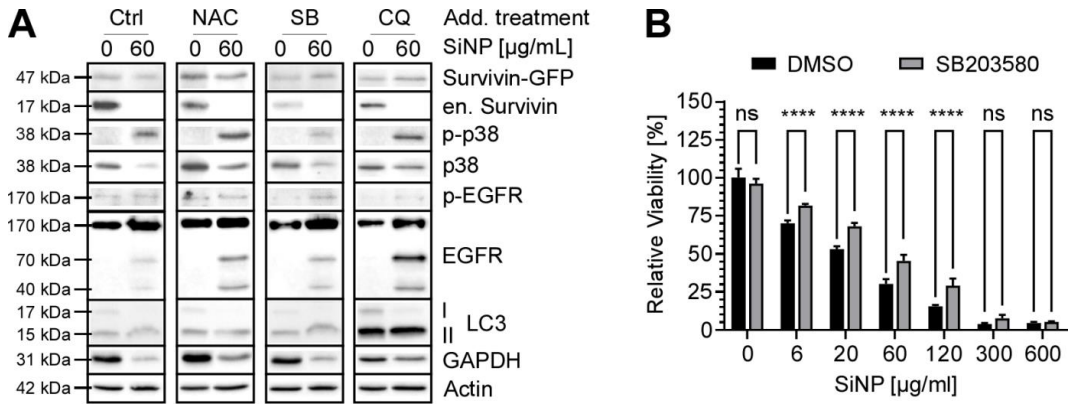

Figure 31. SiNP promoted signaling pathways. A) EGFR signaling. A431 Survivin-GFP expressing cells incubated in FCS with 5 µM NAC, 10 µM SB203580 (SB, p38 inhibitor), or 20 µM CQ for 2 h before incubation with 60 µg/mL SiNP in serum-free medium for 4 h. Western blot analysis was performed for the target protein Survivin as well as MAPK p38 and EGFR. Housekeeping genes GAPDH and Actin were applied as loading controls. B) Cell protective

ability of p38 inhibitor SB203580 in combination with increasing SiNP concentrations. A431 Survivin-GFP expressing cells incubated 2 h before SiNP treatment with 10 µM SB203580 or DMSO as controls. SiNP treatment was performed in a serum-deprived medium for 2 h. Viability was measured via the Alamar Blue Viability Assay (4.2.9.1). Anova two-way test was performed accounting significances with p****<0.0001, ns= not significant.

The selective p38 inhibitor SB203580 blocks the ATP-binding pocket of p38, thereby impairing its kinase function and further p38-mediated signal transduction without affecting p38 phosphorylation (Kumar et al., 1999). The inhibition of p38 with SB203580 elevated the fraction of EGFR isoforms, but less than the additional NAC treatment, in comparison to the control. The inhibition of the late-stage autophagy increased the light-molecular-weight-EGFR bands in comparison to control cells, which correlated with an increased LC3 conversion. Like p38 inhibitor SB203580, CQ attenuated the EGFR expression during serum deprivation without SiNP incubation (Figure 31 A). These findings support the assumption that the SiNP-mediated p38 activation promotes the internalization and degradation of inactive EGFR as described by Thomas et al. (2017) and further promotes the autophagy initiation (Tomas et al., 2017). Altogether, these data indicated that SiNP-mediated stress is at least in part caused by SiNP-generated ROS, inducing stress kinase p38 and finally resulting in the EGFR internalization and degradation as well as downregulation of endogenous Survivin (Figure 31 A). The inhibition of the stress kinase p38 with SB203580 attenuated the SiNP-mediated toxicity in Survivin-GFP expressing cells, supporting this assumption (Figure 31 B). In contrast, A431 wt cells did not show any differences regarding SiNP-mediated cell toxicity, when treated with the p38 inhibitor SB203580 under the same treatment conditions (Supplementary Figure 11). An extended experiment using the p38 inhibitor SB203580 in combination with SiNP had no positive or negative effect on the cell viability of A431 wt cells which were transiently transfected with siCTRL and siBIRC5 (Supplementary Figure 12). Hence Survivin-GFP long-term expressing cells respond to p38 inhibition with increased resistance against SiNP but A431wt cells do not, (Figure 31, Supplementary Figure 11, Supplementary Figure 12), it is ambiguous which role p38 plays in the SiNP-mediated cell toxicity. If genetic mutations or the absent formation of p38 dimers in Survivin-GFP expressing cells promote resistance against SiNP has to be examined in further experiments.

2.6.3 FoxO Signaling in the Context of SiNP-dependent ROS Generation and Survivin Overexpression

ROS are signaling molecules promoting tumor proliferation, metastasis, survival, and angiogenesis as well as autophagy and apoptosis (Redza-Dutordoir & Averill-Bates, 2016; Sabharwal & Schumacker, 2014). The family forkhead box class one (FOXO) transcription factors regulated the gene expression of antioxidant proteins in response to oxidative stress (Gorrini et al., 2013). Mainly three kinases (IKK, Akt, p44/42) suppress the FoxO protein activity

via phosphorylation. In turn phosphorylation through other kinases like p38 and c-Jun-N-terminal kinase (JNK) can activate the FoxO family members in response to stress stimuli. The phosphorylation by IκB kinase (IKK), Akt, and p44/42 promotes the nuclear exclusion and inactivity of FoxO proteins 1 and 3. The dephosphorylation of FoxO1/3 proteins leads to nuclear translocation, which can induce apoptosis by suppressing anti-apoptotic proteins such as Survivin, and inducing the transcription of pro-apoptotic proteins such as Fas and Bim (Figure 38) (Klotz et al., 2015; Wani et al., 2021). Furthermore, Nakamura (2008) showed that the transcription of FoxO3 targeted genes is essential for ROS-induced apoptosis (Nakamura & Sakamoto, 2008). How FoxO signaling is affected by different Survivin expression levels was examined via immunoblot analysis and immunofluorescence staining (Figure 32A).

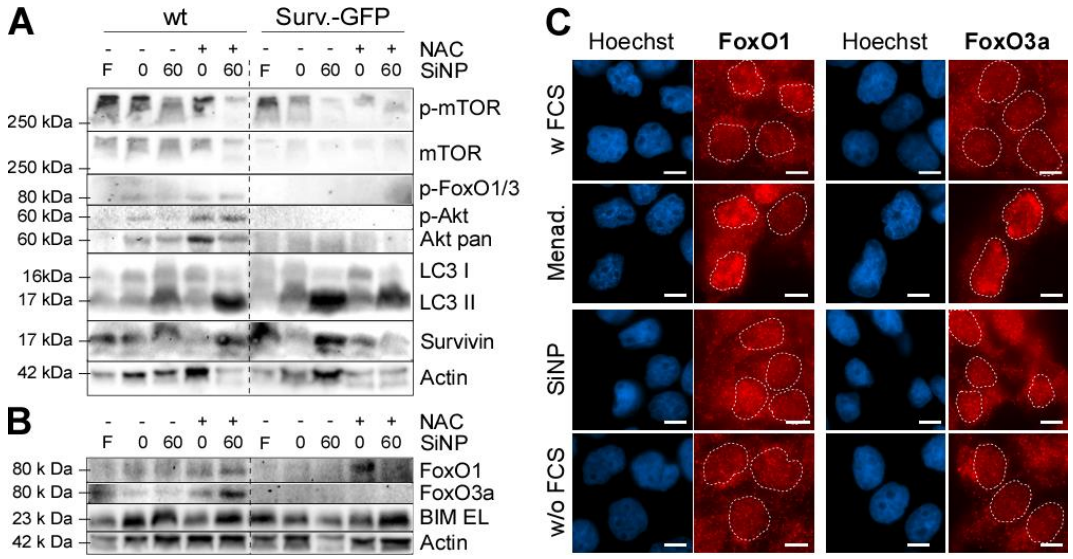

Figure 32. The Akt/FoxO/BIM signaling after long-term Survivin-GFP expression. A) Immunoblot analysis of A431 wt and Survivin-GFP (Surv.-GFP) expressing cells incubated for 2 h with 5 µM NAC before treatment with (w) or without (w/o) 60 µg/mL SiNP for additional 2 h in serum-deprived medium. Cells cultivated only in serum-containing medium (F) added as a control for the normal cell status. B) Immunoblot analysis as in A with the focus on FoxO and BIM EL interaction. C) Immunofluorescent staining of FoxO1 and FoxO3a in A431 wt cells. Cells were cultivated in a serum-containing medium without additional treatments (w FCS), or with additional treatment (50 µM Menadione (Menad.) for 1 h). Furthermore, cells were treated with a serum-free medium (w/oFCS) with or without 60 µg/mL SiNP for 30 min. For detailed mask settings, see Supplementary Figure 12. Scale bars indicates 25 µm.

The immunoblot analysis showed that the treatment with SiNP was followed by a decrease in active Akt (p-Akt) and simultaneously by a decrease in p-FoxO1/3 expression in A431 wt cells (Figure 32 A, B). Interestingly the expression and activation of Akt and FoxO1/3 were suppressed or rather absent in A431 Survivin-GFP expressing cells compared to A431 wt cells (Figure 32 A, B). Recent findings showed that BIM EL is regulated by the PI3K/Akt/FoxO3a axis (Ciechomska et al., 2020). Consequently, the pro-apoptotic protein BIM EL is regulated by FoxO and was further investigated by immunoblot analysis in Figure 32 B, Supplementary Figure 15 (Gilley et al., 2003). The analysis showed that the BIM EL level in A431 wt cells was

low under normal serum-containing growth conditions (Figure 32 B). Serum deprivation without or with an additional SiNP treatment increased the BIM EL expression. The ROS scavenger NAC attenuated the starvation-dependent BIM EL expression but not that of SiNP-treated cells (Supplementary Figure 15), indicating that SiNP addressed the FoxO/BIM EL pathway independent of ROS signaling. In contrast, Survivin-GFP expressing cells showed a significantly higher BIM EL basal level than A431 wt cells (Figure 32B). Furthermore, the BIM EL expression level was lower than that of A431 wt cells in response to serum deprivation, but not in response to SiNP (Supplementary Figure 15). However, ROS scavenger NAC did not decrease the BIM EL expression in response to SiNP in A431 Survivin-GFP expressing cells. In sum, these findings indicated that BIM EL might play a role in SiNP-mediated toxicity and that Survivin might manipulate the BIM EL expression pattern. More experiments are required to confirm that SiNP address the Akt/FoxO/BIM EL pathway and that cancer cells overexpressing Survivin interrupt this pathway as a survival strategy.

To clarify FoxO gene regulation the cellular translocation of FoxO1 and FoxO3awas examined via immunofluorescence staining and microscopic examination of FoxO1 and FoxO3a in A431 wt cells (Figure 32C, Supplementary Figure 12, 13). The dynamic regulation of FoxO proteins via specific phosphorylations and acetylations leads to an equal distribution between nuclei and cytoplasm (Klotz et al., 2015), as seen in control samples cultivated in serum-containing medium (Figure 32 C).Treatment with ROS-inducing agent Menadione induced the translocation of FoxO1 and FoxO3a into nuclei. Previous experiments showed that a ROS burst occurred after 30 min of incubation in a serum-deprived medium with and without SiNP (Figure 25). In this context, FoxO distribution was examined after the same treatment time, but a nuclear translocation of FoxO proteins was not observed in serum-deprived cells (Figure 32C). However, SiNP treatment might induce nuclear translocation of FoxO1 and FoxO3a, but not as significant as ROS-inducing agent Menadione. The quality of images and resulting statement using fluorescence microscopy depends on the grade of specificity of the used primary and secondary antibody and the protein expression level of the target protein. Due to high background staining of the secondary antibody as a consequence of low primary antibody binding the result interpretation is limited to clear translocations of the FoxO proteins into the nuclei, which were only clearly seen in cells treated with ROS-inducing agent Menadione (Figure 32 C,

Supplementary Figure 13,

Supplementary Figure 14). Furthermore, FoxO1/3a/Cy3 antibodies caused artifacts in combination with SiNP, increasing the difficulty of the result interpretation (Supplementary Figure 13).

Summarizing, ROS induced the translocation of FoxO1 and FoxO3a into the nucleus. The treatment with SiNP showed a potential cytoplasmic shift of FoxO1 and FoxO3a into nuclei in

A431 wt cells, while long-term expression of Survivin-GFP suppressed the expression and activation of Akt and FoxO proteins in general. In consequence, Survivin-GFP expressing cells exhibit a higher basal BIM EL level than the wild-type. Nevertheless, the BIM EL level increases in response to the treatment with SiNP, indicating that SiNP might mediate cell toxicity by addressing the FoxO/BIM EL apoptotic pathway.

2.6.4 SUMMARY

Summerizing the relationship between Survivin and ROS-dependent signaling the SiNP-dependent ROS generation caused the activation of stress kinase p38, as well as the formation of p38 dimers in A431 wt cells, which were absent in Survivin-GFP expressing cells (Figure 29). The role of p38 remains controversial since the inhibition of p38 increased the viability of Survivin-GFP expressing cells in response to SiNP but had to influence onto A431 wt cells without and with a Survivin knockdown (Figure 31, Supplementary Figure 11, Supplementary Figure 12). However, SiNP triggered the degradation of EGFR, indicating cell stress (Figure 31A). In addition, SiNP decreased the p44/42 pro-survival signaling pathway and might address the JNK, the NF-kB, and the FoxO/BIM EL pathways as well, while Survivin overexpression suppressed the Akt/FoxO pathway (Figure 29A, B, Supplementary Figure 8, Supplementary Figure 15).

2.7 AUTOPHAGY MODULATORS

2.7.1 INFLUENCE OF AMPK INHIBITOR COMPOUND C ON THE NANOPARTICLE TOXICITY

Serum deprivation is an important factor in the experimental setup, as SiNP otherwise gain a protein corona losing their cell interacting potential (Docter et al., 2014). One of the main cellular regulators, the AMPK, is stimulated by ROS in response to serum deprivation leading to mTOR suppression and autophagy initiation (Wu et al., 2013). The additional generation of ROS above the signaling level deactivates the AMPK and prevents the AMPK-dependent mTOR inactivation and autophagy initiation (Hernandez et al., 2011). Considering this mechanism, the AMPK-dependent autophagy was inhibited by the AMPK-specific inhibitor Compound C (CC) to potentially increase the toxicity of SiNP. The Compound C-related effects were examined via Lysotracker staining, immunoblot analysis, and cell viability tests (Figure 33).

The use of AMPK inhibitor Compound C (CC) increased the number of acidic puncta in response to starvation conditions (Figure 33 A-D); A431 wt cells showed a cytosolic distribution (A3), while Survivin-GFP expressing cells exhibited a significant perinuclear

localization (C3). Additional treatment with CQ revealed that Compound C increased the generation of acidic bodies in comparison to DMSO controls under serum deprivation, especially in the wild-type (B3). Survivin-GFP expressing cells did not increase acidic puncta, and puncta possessed a smaller size. Compared to A431 wt cells (B3), Survivin-GFP expressing cells showed an altered distribution phenotype (D3). In combination with AMPK inhibitor CC, SiNP did not increase the number of acidic puncta above the level of starvation-induced autophagy and CC treatment alone (A431 wt: C4, D4; A431 Survivin-GFP: A4, B4). The CC treatment reduced SiNP-induced acidic puncta formation (B4) in comparison to SiNP incubation with DMSO (B2). Furthermore, Survivin-GFP expressing cells with prior CQ treatment showed repeatedly significantly smaller acidic puncta (D4) than wt cells with a similar treatment (B4). The cell viability reflected the controversial phenotypes. In general, CC decreased the cell viability of A431 wt and Survivin-GFP expressing cells. However, compared to CC alone the combination of CC with SiNP showed the tendency to increase the cell viability again, especially in Survivin-GFP expressing cells (Figure 33C, D). The autophagy flux was further examined using immunoblot analysis for autophagy-relevant markers (Figure 33 E).

A431 wt and Survivin-GFP expressing cells treated with CC and SiNP for 4 h showed the phosphorylated form of mTOR, indicating mTOR reactivation due to prolonged autophagy, after which essential building blocks regained (Figure 33, see also Figure 30). The reactivation of mTOR was not observed in starved Survivin-GFP expressing cells. Considering CC as an AMPK inhibitor, mTOR dephosphorylation and deactivation should be suppressed, thereby preventing starvation-induced autophagy. Parallel incubation with CC showed no impact on mTOR phosphorylation, indicating an AMPK-independent mTOR activation pathway, which overpasses the AMPK suppression. In this regard, AMPK might initiate autophagy mTOR-independently via the AMPK and JNK/c-Jun signaling pathway (Tanida et al., 2008; Vucicevic et al., 2011). Simultaneous incubation with late-stage autophagy inhibitor CQ inverted the amount of the active mTOR form in Survivin-GFP expressing cells but not in A431 wt cells (Figure 33 G). The accumulation of p-mTOR in CQ-treated, starved cells indicates that p-mTOR degrades in an autophagy-dependent manner. However, in this experiment, the accumulation of LC3-I/II after treatment with SiNP was not observed, as has always been the case in other experiments. This observation might be attributed to the degrading cell death process accompanied by active caspase-3 or might be caused by a failed reblotting procedure resulting in unclear bands.

Nevertheless, distinct differences between Survivin normal (wt) and Survivin overexpressing cells (Surv.-GFP) were found in the expression of Akt and stress MAPK p38: Both cell types expressed Akt and p38, however, in A431 wt cells p38 and Akt dimers or multiphosphorylated forms occurred. The dimerization of p38 was detected in A431 wt cells in several experiments

but never in Survivin overexpressing cells. The dimers might indicate oxidative stress promoting the heterodimerization of the MAPK p38 with MKK3 (Bassi et al., 2017).

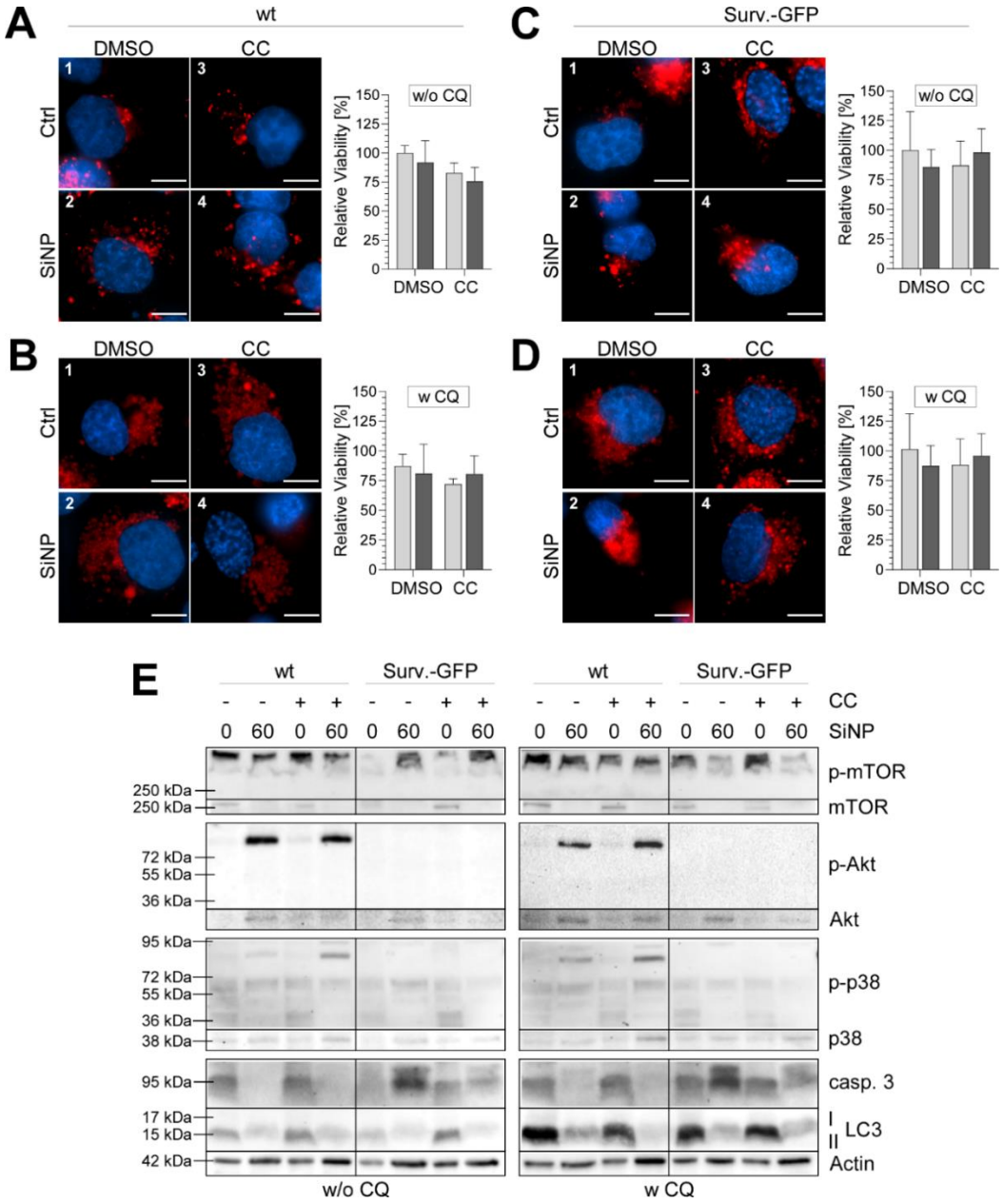

Figure 33. Role of AMPK in SiNP-mediated autophagy and toxicity. A-D) A431 wt and Survivin-GFP expressing cells analyzed microscopically for acidic body formations and cell viability. Cells were pretreated with 5 µM Compound C (CC) or DMSO as a control for 2 h. Then, the cells were treated with 60 µg/mL SiNP in the presence of CC or DMSO in a serum-deprived medium for 2 h. For the microscopical observation samples were stained alive with 2 µg/mL Hoechst for 10 min before Lysotracker red staining (50 nM) was performed (4.2.5). Images were taken immediately after staining. Scale bar indicates 10 µm. The cell viability was measured by Alamar Blue Viability assays (4.2.9.1). The experiment was performed in three independent approaches, each consisting of triplicates. Data normalized for each cell type to untreated controls without CQ pretreatment. Statistics were analyzed with the

ANOVA-two-way test, but no significant differences were found. E) Immunoblot analysis. A431 wt and Survivin-GFP expressing cells were cultivated for 24 h in the presence or absence of CQ. The treatment with Compound C (5 µM) was performed parallel to the incubation with SiNP (60 µg/mL) in a serum-deprived medium for 4 h. Autophagy and apoptosis-related proteins were examined via immunoblot (4.2.3.4)

2.7.2 Influence of PI3K Inhibitor LY294002 and Wortmannin on Nanoparticle Toxicity

Since Survivin-GFP expressing cells showed constantly suppressed Akt expression the role of Akt upstream activator PI3K was examined by use of PI3K inhibitors LY294002 (LY) and Wortmannin (W) (Figure 34, Figure 35, Supplementary Figure 16).

Immunoblot analysis showed that the serum-deprived DMSO control treatment exhibited a normal autophagy flux with inactivated mTOR and a low Akt activation and expression, accompanied by a low LC3 level in wild-type andin Survivin-GFP expressing cells. However, differences between wild-type and Survivin-GFP expressing cells consisted in the expression of Akt: While Akt was constitutively expressed in A431 wt cells, Survivin-GFP expressing cells expressed Akt only under the condition of SiNP treatment (Figure 34).

In the presence of low Wortmannin concentrations (0.2 µM), the Akt expression and activation, and LC3 accumulation increased under serum deprivation in comparison to DMSO control treatments (Figure 34 A). However, due to the unclear protein separation, it was not possible to analyze the LC3 conversion in more detail, but in general, SiNP increased the LC3 accumulation. In combination with the PI3K inhibitor LY294002, the LC3 protein expression decreased in comparison to DMSO controls (Figure 34 B). When A431 wt cells were treated with a combination of SiNP and PI3K inhibitors, Wortmannin or LY294002, the autophagy-suppressing factor mTOR was highly active although LC3 accumulated. Interestingly, Survivin-GFP expressing cells activated mTOR in response to the PI3K inhibitor LY294002 but not in response to Wortmannin. In addition, Survivin-GFP expressing cells showed a LY294002-dependent decrease of the Akt expression but not when treated with Wortmannin (Figure 34).

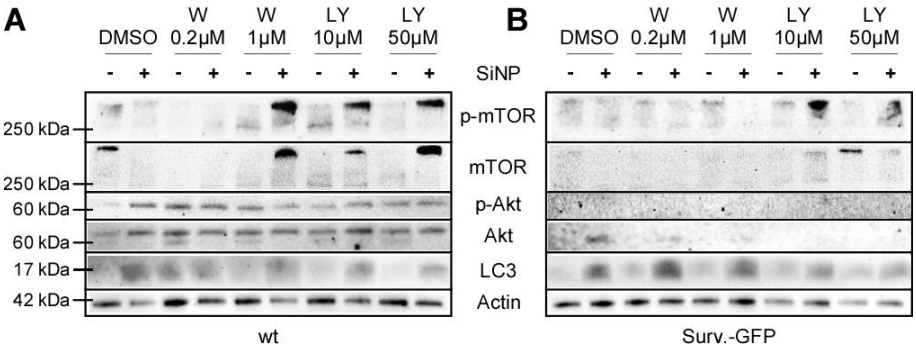

Figure 34. Role of PI3K on the Akt/mTOR pathway. Two different PI3K inhibitors LY294002 (LY) and Wortmannin (W) were examined via immunoblot analysis. Wortmannin and LY294002 were incubated for 2 h in a serum-containing medium before SiNP treatment in a serum-free medium (60 µg/mL, 4 h).

In sum, LY294002 was more potent in inhibiting PI3K/Akt in Survivin-GFP expressing cells than Wortmannin, but not in wild-type cells, indicating Survivins specific role in the PI3K/Akt signaling pathway. However, the PI3K inhibitor LY294002 increased the mTOR activation in combination with SiNP, but not with DMSO. In addition, LC3 accumulated despite mTOR activation. Together the results indicate that SiNP triggered autophagy in a PI3K/Akt/mTOR-independent manner (Figure 34).

The influence of the PI3K/Akt pathway on SiNP toxicity was further examined via cell viability assays. A431 wt and Survivin-GFP expressing cells were incubated with PI3K inhibitors Wortmannin and LY294002 and then exposed to SiNP (Figure 35, Supplementary Figure 16).

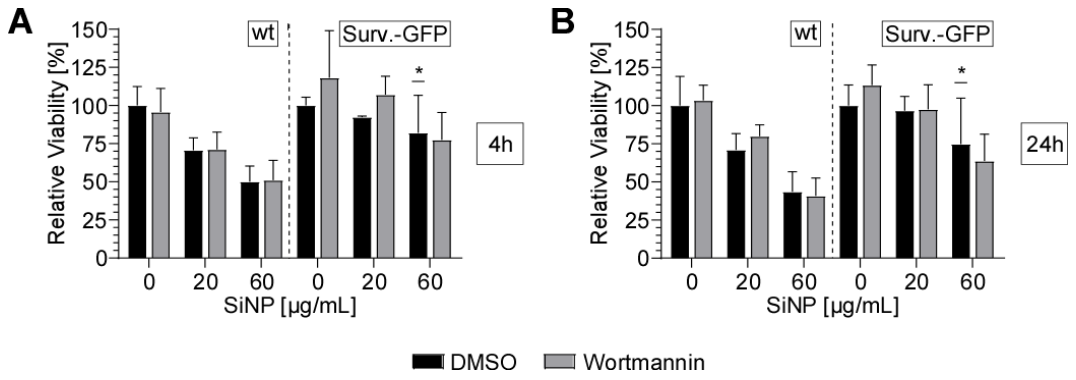

Figure 35. Toxicity of PI3K inhibitor Wortmannin in combination with SiNP. The inhibitor Wortmannin (0.2 µM). was pre-incubated for 2 h in a serum-containing medium before cells were treated with SiNP (60 µg/mL) in a serum-deprived medium for 4 h and up to 24 h. The experiment was exercised three times in triplicates. Statistical analysis was performed via the Anova two-way test, but no significant differences were found comparing DMSO and Wortmannin-treated cells. In addition, A431 wt cells were compared with similar treated Survivin-GFP (Surv.-GFP) expressing cells, exhibiting significances with p*>0.05.

The PI3K inhibitor Wortmannin protected Survivin-GFP expressing cells against starvation and SiNP-induced cell toxicity. In comparison to A431 wt cells, Survivin-GFP expressing cells showed higher viability in the presence and absence of 0.2 µM Wortmannin (Figure 35). Higher Wortmannin concentrations (1 µM) showed no further effect on Survivin-GFP expressing cells. On the contrary, the cell viability decreased with time (Supplementary Figure 16). However, A431 wt cells showed a trend in the presence of 1 µM Wortmannin, improving the cell viability after 4h and after and an additional recovery time of 20 h (Supplementary Figure 16 A). On the other hand, the immunoblot analysis suggested LY294002 to be more potent as PI3K/Akt inhibitor and mTOR activator than Wortmannin, but the cell viability was not significantly influenced in the presence of lower (10 µM) or higher (50 µm) LY294002 concentrations in A431 wt and Survivin-GFP expressing cells (Supplementary Figure 16 B, C). In sum, no. clear synergistic effects were found when SiNP were combined with the PI3K inhibitors Wortmannin and LY294002.

2.7.3 Influence of Autophagy Late-Stage Inhibitor Chloroquine on the Nanoparticle Toxicity

Late-stage autophagy inhibition with the compound Chloroquine (CQ) decreased the cell viability of A431 wt and Survivin-GFP expressing cells in a similar and significant way (Figure 36). The combination of SiNP with CQ decreased the cell viability further, but no synergistic effects were observed, when the combined treatment results were normalized to the single CQ treatment (Figure 36). Over the total treatment range, the combination of CQ with SiNP decreased the cell viability by about 4.48 ± 4.91% in wild-type and 2.98 ± 5.91% in Survivin-GFP expressing cells, compared to SiNP alone. This finding suggests that the cell toxic effects of CQ and SiNP toxicity occur independently from each other.

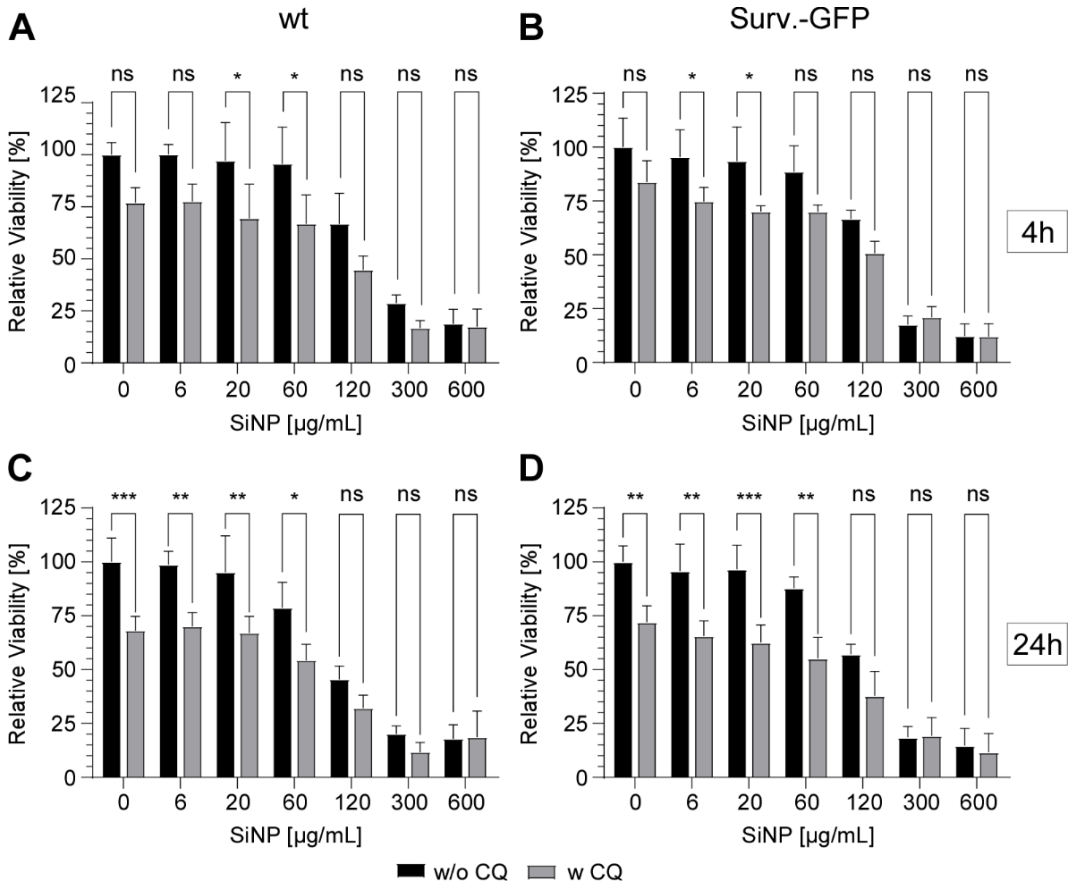

Figure 36. Combinatorial treatment of SiNP with late-stage inhibitor CQ. A-D) Viability test after treatment without (w/o) or with (w) CQ in combination with increasing SiNP concentrations. Autophagy was blocked with 20 µM CQ for 24 h before and during the SiNP treatment. SiNP (60 µg/mL) treatment was performed in a serum-deprived medium for 4 h. Viability was measured via Alamar Blue Assay (4.2.9.1) in the presence (A) or absence (C) of CQ. Alamar Blue Assay for time point 24 h performed without CQ (B, D). The experiments were performed in three independent approaches (n=3). Anova two-way test was used for statistical analysis with p*>0.05, p**<0.005, p***<0.0005, ns=not significant, comparing CQ treated and untreated cells.

2.7.4 SUMMARY

Compound C, and PI3K inhibitors Wortmannin and LY294002 did not enhance the toxicity of SiNP (Figure 33). Furthermore, Compound C decreased the cell viability of A431 wt cells but in turn increased the cell viability of Survivin-GFP expressing cells (Figure 33, Figure 35, Supplementary Figure 16). In sum, the results indicate that the SiNP-mediated autophagy initiation might be PI3K/Akt/mTOR-independent and initiated by alternative pathways such as p38 and/or EGFR (2.6.2). However, interrupting autophagy with late-stage autophagy inhibitor Chloroquine bears a greater potential to increase the toxicity of SiNP than the mTOR addressing, and autophagy suppressing PI3K inhibitors, Wortmannin and LY294002, or autophagy enhancing Compound C.

3 CONCLUSION AND OUTLOOK

3.1 LINEUP OF THE THESIS

The expression of Survivin is limited to mitosis in adult non-malignant tissue except for bone marrow stem cells, thymocytes, and the basal epithelium (Sah et al., 2006; Stauber et al., 2007). The Survivin overexpression is used as diagnostic marker for cancer progression, correlating with enhanced chemoresistance, and a poor survival prognosis (Capalbo et al., 2007; Knauer et al., 2013; Rodel et al., 2012). In addition, recent findings indicated new insight into the Survivin function as a switch between autophagy and apoptosis to promote cancer resistance (Cheung et al., 2020; Hay-Koren et al., 2017). The development of new treatment strategies to bypass these resistance mechanisms is an ongoing process. In the context of new treatment approaches, nanotechnology has gained popularity in the medical field including cancer treatment applications (see section 1.7.1). In the thesis, uncoated amorphous silica nanoparticles (SiNP) of 20 nm size were used as model particles to evaluate Survivins potential role in regulating SiNP-mediated toxicity. To elucidate underlying mechanisms, Survivin expression levels were varied and effects on cell viability and signaling pathways were determined. In a final step, SiNP were combined with various compounds to improve the anti-cancer effect by specifically influencing the autophagy process. The results for each part are discussed in an embedded context.

3.2 SINP-MEDIATED TOXICITY

Initially, the toxicity of SiNP was assessed across a concentration spectrum spanning 0 - 600 µg/mL and delineating non-toxic (0 - 6 µg/mL), subtoxic (>20 - 60 µg/mL), and highly toxic (>60 µg/mL) concentrations, using the epithelial cell line A431. The epithelial cell line A431 was modified to express high Survivin levels via a stable transfected Survivin-GFP plasmid, and on the other hand, was transiently transfected with siRNA against Survivin coding mRNA BIRC5 to knock down the Survivin expression. The experiments unveiled that SiNP of type AmSil20 exert concentration and time-dependent cell toxicity effects on A431 wt and Survivin-GFP expressing cells. Notably, Survivin-GFP-expressing cells demonstrated marked resilience against escalating SiNP concentrations. Variating the experimental settings and handling procedures for the SiNP treatment revealed that the toxicity of SiNP is strongly dependent on the initial exposure time in a serum-deprived medium. The SiNP attached briefly to the cell membrane and 10 min of exposure was enough to decrease the cell viability of A431 cells significantly. On the other hand, the addition of serum to the treatment medium significantly attenuated SiNP toxicity, as a protein corona is likely to form (Docter et al., 2014).

3.3 Survivins Defense Mechanisms against SiNP Toxicity

3.3.1 Survivin-dependent Galectin-1 Regulation as a Defense Mechanism against SiNP Toxicity

The carbohydrate-binding protein family of galectins affects various cell processes in dependence on the localization, cell adhesion, migration, proliferation, and phagocytosis, and manipulates the immunological response (Kruk et al., 2023). Galectins can localize in the cytoplasmic or the nuclear region or be secreted into the extracellular space aside from the typical vesical-based secretion pathways (Vladoiu et al., 2014; Vyakarnam et al., 1998 256).
Immunofluorescence staining of galectin-1 unveiled a distinct cytosolic localization in Survivin-GFP-expressing cells, and a prominent nuclear galectin-1 accumulation in wild-type cells, indicating a relationship between Survivin expression and galectin localization and potentially cytoprotective function.
Indeed, Nam et al. (2017) showed that the extracellular galectin-1 expression promoted the Survivin expression through the integrin β1/FAK/c-Src/ERK/STAT3 signaling pathway in triple-negative breast cancer cells (TNB) (Nam et al., 2017). Downregulation of galectin-1 via siRNA sensitized hepatocellular carcinoma (HCC) cells against apoptosis mediated by the tumor necrosis factor-related apoptosis-inducing ligand (TRAIL), while overexpression of either Bcl-2 or Survivin rescued the cells from galectin-1 dependent apoptosis (Li et al., 2015). Furthermore, Li et al. (2015) unveiled that the galectin-1 expression in HCC correlated with Survivin and Bcl-2 expression, while a knockdown of galectin-1 resulted in Survivin and Bcl-2 attenuation (Li et al., 2015).
The functions of galectins are highly dependent on their cellular localization. Galectin-1 and 3, when present in the nucleus, interact with Gemin 4, which is necessary for the assembly of the spliceosome complex (Park et al., 2001). The nuclear localization of galectin-1 and galectin-3 has been associated with the processes that precede mRNA splicing. Depletion of either galectin has been found to significantly reduce mRNA splicing (Vyakarnam et al., 1997). In addition, Gao et al. (2018) revealed an interaction of galectin-1 with the FKH DNA binding domain of FOXP3, predominantly in nuclei and not in the cytoplasmic area. This interaction interferes with FOXP3 DNA binding and gene regulation abilities, increasing the transcription of oncogenes like Bcl-2 (Gao et al., 2018).
The cytoplasmic localization of galectin-1 and 3 activates the PI3K/Akt pathway, resulting in the phosphorylation and nuclear translocation of beta-catenin (Fang et al., 2007). In the context of cancer cells, nuclear beta-catenin enhances the transcriptional activity, which promotes tumor progression (Ose et al., 2012). However, the cytoplasmic accumulation of galectin-3 activates the anti-apoptotic function of galectin-3 through interaction with Bcl-2 on mitochondria

(Takenaka et al., 2004). The galectin-dependent stimulation of apoptosis in T-cells attenuates the immunological responses against cancer cells promoting the cancer progression (Dalotto-Moreno et al., 2013; Rabinovich et al., 2000). Further, the extracellular galectins play an important role in the immune response development as well (Casals et al., 2018).

In general, galectin-1 carries six cysteine residues, of which three are exposed on the protein surface. Galectin-1 regulatory functions are thereafter redox-sensitive, while the oxidative state is reversible (Guardia et al., 2014). As the experiments revealed an oxidative burst after 30 min, galectin-1 functions are likely affected by oxidation, which might result in an alternate galectin-1 localization. The concentration of cellular ROS plays an important part in galectin dimerization; low ROS levels oxidize monomeric galectin-1 molecules, and high ROS levels can lead to multimer formation or rather galectin aggregations. Galectin-1-dimerization induced by binding to specific ligands can protect galectin-1 from oxidative inactivation (Stowell et al., 2009). On the other hand, the multimeric galectin-1-aggregates form disulfide bridges, disabling galectin-1 binding abilities to glycans and losing pro-apoptotic function in T-cells. (Arthur et al., 2015; Stowell et al., 2009).

Since enhanced Survivin levels influenced the localization of galectin-1 in response to serum deprivation and SiNP exposure the possible advantages behind cytoplasmic and nuclear localization of galectin-1 will be discussed on the base of relevant signaling pathway p44/42 examined in the study.

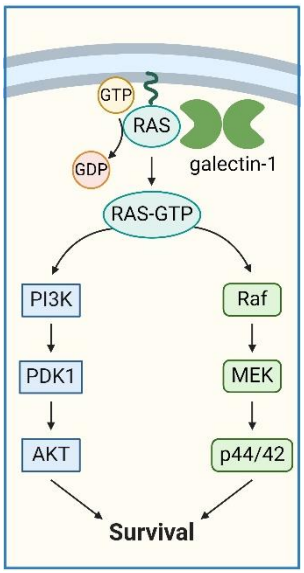

Figure 37. Ras signaling pathway stabilized by galectin-1 at the cytosolic side of the cell membrane. The activation of RAS induces the signal transduction through PI3K/PDK1/Akt and Raf/MEK/p44/42 (ERK) pathways to promote cell survival.

Paz et al. (2001) showed that high expression of galectin-1 correlated with increased levels of H-Ras proteins localized to the inner cell membrane, which is essential for Ras-specific signal transduction. In addition, the workgroup unveiled that active H-Ras recruited galectin-1 to the cell membrane and not the other way around to enhance ERK (p44/42) signaling (Paz et al., 2001; Prior & Hancock, 2012). Furthermore, Ras genes are often highly mutated in tumor cells promoting the malignant transformation of the cell (Prior et al., 2012).

Survivin-GFP expressing cells promoted the cytosolic or rather the membrane-localized galectin-1. The pro-survival MAPK p44/42 was activated fast in response to serum deprivation in Survivin-GFP expressing cells and less in wild-type cells. The results suggest that enhanced Survivin levels favor the cytosolic accumulation of galectin-1, which might stabilize the H-Ras/ERK signaling pathway counteracting moderate cell stress. However, SiNP attenuated the p44/42 activation, indicating that galectin-1 mediated H-Ras stabilization and p44/42 expression cannot withstand high-stress levels. If the galectin-1/Ras/ERK signaling pathway plays a role in Survivin-mediated resistance, has to be evaluated in further experiments by targeting the galectin-1/Ras/ERK signaling cascade with specific inhibitors or other approaches.

3.4 Survivin influences Starvation and SiNP induced Signaling Pathways

3.4.1 Influence of Survivin on the Akt/mTOR and Akt/FoxO Pathway

Under normal growth conditions, Akt acts as a promotor for cell growth by promoting mTOR activity (Dan et al., 2014). The Akt-dependent mTOR phosphorylation leads to a negative feedback loop downregulating the Akt expression after assembly of the mTOR complex 1 (mTORC1) (Bhaskar & Hay, 2007). Several cancer types hyperactivate the serine/threonine kinase Akt to suppress apoptosis by inhibiting the cytochrome C release from mitochondria (Majewski et al., 2004). However, Akt can induce the state of replicative senescence or premature senescence (Nogueira et al., 2008). Noguiera et al. (2008) showed that overexpression of Akt cannot prevent ROS-induced cell death and is, in contrast, sensitizing cells to ROS-mediated apoptosis by inhibiting sestrin 3, a ROS scavenger downstream of FoxO and negative regulator of the Rag/mTORC1 axis (Chen et al., 2010; Nogueira et al., 2008). Further Lu et al. (2013) showed that suppression of FoxO3a via Akt-dependent phosphorylation prevents the expression of ROS scavenger MnSOD (Lu et al., 2013; Nogueira et al., 2008). In addition, Zhao et al. (2010) showed that acetylated FoxO1 in the cytoplasm promotes autophagy and cell death through the interaction with ATG7 (Zhao et al., 2010). This role of FoxO1 is dependent on the dissociation from NAD-dependent deacetylase sirtuin-2 (Sirt2). Since FoxO3 suppressed the expression of FoxO1 the Akt-dependent FoxO3 phosphorylation and inactivation favors the FoxO1 cytoplasmic localization and autophagy initiation (Zhou et al., 2012).

In this context, A431 wt cells responded with an increased Akt activation and increased FoxO1/3 inactivation level to serum-deprived medium and showed a decreased p-Akt and p-

FoxO1/3 level after treatment with SiNP. Elevated Survivin protein levels suppressed the expression and activation of Akt and FoxO1/3a.

The lack of the FoxO1/3a signaling in Survivin overexpressing cells might mediate the resistance against SiNP-mediated toxicity via upregulation of ROS scavenger's sestrin 3 and MnSOD as proposed by different studies (Lu et al., 2013; Nogueira et al., 2008). However, Akt and FoxO1/3a expression and activation as well as autophagy were suppressed in Survivin-GFP expressing cells, compared to wild-type cells. The results suggest a that Survivin expressing cancer cells inactivate the Akt/FOXO pathway to prevent the SiNP induced autophagy-dependent cell death. Simultaneously, enhanced Survivin levels might increase ROS scavenger genes to counteract SiNP-generated ROS.

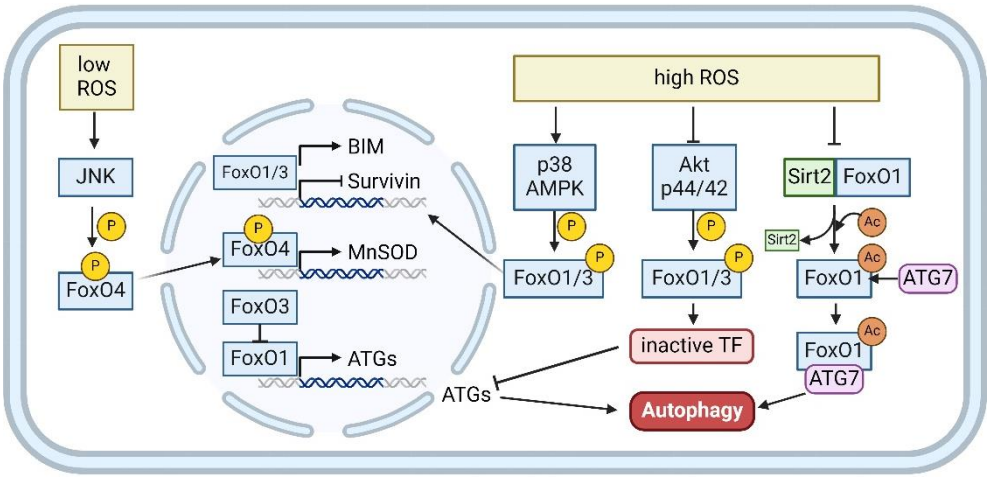

Figure 38. FoxO regulation in response to low and high ROS levels. Low ROS levels active kinase JNK, which phosphorylates FoxO4 leading to the translocation and transcriptional activation to enhance the expression of ROS scavenger MnSOD. High ROS levels stimulate different kinds of kinases such as p38, Akt, and p44/42. The stress kinase p38 phosphorylates FoxO proteins, inducing the transcription of pro-apoptotic genes such as BIM and suppressing pro-survival genes such as Survivin. In general, Akt and p44/42 inhibit the transcriptional activation of FoxO proteins leading to the arrest of FoxO members in the cytosol. Hence the transcription of autophagy-related genes by FoxO1 suppresses autophagy too. FoxO3 can suppress the FoxO1-related gene transcription providing another control switch to the autophagy process. In addition, high ROS levels impair the Sirt2/FoxO1 complex, triggering the acetylation (Ac) of FoxO1. In turn, the autophagy-related gene ATG7 replaces Sirt2 as a complex partner and initiates autophagy. Overall, a feedback loop is established controlling the autophagy flux in response to high ROS levels. Created with Biorender.com

Since several experiments showed that SiNP affect important pro-survival kinases like Akt and p44/42, and on the other hand stress stress-related MAPK p38, they will be discussed here in the context of FoxO signaling.

Overall, Akt-mediated phosphorylation promotes the inactivation of FoxO-dependent gene expression, while MAPK p38 and JNK-dependent phosphorylation of FoxO proteins modulate FoxO protein activity (Figure 38) (Asada et al., 2007; Essers et al., 2004:Yang, 2008 #368). Pan et al. (2017) proposed a mechanism where Akt-dependent phosphorylation of FoxO1

causes the inhibition of FoxO1 tumor suppressive abilities; Akt-mediated phosphorylation of FoxO1 at Ser 319 promotes FoxO1 interaction with the scaffold protein IQ Motif Containing GTPase Activating Protein 1 (IQGAP1) in the cytoplasm, interrupting IQGAP1-mediated phosphorylation of MAPK p44/42 (ERK). Hence Survivin-dependent Akt downregulation might promote IQGAP1-dependent activation of the pro-survival MAPK p44/42 (ERK), which then results in an enhanced resistance against chemotherapeutics and might promote resistance against SiNP toxicity in the thesis context (Pan et al., 2017).

The treatment with SiNP led to a time-dependent activation of stress kinase p38 in A431 wt cells, while p38 was suppressed or delayed in Survivin-GFP expressing cells.

Ho et al. (2012) treated MCF-7 breast cancer cells with a well-documented ROS-inducing agent, Doxorubicin. The treatment activated MAPK p38, which in turn phosphorylated Ser7 on the FoxO3a protein, and induced its nuclear relocation. The p38-activated FoxO3 transcription factor promoted the transcription of cell stress and apoptosis-related genes such as BIM and further suppressed pro-survival factors such as Survivin (Ho et al., 2012) ,(Figure 38).

In this context, suppression of the p38/FoxO3a pro-apoptotic axis might present a resistance mechanism against SiNP toxicity mediated by high Survivin expression levels in cancer cells. FoxO3a was partially relocated into nuclei in A431 wt cells treated with ROS-inducing agent menadione, and SiNP. Furthermore, the enhanced expression of Survivin suppressed the overall expression of the FoxO3a proteins. Together these results support the assumption that Survivin might inhibit the p38/FoxO3a pro-apoptotic axis to act against SiNP toxicity. Indeed, the absence of FoxO transcription factors is related to several cancer types. Those cancer cells exhibit often chromosomal translocations of FOXO genes or have an enhanced miRNA dependent FoxO protein degradation level (Liu et al., 2011; Parry et al., 1994). Overall, the results presented highlight the role of Survivin in the dysregulation of FoxO transcription factors in cancer cells.

3.4.2 Relationship between p38 and Akt

MAPK p38 can directly activate the Akt transcription, elevating the Akt protein level and activity through Akt phosphorylation during myogenesis, but not the other way around (Cabane et al., 2004). A constitutive Akt activity decreases p38 activity, while Akt suppression increases p-p38 under hyperglycemic long-term conditions (Rane et al., 2010). In endothelial cells, the interplay between Akt and p38 decides between survival and apoptosis. Constitutive active Akt inhibits MKK3 due to the Akt-dependent phosphorylation resulting in a declined MKK3/6 activity, which is followed by a suppressed p38 activity, promoting cell survival. On the other hand, a declined Akt activity was related to an increased MKK3/p38 activation and apoptosis (Gratton et al., 2001). Artificially enhanced expression of Survivin suppressed the expression and activation of Akt, but the p38 activity was not enhanced. In contrast, p38 activation was

delayed in response to serum deprivation when Survivin was overexpressed. Further, inhibition of p38 in Survivin-GFP expressing cells increased the resistance against SiNP but did not affect A431 wt cells without and with a siRNA-induced Survivin knockdown. The p38-inhibitor SB203580 can suppress the Akt activation (Lali et al., 2000), but this effect was unfortunately not examined in this relation. However, in addition to serum deprivation SiNP increased the activation of p38, and attenuated Akt in A431 wt cells. A Survivin knockdown amplified the effects, while enhanced Survivin levels attenuated the p38 activation. Overall, these findings suggest suggesting a tight regulative network connecting Survivin, Akt, and p38 that might promote cancer cell resistance against nanoparticle-based drug formulations.

3.4.3 Relationship between Survivin, p38 and SiNP-generated ROS

The interaction between p38 and mTOR and their outcome signal transduction depends strongly on the context of the applied test system. A serum-deprived medium can enhance the cellular ROS level, stimulating AMPK and inactivating mTOR, while additional ROS can overpass AMPK-dependent mTOR inhibition (Hernandez et al., 2011). Hernandez et al. (2011) showed that mTOR is activated by p38 as a survival pathway due to enhanced ROS levels induced by H_2O_2 in cardiomyocytes (Hernandez et al., 2011). This study is supported by findings from Herbele et al. (2019) showing that PI3K/p38 activation under stress conditions can activate mTOR (Heberle et al., 2019). In the used test system, the activation of p38 did not correlate with mTOR activation. On the contrary, mTOR and p38 showed rather both-sided negative regulation. Muranen et al. (2016) showed that mTOR can act as an upstream suppressor of p38, the other way around prolonged mTOR suppression increases p38 activation initiating a proliferation arrest to prevent apoptosis (Muranen et al., 2016).
In addition, activation of MAPK p38 via phosphorylation is a marker for ROS-induced cell stress (Jia et al., 2007). Stress kinase p38 contains a redox-sensitive loop, which is responsible for the dimerization with MKK3 via covalent disulfide bridges (Bassi et al., 2017). Ma et al. (2007) gave evidence that the interaction of p38 with MKK3 is necessary to initiate ROS-induced apoptosis in tubular epithelial cells (Ma et al., 2007). Another study described the MKK3-mediated phosphorylation of p38 as a tumor growth and migration-promoting axis in nasopharyngeal carcinoma. Hence p38 expression correlated with tumor migration and metastasis in metastatic melanoma (Chiang et al., 2020; Naffa et al., 2020). Further, p38 can form heterodimers with MK2 in a phosphorylated or unphosphorylated form. The complexation with the unphosphorylated p38 keeps the complex inside the nucleus by blocking the phosphorylation of MK2. MK2 phosphorylation activates the nucleus export signal translocating the p38-MK2 complex into the cytosol leading to further activation of signal transducing MAPKs (Lukas et al., 2004; Sok et al., 2020). Survivin-overexpressing cells did

not show these dimers in any experiment, but A431 wt exhibited bands corresponding to the p38 complex.

In sum, the expression and activation of MAPK p38 is a crucial regulator determining the faith of cells under stress, promoting cell survival or death. Here, the activation of MAPK p38 is most likely a marker for ROS-mediated stress, inducing cell apoptotic processes (Jia et al., 2007). In addition, MAPK p38 can suppress basal autophagy as well as starvation-dependent autophagy by acting as an allosteric inhibitor for the mATG9-p38IP interaction (Webber & Tooze, 2010). On the other hand, Survivin has a suppressive function onto the p38 activation and p38 dimer formation, leading to the assumption that the suppression of p-p38, and especially the dimer formation might be a main protective mechanism against SiNP-mediated toxicity in Survivin overexpressing cancer cells. The mechanism behind this could involve ROS-reducing processes like the Warburg effect, which was shown to be controlled by Survivin and further indicated in the thesis work (Townley & Wheatley, 2020).

3.4.4 SiNP INDUCE EGFR-MEDIATED EXTRACELLULAR SIGNALING

EGFR is overexpressed in various solid tumors as well as in the used cell line A431 (Zhang et al., 2015). Under normal conditions, EGFR promotes cell survival by activating PI3K/Akt signaling and enhancing mTOR activity, resulting in autophagy suppression (Kwon et al., 2019) and in an enhanced Survivin expression (Wang & Greene, 2005). Various stress stimuli induce the internalization of EGFR without previous activation through phosphorylation by ligands (Tomas et al., 2017). Among others, stress-activated MAPK kinase p38 is responsible for the internalization of EGFR (Tomas et al., 2017). In turn, EGFR stimulates cell survival pathways, including autophagy. The prolonged p38 activation promotes the lysosomal degradation and/or recycling of the internalized EGFR back to the cell surface (Perez Verdaguer et al., 2021; Zwang & Yarden, 2006). In the scope of this work, SiNP activated stress-related MAPK p38 and parallel led to the degradation of EGFR. Introducing ROS scavenger NAC attenuated but did not prevented the EGFR degradation and p38 activation. Kümper et al. (2017) showed that SiNP could directly interfere with EGFR ligand-dependent activation leading to Akt suppression, resulting in decreased cell proliferation (Kümper, 2017). Overall, it is likely that SiNP address the EGFR/PI3K/Akt pathway in EGFR overexpressing cell line A431. The pathway might declare the Akt suppression and the decline of cell viability in A431 wt cells due to SiNP exposure. However, p38 is also mediating EGFR-induced cell death in the EGFR overexpressing cell line A431 (Kozyulina et al., 2013), which might explain the enhanced resistance against SiNP by use of p38 inhibitor SB203580 in Survivin-GFP expressing cells.

3.5 AUTOPHAGY MODULATORS

3.5.1 AMPK-DEPENDENT AUTOPHAGY INITIATION

AMPK is an mTOR inhibitor inducing autophagy under serum-deprived conditions. Starvation of growth factors or amino acids induces the nuclear translocation of AMPK, promoting the expression of autophagy-related genes by stabilizing the coactivator of TFEB-mediated gene transcription, CARM-1 (Shin et al., 2016). Compound C (CC) as an AMPK inhibitor, inhibits AMPK activation and consequently should prevent autophagy, but on the contrary, CC increased autophagy markers. The combination of AMPK inhibitor CC and SiNP did not show synergistic effects. Since AMPK inhibitor CC did not prevent the autophagy characteristic organelle shift in SiNP treated cells, the results indicate an AMPK/mTOR-independent autophagy initiation pathway triggered by SiNP.

Activation of AMPK promotes the change from phosphorylated oxidation to glycolysis by removing mitochondria through mitophagy, reducing the ATP and ROS production (Domenech et al., 2015). In turn, the mitochondrial dysfunction impairs the lysosomal degradation pathway leading to increased lysosomal size and the accumulation of lysosomes and ROS (Demers-Lamarche et al., 2016). Enhanced intracellular ROS levels can activate the MCOLN1 calcium channel on lysosomes to release Ca^{2+}. An increased Ca^{2+} level can activate TFEB as well as autophagy and lysosome-related genes, stimulating the clearance of mitochondria through mitophagy (Zhang et al., 2016). Altogether, an increased ROS level can activate autophagy and in turn, mTORC1 is reactivated due to autophagy-derived amino acids entering the cell cycle process (Rodgers et al., 2014).

The deprivation of glucose and serum promotes the nuclear translocation of GAPDH. The starvation conditions activate AMPK, which initiates the translocation of GAPDH through phosphorylation. In turn, GAPDH activates Sirt1 in the nucleus and stimulates autophagy initiation. The interaction of p-GAPDH with Sirt1 stimulates apoptotic processes in response to permanent stress. (Chang et al., 2015). In more detail the translocation of GAPDH is fine-tuned by AMPK and Akt-mediated phosphorylation; AMPK-dependent phosphorylation induces the nuclear translocation and results in autophagy and apoptosis, while the Akt-dependent phosphorylation arrests GAPDH in the cytoplasm promoting its anti-apoptotic functions (Kwon et al., 2010). Therefore, Akt2 stabilizes GAPDH by complexation and preventing the caspase-independent apoptotic death (Jacquin et al., 2013). Hence GAPDH is downregulated in response to SiNP, treated cells might address the AMPK/GAPDH signaling axis to promote autophagy and apoptosis. However, further examination is required to prove this assumption.

3.5.2 PI3K/AKT/MTOR DEPENDENT AUTOPHAGY REGULATION

Since the Akt expression and activation were inhibited in A431 Survivin-GFP expressing cells the PI3K inhibitors LY294002 and Wortmannin were used in the attempt to decrease the cell viability. The combination achieved no additional cytotoxicity, but the presented data showed that both PI3K inhibitors promoted the activation of the pro-survival regulator mTOR in A431 wild-type and were less effective in Survivin-GFP expressing cells. The results support the assumption of a contra-productive use of PI3K inhibitors alone or in combination with SiNP. In this context, Wang et al. (2017) showed that LY294002 enhances the activation of the pro-survival Akt by phosphorylation specifically in gemcitabine (GEM) resistant pancreatic cancer cells (Y. Wang et al., 2017).

Normal growth conditions promote the PI3K/PDK-1/Akt pathway, while serum and growth factor deprivation enhance the PDK-1 independent calcium/calmodulin-dependent protein kinase kinase 2 (CaMMK2) pathway to phosphorylate Akt at Thr308. The PI3K-independent activation of Akt during starvation improves the cell viability of cancer cells, which might explain the observed vitality of A431 wt cells in a serum-free medium (S. Dai et al., 2016).

Lee et al. (2019) described two pathways that occurred during the SiNP-induced cell death. Besides the caspase-3-dependent cell death induced due to ER stress, Lee showed that SiNP led to the activation of autophagy-mediated necroptosis. Necroptosis was mediated by the PI3K/Akt/eNOS-induced formation of the necroptosome, indicated by receptor-interacting serine/threonine-protein kinase 1 (RIPK1) dependent activation of RIPK3 (Lee et al., 2019). Hence, Survivin-GFP expressing cells suppressed the Akt expression and activation as well as the autophagy initiation; it would be plausible that Survivin overexpression prevents the formation of the necroptosom, elucidating Survivin-mediated resistance against SiNP-induced toxicity. However, further analysis is required to prove this theory in the thesis context.

Overall, PI3K inhibition with Wortmannin or LY294002 had a high impact on the mTOR activation status in SiNP-treated A431 wt and Survivin-GFP expressing cells. Despite Wortmannin being shown to inhibit cell proliferation and further increase cell death in combination with LY294002 (Y. Wang et al., 2017) the PI3K inhibitors showed no significant influence on the SiNP-induced cell toxicity. Conclusively, the combination of PI3K inhibitors LY294002 or Wortmannin with SiNP should be excluded from Survivin-targeting cancer therapies, which are based on SiNP.

4 MATERIALS AND METHODS

4.1 MATERIALS

4.1.1 APPLIANCES

Table 1: Appliances

Appliance	Model	Manufacturer
Agarose Gel System	Mini L	peqLab, VWR, Darmstadt
Array Scan	VTI	Thermo Fisher Scientific, Dreieich
Autoclave	5050 ELV	Tuttnauer, Breda
Cell Counting Device	CASY TTC	OMNI Life Science, Hamburg
Cell Culture Hood	Hera safe	Heraeus Holding GmbH, Hanau
Cell Freezing Container	CoolCell	Biocision, USA
Centrifuge, Benchtop	Mini Spin	Eppendorf, Hamburg
Centrifuge, Benchtop	Centrifuge 5415D	Eppendorf, Hamburg
Centrifuge, Falcons	Heraeus Multifuge 1L-R	Thermo Scientific, Tuttlingen
Chemidoc	MP Imaging System	Bio-Rad Laboratories, München
Crushed Ice Machine	AF 80	Scotsman, Vernon Hills, USA
Fluorescence Reader	Tecan Spark	Tecan, Crailsheim
Freezer (-20 °C)		Liebherr, Bulle, Schweiz
Freezer (-80 °C)	TSX	Thermo Scientific, Dreieich
Fridge		Liebherr, Bulle, Schweiz
Gel Documentation	Multi Genius, Bioimaging system	Syngene, Cambridge
Heating Block	Thermomixer	Eppendorf, Hamburg
Incubator	Hera Cell	Thermo Fisher Scientifc, Dreieich
Incubator	CB 60	Binder, Tuttlingen
Micro Scale	PCB250-3 PCB8000-1	Kern&Sohn, Balingen-Frommern

Appliance	Model	Manufacturer
Microscope, Fluorescence	Axiovert 200M	Zeiss, Oberkochen
Microscope, Cell Culture	Nikon TMS	Nikon, Düsseldorf
Microscope, 2PE	Leica TCS SP8 DIVE	Leica, Wetzlar
Microwave	M730	Philips, Hamburg
Nanophotometer	NanoDrop	Thermo Fisher Scientific, Dreieich
Nitrogen Tank	GT 38	Omnilab AG, Mettmennstetten
pH-Meter	EasyFive	Mettler Toledo, Gießen
Pipette (Multi Channel)	Research plus	Eppendorf, Hamburg
Pipettes	Pipetman Neo P2N, P200N, P1000N, P5000N	Gilson, Limburg-Offenheim
Pipette	Pipetboy acu	INTEGRA Biosciences, Fernwald
Power Supply	PowerPac	Bio-Rad Laboratories, München
Roller mixer	RollerMixer SRT6	Stuart Scientific, Asbach
Scale	ABT 120-SDM	Kern&Sohn, Balingen
SDS Gel System	Mini Protean Cell	Bio-Rad Laboratories, München
Shaker	WS 10	Edmung Bühler GmbH, Hechingen
	Rocker 2d digital	IKA, Staufen
	3D Rocking Shaker	StarLab, Hamburg
Sonicator	Sonoplus mini20	Bandelin, Berlin
	Sonoplus 2070	Bandelin, Berlin
Stirring Plate	Ikama RCT	Ika, Staufen
Thermocycler	T Personal	Biometra, Jena
Thermocycler	One Cycler	VWR, Darmstadt
Turbo-Blotter	Trans-Blot Turbo Transfer System	Bio-Rad Laboratories, München
Ultrafine scale	ABT 120-5DM	Kern&Sohn, Balingen-Frommern
Vortex Mixer	VWR VV3	VWR, Darmstadt
	REAX 2000	Heidolph, Schwabach

4.1.2 CONSUMABLES

Table 2: Chemicals and medium additives

Type	Supplier
Acrylamide (Rotiphorese 30)	Carl Roth, Karlsruhe
Amphotericin B	Sigma Aldrich, Merck, Darmstadt
AlamarBlue	Thermo Fisher Scientific, Dreieich
Agarose	Invitrogen, Karlsruhe
Ammonium persulfate (APS)	AppliChem, Darmstadt
Bovines Serum Albumin (BSA)	AppliChem, Darmstadt
Bradford Protein Assay	Bio-Rad, Dreieich
Bromophenol blue	Sigma Aldrich, Merck, Darmstadt
Casy-Blue	OMNI Life Science, Hamburg
Casy-Ton	OMNI Life Science, Hamburg
Complete Protease Inhibitor	Roche, Penzberg
D-Glucose	AppliChem, Darmstadt
Dimethyl sulfoxide (DMSO)	AppliChem, Darmstadt
Dithiothreitol (DTT)	Carl Roth, Karslruhe
Dulbeccos Modified Eagle Medium (DMEM)	Gibco, Invitrogen, Karlsruhe
Ethylenediaminetetraacetic acid (EDTA)	AppliChem, Darmstadt
Ethidium Bromide	Sigma Aldrich, Merck, Darmstadt
Ethanol	Carl Roth, Karlsruhe
Ethanol, denatured	Höfer Chemie,
Fetal Calf Serum (FCS)	Gibco, Invitrogen, Karlsruhe
G418 – BC	Biochrom AG, Berlin
Glutamin	Gibco, Invitrogen, Karlsruhe
Glycin	AppliChem, Darmstadt
Hoechst 33342	Sigma Aldrich, Merck, Darmstadt
Isopropanol	Fisher Scientific, Schwerte
Lipofectamine® RNAiMax	Invitrogen, Karlsruhe
KCl	Carl Roth, Karslruhe
KH_2PO_4	Carl Roth, Karslruhe
Skim Milk Powder	AppliChem, Darmstadt
Mercaptoethanol	Carl Roth, Karslruhe
$MgSO_4$	AppliChem, Darmstadt
Methanol	Carl Roth, Karslruhe

Type	Supplier
NaCl	Carl Roth, Karlsruhe
$NaHCO_3$	Carl Roth, Karlsruhe
NEAA	Gibco, Invitrogen, Karlsruhe
Opti-Minimal Essential Medium (MEM)	Gibco, Invitrogen, Karlsruhe
PageRuler Plus Prestained Protein Ladder	Thermo Fisher Scientific, Dreieich
Paraformaldehyde	Serva Electrophoresis, Heidelberg
Phosphate Buffered Saline (PBS), sterile	Gibco, Invitrogen, Karlsruhe
Penicillin/Streptomycin (PenStrep)	Gibco, Invitrogen, Karlsruhe
ReBlot strong (10x) Stripping Buffer	Chemicon International
Roswell Park Memorial Institute (RPMI)	Gibco, Invitrogen, Karlsruhe
Sodium Dodecyl Sulfate (SDS)	Carl Roth, Karlsruhe
Tetramethylethylenediamine (TEMED)	Serva Electrophoresis, Heidelberg
Tris(hydroxymethyl)-aminomethane (Tris)	Neolab, Heidelberg
Triton X-100	Sigma Aldrich, Merck, Darmstadt
Tween 20	AppliChem, Darmstadt
Urea	Merck, Darmstadt

Table 3: Laboratory consumables

Type	Supplier
Casy tubes	OMNI Life Science, Hamburg
Cell Culture Bottles T25, T75, T225	Greiner Bio-One, Österreich
Cell Culture Plates 10 cm	Greiner Bio-One, Österreich
Cell Culture Plates 24 well	Greiner Bio-One, Österreich
Cell Culture Plates 96 well	Greiner Bio-One, Österreich
Cell Culture Plates, 8 well	Ibidi, Martinsried
Cell Culture Disks, Microscopy	Mattek, USA
Cell Culture Disks, 4 well Microscopy	Mattek, USA
Cryopreservation Tubes: CryzoTraq Tube 2D	Biozym Scientific GmbH, Hessisch Oldendorf
Falcon Tubes (15 mL, 50 mL)	Greiner Bio-One, Österreich
Micro reaction tubes (0,5 mL, 1,5 mL, 2 mL)	Ratiolab, Dreieich
Micro reaction tubes (5 mL)	Eppendorf, Hamburg
Mini-PROTEAN TGX Precast Gels	Bio-Rad Laboratories, Dreieich

Type	Supplier
Pipettes (2 mL)	Corning, USA
Pipettes (5 mL, 10 mL, 25 mL)	Greiner Bio-One, Österreich
Pipette Tips (10 µL)	Starlab, Hamburg
Pipette Tips (200 µL, 1.000 µL, 5.000 µL)	Falcon, Corning, USA Greiner Bio-One, Österreich Sarstedt, Nümbrecht
Syringe Filter (sterile, 0.22 µm pore size)	Merck Milipore, Darmstadt

4.1.3 ENZYMES

Table 4: Enzymes

Enzyme	Supplier
RNase-free DNase	Qiagen, Hilden
Trypsin LE Express	Gibco, Invitrogen, Karlsruhe

4.1.4 BUFFERS AND SOLUTIONS

Table 5: Buffers and solutions

Type	Composition
0.1% Tween	0.1% Tween 20 in PBS
1% Agarose gel	1% agarose in TAE
1x Dissociation Buffer	62.5 mM Tris, 10% glycerin, 2% SDS, 50 mM DTT, 0.01% bromophenol blue
6x Dissociation Buffer	350 mM Tris-HCl, 30% β-mercaptoethanol, 10% SDS, 30% glycerin, 0.02% bromophenol blue
DNA Loading Buffer	15% glycerin (87%), 3 mM EDTA, 600 mg/l bromophenol blue
Hutner's Trace Elements (HTE)	2.2 g $ZnSO_4 \cdot 7\ H_2O$, 1.1 g H_3BO_3, 0.5 g $MnCl_2 \cdot 4\ H_2O$, 0.5 g $FeSO_4 \cdot 7\ H_2O$, 0.16 g $CoCl_2 \cdot 6\ H_2O$, 0.16 g $CuSO_4 \cdot 5\ H_2O$, 0.11 g $(NH_4)Mo_7O_{24} \cdot 4\ H_2O$, 5 g EDTA, *ad* 100 mL H_2O, pH 6.5
Lysis Buffer	8 M urea, 2% CHAPS, 0.01% bromophenol blue
Milk/PBS	5% skim milk powder in PBS

Type	Composition
PBS	4.3 mM Na_2PO_4, 1.4 mM KH_2PO_4, 137 mM NaCl, 2.7 mM KCl, pH 7.4
PBS-T	0.1% Tween 20 in PBS
PBSTD	0.3% Triton X-100, 1% DMSO in PBS
PBSTD/BSA	1% BSA in PBSTD
PBSTD/FCS	5% FCS in PBSTD
Radioimmunoprecipitation assay buffer (RIPA) Buffer	150 mM NaCl, 50 mM Tris-HCl, 1 mM EDTA, 1% NP-40, 1% Na-deoxycholate, 0.5 mM PMSF, Complete 1/50 mL, 0.1% SDS
SDS Buffer (Stacking gel)	26.6 mL Rotiphorese 30, 125 mM Tris-HCl (pH 6.8), 0.1% SDS, ad 200 mL
SDS Buffer	3 g/l Tris, 14,4 g/l Tris, 1 g/l SDS
Tris-Acetate-EDTA-Puffer (TAE)	4.84 g/l Tris, 2.29 g/l Na·3 H_2O, 1 mM EDTA, pH 8 (HCl)
Tris-HCl	0.5 M Tris, pH 6.8 (HCl)

4.1.5 Commercial Kits and Staining

Table 6: Commercial kits and staining

Type	Supplier
CellROX™ Green Reagent	Thermo Fisher Scientific, Dreieich
CellROX™ Orange Reagent	Thermo Fisher Scientific, Dreieich
CellTiterGlo 2.0	Promega, Mannheim
Clarity Western ECL	Bio-Rad Laboratories, Dreieich
Hoechst 33342	Sigma Aldrich, Merck, Darmstadt
LysoTracker Green DND	Fisher Scientific GmbH, Schwerte
LysoTracker Red DND-99	Fisher Scientific GmbH, Schwerte
MitoTracker Deep Red FM	Fisher Scientific GmbH, Schwerte
Mycoplasma Detection Kit for conventional PCR (Venor®GeM Advance)	Minerva-biolabs GmbH, Berlin
Trans-Blot Turbo RTA Mini PVDF Transfer Kit	Bio-Rad Laboratories, Dreieich

4.1.6 CELL LINES

Table 7: Cell lines

Name	Organism, Entity	Medium	ATCC/Reference
A431	Epidermoid carcinoma	DMEM, 10% FCS, Glutamine, PenStrep	CRL-1555
A431 Survivin-GFP or GFP stably transfected	Epidermoid carcinoma	DMEM, 10% FCS, Glutamine, PenStrep G418 - BC	CRL-1555
293T	Human embryonic kidney	DMEM, 10% FCS, Glutamine, PenStrep	CRL-11268 CVCL_0063
FaDu	Human hypopharyngeal squamous cell carcinoma	DMEM, 10% FCS, Glutamine, PenStrep, 1% NEAA, 1% HEPES, 2% Sodium-Bicarbonat	ATCC-HTB43 CVCL_1218
H441	Human lung papillary adenocarcinoma	RPMI, 10% FCS, Glutamine, PenStrep	HTB-174 CVCL_1561
Iso-Has-1	Human skin angiosarcoma	RPMI, 10% FCS, Glutamine, PenStrep	CVCL_C516

4.1.7 ANTIBODIES

Table 8: Primary antibodies for western blot (WB) and immunofluorescence (IF)

No. intern	Antigen	Host	Clone type	Dilution in WB	Dilution in IF	Supplier No. Suppl.
F2	**Actin**	rabbit	poly	1:2000	1:200	Sigma A2066
B1	**Akt (pan) (C67E7)**	rabbit	mono	1:1000	/	Cell Signaling 4691
B2	**Akt phospho (Ser473)**	rabbit		1:1000	/	Cell Signaling 9271
B41	**Akt phospho (Ser473)**	rabbit	mono	1:1000	/	Cell Signaling 3787S
B85	**Bcl-2 phospho (Ser 70) (5H2)**	rabbit	mono	1:1000	/	Cell Signaling 2827
6	**Bcl-2**	rabbit	poly	1:1000	/	Santa Cruz sc-492
B83	**Beclin-1**	rabbit	poly	1:1000	/	Cell Signaling 3738
F5	**BIM**	rabbit	poly	1:1000	/	Sigma B7929
B92	**Bim (C34C5)**	rabbit	mono	1:1000	/	Cell Signaling 2933
B6	**Cleav.Caspase-3 (Asp175)**	rabbit	poly	1:1000	/	Cell Signaling 9661
F104	**galectin 1**	rabbit	mono	/	1:1000	Thermo Fisher MA5-32779
B12	**GFP**	rabbit	poly	1:1000	/	Acris Antibodies SP3005P
157	**Lamp-1**	mouse	mono	1:1000	1:50	Santa Cruz sc-17768
B79	**LC3A/B**	rabbit	poly	1:5000	1:200	Cell Signaling 4108
B20	**MAP Kinase 1/2 (Erk 1/2)**	rabbit	poly	1:1000	/	Upstate(Millipore) 06-182
B19	**MAPK**					Upstate(Millipore)
B21	**MAPK p38**	rabbit	poly	1:1000	/	Cell Signaling 9212

No. intern	Antigen	Host	Clone type	Dilution in WB	Dilution in IF	Supplier No. Suppl.
B22	**MAPK p38 (Thr180/Tyr182)**	rabbit	poly	1:1000	/	Cell Signaling 9211
B54	**MAPK p44/42 (L34F12)**	mouse	mono	1:1000	/	Cell Signaling 4696
B23	**MAPK p44/42 (Thr202/Tyr204)**	rabbit	poly	1:1000	/	Cell Signaling 9101
B24	**MAPK p44/42 (Thr202/Tyr204)**	rabbit	poly	1:1000	/	Cell Signaling 4370
B84	**mTOR (7C10)**	rabbit	mono	1:1000	/	Cell Signaling 2983
B86	**mTOR phospho (Ser2448) (D9C2)**	rabbit	mono	1:1000	/	Cell Signaling 5536
B62	**NfkB p65 (D14E12)**	rabbit		1:1000	/	Cell Signaling 8242
B34	**SAPK/JNK phospho (Thr183/Tyr185)**	rabbit	poly	1:1000	/	Cell Signaling 9251
B78	**Smac/Diablo (D5S3R)**	rabbit	mono	1:1000	/	Cell Signaling 15108
F33	**Survivin**	rabbit	poly	1:1000	/	Novus Biologicals NB500-201
F96	**Survivin (60.11)**	mouse	mono	1:1000	/	OriGene TA301425
F38	**Tubulin α**	mouse	mono	1:1000	/	Sigma T5168
B38	**Tubulin β**	rabbit	mono	1:1000	1:1000	Abcam ab179513
F39	**Tubulin γ**	mouse	mono	1:1000	/	Sigma T6557

Table 9. Secondary antibodies for western blot (WB) and immunofluorescence (IF)

No. intern	Antigen and Fluorophore	Host	Dilution in WB	Dilution in IF	Supplier No. supplier
B73	**α-mouse (HRP)**	horse	1:5000		Cell Signaling 7076
B74	**α-rabbit (HRP)**	goat	1:5000		Cell Signaling 7074
n.a	**α-mouse (FITC)**	donkey		1:200	Abcam ab6812
n.a.	**α-rabbit (FITC)**	goat		1:200	
n.a.	**α-mouse (Cy3)**	goat		1:300	Dianova 115-165-062
n.a.	**α-rabbit (Cy3)**	goat		1:500	Dianova 111-165-003

4.1.8 NANOPARTICLES

Table 10: Nanoparticles

Name	Feature	Supplier/Reference
AmSil20/ NexSil^{TM} 20	Amorphous silica NP, 32 nm, -15 mV	Nyacol, USA
Kisker$^{green/red}$	Commercial silica NP, 50 nm, green/red fluorescent	Kisker Biotech, Steinfurt

4.1.9 SOFTWARE

Table 11: Software

Program	Supplier/Reference
Axiovision	Zeiss, Oberkochen
Benchling	Benchling [Biology Software]. (2020). Available from https://benchling.com.
BLAST, GeneBank	National Center for Biotechnology Information (NCBI). Bethesda (MD): National Library of Medicine (US), National Center for Biotechnology Information. Available from https://www.ncbi.nlm.nih.gov/
Canvas X 2019	Canvas GFX, Inc., Boston, USA
CLASTR	CLASTR, the Cellosaurus STR Similarity Search Tool, Version 1.4.4. Available from https://web.expasy.org/cellosaurus-str-search/
Endnote	Clarivate Analytics, California
Image Lab	Bio-Rad Laboratories GmbH, Feldkirchen
Fiji/ImageJ	See Schindelin et al. (2012) https://imagej.nih.gov/ij/
GraphPad PRISM 8/ 9	Graphpad Software, Inc., San Diego, USA
Leica Image Suite	Leica, Wetzlar

4.2 METHODS

4.2.1 CELL BIOLOGICAL METHODS

4.2.1.1 CELL STOCK PREPARATION

Cell stocks were prepared from confluent flasks and dissolved with trypsin according to the flask size by incubation on a heat plate (37°C) (Table 12). The detached cells were suspended in full growth medium and moved into a falcon for washing (1500 rpm, 5 min, RT). For long-term storage in a nitrogen tank, FCS was prepared with 10% DMSO. The washed cell pellets were gently mixed with the according volume of FCS/ 10% DMSO and aliquoted as 1 mL in cryopreservation tubes (Biozyme, Hess. Oldendorf). The cryopreservation tubes were inserted into a cell freezing container (Biosicion, USA) and cooled down for 24 h in a -80°C freezer (Thermo Scientific, Dreieich) before the samples were moved into the nitrogen tank for long-term storage.

Table 12. Cell stock preparation. Required components for preparing cell stocks for long-term storage in a nitrogen tank according to the number of stocks and used flask size.

Culture area (cm^2)	Trypsin volume (mL)	FCS+ 10% DMSO (mL)	Amount of stocks
25	0.5	1	1
75	1.5	3	3
175	3.0	5	5

4.2.1.2 THAWING OF CELL STOCKS AND CELL CULTURE

Frozen cells in cryopreservation tubes were stored on ice until further steps were performed. The cryopreservative tubes were swirled in a preheated water bath (37°C) until only a little ice remained in the samples. In a sterile environment, cells were suspended in 5 mL FCS and washed and pelleted at 1500 rpm for 5 min at RT. Next, the supernatant was removed with a glass Pasteur pipette. The pellet was suspended in full growth culture medium and seeded into a small culture flask. Cells were cultured at 37°C and 5% CO_2 until further steps such as medium change or cell division (splitting) were required. Splitting was performed in general every two days according to the cell growth rate. For the cell splitting, cells were rinsed once with PBS and trypsinized with the according trypsin volume (Table 12). The treated flasks were incubated on a heat plate (37°C) to detach the cells. Then, cells were suspended in full growth medium and divided according to the required cell density for further cultivation and/or experimental demands.

4.2.1.3 MYCOPLASMA TEST

After one week of cultivation of newly thawed cells, cells were tested for mycoplasma contamination. The test was performed with the Venor®GeM Advance Kit (Minerva-Biolabs, Berlin) according to the manufacturer's instructions. Further test requirements included a 1.5% agarose gel, supplemented with 12 µL ethidium bromide onto 35 mL liquid agarose. The gel electrophoresis was performed for 30 min, 100 V in TAE buffer. Then the Gels were documented with an imaging system using UV light (Multi Genius, Syngene, Cambridge).
Only mycoplasma-negative cells were further cultivated in a normal growth medium, otherwise, cells were treated with a medium supplemented with plasmocin to eliminate the mycoplasma contaminations.

4.2.1.4 CELL SEEDING AND COUNTING

For cell seeding cells were counted with an automated cell counting device (Casy, OMNI Life Science, Hamburg). For automized cell counting, each cell line was pre-established by incubating the cell suspension with 200 µL Casy Blue Reagent for 10 min to determine the parameters for dead cells. Dilution in CasyTon® was prepared to set up parameters for viable cells. Following measurements with the Casy® TTC system (OMNI Life Science, Hamburg) were performed with 50 µL cell suspension in 10 mL CasyTon®. Cells were counted in three cycles while analyzing a 500 µL volume for each round and calculated the mean cell number per milliliter as well as the cell viability. The mean value was used to adjust the cell number to experimental requirements. If not described otherwise, cells were seeded as follows:

Table 13. Cell seeding. General cell seeding numbers to reach the experimental requirements after 24 h cell culture for different test systems.

Experimental system	**Cell number/cavity**	**Medium volume**
96-well plate	$1 \cdot 10^4$	200 µL
48-well plate	$2 \cdot 10^4$	200 µL
24-well plate	$5 \cdot 10^4$	0.5 mL
8-well ibidi slide	$1 \cdot 10^4$	200 µL
4-well cell culture dish	$2 \cdot 10^4$	0.5 mL
Cell culture dish	$1 \cdot 10^5$	2 mL
10 cm cell culture plate	$2 \cdot 10^6$	10 mL

In general, cells were ready to use for treatments after overnight cultivation. For special treatments with a duration of 48 h cells were seeded with an adjusted cell number to meet the experimental requirements for the main treatment time after 48 h.

4.2.2 TREATMENTS

4.2.2.1 TREATMENT WITH SINP

The SiNP concentrations were adjusted first in deionized water in a manner that final concentrations could be prepared 1:1000 in a serum-free medium. Before the SiNP treatment cells were washed three times with a serum-free medium to remove remaining serum proteins. Cells were treated for 2 h or 4 h with SiNP in a serum-free medium or according to the experimental settings. For later time points SiNP containing medium was removed and cells were rinsed three times with PBS, then serum containing full growth medium was added for prolonged incubation for up to 24 h.

Table 14. SiNP treatment volume according to the used cell culture systems.

Experimental system	**Treatment volume**
96-well plate	100 µL
48-well plate	100 µL
24-well plate	500 µL
8-well ibidi slide	100 µL
4-well cell culture dish	500 µL
Cell culture dish	1 mL
10cm cell culture plate	10 mL

4.2.2.2 TREATMENT WITH AUTOPHAGY MODULATORS AND ROS SCAVENGERS AND INDUCERS

The influence of Survivin on SiNP-mediated toxicity in the context of autophagy-mediated processes was investigated using different autophagy modulators and further ROS-inducing or scavenging agents listed in Table 15. Table 15 gives a summary of functions and the treatment procedures as well as used concentrations applied generally in the experiments.

Table 15. Overview of used chemical inhibitors and ROS scavengers or inducers used in the experiments.

Autophagy modulators	**Function**	**Concentration**	**Incubation procedure**
Chloroquine	Late-stage autophagy inhibitor	20 µM	24 h before treatment and during the treatment
Compound C	AMPK inhibitor, autophagy inhibitor	5 µM	2 h before treatment or parallel to treatment
LY294002	PI3K inhibitor, autophagy initiator	10 µM, 50 µM	2 h before treatment
Wortmannin	PI3K inhibitor, autophagy initiator	0.2 µM, 1 µM	2 h before treatment
ROS modulators	**Function**	**Concentration**	**Incubation procedure**
N-acetylcysteine (NAC)	ROS scavenger	5 µM	2 h before treatment
Vitamin C (Vit C)	ROS scavenger	200 µM	2 h before treatment
Menadione	ROS inducer	50 nM	1 h

4.2.3 Protein Analysis

4.2.3.1 Cell Lysate Preparation for Western Blot Analysis

The preparation of cell lysates was carried out on ice during the whole preparation time. Cells were treated in 10 cm cell culture dishes and were scraped from the dish surface for harvesting. Cells were resuspended fast and carefully with a 10 mL pipette. The cell suspension was collected in a 15 mL falcon tube. Pelleting was carried out at 4°C, 1500 rpm for 5 min. Cells were washed once by resuspending in ice-cold PBS and by repeated pelleting. The medium-free cell pellet was mixed gently with 30-100 µL RIPA lysate buffer according to the pellet size. Cell lysis was done by sonification (50-90% amplitude, 0.5 s pulses over 30 s, Sonoplus mini20, Bandelin, Berlin) for 20 minutes. Between the sonification steps the lysates were incubated for 5 min on ice to prevent overheating and protein damage of the samples. After lysis, non-dissolved cell debris were removed by centrifugation (13000 rpm, 4°C, 20 min). The clear supernatant was aliquoted for storage in a -80°C freezer or was used directly for protein analysis. The lysate protein concentration was determined by a Bradford probe (4.2.3.2).

4.2.3.2 Bradford Test determining Protein Concentration

A commercial Bradford stock solution (Bio-Rad, Dreieich) was diluted 1:4 with deionized water. Cell lysates were diluted 1:1000 in deionized water. Each sample was submitted into three wells with 120 µL of the dilution. On a sun-protected surface, 40 µL of the Bradford solution was added to each well. The 96-well plate was incubated in the dark at RT for 5 minutes and read in a commercial plate reader (TECAN Sparks, Crailsheim, Schweiz) immediately after incubation. Absorption was detected at 595 nm. Protein concentration was determined with a standard curve, which was created under the same test conditions with different concentrations of BSA (Figure 39).

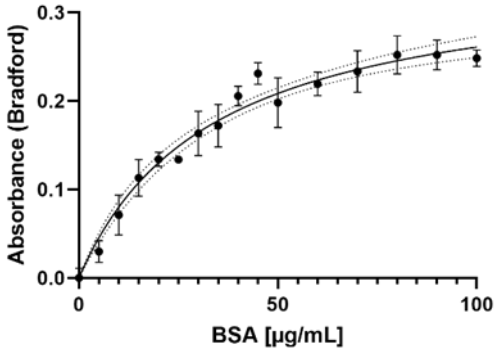

Figure 39. Bradford standard curve for extrapolation. Created with GraphPad Prism Software.

4.2.3.3 Protein Separation via SDS-PAGE

For the SDS page analysis, a 12% SDS gel was prepared and topped with a stacking gel on top. First, the 12% SDS gel was mixed as listed in Table 16. A 1.5 mm thick glass chamber was cleaned with isopropanol before the liquid SDS gel was poured in. The gel edge was smoothed with isopropanol. After 1 h at RT, the gel polymerized completely, and excess isopropanol was removed carefully with a lint-free paper tissue. The stacking gel was prepared as listed below and a pocket comb was inserted. After additional time for polymerization (1 h, RT) the filled glass chamber was transferred into a plastic bag and incubated in a running buffer at 4°C overnight. Alternatively, commercial gels were used in indicated experiments (Mini-PROTEAN TGX Precast Gel, Bio-Rad Laboratories, Dreieich).

Samples with determined protein content were diluted in HPLC-H_2O to 50-100 ng (30 µL for a 10-pocket comb or in 20 µL for a 12-pocket comb) and mixed with 6x dissociation buffer. Then, samples were incubated at 95°C, 300 rpm for 5 min. Impurities were spun down at 2000 rpm for 5 min to prevent clogging during the SDS-Page run. The sample supernatant and a protein ladder (8 µL, PageRuler Plus Pre-Stained Protein Ladder, Thermo Fisher Scientific) were applied into the gel pockets. Electrophoresis was performed at 80 V until samples were concentrated in the stacking gel resp. in a commercial ready-to-use gel. Separation was carried out at 100 V for 1 h or intended protein size separation.

Table 16. SDS-Page. SDS-Page gel is composed of a separating gel and a stacking gel. The gels are composed as follows.

Separating gel (10%)	**Volume**
SDS buffer	2.7 mL
Acrylamide	3.3 mL
Water	4 mL
APS (10%)	100 µL
TEMED	10 µL
Stacking gel	**Volume**
Stacking gel buffer	5 mL
APS (10%)	50 µL
TEMED	5 µL

4.2.3.4 WESTERN BLOT ANALYSIS

The separated SDS-Page gel was blotted onto a PVDF membrane (30-45 min, 0.8 Amp, 20 V). For that, the PVDF membrane was equilibrated in methanol, and commercial transfer stacks (Trans-Blot Turbo Mini-size-Transfer Stacks, Bio-RAD, Dreieich) were soaked in transblot buffer. The gel was detached from the glass chamber and a PVDF membrane was placed on the gel without enclosing air bubbles. A soaked transfer stack was placed on top and air bubbles were removed carefully with a roller. The construct was placed upside down in a cassette of a turbo blotter (Bio-Rad Laboratories, München) and a second stack was put on the gel. Air bubbles were removed again. Additional transblot buffer was poured over the stacks to prevent drying out during the blotting process. After blotting, the membrane was washed with PBS or TBS at 25 rpm, 5 min before blocking with milk/PBST (5% milk, 0.1% Tween, 1x PBS) or BSA/TBST (5% BSA, 0.1% Tween, 1x TBS) for at least 1 h at RT. The primary antibodies were prepared in the respective blocking solution overnight at 4°C while shaking. Membranes were washed three times with PBS or TBS before HRP-coupled antibodies were added for 1 h at RT while shaking at 10 rpm. The washing step was repeated and the ECL substrate was directly added at the ChemiDOC (Bio-RAD Laboratories, München) working place to detect luminescence signals from specific antibody-bound protein bands. Reblotting was performed with a 1x reblotting buffer (Chemicon International) for 10 min at RT while shaking at 10 rpm to strip the used antibodies off the membrane. Washing was repeated and the membrane was finally usable for another round of antibody detection, starting from the membrane blocking. Applied antibodies are listed in Table 8 and Table 9.

4.2.3.5 AUTOPHAGY TURNOVER ASSAY

To track the autophagy process LC3-Iconversion to LC3-II was determined by western blot analysis (4.2.3.4). The ordinary treatment was supplemented with 20 µM Chloroquine (CQ) to prevent LC3-II degradation by interrupting late-stage autophagy. For that, cells were pre-treated for 24 h with CQ, and additional CQ was added to the ordinary treatment. Samples of both approaches were analyzed on one gel run followed by a western blotting of LC3. The introduction of CQ allows autophagy initiation but prevents the degradation of LC3-II resulting in the accumulation of LC3-II. The comparison of both treatments allows us to conclude autophagy initiation, autophagy interruption, and autophagy turnover (Figure 14).

4.2.4 TRANSFECTION

4.2.4.1 REVERSE TRANSIENT TRANSFECTION OF SIRNA WITH LIPOFECTAMINE® RNAIMAX

Reverse transfection was carried out to silence the translation of the Survivin protein by delivering siRNA against Survivin coding BIRC5-mRNA (siBIRC5). Reverse transfection was performed according to the manufacturer's instructions and was further adapted for the experimental demands (Table 17). First, the transfection complex was formed in 24-well plates or cell culture dishes (ø 10 cm), see Table 17. The complex was incubated for 10-20 min at RT protected from light.

Table 17. Composition of the RNAiMax transfection complex for specific treatment volumes and cell numbers. Transfection was performed with a final siRNA concentration of 10 nM.

Complex components	**10 cm dish**	**24-well**	**48-well**	**8-well (ibidi)**	**4-well dish**
siRNA (20 µM)	13.2 µL	4.2 µL	1.05 µL	1.05 µL	0.765 µL
Lipofectamine® RNAiMax/ well	20 µL	3 µL	1 µL	1 µL	1 µL
OptiMEM-medium	2 mL	50 µL	15µL	15.8 µL	115.8 µL
Cells/ well	$1 \cdot 10^6$	$7.5 \cdot 10^4$	$3.5 \cdot 10^4$	$2.7 \cdot 10^4$	$4 \cdot 10^4$
Transfection medium	10 mL	1 mL	350 µL	300 µL	579 µL

Cells were harvested with trypsin (Table 12) and resuspended in a transfection medium (DMEM medium supplemented with FCS and glutamine but without antibiotics). The cell number was determined with the Casy TCC system (4.2.1.4) and the required cell number was transferred into a 15 mL or 50 mL Falcon. Cells were washed with a transfection medium by

centrifugation (1500 rpm, 5 min, RT). The antibiotic-free cell pellet was resuspended in a transfection medium to achieve the required cell number/ mL. The cell suspension was added to the transfection complex and incubated for 24 h in an incubator (37°C, 5% CO_2) before the transfection medium was removed and treatment started.

4.2.5 Fixation and Staining of Cells for Microscopy

4.2.5.1 Fixation Procedure

Microscopy was performed with a determined cell number with living or fixed cells in 8-well ibidi slides, or 4-well and 1-well cell culture dishes with a glass bottom. Living cells were imaged directly when the preferred time point was reached; otherwise, cells were fixed after the treatment with 4% PFA at RT for 15-20 min. For additional staining steps, cells were permeabilized with 0.1% Triton-X 100 in PBS for 5 min at RT. Cells were washed three times with PBS between each step.

4.2.5.2 Staining of Nuclei

Nuclei were stained with Hoechst 33342 reagent. For fixed cells, 12.5 µg/mL Hoechst in PBS was incubated for 10-20 min at RT. Living cells were incubated with 2 µg/mL Hoechst in cell culture medium for a maximum of 10 min at 37°C, 5% CO_2. The remaining staining solution was removed, and cells were washed three times with PBS before additional steps were performed.

4.2.5.3 Staining with Antibodies

For immunofluorescence staining with primary and fluorescence-labeled secondary antibodies cells had to be fixed and permeabilized (4.2.5.1). Optional nuclei staining (4.2.5.2) was performed before antibody staining was carried out.
Primary and secondary antibodies were diluted in 5% BSA/PBS. Antibody dilutions are listed in Table 8 and Table 9. Samples were blocked with 5% BSA/PBS for 30 min at RT before primary antibodies were incubated overnight at 4°C or for 1-2 h at RT respectively. Unbound antibodies were removed by washing three times with PBS. The blocking step was repeated, and the secondary antibody was incubated for 1 h at RT. Then samples were washed with PBS, and additional PBS was added, to keep the cells from drying out during the microscopy session. Stained cells were analyzed directly or stored in PBS at 4°C until analysis was continued.

4.2.5.4 Staining of Mitochondria

Mitochondria were stained with 50 ng/mL live cell staining Mitotracker deep red (Fisher Scientific GmbH, Schwerte) for 30 min in an incubator (37°C, 5% CO_2). Optionally, Hoechst was pre-diluted and added at a final concentration of 2 µg/mL for 10 min before the incubation time for Mitotracker staining had elapsed. Cells were carefully washed three times with PBS and examined microscopically directly in a serum-containing growth medium.

4.2.5.5 Staining of acidic Bodies with Lysotracker Dyes

Acidic bodies were stained with Lysotracker dyes (Fisher Scientific GmbH, Schwerte). First, the Lysotracker dye stock solution was pre-diluted in serum-free medium 1:1000 to a concentration of 1 mM. The final concentration of 50 nM was reached by a 1:20 dilution in a serum-free medium. Before the staining with Lysotracker dyes cells were washed three times and then incubated for 30 min with Lysotracker containing medium at 37°C, 5% CO_2. Imaging was performed directly after incubation time ended to avoid artifacts appearing under life-staining conditions.

4.2.5.6 Staining of ROS with CellROX Reagents

Reactive oxygen species were detected with either live cell staining CellROX orange or fixable staining CellROX green (Thermo Fisher Scientific, Dreieich). After treatment, CellROX reagent was diluted in cell culture medium to a final concentration of 50 ng/mL and incubated for 30 min at 37°C, 5% CO_2. Optional, Hoechst was pre-diluted and added to a final concentration of 2 µg/mL 10 min before incubation time for the CellROX staining was up. Samples stained with CellROX orange were analyzed immediately. Cells stained with CellROX green were fixed as described in section 4.2.5.1 and analyzed directly or otherwise within 24 h, because despite the cell fixation CellROX green is bleaching out and therefore samples were discarded after 24 h. CellROX staining was analyzed via microscopy or array scan high-content screening.

4.2.6 Microscopy

Samples were imaged with a Zeiss Axiovert microscope (Oberkochen, Schweiz) with automated or fixed excitation time adjusted to the experimental demands. Images were analyzed with Leica image suite and Image J software and prepared for export to Canvas X 2019 image software.

4.2.7 Fluorescence-activated Cell Sorting (FACS) via Flow Cytometry

Stably transfected A431 cells were sorted for high, moderate, and low expression of the introduced fusion protein Survivin-GFP for the GFP fluorescent tag by the CFFC PKZI facility, University Medicine Mainz. For the cell sorting procedure, two big cultivation flasks with a confluence of 90% were trypsinized with 3 mL trypsin and incubated on a heat plate (37°C) to detach and harvest the cells. The procedure was stopped with serum-containing medium, and cells washed once at 1500 rpm, 5 min at RT. Then $10 \cdot 10^6$ cells/mL were resuspended in 1 mL sorting solution (PBS/ 2% FCS/ 50 mM EDTA). Negative control cells were harvested from one small culture flask and prepared according to the described protocol. Right before the cell sorting started, cell clumps were removed by putting the cells through a 70 µm nylon mesh to avoid blocking the used nozzle. Finally, sorted cells were collected in FCS to minimize cell death until further cultivation (4.2.1.2).

4.2.8 High-Content-Analysis via Array Scan

High content analysis was applied to analyze treatments on the single-cell level. Measurements were performed on an Array Scan VTI (Thermo Fisher, Dreieich) on live or fixed cells in 96-well or 24-well plate format. Stained nuclei (4.2.5.2) were used to set up a mask to identify objects. The algorithm of the Target Activation Assay was used at fixed excitation times for CellROX orange and the Translocation Assay algorithm for CellROX green stained samples. For the Target Activation Assay, a circular mask was set up to a diameter of either three or five pixels around valid objects to define the region of interest (CellROX orange staining). For the Translocation assay, two regions of interest were defined as follows: First, Hoechst-stained nuclei were validated as objects and determined as the first region of interest. A second circular mask around the nuclei with a diameter of three pixels was created to depict CellROX green intensity in the cytoplasm. For each sample triplicates were prepared and at least 5000 cells were analyzed per well. Data was exported as the average value per cell format and analyzed further with GraphPad PRISM software.

4.2.9 Biochemical Assays

4.2.9.1 Cell Viability Assay via Alamar Blue Assay

Cell viability measured with Alamar Blue was performed after finished treatments with 1:10 diluted Alamar Blue in serum-containing medium (1 h, 5% CO_2, 37°C). In the environment of viable cells, Alamar Blue dye resazurin is reduced to a red fluorescent molecule which can be

detected at 550 nm excitation and 595 nm emission in a Tecan Spark® plate reader (Crailsheim, Schweiz). The background was determined from culture medium samples without cells containing Alamar Blue reagent. The background was subtracted, and the cleared datasets were normalized to untreated control samples. For further analysis, GraphPad Prism software was used. Optionally, cells were washed after the read-out and incubated in a fresh medium until later time points were reached for repeated analysis with Alamar Blue reagent.

4.2.9.2 Cell Viability Assay via CellTiterGlo Reagent

Additionally, cell viability was determined by the ATP content that correlates with the number of viable cells. For ATP measurement CellTiter-Glo® 2.0 (Promega, Mannheim) was performed in 96-well plates in triplicates. The assay was carried out after the treatment. For that, the supernatant was reduced to 100 µL, and an equivalent amount of CellTiterGlo reagent was added to lyse the cells. The plate was incubated for 2 min on a plate shaker at 300 rpm at RT. Additional incubation for 5 min at RT in the dark was applied before the cell lysate was transferred into a white luminescence plate. Quantum dots, which can interfere with the detector, were avoided through equilibration of the luminescence plate for 3 min in the closed Tecan Spark cassette before measurement started.

5 REFERENCES

Abulikemu, A., Zhao, X., Qi, Y., Liu, Y., Wang, J., Zhou, W., Duan, H., Li, Y., Sun, Z., & Guo, C. (2022). Lysosomal impairment-mediated autophagy dysfunction responsible for the vascular endothelial apoptosis caused by silica nanoparticle via ROS/PARP1/AIF signaling pathway. *Environ Pollut, 304*, 119202. https://doi.org/10.1016/j.envpol.2022.119202

Aguirre-Ghiso, J. A., Estrada, Y., Liu, D., & Ossowski, L. (2003). ERK(MAPK) activity as a determinant of tumor growth and dormancy; regulation by p38(SAPK). *Cancer Res*, *63*(7), 1684-1695. https://www.ncbi.nlm.nih.gov/pubmed/12670923

Ahmad, T., Aggarwal, K., Pattnaik, B., Mukherjee, S., Sethi, T., Tiwari, B. K., Kumar, M., Micheal, A., Mabalirajan, U., Ghosh, B., Sinha Roy, S., & Agrawal, A. (2013). Computational classification of mitochondrial shapes reflects stress and redox state. *Cell Death Dis*, *4*(1), e461. https://doi.org/10.1038/cddis.2012.213

Aits, S., & Jaattela, M. (2013). Lysosomal cell death at a glance. *J Cell Sci*, *126*(Pt 9), 1905-1912. https://doi.org/10.1242/jcs.091181

Aits, S., Kricker, J., Liu, B., Ellegaard, A. M., Hamalisto, S., Tvingsholm, S., Corcelle-Termeau, E., Hogh, S., Farkas, T., Holm Jonassen, A., Gromova, I., Mortensen, M., & Jaattela, M. (2015). Sensitive detection of lysosomal membrane permeabilization by lysosomal galectin puncta assay. *Autophagy*, *11*(8), 1408-1424. https://doi.org/10.1080/15548627.2015.1063871

Akamatsu, M., Vasan, R., Serwas, D., Ferrin, M. A., Rangamani, P., & Drubin, D. G. (2020). Principles of self-organization and load adaptation by the actin cytoskeleton during clathrin-mediated endocytosis. *Elife*, *9*. https://doi.org/10.7554/eLife.49840

Akpinar, M. Y., Simsek, G. G., Aksoy, E. K., Sapmaz, F. P., Kantarci, S., Uzman, M., & Nazligul, Y. (2020). Survivin expression starts before hepatocellular cancer development in the liver of chronic hepatitis B patients: a pilot, cross-sectional study. *Prz Gastroenterol*, *15*(2), 138-143. https://doi.org/10.5114/pg.2019.87081

Albadari, N., & Li, W. (2023). Survivin Small Molecules Inhibitors: Recent Advances and Challenges. *Molecules*, *28*(3). https://doi.org/10.3390/molecules28031376

Albitar, L., Pickett, G., Morgan, M., Wilken, J. A., Maihle, N. J., & Leslie, K. K. (2010). EGFR isoforms and gene regulation in human endometrial cancer cells. *Molecular Cancer*, *9*(1), 166. https://doi.org/10.1186/1476-4598-9-166

Alvarez-Meythaler, J. G., Garcia-Mayea, Y., Mir, C., Kondoh, H., & ME, L. L. (2020). Autophagy Takes Center Stage as a Possible Cancer Hallmark. *Front Oncol*, *10*, 586069. https://doi.org/10.3389/fonc.2020.586069

Andersson, K. M., Turkkila, M., Erlandsson, M. C., Bossios, A., Silfversward, S. T., Hu, D., Ekerljung, L., Malmhall, C., Weiner, H. L., Lundback, B., & Bokarewa, M. I. (2017). Survivin controls biogenesis of microRNA in smokers: A link to pathogenesis of rheumatoid arthritis. *Biochim Biophys Acta Mol Basis Dis*, *1863*(3), 663-673. https://doi.org/10.1016/j.bbadis.2016.11.033

Andersson, S. E., Svensson, M. N., Erlandsson, M. C., Dehlin, M., Andersson, K. M., & Bokarewa, M. I. (2012). Activation of Fms-like tyrosine kinase 3 signaling enhances survivin expression in a mouse model of rheumatoid arthritis. *PLoS One*, *7*(10), e47668. https://doi.org/10.1371/journal.pone.0047668

Arruebo, M., Vilaboa, N., Saez-Gutierrez, B., Lambea, J., Tres, A., Valladares, M., & Gonzalez-Fernandez, A. (2011). Assessment of the evolution of cancer treatment therapies. *Cancers (Basel)*, *3*(3), 3279-3330. https://doi.org/10.3390/cancers3033279

Arthur, C. M., Baruffi, M. D., Cummings, R. D., & Stowell, S. R. (2015). Evolving mechanistic insights into galectin functions. *Methods Mol Biol*, *1207*, 1-35. https://doi.org/10.1007/978-1-4939-1396-1_1

Asada, S., Daitoku, H., Matsuzaki, H., Saito, T., Sudo, T., Mukai, H., Iwashita, S., Kako, K., Kishi, T., Kasuya, Y., & Fukamizu, A. (2007). Mitogen-activated protein kinases, Erk and p38, phosphorylate and regulate Foxo1. *Cell Signal*, *19*(3), 519-527. https://doi.org/10.1016/j.cellsig.2006.08.015

Aumuller, G., Renneberg, H., & Hasilik, A. (1997). Distribution and subcellular localization of a lysosome-associated protein in human genital organs. *Cell Tissue Res*, *287*(2), 335-342. https://doi.org/10.1007/s004410050758

Ausserlechner, M. J., & Hagenbuchner, J. (2016). Mitochondrial survivin - an Achilles' heel in cancer chemoresistance. *Mol Cell Oncol*, *3*(2), e1076589. https://doi.org/10.1080/23723556.2015.1076589

Bai, L., Wu, Q., Zhang, X., & Zhao, Y. (2023). Autosis as a selective type of cell death. *Front Cell Dev Biol*, *11*, 1164681. https://doi.org/10.3389/fcell.2023.1164681

Baratchi, S., Kanwar, R. K., & Kanwar, J. R. (2011). Novel survivin mutant protects differentiated SK-N-SH human neuroblastoma cells from activated T-cell neurotoxicity. *J Neuroimmunol*, *233*(1-2), 18-28. https://doi.org/10.1016/j.jneuroim.2010.10.036

Bassi, R., Burgoyne, J. R., DeNicola, G. F., Rudyk, O., DeSantis, V., Charles, R. L., Eaton, P., & Marber, M. S. (2017). Redox-dependent dimerization of p38alpha mitogen-activated protein kinase with mitogen-activated protein kinase kinase 3. *J Biol Chem*, *292*(39), 16161-16173. https://doi.org/10.1074/jbc.M117.785410

Bhaskar, P. T., & Hay, N. (2007). The two TORCs and Akt. *Dev Cell*, *12*(4), 487-502. https://doi.org/10.1016/j.devcel.2007.03.020

Birgisdottir, A. B., Lamark, T., & Johansen, T. (2013). The LIR motif - crucial for selective autophagy. *J Cell Sci*, *126*(Pt 15), 3237-3247. https://doi.org/10.1242/jcs.126128

Blackadar, C. B. (2016). Historical review of the causes of cancer. *World J Clin Oncol*, *7*(1), 54-86. https://doi.org/10.5306/wjco.v7.i1.54

Blechinger, J., Herrmann, R., Kiener, D., Garcia-Garcia, F. J., Scheu, C., Reller, A., & Brauchle, C. (2010). Perylene-labeled silica nanoparticles: synthesis and characterization of three novel silica nanoparticle species for live-cell imaging. *Small*, *6*(21), 2427-2435. https://doi.org/10.1002/smll.201000762

Brand, W., van Kesteren, P. C. E., Peters, R. J. B., & Oomen, A. G. (2021). Issues currently complicating the risk assessment of synthetic amorphous silica (SAS) nanoparticles after oral exposure. *Nanotoxicology*, *15*(7), 905-933. https://doi.org/10.1080/17435390.2021.1931724

Breder-Bonk, C., Docter, D., Barz, M., Strieth, S., Knauer, S. K., Gul, D., & Stauber, R. H. (2023). The Apoptosis Inhibitor Protein Survivin Is a Critical Cytoprotective Resistor against Silica-Based Nanotoxicity. *Nanomaterials (Basel)*, *13*(18). https://doi.org/10.3390/nano13182546

Brunasso, A. M., & Massone, C. (2016). Update on the pathogenesis of Scleroderma: focus on circulating progenitor cells. *F1000Res*, *5*. https://doi.org/10.12688/f1000research.7986.1

Cabane, C., Coldefy, A. S., Yeow, K., & Derijard, B. (2004). The p38 pathway regulates Akt both at the protein and transcriptional activation levels during myogenesis. *Cell Signal*, *16*(12), 1405-1415. https://doi.org/10.1016/j.cellsig.2004.05.003

Capalbo, G., Rodel, C., Stauber, R. H., Knauer, S. K., Bache, M., Kappler, M., & Rodel, F. (2007). The role of survivin for radiation therapy. Prognostic and predictive factor and therapeutic target. *Strahlenther Onkol*, *183*(11), 593-599. https://doi.org/10.1007/s00066-007-1800-4

Carmena, M., Wheelock, M., Funabiki, H., & Earnshaw, W. C. (2012). The chromosomal passenger complex (CPC): from easy rider to the godfather of mitosis. *Nat Rev Mol Cell Biol*, *13*(12), 789-803. https://doi.org/10.1038/nrm3474

Casals, C., Campanero-Rhodes, M. A., Garcia-Fojeda, B., & Solis, D. (2018). The Role of Collectins and Galectins in Lung Innate Immune Defense. *Front Immunol*, *9*, 1998. https://doi.org/10.3389/fimmu.2018.01998

Ceballos-Cancino, G., Espinosa, M., Maldonado, V., & Melendez-Zajgla, J. (2007). Regulation of mitochondrial Smac/DIABLO-selective release by survivin. *Oncogene*, *26*(54), 7569-7575. https://doi.org/10.1038/sj.onc.1210560

Chang, C., Su, H., Zhang, D., Wang, Y., Shen, Q., Liu, B., Huang, R., Zhou, T., Peng, C., Wong, C. C., Shen, H. M., Lippincott-Schwartz, J., & Liu, W. (2015). AMPK-Dependent Phosphorylation of GAPDH Triggers Sirt1 Activation and Is Necessary for Autophagy upon Glucose Starvation. *Mol Cell*, *60*(6), 930-940. https://doi.org/10.1016/j.molcel.2015.10.037

Chantalat, L., Skoufias, D. A., Kleman, J. P., Jung, B., Dideberg, O., & Margolis, R. L. (2000). Crystal structure of human survivin reveals a bow tie-shaped dimer with two unusual alpha-helical extensions. *Mol Cell*, *6*(1), 183-189.

Chen, C. C., Jeon, S. M., Bhaskar, P. T., Nogueira, V., Sundararajan, D., Tonic, I., Park, Y., & Hay, N. (2010). FoxOs inhibit mTORC1 and activate Akt by inducing the expression of Sestrin3 and Rictor. *Dev Cell*, *18*(4), 592-604. https://doi.org/10.1016/j.devcel.2010.03.008

Chen, J., Cao, X., Li, B., Zhao, Z., Chen, S., Lai, S. W. T., Muend, S. A., Nossa, G. K., Wang, L., Guo, W., Ye, J., Lee, P. P., & Feng, M. (2020). Warburg Effect Is a Cancer Immune Evasion Mechanism Against Macrophage Immunosurveillance. *Front Immunol*, *11*, 621757. https://doi.org/10.3389/fimmu.2020.621757

Chen, L., Zhang, J., Lyu, Z., Chen, Y., Ji, X., Cao, H., Jin, M., Zhu, J., Yang, J., Ling, R., Xing, J., Ren, T., & Lyu, Y. (2018). Positive feedback loop between mitochondrial fission and Notch signaling promotes survivin-mediated survival of TNBC cells. *Cell Death Dis*, *9*(11), 1050. https://doi.org/10.1038/s41419-018-1083-y

Chen, L., Zhou, X., Nie, W., Zhang, Q., Wang, W., Zhang, Y., & He, C. (2016). Multifunctional Redox-Responsive Mesoporous Silica Nanoparticles for Efficient Targeting Drug Delivery and Magnetic Resonance Imaging. *ACS Appl Mater Interfaces*, *8*(49), 33829-33841. https://doi.org/10.1021/acsami.6b11802

Chen, X., Duan, N., Zhang, C., & Zhang, W. (2016). Survivin and Tumorigenesis: Molecular Mechanisms and Therapeutic Strategies. *J Cancer*, *7*(3), 314-323. https://doi.org/10.7150/jca.13332

Chen, Y., Li, D., Liu, H., Xu, H., Zheng, H., Qian, F., Li, W., Zhao, C., Wang, Z., & Wang, X. (2011). Notch-1 signaling facilitates survivin expression in human non-small cell lung cancer cells. *Cancer Biol Ther*, *11*(1), 14-21. https://doi.org/10.4161/cbt.11.1.13730

Chen, Y. W., Liu, T. Y., Chang, P. H., Hsu, P. H., Liu, H. L., Lin, H. C., & Chen, S. Y. (2016). A theranostic nrGO@MSN-ION nanocarrier developed to enhance the combination effect of sonodynamic therapy and ultrasound hyperthermia for treating tumor. *Nanoscale*, *8*(25), 12648-12657. https://doi.org/10.1039/c5nr07782f

Cheung, C. H., Chen, H. H., Kuo, C. C., Chang, C. Y., Coumar, M. S., Hsieh, H. P., & Chang, J. Y. (2009). Survivin counteracts the therapeutic effect of microtubule de-stabilizers by stabilizing tubulin polymers. *Mol Cancer*, *8*, 43. https://doi.org/10.1186/1476-4598-8-43

Cheung, C. H. A., Chang, Y. C., Lin, T. Y., Cheng, S. M., & Leung, E. (2020). Anti-apoptotic proteins in the autophagic world: an update on functions of XIAP, Survivin, and BRUCE. *J Biomed Sci*, *27*(1), 31. https://doi.org/10.1186/s12929-020-0627-5

Chiang, C., Zhang, M., Wang, D., Xiao, T., Zhu, L., Chen, K., Huang, J., Huang, J., Zhu, J., Li, L., Chen, C., Chen, Y., Hu, H., Jiang, W., Zou, Y., Wang, T., & Zheng, D. (2020). Therapeutic potential of targeting MKK3-p38 axis with Capsaicin for Nasopharyngeal Carcinoma. *Theranostics*, *10*(17), 7906-7920. https://doi.org/10.7150/thno.45191

Chu, K. F., & Dupuy, D. E. (2014). Thermal ablation of tumours: biological mechanisms and advances in therapy. *Nat Rev Cancer*, *14*(3), 199-208. https://doi.org/10.1038/nrc3672

Chu, Z., Huang, Y., Tao, Q., & Li, Q. (2011). Cellular uptake, evolution, and excretion of silica nanoparticles in human cells. *Nanoscale*, *3*(8), 3291-3299. https://doi.org/10.1039/c1nr10499c

Ciechomska, I. A., Gielniewski, B., Wojtas, B., Kaminska, B., & Mieczkowski, J. (2020). EGFR/FOXO3a/BIM signaling pathway determines chemosensitivity of BMP4-differentiated glioma stem cells to temozolomide. *Exp Mol Med*, *52*(8), 1326-1340. https://doi.org/10.1038/s12276-020-0479-9

Cooper, G. (2000). A Molecular Approach. In *The Cell* (2nd edition ed.). Sinauer Associates. https://www.ncbi.nlm.nih.gov/books/NBK9963/

Cui, H., Zhu, Y., Yang, Q., Zhao, W., Zhang, S., Zhou, A., & Jiang, D. (2016). Necrostatin-1 treatment inhibits osteocyte necroptosis and trabecular deterioration in ovariectomized rats. *Sci Rep*, *6*, 33803. https://doi.org/10.1038/srep33803

da Cruz Schneid, A., Albuquerque, L.J.C., Mondo, G.B., Ceolin M., Picco A.S., Cardoso M.B. (2022). Colloidal stability and degradability of silica nanoparticles in biological fluids: a review. *J Sol-Gel Sci Technol 102*, 41–62 https://doi.org/10.1007/s10971-021-05695-8

Dai, L., Liu, J., Luo, Z., Li, M., & Cai, K. (2016). Tumor therapy: targeted drug delivery systems. *J Mater Chem B*, *4*(42), 6758-6772. https://doi.org/10.1039/c6tb01743f

Dai, S., Gocher, A., Euscher, L., & Edelman, A. (2016). Serum Starvation Induces a Rapid Increase of Akt Phosphorylation in Ovarian Cancer Cells. *The FASEB Journal*, *30*(S1), 714.719-714.719. https://doi.org/https://doi.org/10.1096/fasebj.30.1_supplement.714.9

Dalotto-Moreno, T., Croci, D. O., Cerliani, J. P., Martinez-Allo, V. C., Dergan-Dylon, S., Mendez-Huergo, S. P., Stupirski, J. C., Mazal, D., Osinaga, E., Toscano, M. A., Sundblad, V., Rabinovich, G. A., & Salatino, M. (2013). Targeting galectin-1 overcomes breast cancer-associated immunosuppression and prevents metastatic disease. *Cancer Res*, *73*(3), 1107-1117. https://doi.org/10.1158/0008-5472.CAN-12-2418

Dan, H. C., Ebbs, A., Pasparakis, M., Van Dyke, T., Basseres, D. S., & Baldwin, A. S. (2014). Akt-dependent activation of mTORC1 complex involves phosphorylation of mTOR (mammalian target of rapamycin) by IkappaB kinase alpha (IKKalpha). *J Biol Chem*, *289*(36), 25227-25240. https://doi.org/10.1074/jbc.M114.554881

Darwish, G. H., Asselin, J., Tran, M. V., Gupta, R., Kim, H., Boudreau, D., & Algar, W. R. (2020). Fully Self-Assembled Silica Nanoparticle-Semiconductor Quantum Dot Supra-Nanoparticles and Immunoconjugates for Enhanced Cellular Imaging by Microscopy and Smartphone Camera. *ACS Appl Mater Interfaces*, *12*(30), 33530-33540. https://doi.org/10.1021/acsami.0c09553

Debela, D. T., Muzazu, S. G., Heraro, K. D., Ndalama, M. T., Mesele, B. W., Haile, D. C., Kitui, S. K., & Manyazewal, T. (2021). New approaches and procedures for cancer treatment: Current perspectives. *SAGE Open Med*, *9*, 20503121211034366. https://doi.org/10.1177/20503121211034366

Decan, N., Wu, D., Williams, A., Bernatchez, S., Johnston, M., Hill, M., & Halappanavar, S. (2016). Characterization of in vitro genotoxic, cytotoxic and transcriptomic responses following exposures to amorphous silica of different sizes. *Mutat Res Genet Toxicol Environ Mutagen*, *796*, 8-22. https://doi.org/10.1016/j.mrgentox.2015.11.011

Delacour-Larose, M., Thi, M. N., Dimitrov, S., & Molla, A. (2007). Role of survivin phosphorylation by aurora B in mitosis. *Cell Cycle*, *6*(15), 1878-1885. https://doi.org/10.4161/cc.6.15.4482

Deleyto-Seldas, N., & Efeyan, A. (2021). The mTOR-Autophagy Axis and the Control of Metabolism. *Front Cell Dev Biol*, *9*, 655731. https://doi.org/10.3389/fcell.2021.655731

Demers-Lamarche, J., Guillebaud, G., Tlili, M., Todkar, K., Belanger, N., Grondin, M., Nguyen, A. P., Michel, J., & Germain, M. (2016). Loss of Mitochondrial Function Impairs Lysosomes. *J Biol Chem*, *291*(19), 10263-10276. https://doi.org/10.1074/jbc.M115.695825

Deveraux, Q. L., & Reed, J. C. (1999). IAP family proteins--suppressors of apoptosis. *Genes Dev*, *13*(3), 239-252. https://doi.org/10.1101/gad.13.3.239

Diab, R., Canilho, N., Pavel, I. A., Haffner, F. B., Girardon, M., & Pasc, A. (2017). Silica-based systems for oral delivery of drugs, macromolecules and cells. *Adv Colloid Interface Sci*, *249*, 346-362. https://doi.org/10.1016/j.cis.2017.04.005

Dilnawaz, F., & Sahoo, S. K. (2018). Augmented Anticancer Efficacy by si-RNA Complexed Drug-Loaded Mesoporous Silica Nanoparticles in Lung Cancer Therapy. *ACS Applied Nano Materials*, *1*(2). https://doi.org/10.1021/acsanm.7b00196

Docter, D., Bantz, C., Westmeier, D., Galla, H. J., Wang, Q., Kirkpatrick, J. C., Nielsen, P., Maskos, M., & Stauber, R. H. (2014). The protein corona protects against size- and dose-dependent toxicity of amorphous silica nanoparticles. *Beilstein J Nanotechnol*, *5*, 1380-1392. https://doi.org/10.3762/bjnano.5.151

Dohi, T., Beltrami, E., Wall, N. R., Plescia, J., & Altieri, D. C. (2004). Mitochondrial survivin inhibits apoptosis and promotes tumorigenesis. *J Clin Invest*, *114*(8), 1117-1127. https://doi.org/10.1172/JCI22222

Domenech, E., Maestre, C., Esteban-Martinez, L., Partida, D., Pascual, R., Fernandez-Miranda, G., Seco, E., Campos-Olivas, R., Perez, M., Megias, D., Allen, K., Lopez, M., Saha, A. K., Velasco, G., Rial, E., Mendez, R., Boya, P., Salazar-Roa, M., & Malumbres, M. (2015). AMPK and PFKFB3 mediate glycolysis and survival in response to mitophagy during mitotic arrest. *Nat Cell Biol*, *17*(10), 1304-1316. https://doi.org/10.1038/ncb3231

Du, L., & Pertsemlidis, A. (2012). microRNA regulation of cell viability and drug sensitivity in lung cancer. *Expert Opin Biol Ther*, *12*(9), 1221-1239. https://doi.org/10.1517/14712598.2012.697149

Duan, X., & Li, Y. (2013). Physicochemical characteristics of nanoparticles affect circulation, biodistribution, cellular internalization, and trafficking. *Small*, *9*(9-10), 1521-1532. https://doi.org/10.1002/smll.201201390

Dunajova, L., Cash, E., Markus, R., Rochette, S., Townley, A. R., & Wheatley, S. P. (2016). The N-terminus of survivin is a mitochondrial-targeting sequence and Src regulator. *J Cell Sci*, *129*(14), 2707-2712. https://doi.org/10.1242/jcs.183277

Elmore, S. (2007). Apoptosis: a review of programmed cell death. *Toxicol Pathol*, *35*(4), 495-516. https://doi.org/10.1080/01926230701320337

Engels, K., Knauer, S. K., Metzler, D., Simf, C., Struschka, O., Bier, C., Mann, W., Kovacs, A. F., & Stauber, R. H. (2007). Dynamic intracellular survivin in oral squamous cell carcinoma: underlying molecular mechanism and potential as an early prognostic marker. *J Pathol*, *211*(5), 532-540. https://doi.org/10.1002/path.2134

Engelsma, D., Rodriguez, J. A., Fish, A., Giaccone, G., & Fornerod, M. (2007). Homodimerization antagonizes nuclear export of survivin. *Traffic*, *8*(11), 1495-1502. https://doi.org/10.1111/j.1600-0854.2007.00629.x

Essers, M. A., Weijzen, S., de Vries-Smits, A. M., Saarloos, I., de Ruiter, N. D., Bos, J. L., & Burgering, B. M. (2004). FOXO transcription factor activation by oxidative stress

mediated by the small GTPase Ral and JNK. *EMBO J*, *23*(24), 4802-4812. https://doi.org/10.1038/sj.emboj.7600476

Fang, D., Hawke, D., Zheng, Y., Xia, Y., Meisenhelder, J., Nika, H., Mills, G. B., Kobayashi, R., Hunter, T., & Lu, Z. (2007). Phosphorylation of beta-catenin by AKT promotes beta-catenin transcriptional activity. *J Biol Chem*, *282*(15), 11221-11229. https://doi.org/10.1074/jbc.M611871200

Fang, S., Lin, J., Li, C., Huang, P., Hou, W., Zhang, C., Liu, J., Huang, S., Luo, Y., Fan, W., Cui, D., Xu, Y., & Li, Z. (2017). Dual-Stimuli Responsive Nanotheranostics for Multimodal Imaging Guided Trimodal Synergistic Therapy. *Small*, *13*(6). https://doi.org/10.1002/smll.201602580

Fytianos, G., Rahdar, A., & Kyzas, G. Z. (2020). Nanomaterials in Cosmetics: Recent Updates. *Nanomaterials (Basel)*, *10*(5). https://doi.org/10.3390/nano10050979

Gao, Y., Gao, D., Shen, J., & Wang, Q. (2020). A Review of Mesoporous Silica Nanoparticle Delivery Systems in Chemo-Based Combination Cancer Therapies. *Front Chem*, *8*, 598722. https://doi.org/10.3389/fchem.2020.598722

Gao, Y., Li, X., Shu, Z., Zhang, K., Xue, X., Li, W., Hao, Q., Wang, Z., Zhang, W., Wang, S., Zeng, C., Fan, D., Zhang, W., Zhang, Y., Zhao, H., Li, M., & Zhang, C. (2018). Nuclear galectin-1-FOXP3 interaction dampens the tumor-suppressive properties of FOXP3 in breast cancer. *Cell Death Dis*, *9*(4), 416. https://doi.org/10.1038/s41419-018-0448-6

Geeraert, C., Ratier, A., Pfisterer, S. G., Perdiz, D., Cantaloube, I., Rouault, A., Pattingre, S., Proikas-Cezanne, T., Codogno, P., & Pous, C. (2010). Starvation-induced hyperacetylation of tubulin is required for the stimulation of autophagy by nutrient deprivation. *J Biol Chem*, *285*(31), 24184-24194. https://doi.org/10.1074/jbc.M109.091553

Gilley, J., Coffer, P. J., & Ham, J. (2003). FOXO transcription factors directly activate bim gene expression and promote apoptosis in sympathetic neurons. *J Cell Biol*, *162*(4), 613-622. https://doi.org/10.1083/jcb.200303026

Giodini, A., Kallio, M. J., Wall, N. R., Gorbsky, G. J., Tognin, S., Marchisio, P. C., Symons, M., & Altieri, D. C. (2002). Regulation of microtubule stability and mitotic progression by survivin. *Cancer Res*, *62*(9), 2462-2467. https://www.ncbi.nlm.nih.gov/pubmed/11980633

Glaviano, A., Foo, A. S. C., Lam, H. Y., Yap, K. C. H., Jacot, W., Jones, R. H., Eng, H., Nair, M. G., Makvandi, P., Geoerger, B., Kulke, M. H., Baird, R. D., Prabhu, J. S., Carbone, D., Pecoraro, C., Teh, D. B. L., Sethi, G., Cavalieri, V., Lin, K. H., . . . Kumar, A. P. (2023). PI3K/AKT/mTOR signaling transduction pathway and targeted therapies in cancer. *Mol Cancer*, *22*(1), 138. https://doi.org/10.1186/s12943-023-01827-6

Go, M. R., Bae, S. H., Kim, H. J., Yu, J., & Choi, S. J. (2017). Interactions between Food Additive Silica Nanoparticles and Food Matrices. *Front Microbiol*, *8*, 1013. https://doi.org/10.3389/fmicb.2017.01013

Gorrini, C., Harris, I. S., & Mak, T. W. (2013). Modulation of oxidative stress as an anticancer strategy. *Nat Rev Drug Discov*, *12*(12), 931-947. https://doi.org/10.1038/nrd4002

Gratton, J. P., Morales-Ruiz, M., Kureishi, Y., Fulton, D., Walsh, K., & Sessa, W. C. (2001). Akt down-regulation of p38 signaling provides a novel mechanism of vascular endothelial growth factor-mediated cytoprotection in endothelial cells. *J Biol Chem*, *276*(32), 30359-30365. https://doi.org/10.1074/jbc.M009698200

Gravina, G., Wasen, C., Garcia-Bonete, M. J., Turkkila, M., Erlandsson, M. C., Toyra Silfversward, S., Brisslert, M., Pullerits, R., Andersson, K. M., Katona, G., & Bokarewa, M. I. (2017). Survivin in autoimmune diseases. *Autoimmun Rev*, *16*(8), 845-855. https://doi.org/10.1016/j.autrev.2017.05.016

Greenberg, M. I., Waksman, J., & Curtis, J. (2007). Silicosis: a review. *Dis Mon*, *53*(8), 394-416. https://doi.org/10.1016/j.disamonth.2007.09.020

Guardia, C. M., Caramelo, J. J., Trujillo, M., Mendez-Huergo, S. P., Radi, R., Estrin, D. A., & Rabinovich, G. A. (2014). Structural basis of redox-dependent modulation of galectin-1 dynamics and function. *Glycobiology*, *24*(5), 428-441. https://doi.org/10.1093/glycob/cwu008

Gundamaraju, R., Lu, W., Paul, M. K., Jha, N. K., Gupta, P. K., Ojha, S., Chattopadhyay, I., Rao, P. V., & Ghavami, S. (2022). Autophagy and EMT in cancer and metastasis: Who controls whom? *Biochim Biophys Acta Mol Basis Dis*, *1868*(9), 166431. https://doi.org/10.1016/j.bbadis.2022.166431

Guo, C., Yang, M., Jing, L., Wang, J., Yu, Y., Li, Y., Duan, J., Zhou, X., Li, Y., & Sun, Z. (2016). Amorphous silica nanoparticles trigger vascular endothelial cell injury through apoptosis and autophagy via reactive oxygen species-mediated MAPK/Bcl-2 and PI3K/Akt/mTOR signaling. *Int J Nanomedicine*, *11*, 5257-5276. https://doi.org/10.2147/IJN.S112030

Hagemann, S., Wohlschlaeger, J., Bertram, S., Levkau, B., Musacchio, A., Conway, E. M., Moellmann, D., Kneiseler, G., Pless-Petig, G., Lorenz, K., Sitek, B., & Baba, H. A. (2013). Loss of Survivin influences liver regeneration and is associated with impaired Aurora B function. *Cell Death Differ*, *20*(6), 834-844. https://doi.org/10.1038/cdd.2013.20

Hagenbuchner, J., Kiechl-Kohlendorfer, U., Obexer, P., & Ausserlechner, M. J. (2016). BIRC5/Survivin as a target for glycolysis inhibition in high-stage neuroblastoma. *Oncogene*, *35*(16), 2052-2061. https://doi.org/10.1038/onc.2015.264

Hagenbuchner, J., Kuznetsov, A. V., Obexer, P., & Ausserlechner, M. J. (2013). BIRC5/Survivin enhances aerobic glycolysis and drug resistance by altered regulation of the mitochondrial fusion/fission machinery. *Oncogene*, *32*(40), 4748-4757. https://doi.org/10.1038/onc.2012.500

Hagenbuchner, J., Oberacher, H., Arnhard, K., Kiechl-Kohlendorfer, U., & Ausserlechner, M. J. (2019). Modulation of Respiration and Mitochondrial Dynamics by SMAC-Mimetics for Combination Therapy in Chemoresistant Cancer. *Theranostics*, *9*(17), 4909-4922. https://doi.org/10.7150/thno.33758

Haleem, A., Javaid, M., Singh, R. P., Rab, S., & Suman, R. (2023). Applications of nanotechnology in medical field: a brief review. *Global Health Journal*, *7*(2), 70-77. https://doi.org/10.1016/j.glohj.2023.02.008

Hay-Koren, A., Bialik, S., Levin-Salomon, V., & Kimchi, A. (2017). Changes in cIAP2, survivin and BimEL expression characterize the switch from autophagy to apoptosis in prolonged starvation. *J Intern Med*, *281*(5), 458-470. https://doi.org/10.1111/joim.12616

He, C., & Klionsky, D. J. (2009). Regulation mechanisms and signaling pathways of autophagy. *Annu Rev Genet*, *43*, 67-93. https://doi.org/10.1146/annurev-genet-102808-114910

Heberle, A. M., Razquin Navas, P., Langelaar-Makkinje, M., Kasack, K., Sadik, A., Faessler, E., Hahn, U., Marx-Stoelting, P., Opitz, C. A., Sers, C., Heiland, I., Schauble, S., & Thedieck, K. (2019). The PI3K and MAPK/p38 pathways control stress granule assembly in a hierarchical manner. *Life Sci Alliance*, *2*(2). https://doi.org/10.26508/lsa.201800257

Hernandez-Caceres, M. P., Munoz, L., Pradenas, J. M., Pena, F., Lagos, P., Aceiton, P., Owen, G. I., Morselli, E., Criollo, A., Ravasio, A., & Bertocchi, C. (2021). Mechanobiology of Autophagy: The Unexplored Side of Cancer. *Front Oncol*, *11*, 632956. https://doi.org/10.3389/fonc.2021.632956

Hernandez, G., Lal, H., Fidalgo, M., Guerrero, A., Zalvide, J., Force, T., & Pombo, C. M. (2011). A novel cardioprotective p38-MAPK/mTOR pathway. *Exp Cell Res*, *317*(20), 2938-2949. https://doi.org/10.1016/j.yexcr.2011.09.011

Heuser, J. (1989). Changes in lysosome shape and distribution correlated with changes in cytoplasmic pH. *J Cell Biol*, *108*(3), 855-864. https://doi.org/10.1083/jcb.108.3.855

Ho, K. K., McGuire, V. A., Koo, C. Y., Muir, K. W., de Olano, N., Maifoshie, E., Kelly, D. J., McGovern, U. B., Monteiro, L. J., Gomes, A. R., Nebreda, A. R., Campbell, D. G., Arthur, J. S., & Lam, E. W. (2012). Phosphorylation of FOXO3a on Ser-7 by p38 promotes its nuclear localization in response to doxorubicin. *J Biol Chem*, *287*(2), 1545-1555. https://doi.org/10.1074/jbc.M111.284224

Hu, F., Pan, D., Zheng, W., Yan, T., He, X., Ren, F., Lu, Y., & Ma, X. (2017). Elucidating respective functions of two domains BIR and C-helix of human IAP survivin for precise targeted regulating mitotic cycle, apoptosis and autophagy of cancer cells. *Oncotarget*, *8*(69), 113687-113700. https://doi.org/10.18632/oncotarget.22823

Huang, W., Mao, Y., Zhan, Y., Huang, J., Wang, X., Luo, P., Li, L. I., Mo, D., Liu, Q., Xu, H., & Huang, C. (2016). Prognostic implications of survivin and lung resistance protein in advanced non-small cell lung cancer treated with platinum-based chemotherapy. *Oncol Lett*, *11*(1), 723-730. https://doi.org/10.3892/ol.2015.3913

Humphry, N. J., & Wheatley, S. P. (2018). Survivin inhibits excessive autophagy in cancer cells but does so independently of its interaction with LC3. *Biol Open*, *7*(10). https://doi.org/10.1242/bio.037374

IARC, C. T.-. (2024, GLOBOCAN 2020). *Estimated age-standardized incidence and mortality rates (World) in 2020, World, both sexes, all ages (excl. NMSC)*. https://gco.iarc.fr/today/online-analysis-multi-bars?v=2020&mode=cancer&mode_population=countries&population=900&populations=900&key=asr&sex=0&cancer=39&type=0&statistic=5&prevalence=0&population_group=0&ages_group%5B%5D=0&ages_group%5B%5D=17&nb_items=10&group_cancer=1&include_nmsc=0&include_nmsc_other=1&type_multiple=%257B%2522inc%2522%253Atrue%252C%2522mort%2522%253Atrue%252C%2522prev%2522%253Afalse%257D&orientation=horizontal&type_sort=0&type_nb_items=%257B%2522top%2522%253Atrue%252C%2522bottom%2522%253Afalse%257D

Jacquin, M. A., Chiche, J., Zunino, B., Beneteau, M., Meynet, O., Pradelli, L. A., Marchetti, S., Cornille, A., Carles, M., & Ricci, J. E. (2013). GAPDH binds to active Akt, leading to Bcl-xL increase and escape from caspase-independent cell death. *Cell Death Differ*, *20*(8), 1043-1054. https://doi.org/10.1038/cdd.2013.32

Jahreiss, L., Menzies, F. M., & Rubinsztein, D. C. (2008). The itinerary of autophagosomes: from peripheral formation to kiss-and-run fusion with lysosomes. *Traffic*, *9*(4), 574-587. https://doi.org/10.1111/j.1600-0854.2008.00701.x

Jan, R., & Chaudhry, G. E. (2019). Understanding Apoptosis and Apoptotic Pathways Targeted Cancer Therapeutics. *Adv Pharm Bull*, *9*(2), 205-218. https://doi.org/10.15171/apb.2019.024

Janjua, T. I., Cao, Y., Kleitz, F., Linden, M., Yu, C., & Popat, A. (2023). Silica nanoparticles: A review of their safety and current strategies to overcome biological barriers. *Adv Drug Deliv Rev*, *203*, 115115. https://doi.org/10.1016/j.addr.2023.115115

Jeyaprakash, A. A., Klein, U. R., Lindner, D., Ebert, J., Nigg, E. A., & Conti, E. (2007). Structure of a Survivin-Borealin-INCENP core complex reveals how chromosomal passengers travel together. *Cell*, *131*(2), 271-285. https://doi.org/10.1016/j.cell.2007.07.045

Ji, Z., Guo, W., Sakkiah, S., Liu, J., Patterson, T. A., & Hong, H. (2021). Nanomaterial Databases: Data Sources for Promoting Design and Risk Assessment of Nanomaterials. *Nanomaterials (Basel)*, *11*(6). https://doi.org/10.3390/nano11061599

Jia, Y. T., Wei, W., Ma, B., Xu, Y., Liu, W. J., Wang, Y., Lv, K. Y., Tang, H. T., Wei, D., & Xia, Z. F. (2007). Activation of p38 MAPK by reactive oxygen species is essential in a

rat model of stress-induced gastric mucosal injury. *J Immunol*, *179*(11), 7808-7819. https://doi.org/10.4049/jimmunol.179.11.7808

Jiang, Y., de Bruin, A., Caldas, H., Fangusaro, J., Hayes, J., Conway, E. M., Robinson, M. L., & Altura, R. A. (2005). Essential role for survivin in early brain development. *J Neurosci*, *25*(30), 6962-6970. https://doi.org/10.1523/JNEUROSCI.1446-05.2005

Joudeh, N., & Linke, D. (2022). Nanoparticle classification, physicochemical properties, characterization, and applications: a comprehensive review for biologists. *J Nanobiotechnology*, *20*(1), 262. https://doi.org/10.1186/s12951-022-01477-8

Jung, C. H., Ro, S. H., Cao, J., Otto, N. M., & Kim, D. H. (2010). mTOR regulation of autophagy. *FEBS Lett*, *584*(7), 1287-1295. https://doi.org/10.1016/j.febslet.2010.01.017

Jung, S., Jeong, H., & Yu, S. W. (2020). Autophagy as a decisive process for cell death. *Exp Mol Med*, *52*(6), 921-930. https://doi.org/10.1038/s12276-020-0455-4

Kallio, M. J., Nieminen, M., & Eriksson, J. E. (2001). Human inhibitor of apoptosis protein (IAP) survivin participates in regulation of chromosome segregation and mitotic exit. *FASEB J*, *15*(14), 2721-2723. https://doi.org/10.1096/fj.01-0280fje

Kawahara, A., Ohsawa, Y., Matsumura, H., Uchiyama, Y., & Nagata, S. (1998). Caspase-independent cell killing by Fas-associated protein with death domain. *J Cell Biol*, *143*(5), 1353-1360. https://doi.org/10.1083/jcb.143.5.1353

Khan, M. W., Layden, B. T., & Chakrabarti, P. (2018). Inhibition of mTOR complexes protects cancer cells from glutamine starvation induced cell death by restoring Akt stability. *Biochim Biophys Acta Mol Basis Dis*, *1864*(6 Pt A), 2040-2052. https://doi.org/10.1016/j.bbadis.2018.03.013

Kimura, S., Noda, T., & Yoshimori, T. (2008). Dynein-dependent movement of autophagosomes mediates efficient encounters with lysosomes. *Cell Struct Funct*, *33*(1), 109-122. https://doi.org/10.1247/csf.08005

Klotz, L. O., Sanchez-Ramos, C., Prieto-Arroyo, I., Urbanek, P., Steinbrenner, H., & Monsalve, M. (2015). Redox regulation of FoxO transcription factors. *Redox Biol*, *6*, 51-72. https://doi.org/10.1016/j.redox.2015.06.019

Knauer, S. K., Bier, C., Habtemichael, N., & Stauber, R. H. (2006). The Survivin-Crm1 interaction is essential for chromosomal passenger complex localization and function. *EMBO Rep*, *7*(12), 1259-1265. https://doi.org/10.1038/sj.embor.7400824

Knauer, S. K., Unruhe, B., Karczewski, S., Hecht, R., Fetz, V., Bier, C., Friedl, S., Wollenberg, B., Pries, R., Habtemichael, N., Heinrich, U. R., & Stauber, R. H. (2013). Functional characterization of novel mutations affecting survivin (BIRC5)-mediated therapy resistance in head and neck cancer patients. *Hum Mutat*, *34*(2), 395-404. https://doi.org/10.1002/humu.22249

Kocot, A. M., & Wroblewska, B. (2022). Nutritional strategies for autophagy activation and health consequences of autophagy impairment. *Nutrition*, *103-104*, 111686. https://doi.org/10.1016/j.nut.2022.111686

Kohda, D., Odaka, M., Lax, I., Kawasaki, H., Suzuki, K., Ullrich, A., Schlessinger, J., & Inagaki, F. (1993). A 40-kDa epidermal growth factor/transforming growth factor alpha-binding domain produced by limited proteolysis of the extracellular domain of the epidermal growth factor receptor. *J Biol Chem*, *268*(3), 1976-1981. https://www.ncbi.nlm.nih.gov/pubmed/8420971

Kondapuram, S. K., Ramachandran, H. K., Arya, H., & Coumar, M. S. (2023). Targeting survivin for cancer therapy: Strategies, small molecule inhibitors and vaccine based therapeutics in development. *Life Sci*, *335*, 122260. https://doi.org/10.1016/j.lfs.2023.122260

Kornberg, M. D. (2020). The immunologic Warburg effect: Evidence and therapeutic opportunities in autoimmunity. *Wiley Interdiscip Rev Syst Biol Med*, *12*(5), e1486. https://doi.org/10.1002/wsbm.1486

Kozyulina, P. Y., Okorokova, L. S., Nikolsky, N. N., & Grudinkin, P. S. (2013). p38 MAP kinase enhances EGF-induced apoptosis in A431 carcinoma cells by promoting tyrosine phosphorylation of STAT1. *Biochem Biophys Res Commun*, *430*(1), 331-335. https://doi.org/10.1016/j.bbrc.2012.11.041

Kruk, L., Braun, A., Cosset, E., Gudermann, T., & Mammadova-Bach, E. (2023). Galectin functions in cancer-associated inflammation and thrombosis. *Front Cardiovasc Med*, *10*, 1052959. https://doi.org/10.3389/fcvm.2023.1052959

Kumar, S., Jiang, M. S., Adams, J. L., & Lee, J. C. (1999). Pyridinylimidazole compound SB 203580 inhibits the activity but not the activation of p38 mitogen-activated protein kinase. *Biochem Biophys Res Commun*, *263*(3), 825-831. https://doi.org/10.1006/bbrc.1999.1454

Kümper, A. (2017). *Einfluss von kolloidalen Silikananopartikeln auf die EGFR-abhängige Signaltransduktion* [Inaugural-Dissertation, Heinrich-Heine-Universität Düsseldorf]. Katalog der deutschen Nationalbibliothek. https://d-nb.info/1138436860/34

Kwon, H. J., Rhim, J. H., Jang, I. S., Kim, G. E., Park, S. C., & Yeo, E. J. (2010). Activation of AMP-activated protein kinase stimulates the nuclear localization of glyceraldehyde 3-phosphate dehydrogenase in human diploid fibroblasts. *Exp Mol Med*, *42*(4), 254-269. https://doi.org/10.3858/emm.2010.42.4.025

Kwon, Y., Kim, M., Jung, H. S., Kim, Y., & Jeoung, D. (2019). Targeting Autophagy for Overcoming Resistance to Anti-EGFR Treatments. *Cancers (Basel)*, *11*(9). https://doi.org/10.3390/cancers11091374

Lali, F. V., Hunt, A. E., Turner, S. J., & Foxwell, B. M. (2000). The pyridinyl imidazole inhibitor SB203580 blocks phosphoinositide-dependent protein kinase activity, protein kinase B phosphorylation, and retinoblastoma hyperphosphorylation in interleukin-2-stimulated T cells independently of p38 mitogen-activated protein kinase. *J Biol Chem*, *275*(10), 7395-7402. https://doi.org/10.1074/jbc.275.10.7395

Lee, K., Lee, J., Kwak, M., Cho, Y. L., Hwang, B., Cho, M. J., Lee, N. G., Park, J., Lee, S. H., Park, J. G., Kim, Y. G., Kim, J. S., Han, T. S., Cho, H. S., Park, Y. J., Lee, S. J., Lee, H. G., Kim, W. K., Jeung, I. C., . . . Min, J. K. (2019). Two distinct cellular pathways leading to endothelial cell cytotoxicity by silica nanoparticle size. *J Nanobiotechnology*, *17*(1), 24. https://doi.org/10.1186/s12951-019-0456-4

Lee, S. B., Kim, J. J., Kim, T. W., Kim, B. S., Lee, M. S., & Yoo, Y. D. (2010). Serum deprivation-induced reactive oxygen species production is mediated by Romo1. *Apoptosis*, *15*(2), 204-218. https://doi.org/10.1007/s10495-009-0411-1

Lei, Z. N., Tian, Q., Teng, Q. X., Wurpel, J. N. D., Zeng, L., Pan, Y., & Chen, Z. S. (2023). Understanding and targeting resistance mechanisms in cancer. *MedComm (2020)*, *4*(3), e265. https://doi.org/10.1002/mco2.265

Leung, C. C., Yu, I. T., & Chen, W. (2012). Silicosis. *Lancet*, *379*(9830), 2008-2018. https://doi.org/10.1016/S0140-6736(12)60235-9

Leung, C. G., Xu, Y., Mularski, B., Liu, H., Gurbuxani, S., & Crispino, J. D. (2007). Requirements for survivin in terminal differentiation of erythroid cells and maintenance of hematopoietic stem and progenitor cells. *J Exp Med*, *204*(7), 1603-1611. https://doi.org/10.1084/jem.20062395

Li, F., Aljahdali, I., & Ling, X. (2019). Cancer therapeutics using survivin BIRC5 as a target: what can we do after over two decades of study? *J Exp Clin Cancer Res*, *38*(1), 368. https://doi.org/10.1186/s13046-019-1362-1

Li, J., Sun, R. R., Yu, Z. J., Liang, H., Shen, S., & Kan, Q. (2015). Galectin-1 Modulates the Survival and Tumor Necrosis Factor-Related Apoptosis-Inducing Ligand (TRAIL)

Sensitivity in Human Hepatocellular Carcinoma Cells. *Cancer Biother Radiopharm*, *30*(8), 336-341. https://doi.org/10.1089/cbr.2015.1857

Li, Y., Lu, W., Yang, J., Edwards, M., & Jiang, S. (2021). Survivin as a biological biomarker for diagnosis and therapy. *Expert Opin Biol Ther*, *21*(11), 1429-1441. https://doi.org/10.1080/14712598.2021.1918672

Lin, J. T., Liu, Z. K., Zhu, Q. L., Rong, X. H., Liang, C. L., Wang, J., Ma, D., Sun, J., & Wang, G. H. (2017). Redox-responsive nanocarriers for drug and gene co-delivery based on chitosan derivatives modified mesoporous silica nanoparticles. *Colloids Surf B Biointerfaces*, *155*, 41-50. https://doi.org/10.1016/j.colsurfb.2017.04.002

Lin, T. Y., Chan, H. H., Chen, S. H., Sarvagalla, S., Chen, P. S., Coumar, M. S., Cheng, S. M., Chang, Y. C., Lin, C. H., Leung, E., & Cheung, C. H. A. (2019). BIRC5/Survivin is a novel ATG12-ATG5 conjugate interactor and an autophagy-induced DNA damage suppressor in human cancer and mouse embryonic fibroblast cells. *Autophagy*, 1-18. https://doi.org/10.1080/15548627.2019.1671643

Liu, G., Pei, F., Yang, F., Li, L., Amin, A. D., Liu, S., Buchan, J. R., & Cho, W. C. (2017). Role of Autophagy and Apoptosis in Non-Small-Cell Lung Cancer. *Int J Mol Sci*, *18*(2). https://doi.org/10.3390/ijms18020367

Liu, H.-J., Luan, X., Feng, H.-Y., Dong, X., Yang, S.-C., Chen, Z.-J., Cai, Q.-Y., Lu, Q., Zhang, Y., Sun, P., Zhao, M., Chen, H.-Z., Lovell, J. F., & Fang, C. (2018). Integrated Combination Treatment Using a "Smart" Chemotherapy and MicroRNA Delivery System Improves Outcomes in an Orthotopic Colorectal Cancer Model. *Advanced Functional Materials*, *28*(28), 1801118. https://doi.org/https://doi.org/10.1002/adfm.201801118

Liu, J., & Cao, X. (2016). Cellular and molecular regulation of innate inflammatory responses. *Cell Mol Immunol*, *13*(6), 711-721. https://doi.org/10.1038/cmi.2016.58

Liu, J. Y., & Sayes, C. M. (2022). A toxicological profile of silica nanoparticles. *Toxicol Res (Camb)*, *11*(4), 565-582. https://doi.org/10.1093/toxres/tfac038

Liu, X., Zhang, Z., Sun, L., Chai, N., Tang, S., Jin, J., Hu, H., Nie, Y., Wang, X., Wu, K., Jin, H., & Fan, D. (2011). MicroRNA-499-5p promotes cellular invasion and tumor metastasis in colorectal cancer by targeting FOXO4 and PDCD4. *Carcinogenesis*, *32*(12), 1798-1805. https://doi.org/10.1093/carcin/bgr213

Lu, J., Tan, M., & Cai, Q. (2015). The Warburg effect in tumor progression: mitochondrial oxidative metabolism as an anti-metastasis mechanism. *Cancer Lett*, *356*(2 Pt A), 156-164. https://doi.org/10.1016/j.canlet.2014.04.001

Lu, Q., Zhai, Y., Cheng, Q., Liu, Y., Gao, X., Zhang, T., Wei, Y., Zhang, F., & Yin, X. (2013). The Akt-FoxO3a-manganese superoxide dismutase pathway is involved in the regulation of oxidative stress in diabetic nephropathy. *Exp Physiol*, *98*(4), 934-945. https://doi.org/10.1113/expphysiol.2012.068361

Lukas, S. M., Kroe, R. R., Wildeson, J., Peet, G. W., Frego, L., Davidson, W., Ingraham, R. H., Pargellis, C. A., Labadia, M. E., & Werneburg, B. G. (2004). Catalysis and function of the p38 alpha.MK2a signaling complex. *Biochemistry*, *43*(31), 9950-9960. https://doi.org/10.1021/bi049508v

Ma, F. Y., Tesch, G. H., Flavell, R. A., Davis, R. J., & Nikolic-Paterson, D. J. (2007). MKK3-p38 signaling promotes apoptosis and the early inflammatory response in the obstructed mouse kidney. *Am J Physiol Renal Physiol*, *293*(5), F1556-1563. https://doi.org/10.1152/ajprenal.00010.2007

Ma, L., Hernandez, M. O., Zhao, Y., Mehta, M., Tran, B., Kelly, M., Rae, Z., Hernandez, J. M., Davis, J. L., Martin, S. P., Kleiner, D. E., Hewitt, S. M., Ylaya, K., Wood, B. J., Greten, T. F., & Wang, X. W. (2019). Tumor Cell Biodiversity Drives Microenvironmental Reprogramming in Liver Cancer. *Cancer Cell*, *36*(4), 418-430 e416. https://doi.org/10.1016/j.ccell.2019.08.007

Majewski, N., Nogueira, V., Bhaskar, P., Coy, P. E., Skeen, J. E., Gottlob, K., Chandel, N. S., Thompson, C. B., Robey, R. B., & Hay, N. (2004). Hexokinase-mitochondria interaction mediated by Akt is required to inhibit apoptosis in the presence or absence of Bax and Bak. *Mol Cell*, *16*(5), 819-830. https://doi.org/10.1016/j.molcel.2004.11.014

Mauthe, M., Orhon, I., Rocchi, C., Zhou, X., Luhr, M., Hijlkema, K. J., Coppes, R. P., Engedal, N., Mari, M., & Reggiori, F. (2018). Chloroquine inhibits autophagic flux by decreasing autophagosome-lysosome fusion. *Autophagy*, *14*(8), 1435-1455. https://doi.org/10.1080/15548627.2018.1474314

Mebert, A. M., Baglole, C. J., Desimone, M. F., & Maysinger, D. (2017). Nanoengineered silica: Properties, applications and toxicity. *Food Chem Toxicol*, *109*(Pt 1), 753-770. https://doi.org/10.1016/j.fct.2017.05.054

Micheau, O. (2018). Regulation of TNF-Related Apoptosis-Inducing Ligand Signaling by Glycosylation. *Int J Mol Sci*, *19*(3). https://doi.org/10.3390/ijms19030715

Min, H. Y., & Lee, H. Y. (2022). Molecular targeted therapy for anticancer treatment. *Exp Mol Med*, *54*(10), 1670-1694. https://doi.org/10.1038/s12276-022-00864-3

Mizushima, N. (2020). The ATG conjugation systems in autophagy. *Curr Opin Cell Biol*, *63*, 1-10. https://doi.org/10.1016/j.ceb.2019.12.001

Mizushima, N., & Komatsu, M. (2011). Autophagy: renovation of cells and tissues. *Cell*, *147*(4), 728-741. https://doi.org/10.1016/j.cell.2011.10.026

Moses, M. A., Brem, H., & Langer, R. (2003). Advancing the field of drug delivery: taking aim at cancer. *Cancer Cell*, *4*(5), 337-341. https://doi.org/10.1016/s1535-6108(03)00276-9

Mu, W., Chu, Q., Liu, Y., & Zhang, N. (2020). A Review on Nano-Based Drug Delivery System for Cancer Chemoimmunotherapy. *Nanomicro Lett*, *12*(1), 142. https://doi.org/10.1007/s40820-020-00482-6

Muranen, T., Selfors, L. M., Hwang, J., Gallegos, L. L., Coloff, J. L., Thoreen, C. C., Kang, S. A., Sabatini, D. M., Mills, G. B., & Brugge, J. S. (2016). ERK and p38 MAPK Activities Determine Sensitivity to PI3K/mTOR Inhibition via Regulation of MYC and YAP. *Cancer Res*, *76*(24), 7168-7180. https://doi.org/10.1158/0008-5472.CAN-16-0155

Murugadoss, S., Lison, D., Godderis, L., Van Den Brule, S., Mast, J., Brassinne, F., Sebaihi, N., & Hoet, P. H. (2017). Toxicology of silica nanoparticles: an update. *Arch Toxicol*, *91*(9), 2967-3010. https://doi.org/10.1007/s00204-017-1993-y

Naffa, R., Vogel, L., Hegedus, L., Paszty, K., Toth, S., Kelemen, K., Singh, N., Remenyi, A., Kallay, E., Cserepes, M., Tovari, J., Grusch, M., & Enyedi, A. (2020). P38 MAPK Promotes Migration and Metastatic Activity of BRAF Mutant Melanoma Cells by Inducing Degradation of PMCA4b. *Cells*, *9*(5). https://doi.org/10.3390/cells9051209

Nakamura, S., & Yoshimori, T. (2017). New insights into autophagosome-lysosome fusion. *J Cell Sci*, *130*(7), 1209-1216. https://doi.org/10.1242/jcs.196352

Nakamura, T., & Sakamoto, K. (2008). Forkhead transcription factor FOXO subfamily is essential for reactive oxygen species-induced apoptosis. *Mol Cell Endocrinol*, *281*(1-2), 47-55. https://doi.org/10.1016/j.mce.2007.10.007

Nam, K., Son, S. H., Oh, S., Jeon, D., Kim, H., Noh, D. Y., Kim, S., & Shin, I. (2017). Binding of galectin-1 to integrin beta1 potentiates drug resistance by promoting survivin expression in breast cancer cells. *Oncotarget*, *8*(22), 35804-35823. https://doi.org/10.18632/oncotarget.16208

Navegantes, K. C., de Souza Gomes, R., Pereira, P. A. T., Czaikoski, P. G., Azevedo, C. H. M., & Monteiro, M. C. (2017). Immune modulation of some autoimmune diseases: the critical role of macrophages and neutrophils in the innate and adaptive immunity. *J Transl Med*, *15*(1), 36. https://doi.org/10.1186/s12967-017-1141-8

Nazio, F., Bordi, M., Cianfanelli, V., Locatelli, F., & Cecconi, F. (2019). Autophagy and cancer stem cells: molecular mechanisms and therapeutic applications. *Cell Death Differ*, *26*(4), 690-702. https://doi.org/10.1038/s41418-019-0292-y

Nirmala, J. G., & Lopus, M. (2020). Cell death mechanisms in eukaryotes. *Cell Biol Toxicol*, *36*(2), 145-164. https://doi.org/10.1007/s10565-019-09496-2

Nogueira, V., Park, Y., Chen, C. C., Xu, P. Z., Chen, M. L., Tonic, I., Unterman, T., & Hay, N. (2008). Akt determines replicative senescence and oxidative or oncogenic premature senescence and sensitizes cells to oxidative apoptosis. *Cancer Cell*, *14*(6), 458-470. https://doi.org/10.1016/j.ccr.2008.11.003

Ongnok, B., Chattipakorn, N., & Chattipakorn, S. C. (2020). Doxorubicin and cisplatin induced cognitive impairment: The possible mechanisms and interventions. *Exp Neurol*, *324*, 113118. https://doi.org/10.1016/j.expneurol.2019.113118

Ose, R., Oharaa, O., & Nagase, T. (2012). Galectin-1 and Galectin-3 Mediate Protocadherin-24-Dependent Membrane Localization of beta-catenin in Colon Cancer Cell Line HCT116. *Curr Chem Genomics*, *6*, 18-26. https://doi.org/10.2174/1875397301206010018

Osminkina, L. A., Nikolaev, A. L., Sviridov, A. P., Andronova, N. V., Tamarov, K. P., Gongalsky, M. B., Kudryavtsev, A. A., Treshalina, H. M., & Timoshenko, V. Y. (2015). orous silicon nanoparticles as efficient sensitizers for sonodynamic therapy of cancer. *Microporous and Mesoporous Materials*, *210*, 169-175. https://doi.org/10.1016/j.micromeso.2015.02.037

Pahlavan, Y., Samadi, N., Ansarin, K., & Khabbazi, A. (2020). Phosphorylation Modulates Survivin Function in Behcet's Disease. *Adv Pharm Bull*, *10*(2), 278-283. https://doi.org/10.34172/apb.2020.033

Pan, C. W., Jin, X., Zhao, Y., Pan, Y., Yang, J., Karnes, R. J., Zhang, J., Wang, L., & Huang, H. (2017). AKT-phosphorylated FOXO1 suppresses ERK activation and chemoresistance by disrupting IQGAP1-MAPK interaction. *EMBO J*, *36*(8), 995-1010. https://doi.org/10.15252/embj.201695534

Papadopoulos, C., Kravic, B., & Meyer, H. (2020). Repair or Lysophagy: Dealing with Damaged Lysosomes. *J Mol Biol*, *432*(1), 231-239. https://doi.org/10.1016/j.jmb.2019.08.010

Park, J. W., Voss, P. G., Grabski, S., Wang, J. L., & Patterson, R. J. (2001). Association of galectin-1 and galectin-3 with Gemin4 in complexes containing the SMN protein. *Nucleic Acids Res*, *29*(17), 3595-3602. https://doi.org/10.1093/nar/29.17.3595

Parry, P., Wei, Y., & Evans, G. (1994). Cloning and characterization of the t(X;11) breakpoint from a leukemic cell line identify a new member of the forkhead gene family. *Genes Chromosomes Cancer*, *11*(2), 79-84. https://doi.org/10.1002/gcc.2870110203

Parzych, K. R., & Klionsky, D. J. (2014). An overview of autophagy: morphology, mechanism, and regulation. *Antioxid Redox Signal*, *20*(3), 460-473. https://doi.org/10.1089/ars.2013.5371

Pavlyukov, M. S., Antipova, N. V., Balashova, M. V., Vinogradova, T. V., Kopantzev, E. P., & Shakhparonov, M. I. (2011). Survivin monomer plays an essential role in apoptosis regulation. *J Biol Chem*, *286*(26), 23296-23307. https://doi.org/10.1074/jbc.M111.237586

Paz, A., Haklai, R., Elad-Sfadia, G., Ballan, E., & Kloog, Y. (2001). Galectin-1 binds oncogenic H-Ras to mediate Ras membrane anchorage and cell transformation. *Oncogene*, *20*(51), 7486-7493. https://doi.org/10.1038/sj.onc.1204950

Perez Verdaguer, M., Zhang, T., Paulo, J. A., Gygi, S., Watkins, S. C., Sakurai, H., & Sorkin, A. (2021). Mechanism of p38 MAPK-induced EGFR endocytosis and its crosstalk with ligand-induced pathways. *J Cell Biol*, *220*(7). https://doi.org/10.1083/jcb.202102005

Perricone, C., Versini, M., Ben-Ami, D., Gertel, S., Watad, A., Segel, M. J., Ceccarelli, F., Conti, F., Cantarini, L., Bogdanos, D. P., Antonelli, A., Amital, H., Valesini, G., & Shoenfeld, Y. (2016). Smoke and autoimmunity: The fire behind the disease. *Autoimmun Rev*, *15*(4), 354-374. https://doi.org/10.1016/j.autrev.2016.01.001

Prior, I. A., & Hancock, J. F. (2012). Ras trafficking, localization and compartmentalized signalling. *Semin Cell Dev Biol*, *23*(2), 145-153. https://doi.org/10.1016/j.semcdb.2011.09.002

Prior, I. A., Lewis, P. D., & Mattos, C. (2012). A comprehensive survey of Ras mutations in cancer. *Cancer Res*, *72*(10), 2457-2467. https://doi.org/10.1158/0008-5472.CAN-11-2612

Rabinovich, G. A., Alonso, C. R., Sotomayor, C. E., Durand, S., Bocco, J. L., & Riera, C. M. (2000). Molecular mechanisms implicated in galectin-1-induced apoptosis: activation of the AP-1 transcription factor and downregulation of Bcl-2. *Cell Death Differ*, *7*(8), 747-753. https://doi.org/10.1038/sj.cdd.4400708

Raetz, E. A., Morrison, D., Romanos-Sirakis, E., Gaynon, P., Sposto, R., Bhojwani, D., Bostrom, B. C., Brown, P., Eckroth, E., Cassar, J., Malvar, J., Buchbinder, A., & Carroll, W. L. (2014). A phase I study of EZN-3042, a novel survivin messenger ribonucleic acid (mRNA) antagonist, administered in combination with chemotherapy in children with relapsed acute lymphoblastic leukemia (ALL): a report from the therapeutic advances in childhood leukemia and lymphoma (TACL) consortium. *J Pediatr Hematol Oncol*, *36*(6), 458-463. https://doi.org/10.1097/MPH.0b013e3182a8f58f

Rane, M. J., Song, Y., Jin, S., Barati, M. T., Wu, R., Kausar, H., Tan, Y., Wang, Y., Zhou, G., Klein, J. B., Li, X., & Cai, L. (2010). Interplay between Akt and p38 MAPK pathways in the regulation of renal tubular cell apoptosis associated with diabetic nephropathy. *Am J Physiol Renal Physiol*, *298*(1), F49-61. https://doi.org/10.1152/ajprenal.00032.2009

Redza-Dutordoir, M., & Averill-Bates, D. A. (2016). Activation of apoptosis signalling pathways by reactive oxygen species. *Biochim Biophys Acta*, *1863*(12), 2977-2992. https://doi.org/10.1016/j.bbamcr.2016.09.012

Rodel, F., Sprenger, T., Kaina, B., Liersch, T., Rodel, C., Fulda, S., & Hehlgans, S. (2012). Survivin as a prognostic/predictive marker and molecular target in cancer therapy. *Curr Med Chem*, *19*(22), 3679-3688. https://doi.org/10.2174/092986712801661040

Rodgers, J. T., King, K. Y., Brett, J. O., Cromie, M. J., Charville, G. W., Maguire, K. K., Brunson, C., Mastey, N., Liu, L., Tsai, C. R., Goodell, M. A., & Rando, T. A. (2014). mTORC1 controls the adaptive transition of quiescent stem cells from G0 to G(Alert). *Nature*, *510*(7505), 393-396. https://doi.org/10.1038/nature13255

Rosa, J., Canovas, P., Islam, A., Altieri, D. C., & Doxsey, S. J. (2006). Survivin modulates microtubule dynamics and nucleation throughout the cell cycle. *Mol Biol Cell*, *17*(3), 1483-1493. https://doi.org/10.1091/mbc.e05-08-0723

Rubinstein, A. D., Eisenstein, M., Ber, Y., Bialik, S., & Kimchi, A. (2011). The autophagy protein Atg12 associates with antiapoptotic Bcl-2 family members to promote mitochondrial apoptosis. *Mol Cell*, *44*(5), 698-709. https://doi.org/10.1016/j.molcel.2011.10.014

Sabharwal, S. S., & Schumacker, P. T. (2014). Mitochondrial ROS in cancer: initiators, amplifiers or an Achilles' heel? *Nat Rev Cancer*, *14*(11), 709-721. https://doi.org/10.1038/nrc3803

Sabnis, A. J., & Bivona, T. G. (2019). Principles of Resistance to Targeted Cancer Therapy: Lessons from Basic and Translational Cancer Biology. *Trends Mol Med*, *25*(3), 185-197. https://doi.org/10.1016/j.molmed.2018.12.009

Sah, N. K., Munshi, A., Hobbs, M., Carter, B. Z., Andreeff, M., & Meyn, R. E. (2006). Effect of downregulation of survivin expression on radiosensitivity of human epidermoid carcinoma cells. *Int J Radiat Oncol Biol Phys*, *66*(3), 852-859. https://doi.org/10.1016/j.ijrobp.2006.06.049

Sano, R., & Reed, J. C. (2013). ER stress-induced cell death mechanisms. *Biochim Biophys Acta*, *1833*(12), 3460-3470. https://doi.org/10.1016/j.bbamcr.2013.06.028

Schutz, I., Lopez-Hernandez, T., Gao, Q., Puchkov, D., Jabs, S., Nordmeyer, D., Schmudde, M., Ruhl, E., Graf, C. M., & Haucke, V. (2016). Lysosomal Dysfunction Caused by Cellular Accumulation of Silica Nanoparticles. *J Biol Chem*, *291*(27), 14170-14184. https://doi.org/10.1074/jbc.M115.710947

Serrano-Puebla, A., & Boya, P. (2018). Lysosomal membrane permeabilization as a cell death mechanism in cancer cells. *Biochem Soc Trans*, *46*(2), 207-215. https://doi.org/10.1042/BST20170130

Shi, Z. D., Pang, K., Wu, Z. X., Dong, Y., Hao, L., Qin, J. X., Wang, W., Chen, Z. S., & Han, C. H. (2023). Tumor cell plasticity in targeted therapy-induced resistance: mechanisms and new strategies. *Signal Transduct Target Ther*, *8*(1), 113. https://doi.org/10.1038/s41392-023-01383-x

Shin, H. J., Kim, H., Oh, S., Lee, J. G., Kee, M., Ko, H. J., Kweon, M. N., Won, K. J., & Baek, S. H. (2016). AMPK-SKP2-CARM1 signalling cascade in transcriptional regulation of autophagy. *Nature*, *534*(7608), 553-557. https://doi.org/10.1038/nature18014

Sok, P., Gogl, G., Kumar, G. S., Alexa, A., Singh, N., Kirsch, K., Sebo, A., Drahos, L., Gaspari, Z., Peti, W., & Remenyi, A. (2020). MAP Kinase-Mediated Activation of RSK1 and MK2 Substrate Kinases. *Structure*, *28*(10), 1101-1113 e1105. https://doi.org/10.1016/j.str.2020.06.007

Sriramoju, B., Kanwar, R. K., & Kanwar, J. R. (2015). Nanoformulated Mutant SurR9-C84A: a Possible Key for Alzheimer's and its Associated Inflammation. *Pharm Res*, *32*(8), 2787-2797. https://doi.org/10.1007/s11095-015-1664-8

Stauber, R. H., Knauer, S. K., Habtemichael, N., Bier, C., Unruhe, B., Weisheit, S., Spange, S., Nonnenmacher, F., Fetz, V., Ginter, T., Reichardt, S., Liebmann, C., Schneider, G., & Kramer, O. H. (2012). A combination of a ribonucleotide reductase inhibitor and histone deacetylase inhibitors downregulates EGFR and triggers BIM-dependent apoptosis in head and neck cancer. *Oncotarget*, *3*(1), 31-43. https://doi.org/10.18632/oncotarget.430

Stauber, R. H., Mann, W., & Knauer, S. K. (2007). Nuclear and cytoplasmic survivin: molecular mechanism, prognostic, and therapeutic potential. *Cancer Res*, *67*(13), 5999-6002. https://doi.org/10.1158/0008-5472.CAN-07-0494

Stauber, R. H., Rabenhorst, U., Rekik, A., Engels, K., Bier, C., & Knauer, S. K. (2006). Nucleocytoplasmic shuttling and the biological activity of mouse survivin are regulated by an active nuclear export signal. *Traffic*, *7*(11), 1461-1472. https://doi.org/10.1111/j.1600-0854.2006.00486.x

Stern, R., Shuster, S., Neudecker, B. A., & Formby, B. (2002). Lactate stimulates fibroblast expression of hyaluronan and CD44: the Warburg effect revisited. *Exp Cell Res*, *276*(1), 24-31. https://doi.org/10.1006/excr.2002.5508

Stowell, S. R., Karmakar, S., Arthur, C. M., Ju, T., Rodrigues, L. C., Riul, T. B., Dias-Baruffi, M., Miner, J., McEver, R. P., & Cummings, R. D. (2009). Galectin-1 induces reversible phosphatidylserine exposure at the plasma membrane. *Mol Biol Cell*, *20*(5), 1408-1418. https://doi.org/10.1091/mbc.e08-07-0786

Svensson, B., Hafstrom, I., Forslind, K., Albertsson, K., Tarkowski, A., & Bokarewa, M. (2010). Increased expression of proto-oncogene survivin predicts Joint destruction and persistent disease activity in early rheumatoid arthritis. *Ann Med*, *42*(1), 45-54. https://doi.org/10.3109/07853890903376280

Takai-Yamashita, C., & Fuji, M. (2020). Hollow silica nanoparticles: A tiny pore with big dreams. *Advanced Powder Technology*, *31*(2), 804-807. https://doi.org/10.1016/j.apt.2019.11.034

Takenaka, Y., Fukumori, T., Yoshii, T., Oka, N., Inohara, H., Kim, H. R., Bresalier, R. S., & Raz, A. (2004). Nuclear export of phosphorylated galectin-3 regulates its antiapoptotic activity in response to chemotherapeutic drugs. *Mol Cell Biol*, *24*(10), 4395-4406. https://doi.org/10.1128/MCB.24.10.4395-4406.2004

Tan, X., Lambert, P. F., Rapraeger, A. C., & Anderson, R. A. (2016). Stress-Induced EGFR Trafficking: Mechanisms, Functions, and Therapeutic Implications. *Trends Cell Biol*, *26*(5), 352-366. https://doi.org/10.1016/j.tcb.2015.12.006

Tanida, I., Ueno, T., & Kominami, E. (2008). LC3 and Autophagy. *Methods Mol Biol*, *445*, 77-88. https://doi.org/10.1007/978-1-59745-157-4_4

Tian, Z., Yu, X., Ruan, Z., Zhu, M., Zhu, Y., & Hanagata, N. (2018). Magnetic mesoporous silica nanoparticles coated with thermo-responsive copolymer for potential chemo- and magnetic hyperthermia therapy. *Microporous and Mesoporous Materials*, *256*(1387-1811), 1-9. https://doi.org/10.1016/j.micromeso.2017.07.053

Tikekar, R. V., Pan, Y., & Nitin, N. (2013). Fate of curcumin encapsulated in silica nanoparticle stabilized Pickering emulsion during storage and simulated digestion. *Food Research International*, *Volume 51*(Issue 1), 370-377. https://doi.org/10.1016/j.foodres.2012.12.027

Tirro, E., Consoli, M. L., Massimino, M., Manzella, L., Frasca, F., Sciacca, L., Vicari, L., Stassi, G., Messina, L., Messina, A., & Vigneri, P. (2006). Altered expression of c-IAP1, survivin, and Smac contributes to chemotherapy resistance in thyroid cancer cells. *Cancer Res*, *66*(8), 4263-4272. https://doi.org/10.1158/0008-5472.CAN-05-3248

Tomas, A., Jones, S., Vaughan, S. O., Hochhauser, D., & Futter, C. E. (2017). Stress-specific p38 MAPK activation is sufficient to drive EGFR endocytosis but not its nuclear translocation. *J Cell Sci*, *130*(15), 2481-2490. https://doi.org/10.1242/jcs.202358

Townley, A. R., & Wheatley, S. P. (2020). Mitochondrial survivin reduces oxidative phosphorylation in cancer cells by inhibiting mitophagy. *J Cell Sci*, *133*(21). https://doi.org/10.1242/jcs.247379

Tsai, P. H., Wang, M. L., Chang, J. H., Yarmishyn, A. A., Nhi Nguyen, P. N., Chen, W., Chien, Y., Huo, T. I., Mou, C. Y., & Chiou, S. H. (2019). Dual Delivery of HNF4alpha and Cisplatin by Mesoporous Silica Nanoparticles Inhibits Cancer Pluripotency and Tumorigenicity in Hepatoma-Derived CD133-Expressing Stem Cells. *ACS Appl Mater Interfaces*, *11*(22), 19808-19818. https://doi.org/10.1021/acsami.9b04474

Tsapras, P., & Nezis, I. P. (2017). Caspase involvement in autophagy. *Cell Death Differ*, *24*(8), 1369-1379. https://doi.org/10.1038/cdd.2017.43

Uchimoto, T., Nohara, H., Kamehara, R., Iwamura, M., Watanabe, N., & Kobayashi, Y. (1999). Mechanism of apoptosis induced by a lysosomotropic agent, L-Leucyl-L-Leucine methyl ester. *Apoptosis*, *4*(5), 357-362. https://doi.org/10.1023/a:1009695221038

Vance, M. E., Kuiken, T., Vejerano, E. P., McGinnis, S. P., Hochella, M. F., Jr., Rejeski, D., & Hull, M. S. (2015). Nanotechnology in the real world: Redeveloping the nanomaterial consumer products inventory. *Beilstein J Nanotechnol*, *6*, 1769-1780. https://doi.org/10.3762/bjnano.6.181

Velculescu, V. E., Madden, S. L., Zhang, L., Lash, A. E., Yu, J., Rago, C., Lal, A., Wang, C. J., Beaudry, G. A., Ciriello, K. M., Cook, B. P., Dufault, M. R., Ferguson, A. T., Gao, Y., He, T. C., Hermeking, H., Hiraldo, S. K., Hwang, P. M., Lopez, M. A., . . . et al. (1999). Analysis of human transcriptomes. *Nat Genet*, *23*(4), 387-388. https://doi.org/10.1038/70487

Vequaud, E., Desplanques, G., Jezequel, P., Juin, P., & Barille-Nion, S. (2016). Survivin contributes to DNA repair by homologous recombination in breast cancer cells. *Breast Cancer Res Treat*, *155*(1), 53-63. https://doi.org/10.1007/s10549-015-3657-z

Verdecia, M. A., Huang, H., Dutil, E., Kaiser, D. A., Hunter, T., & Noel, J. P. (2000). Structure of the human anti-apoptotic protein survivin reveals a dimeric arrangement. *Nat Struct Biol*, *7*(7), 602-608. https://doi.org/10.1038/76838

Villar, V. H., Nguyen, T. L., Delcroix, V., Teres, S., Bouchecareilh, M., Salin, B., Bodineau, C., Vacher, P., Priault, M., Soubeyran, P., & Duran, R. V. (2017). mTORC1 inhibition

in cancer cells protects from glutaminolysis-mediated apoptosis during nutrient limitation. *Nat Commun*, *8*, 14124. https://doi.org/10.1038/ncomms14124

Vladoiu, M. C., Labrie, M., & St-Pierre, Y. (2014). Intracellular galectins in cancer cells: potential new targets for therapy (Review). *Int J Oncol*, *44*(4), 1001-1014. https://doi.org/10.3892/ijo.2014.2267

Vucicevic, L., Misirkic, M., Janjetovic, K., Vilimanovich, U., Sudar, E., Isenovic, E., Prica, M., Harhaji-Trajkovic, L., Kravic-Stevovic, T., Bumbasirevic, V., & Trajkovic, V. (2011). Compound C induces protective autophagy in cancer cells through AMPK inhibition-independent blockade of Akt/mTOR pathway. *Autophagy*, *7*(1), 40-50. https://doi.org/10.4161/auto.7.1.13883

Vyakarnam, A., Dagher, S. F., Wang, J. L., & Patterson, R. J. (1997). Evidence for a role for galectin-1 in pre-mRNA splicing. *Mol Cell Biol*, *17*(8), 4730-4737. https://doi.org/10.1128/MCB.17.8.4730

Vyakarnam, A., Lenneman, A. J., Lakkides, K. M., Patterson, R. J., & Wang, J. L. (1998). A comparative nuclear localization study of galectin-1 with other splicing components. *Exp Cell Res*, *242*(2), 419-428. https://doi.org/10.1006/excr.1998.4111

Wang, H., Holloway, M. P., Ma, L., Cooper, Z. A., Riolo, M., Samkari, A., Elenitoba-Johnson, K. S., Chin, Y. E., & Altura, R. A. (2010). Acetylation directs survivin nuclear localization to repress STAT3 oncogenic activity. *J Biol Chem*, *285*(46), 36129-36137. https://doi.org/10.1074/jbc.M110.152777

Wang, J., Seebacher, N., Shi, H., Kan, Q., & Duan, Z. (2017). Novel strategies to prevent the development of multidrug resistance (MDR) in cancer. *Oncotarget*, *8*(48), 84559-84571. https://doi.org/10.18632/oncotarget.19187

Wang, Q., & Greene, M. I. (2005). EGFR enhances Survivin expression through the phosphoinositide 3 (PI-3) kinase signaling pathway. *Exp Mol Pathol*, *79*(2), 100-107. https://doi.org/10.1016/j.yexmp.2005.05.002

Wang, Q., Wu, P. C., Roberson, R. S., Luk, B. V., Ivanova, I., Chu, E., & Wu, D. Y. (2011). Survivin and escaping in therapy-induced cellular senescence. *Int J Cancer*, *128*(7), 1546-1558. https://doi.org/10.1002/ijc.25482

Wang, R. C., & Levine, B. (2010). Autophagy in cellular growth control. *FEBS Lett*, *584*(7), 1417-1426. https://doi.org/10.1016/j.febslet.2010.01.009

Wang, Y., Kuramitsu, Y., Baron, B., Kitagawa, T., Tokuda, K., Akada, J., Maehara, S. I., Maehara, Y., & Nakamura, K. (2017). PI3K inhibitor LY294002, as opposed to wortmannin, enhances AKT phosphorylation in gemcitabine-resistant pancreatic cancer cells. *Int J Oncol*, *50*(2), 606-612. https://doi.org/10.3892/ijo.2016.3804

Wani, T. H., Chowdhury, G., & Chakrabarty, A. (2021). Generation of reactive oxygen species is the primary mode of action and cause of survivin suppression by sepantronium bromide (YM155). *RSC Med Chem*, *12*(4), 566-578. https://doi.org/10.1039/d0md00383b

Wasen, C., Turkkila, M., Bossios, A., Erlandsson, M., Andersson, K. M., Ekerljung, L., Malmhall, C., Brisslert, M., Toyra Silfversward, S., Lundback, B., & Bokarewa, M. I. (2017). Smoking activates cytotoxic CD8(+) T cells and causes survivin release in rheumatoid arthritis. *J Autoimmun*, *78*, 101-110. https://doi.org/10.1016/j.jaut.2016.12.009

Webber, J. L., & Tooze, S. A. (2010). Coordinated regulation of autophagy by p38alpha MAPK through mAtg9 and p38IP. *EMBO J*, *29*(1), 27-40. https://doi.org/10.1038/emboj.2009.321

Wei, Y., Pattingre, S., Sinha, S., Bassik, M., & Levine, B. (2008). JNK1-mediated phosphorylation of Bcl-2 regulates starvation-induced autophagy. *Mol Cell*, *30*(6), 678-688. https://doi.org/10.1016/j.molcel.2008.06.001

Wei, Y., Sinha, S., & Levine, B. (2008). Dual role of JNK1-mediated phosphorylation of Bcl-2 in autophagy and apoptosis regulation. *Autophagy*, *4*(7), 949-951. https://doi.org/10.4161/auto.6788

Wheatley, S. P., & Altieri, D. C. (2019). Survivin at a glance. *J Cell Sci*, *132*(7). https://doi.org/10.1242/jcs.223826

White, E. Z., Pennant, N. M., Carter, J. R., Hawsawi, O., Odero-Marah, V., & Hinton, C. V. (2020). Serum deprivation initiates adaptation and survival to oxidative stress in prostate cancer cells. *Sci Rep*, *10*(1), 12505. https://doi.org/10.1038/s41598-020-68668-x

Wiechno, P., Somer, B. G., Mellado, B., Chlosta, P. L., Cervera Grau, J. M., Castellano, D., Reuter, C., Stockle, M., Kamradt, J., Pikiel, J., Duran, I., Wedel, S., Callies, S., Andre, V., Hurt, K., Brown, J., Lahn, M., & Heinrich, B. (2014). A randomised phase 2 study combining LY2181308 sodium (survivin antisense oligonucleotide) with first-line docetaxel/prednisone in patients with castration-resistant prostate cancer. *Eur Urol*, *65*(3), 516-520. https://doi.org/10.1016/j.eururo.2013.10.039

Wolanin, K., & Piwocka, K. (2007). [Role of survivin in mitosis]. *Postepy Biochem*, *53*(1), 10-18. https://www.ncbi.nlm.nih.gov/pubmed/17718383 (Rola i znaczenie surwiwiny w przebiegu mitozy.)

Wu, C. A., Chao, Y., Shiah, S. G., & Lin, W. W. (2013). Nutrient deprivation induces the Warburg effect through ROS/AMPK-dependent activation of pyruvate dehydrogenase kinase. *Biochim Biophys Acta*, *1833*(5), 1147-1156. https://doi.org/10.1016/j.bbamcr.2013.01.025

Xi, H., Wang, S., Wang, B., Hong, X., Liu, X., Li, M., Shen, R., & Dong, Q. (2022). The role of interaction between autophagy and apoptosis in tumorigenesis (Review). *Oncol Rep*, *48*(6). https://doi.org/10.3892/or.2022.8423

Yakkala, C., Chiang, C. L., Kandalaft, L., Denys, A., & Duran, R. (2019). Cryoablation and Immunotherapy: An Enthralling Synergy to Confront the Tumors. *Front Immunol*, *10*, 2283. https://doi.org/10.3389/fimmu.2019.02283

Yang, Y., Feng, L. Q., & Zheng, X. X. (2011). Microtubule and kinesin/dynein-dependent, bi-directional transport of autolysosomes in neurites of PC12 cells. *Int J Biochem Cell Biol*, *43*(8), 1147-1156. https://doi.org/10.1016/j.biocel.2011.04.007

Yao, R. Q., Ren, C., Xia, Z. F., & Yao, Y. M. (2021). Organelle-specific autophagy in inflammatory diseases: a potential therapeutic target underlying the quality control of multiple organelles. *Autophagy*, *17*(2), 385-401. https://doi.org/10.1080/15548627.2020.1725377

Yogalingam, G., Hwang, S., Ferreira, J. C., & Mochly-Rosen, D. (2013). Glyceraldehyde-3-phosphate dehydrogenase (GAPDH) phosphorylation by protein kinase Cdelta (PKCdelta) inhibits mitochondria elimination by lysosomal-like structures following ischemia and reoxygenation-induced injury. *J Biol Chem*, *288*(26), 18947-18960. https://doi.org/10.1074/jbc.M113.466870

Yousefi, S., Perozzo, R., Schmid, I., Ziemiecki, A., Schaffner, T., Scapozza, L., Brunner, T., & Simon, H. U. (2006). Calpain-mediated cleavage of Atg5 switches autophagy to apoptosis. *Nat Cell Biol*, *8*(10), 1124-1132. https://doi.org/10.1038/ncb1482

Yu, L., Chen, Y., & Tooze, S. A. (2018). Autophagy pathway: Cellular and molecular mechanisms. *Autophagy*, *14*(2), 207-215. https://doi.org/10.1080/15548627.2017.1378838

Zhang, L., Yang, X., Zhao, B., & Cai, Z. (2015). Acquired resistance to EGFR tyrosine kinase inhibitor in A431 squamous cell carcinoma xenografts is mediated by c-Kit pathway transduction. *Tumour Biol*, *36*(4), 2993-2999. https://doi.org/10.1007/s13277-014-2932-7

Zhang, X., Cheng, X., Yu, L., Yang, J., Calvo, R., Patnaik, S., Hu, X., Gao, Q., Yang, M., Lawas, M., Delling, M., Marugan, J., Ferrer, M., & Xu, H. (2016). MCOLN1 is a ROS sensor in lysosomes that regulates autophagy. *Nat Commun*, *7*, 12109. https://doi.org/10.1038/ncomms12109

Zhang, Y., Liu, D., Hu, H., Zhang, P., Xie, R., & Cui, W. (2019). HIF-1alpha/BNIP3 signaling pathway-induced-autophagy plays protective role during myocardial ischemia-reperfusion injury. *Biomed Pharmacother*, *120*, 109464. https://doi.org/10.1016/j.biopha.2019.109464

Zhao, Y., Yang, J., Liao, W., Liu, X., Zhang, H., Wang, S., Wang, D., Feng, J., Yu, L., & Zhu, W. G. (2010). Cytosolic FoxO1 is essential for the induction of autophagy and tumour suppressor activity. *Nat Cell Biol*, *12*(7), 665-675. https://doi.org/10.1038/ncb2069

Zhitomirsky, B., Farber, H., & Assaraf, Y. G. (2018). LysoTracker and MitoTracker Red are transport substrates of P-glycoprotein: implications for anticancer drug design evading multidrug resistance. *J Cell Mol Med*, *22*(4), 2131-2141. https://doi.org/10.1111/jcmm.13485

Zhou, J., Liao, W., Yang, J., Ma, K., Li, X., Wang, Y., Wang, D., Wang, L., Zhang, Y., Yin, Y., Zhao, Y., & Zhu, W. G. (2012). FOXO3 induces FOXO1-dependent autophagy by activating the AKT1 signaling pathway. *Autophagy*, *8*(12), 1712-1723. https://doi.org/10.4161/auto.21830

Zorov, D. B., Juhaszova, M., & Sollott, S. J. (2014). Mitochondrial reactive oxygen species (ROS) and ROS-induced ROS release. *Physiol Rev*, *94*(3), 909-950. https://doi.org/10.1152/physrev.00026.2013

Zwang, Y., & Yarden, Y. (2006). p38 MAP kinase mediates stress-induced internalization of EGFR: implications for cancer chemotherapy. *EMBO J*, *25*(18), 4195-4206. https://doi.org/10.1038/sj.emboj.7601297

6 APPENDIX

6.1 ABBREVIATIONS

µL	microliter
µM	micromolar
2DG	2-deoxy-D-glucose
Akt	Ak strain transforming
AMP	adenosine monophosphate
AMPK	AMP-activated protein kinase
Apaf-1	apoptotic protease activating factor 1
APS	ammonium persulfate
aSiNP	amorphous silica nanoparticle
ATF6	activating transcription factor 6
ATG	Autophagy-related genes
ATP	adenosine triphosphate
Bcl-2	B-cell lymphoma 2
BD	Behecet`s Disease
BIM/Bim	Bcl-2-interacting mediator of cell death
BIR	baculovirus inhibitor of apoptosis repeat
BIRC5	baculoviral inhibitor of apoptosis repeat-containing 5
BLAST	Basic Local Alignment Search Tool
BNIP3	CL2/adenovirus E1B 19 kDa interacting protein 3
BRUCE	Bir containing Ub-Conjugating Enzyme
BSA	Bovines Serum Albumin
CAD	caspase-activated DNase
CaMMK2	calcium/calmodulin-dependent protein kinase kinase 2
CARM-1	coactivator-associated arginine methyltransferase 1
CBP	CREB-binding protein
CC	Compound C
CD44	cluster of differentiation 44
CHOP	C/EBP homologous protein
CLASTR	Cell Line Authentication using STR
cm	centimeter
CMA	chaperone-mediated autophagy
CQ	Chloroquine
CRM1	Chromosomal Maintenance 1
Ctrl/CTRL	control
Cy3	cyanine3
DIABLO	direct Inhibitor of Apoptosis-Binding protein with LOw pI
DISC	death-inducing signaling complex
DLS	dynamic light scattering
DMEM	Dulbeccos Modified Eagle Medium
DMSO	Dimethyl sulfoxide
DNA	desoxyribonucleic acid
dNTPs	nucleoside triphosphate
Drp-1	dynamic-like-protein 1
DTT	Dithiothreitol
DTT	Dithiothreitol

ECL	enhanced chemiluminescence
EDTA	Ethylenediaminetetraacetic acid
EGFR	epidermal growth factor receptor
EMT	epithelial-mesenchymal transition
EMT	epithelial-to-mesenchymal transition
en.	endogenous
eNOS	endothelial nitric oxide synthase
ER	endoplasmic reticulum
ERAD	ER-assisted degradation
ERK	extracellular-signal regulated kinases
EthD-1	ethidium homodimer 1
FACS	fluorescence-activated cell sorting
FAK	focal adhesion kinase
Fas	FS7-associated cell surface antigen
FCS	Fetal Calf Serum
FIP200	FAK family-interacting protein of 200 kDa
FITC	fluorescein isothiocyanate
FOXO/FoxO	forkhead box class one
FOXP3	forkhead-Box-Protein P3
GAPDH	glycerinaldehyd-3-phosphat-Dehydrogenase
GEM	gemcitabine
GFP	green fluorescent protein
GFP	Green fluorescent protein
GST	gluthatione S-transferase
h	hour
HCC	hepatocellular carcinoma
HIF	hypoxia-inducible factor
HOPS	homotypic fusion and vacuole protein sorting
HPLC	High Performance Liquid Chromatography
HRP	horseraddish peroxidase
HTE	Hutner’s Trace Elements
IAP	inhibitors of apoptosis
IARS	International Agency for Research on Cancer
IKK	IκB kinase
INCENP	inner centromere protein
IP	immunoprecipitation
IQGAP1	IQ Motif Containing GTPase Activating Protein 1
IRE1α	inositol-requiring protein-1α
JAK	janus kinase
JNK	c-Jun-N-terminal kinase
kDa	kilo Dalton
LAMP-1	Lysosomal Associated Membrane Protein 1
LC	microtubule-associated proteins 1A/1B light chain 3
LDH	lactate dehydrogenase
LLMOe	L-Leucyl-L-Leucine methyl ester (hydrochloride)
LND	lonidamine
log	logarithm
LY	LY294002
MAPK	mitogen-activated protein kinase
MCF-7	Michigan Cancer Foundation - 7
Mcl-1	myeloid cell leukemia-1

MCOLN1	mucolipin TRP (transient receptor potential) cation channel 1
MEM	Opti-Minimal Essential Medium
Menad.	menadione
min	minute
miRNA	micro-RNA
MK2	mitogen-activated protein kinase-activated protein kinase-2
MKK3	mitogen-activated protein kinase-activated protein kinase-kinase-3
mL	milliliter
MnSOD	manganese-dependent superoxide dismutase
mRNA	messenger RNA
MSN	mesoporous silica nanoparticles
mTOR	mammalian target of rapamycin
mTORC1	mTOR complex 1
MTS	mitochondrial targeting sequence
NAC	N-acetylcysteine
NAIP	Neuronal Apoptosis Inhibitory Protein
NEAA	Non-Essential Amino Acids
NES	nuclear export signal
NET	neutrophil extracellular traps
NfKB	Nuclear factor kappa-light-chain-enhancer of activated B cells
NICD1	Notch1 intracellular domain
nM	nanomolar
NP	Nanoparticle/s
p	protein
p-	phospho-
PAGE	polyacrylamide gel electrophoresis
PARK2	parkin RBR E3 ubiquitin protein ligase
PBS	Phosphate Buffered Saline
PBS-T	Phosphate Buffered Saline-Tween
PBSTD	Phosphate Buffered Saline-Triton X-100-DMSO
PDK1	pyruvate dehydrogenase kinase isoform 1
PE	phosphatidylethanolamine
PenStrep	Penicillin/Streptomycin
PERK	protein kinase RNA (PKR)-like ER kinase
PFA	paraformaldehyde
PI(3)P	phosphatidylinositol-3-phosphate
PI3K	Phosphoinositide 3-kinases
PINK-1	PTEN-induced-kinase-1
PKB	Protein kinase B
PTEN	Phosphatase and TENsin homolog deleted on chromosome 10
PVDF	polyvinylidenfluoride
R	residues
RAB	Ras-like GTPase
RAS/Ras	rat sarcoma
RBP-Jκ	Recombination Signal Binding Protein for Immunoglobulin Kappa J Region
READ	ER-assisted degradation
RING	Really Interesting New Gene
RIPA	radioimmunoprecipitation assay buffer
RIPK	receptor interaction protein kinases 1
RNA	ribonucleic acid
ROS	reactive oxygen species

RPC	relative protein content
rpm	revolutions per minute
RPMI	Roswell Park Memorial Institute
RT	room temperature
SAPK	stress-activated protein kinases
SDS	sodium Dodecyl Sulfate
Ser	serine
shRNA	short hairpin RNA
SiNP	silica nanoparticle/s
siRNA	short interfering RNA
SIRT/Sirt	sirtuin
Smac	second mitochondria-derived activator of caspase
SNAP29	SNARE-binding protein synaptosomal-associated protein of 29 kDa
SNARE	soluble N-ethylmaleimide-sensitive-factor attachment receptor
STAT3	signal transducers and activators of transcription 3
STX17	syntaxin 17
Surv.	Survivin
TAE	tris acetat EDTA buffer
TAE	Tris-Acetate-EDTA-Puffer
Tat	transactivator of transcription
TEMED	tetramethylethylenediamine
TF	transcription factor
TFEB	transcription factor EB
Thr	threonine
TME	tumor microenvironment
TNF	tumor necrosis factor
TNFR	tumor necrosis factor
TRAIL	TNF-related apoptosis-inducing ligand
TRIS /Tris	tris(hydroxymethyl)-aminomethane
Tyr	tyrosine
ULK-1	unc-51-like kinase 1
UPR	unfolded protein response
UV	ultraviolet
VAMP8	vesicle-associated membrane protein 8
VE	deionized
Vit C	vitamin C
VPS	vacuolar protein sorting proteins
W	wortmannin
w	with
w/o	without
WB	western blot
WHO	World Health Organization
WIPI	WD-repeat protein interacting with phosphoinositides
Wnt	wingless-type MMTV integration site
WT	wildtype
XIAP	X-linked inhibitor of apoptosis protein
YM155	sepantronium bromide

6.2 CONTENT OF FIGURES

Figure 1. Illustration of the extrinsic and intrinsic apoptotic pathway 5
Figure 2. Canonical autophagy 7
Figure 3. Tethering and fusion of autophagosomes with lysosomes8
Figure 4. Molecular structure of Survivin 11
Figure 5. Survivin in apoptosis and autophagy 13
Figure 6. Silica nanoparticle types and functionalization 17
Figure 7. Types of cell death triggered by SiNP 19
Figure 8. Time and concentration dependent SiNP cell toxicity 26
Figure 9. Survivin enhances resistance against SiNP 27
Figure 10. Time-dependent uptake of Kisker (red) NPs 28
Figure 11. Contact and time dependent SiNP toxicity 29
Figure 12. Autophagy-related lysosomal shift 31
Figure 13. Localization of lysosomes and autophagosomes 32
Figure 14. LC3 conversion in response to different stimuli 33
Figure 15. Autophagy is triggered by serum deprivation and SiNP 34
Figure 16. Tracing of the acidic body generation via Lysotracker staining 35
Figure 17. Influence of Survivin knockdown on the localization of autophagy-related organelles 37
Figure 18. Influence of Survivin on the autophagy flux 38
Figure 19. Impact of SiNP on the actin network 40
Figure 20. Impact of SiNP onto microtubule dynamics of β-tubulin 41
Figure 21. Time-dependent ROS regulation 43
Figure 22. Mitochondrial fusion and fission 45
Figure 23. Mitophagy induction as a survival strategy or gate to cell death 46
Figure 24. ROS measurement via CellROX orange 47
Figure 25. Influence of Survivin knockdown on ROS generation upon SiNP exposure 48
Figure 26. Localization of SiNP in autophagy-related compartments 50
Figure 27. Galectin-1-assay 51
Figure 28. Time-related galectin-1 puncta assay 52
Figure 29. Relationship between p38 activation and Survivin downregulation in the context of elevated ROS levels 54
Figure 30. Dynamic autophagy regulation 56
Figure 31. SiNP promoted signaling pathways 57
Figure 32. The Akt/FoxO/BIM signaling after long-term Survivin-GFP expression 59
Figure 33. Role of AMPK in SiNP-mediated autophagy and toxicity 63
Figure 34. Role of PI3K on the Akt/mTOR pathway 64
Figure 35. Toxicity of PI3K inhibitor Wortmannin in combination with SiNP 65
Figure 36. Combinatorial treatment of SiNP with late-stage inhibitor CQ 66
Figure 37. Ras signaling pathway stabilized by galectin-1 at the cytosolic side of the cell membrane 70
Figure 38. FoxO regulation in response to low and high ROS levels 72
Figure 39. Bradford standard curve for extrapolation 93

6.3 CONTENT OF TABLES

Table 1: Appliances....78
Table 2: Chemicals and medium additives....80
Table 3: Laboratory consumables....81
Table 4: Enzymes....82
Table 5: Buffers and solutions....82
Table 6: Commercial kits and staining....83
Table 7: Cell lines....84
Table 8: Primary antibodies....85
Table 9. Secondary antibodies....87
Table 10: Nanoparticles....87
Table 11: Software....88
Table 12. Cell stock preparation....89
Table 13. Cell seeding....90
Table 14. SiNP treatment volume according to the used cell culture systems....91
Table 15. Overview of used chemical inhibitors and ROS scavengers or inducers used in the experiments....92
Table 16. SDS-Page....94
Table 17. Composition of the RNAiMax transfection complex for specific treatment volumes and cell numbers....95

6.4 SUPPLEMENTARY FIGURES

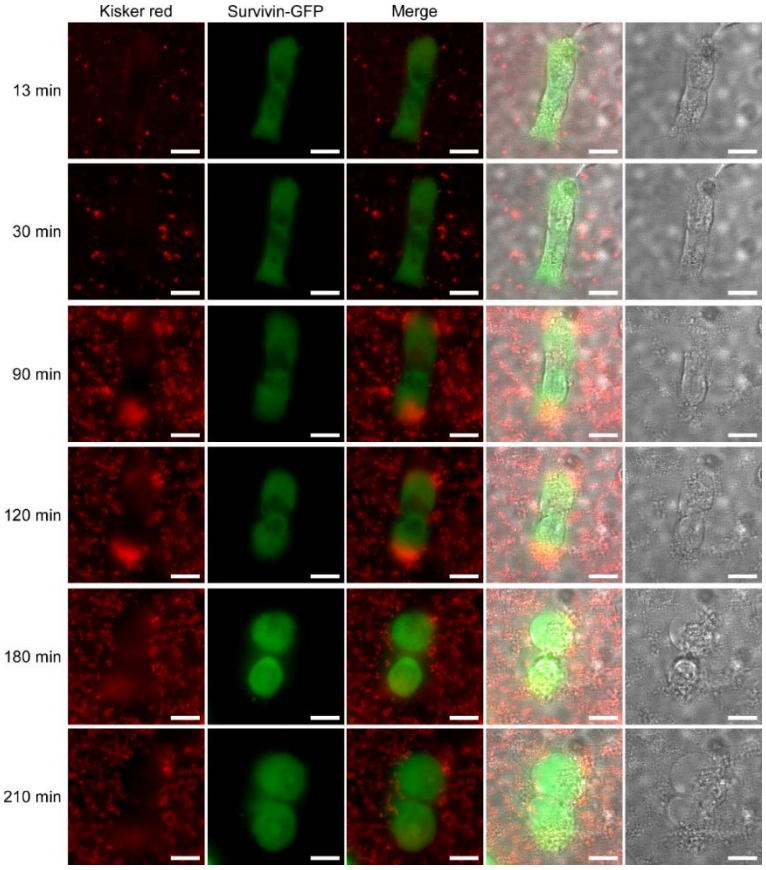

Supplementary Figure 1. Time kinetic of SiNP uptake in the absence of CQ. A431 Survivin-GFP stably transfected cells were treated with 60 µg/mL Kisker red particles. A431 low cells were cultivated after seeding for 24 h. The serum-containing medium was removed, and cells were washed three times with serum-free medium before treatment with 60 µg/mL Kisker red NP. Particle-containing medium was added directly under the microscope and images were taken continuously. Selected time points of 26.5h kinetics are shown. The scale bar indicates 50 µm.

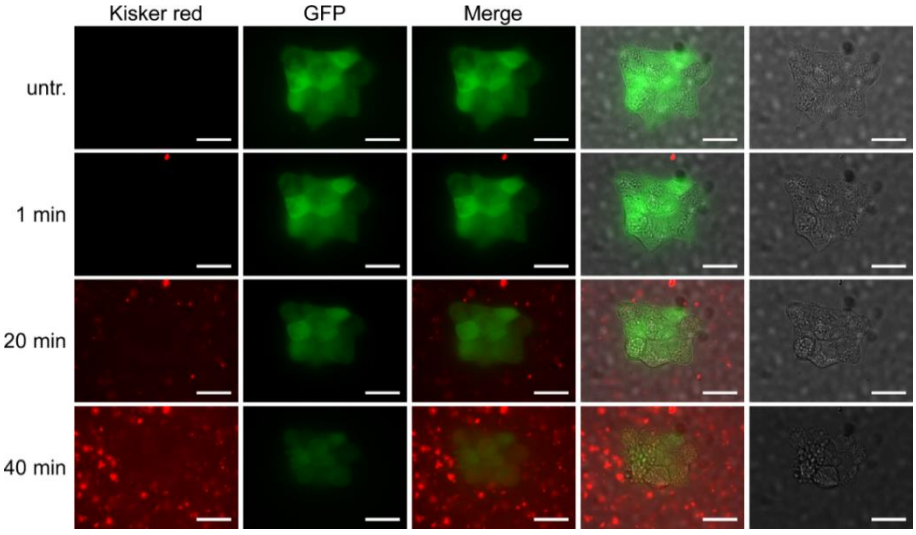

Supplementary Figure 2. A431 GFP stably transfected cells were treated with 60 µg/mL Kisker red particles. A431 GFP cells were cultivated after seeding for 24 h. The serum-containing medium was removed and cells were washed three times with serum-free medium before treatment with 60 µg/mL Kisker red NP. Particle-containing medium was added directly under the microscope and images were taken continuously. Selected time points are shown. The scale bar indicates 50 µm.

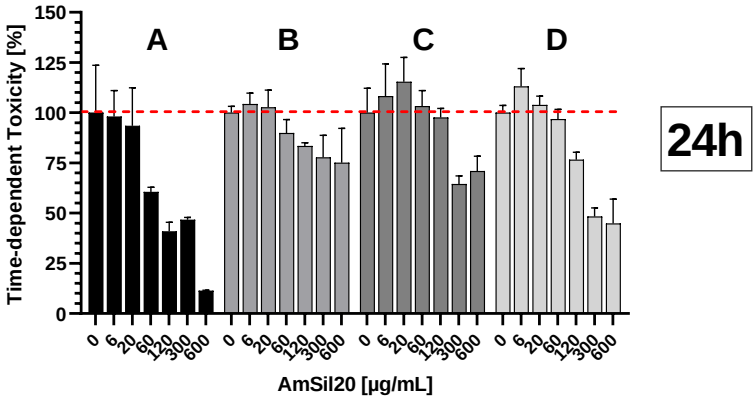

Supplementary Figure 3. Contact and time-dependent SiNP toxicity. A431 wt cells treated with rising SiNP concentrations starting from 0 µg/mL up to 600 µg/mL. Different treatment strategies were applied to investigate SiNP toxicity-related factors. For all approaches, cells were washed before the treatment to remove serum proteins. Then, cells were treated for 10 min with 100 µL serum-free medium containing different SiNP concentrations. After the 10 min incubation cells were treated as follows; A) Cells left in serum-free medium containing SiNP. B) 100 µL of serum-containing medium added to the remaining SiNP-containing medium C) Treatment medium discarded and 100 µL of serum-containing medium added. D) The treatment medium was removed, and cells were washed three times with serum-free medium and substituted with 100 µL of serum-containing medium. A-D) Cells were incubated for 2 h at 37°C, 5% CO_2 before cells were washed three times with PBS. Time-dependent toxicity between time points 2 h and 24 h is visualized through the normalization of time point 24 h to time point 2 h (see Figure 11). The precentral fraction was determined by dividing the mean value for time point 24 h by the mean value for time point 2 h.

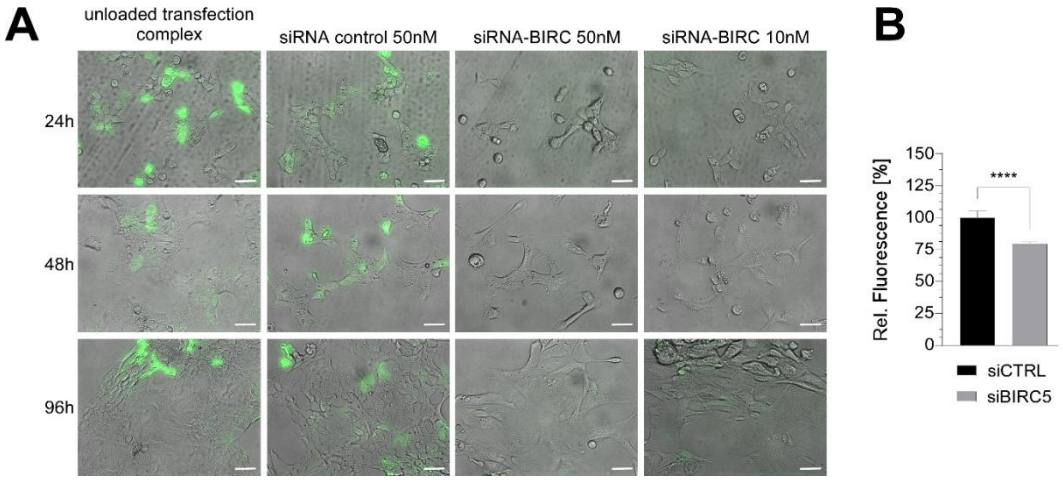

Supplementary Figure 4. Transfection efficiency. A) A431 Survivin-GFP reversely transfected with 50 nM or 10nM siRNA against BIRC 5 gene, coding for Surviving by use of Lipofectamine RNAiMax Transfection Reagent (Invitrogen) see section (4.2.4.1). Cells imaged after transfection time ended (24 h) and additionally after 48h and 96h. B) A) Efficiency of siRNA BIRC5 (siBIRC5) mediated Survivin-GFP knockdown. A431 Survivin-GFP cells were transiently transfected with siBIRC5 and the remaining GFP fluorescence was measured with a plate reader (Tecan).

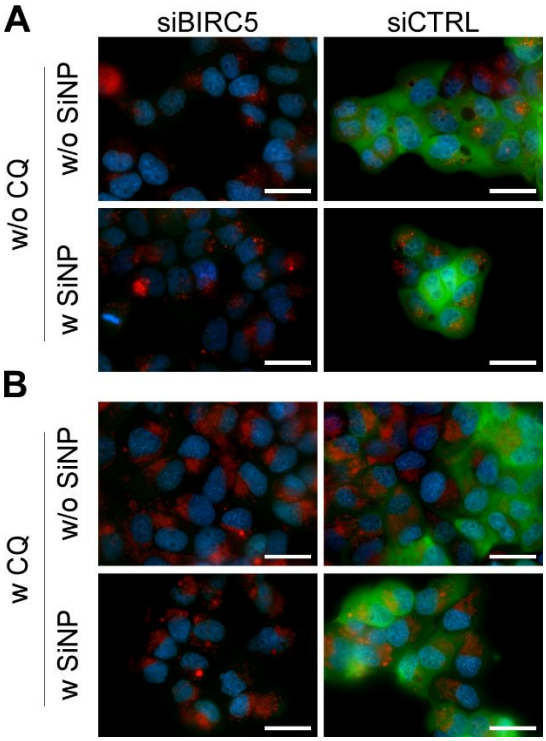

Supplementary Figure 5. The efficiency of the transient transfection with siRNA BIRC5. A431 Survivin-GFP expressing cells transiently transfected with a control siRNA (siCTRL) or siRNA BIRC5 against Survivin. Successful knockdown of Survivin-GFP indicated by the loss of GFP fluorescence. Figure related to (Figure 16).

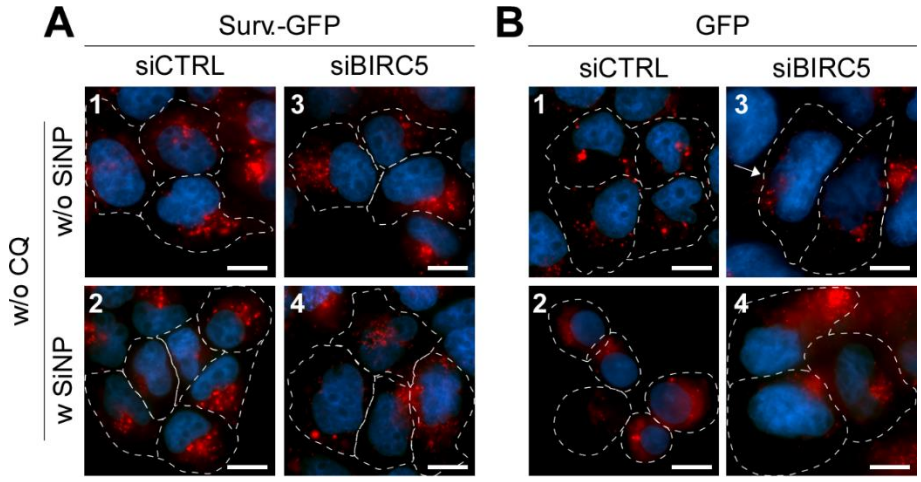

Supplementary Figure 6. Lysotracker staining of A431 cells with different Survivin levels in the absence of CQ. A, B) A431 Survivin-GFP or GFP expressing cells transiently transfected with siBIRC5 or with siCTRL. The successful Survivin knockdown was confirmed by a vanished GFP fluorescence (Supplementary Figure 5). Transiently transfected cells were incubated for 2 h in a serum-deprived medium in the absence or presence of 60 µg/mL SiNP. Samples were stained with 50 nM Lysotracker red dye for 30 min and imaged immediately. The scale bar is equal to 25 µm. Figure related to (Figure 16).

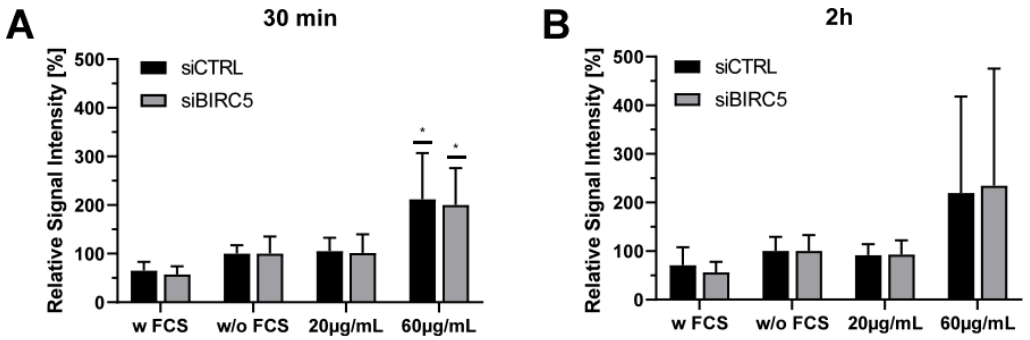

Supplementary Figure 7. Array scan quantitative analysis by use of single-cell measurements of CellROX green fluorescence in nuclei. The data were represented comparatively to visualize the effect of SiNP on ROS level in Survivin normal (CTRL) or deficient cells (siBIRC5) by data normalization to serum-free medium (w/o FCS) in (Figure 25B, D). The data set was compiled from four independent experiments with triplicates. Anova two-way test was performed comparing control groups (w/o FCS) to SiNP-treated samples with p*<0.05.

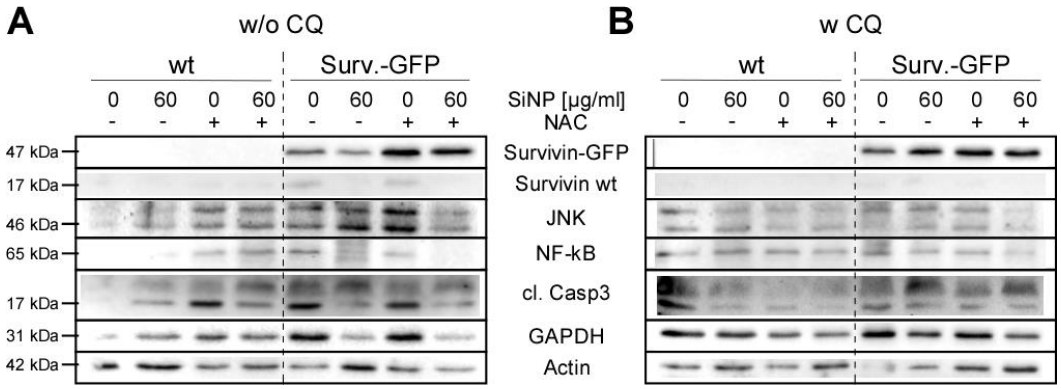

Supplementary Figure 8. SiNP-generated ROS interacts with several signaling pathways. Immunoblot analysis related to Figure 29. A431 wt and Survivin-GFP expressing cells treated without (A) or with (B) late-stage autophagy inhibitor Chloroquine (CQ) 24 h before SiNP treatment. Additionally, 5 µM NAC (+/-) was incubated for 2 h before SiNP were added. Cells incubated in the absence (-) or presence (+) of NAC and/ or CQ in serum-free medium with (+) or without (-) SiNP for 4 h. Western blot analysis was performed for inhibitor of apoptosis protein Survivin, apoptotic caspase 3 (cl. Casp3) and signaling pathways JNK and NF-kB, and housekeeping genes GAPDH and Actin.

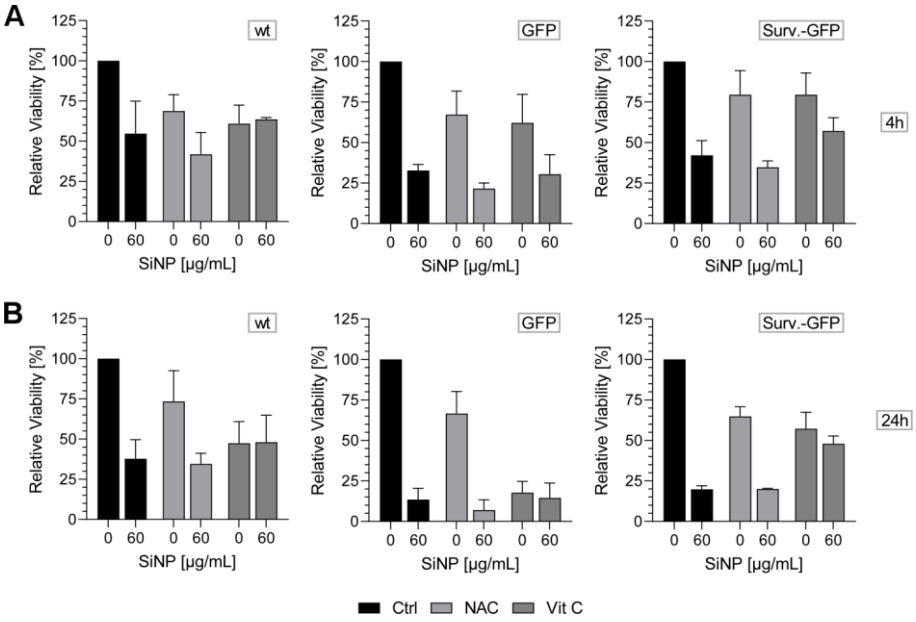

Supplementary Figure 9. Impact of ROS scavengers onto SiNP mediated toxicity. A431 wt, GFP or Survivin-GFP expressing cells seeded within a determined cell number and cultivated for 24 h. Cells were pretreated with 5µM N-Acetylcysteine (NAC) or Ascorbic acid or rather 200 µM Vitamin C (Vit C) for 2 h in the serum-containing medium before the medium was removed and cells were washed three times. Then serum-deprived medium with or without 60 µg/mL SiNP of type AmSil20 was added for 4 h in addition to the ROS scavenger's NAC and Vit C. Viability was determined via Alamar Blue viability assay and repeated after additional incubation in serum-containing medium without additives up to time point 24 h. The Experiment was performed twice with each experiment consisting of four samples.

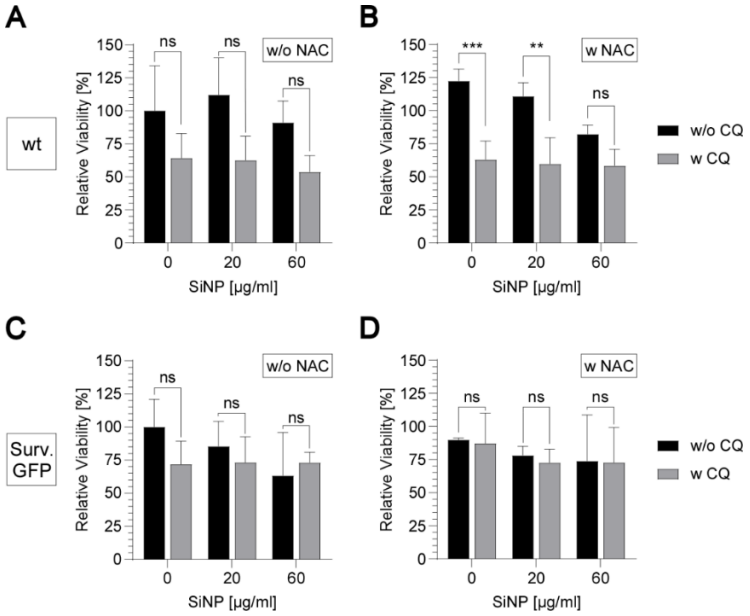

Supplementary Figure 10. Role of ROS in autophagy and SiNP-mediated toxicity. A431 wt and Survivin-GFP incubated without (A, C) or with (B, D) ROS scavenger NAC (5 mM) 2 h. Then, cells were treated in serum-deprived medium without (0) or with SiNP (20 or 60 µg/mL) in the presence or absence of NAC and/or CQ for 4 h. Cell viability was measured in triplicates in three independent experiments via Alamar Blue Reagent Assay. Data were normalized to serum-deprived, but otherwise untreated controls (C). Statistical analysis was performed with an Anova two-way test with p**<0.005, p***<0.0005, ns= not significant.

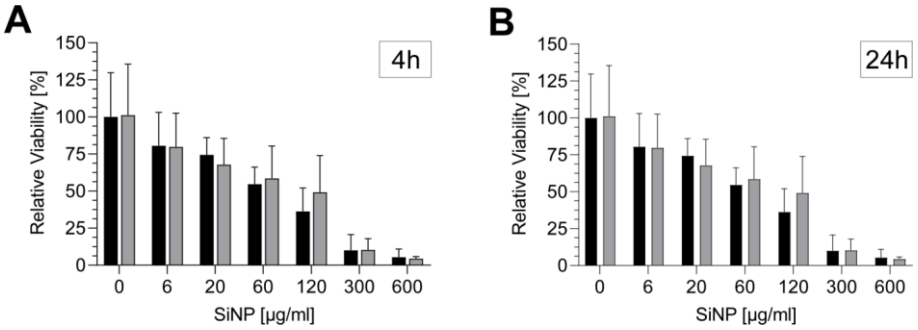

Supplementary Figure 11. Role of p38 activation in SiNP mediated toxicity. A431 wt were incubated for 2 h with inhibitor SB203580 (10µM) or DMSO as control. Then cells were washed three times and a serum-deprived medium containing rising SiNP concentrations was added for 4 h. Viability examination was performed with Alamar Blue Viability Assay (4.2.9.1). Afterward, cells were washed repeatedly and incubated in full growth medium without additional treatment up to time point 24 h. Alamar Blue viability assay was performed again, and data was analyzed with the Anova two-way test to determine statistical differences between samples with or without inhibitor SB203580. No statistical differences were found.

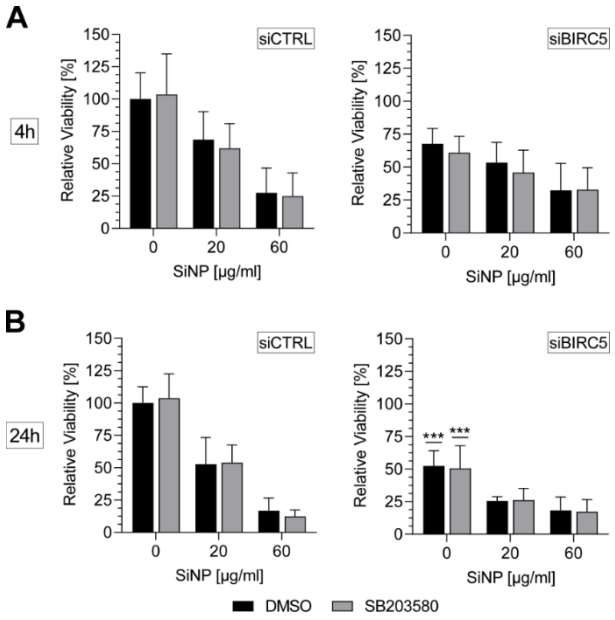

Supplementary Figure 12. Role of stress MAPK p38 in the signal transduction of SiNP toxicity concerning low Survivin expressing levels. Lipofectamin RNAi Max was used to transiently transfect A431 wt cells with siRNA against Survivin coding gene BIRC5 (siBIRC5) or with a control scrambled siRNA (CTRL). Cells were incubated for 2 h with 10 nM p38 inhibitor SB203580 or DMSO as control and then treated for 2 h with 60 µg/mL SiNP. Viability was measured via Alamar Blue viability assay after the 2 h treatment and at time point 24 h (4.2.9.1). Data were analyzed with the Anova two-way test, but no significant differences between samples with or without p38 inhibitor SB203580 were observed. Statistical significance was found for differences between control transfections (CTRL) and siBIRC5 transfected cells for the 24-hour time point with p***<0.0005.

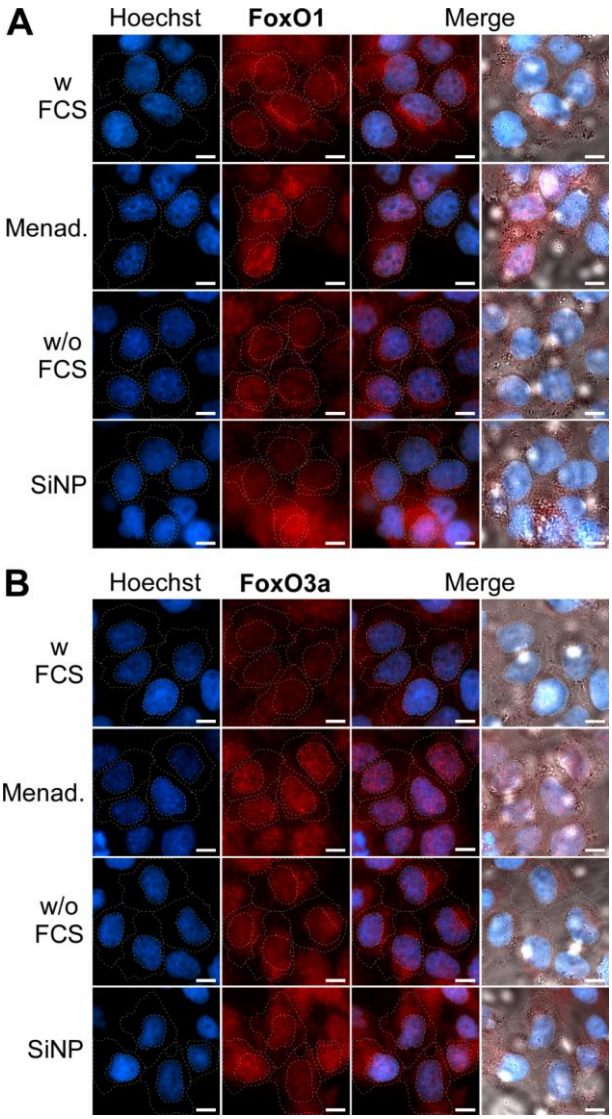

Supplementary Figure 13. Translocation of Fox1 and FoxO3a in A431 wt cells. FoxO1 (A) and FoxO3a (B) were incubated with 60 µg/mL SiNP for 30 minutes in a serum-deprived medium. Cells were incubated for 30 minutes in a serum-deprived medium used as a control (w/o FCS). Further, cells cultivated in serum-containing medium (w FCS) served as a control for normal growth conditions, and the treatment with 50 µm Menadione (Menad.) as a positive control for ROS-induced nuclear translocation of FoxO1. The scale bar indicates for 25 µm.

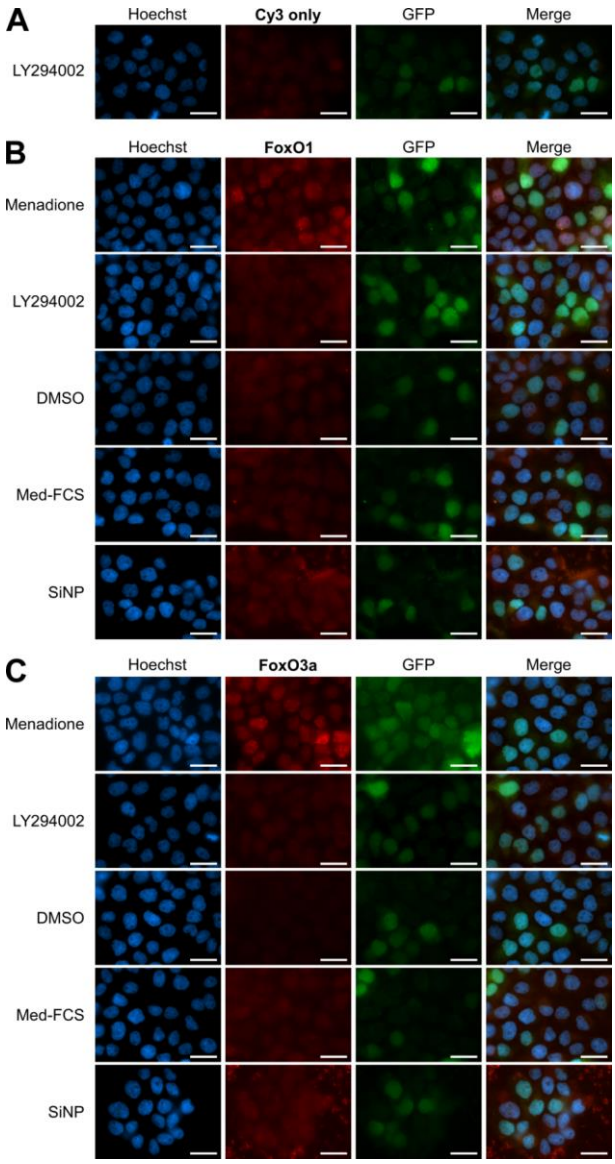

Supplementary Figure 14. Control staining for FoxO1 and FoxO3a and Cy3-coupled secondary antibody. A431 GFP expressing cells were treated with LY294002 (PI3K inhibitor) and Menadione (ROS inducer) as control FoxO1 and FoxO3a nuclear translocation. In addition, cells were incubated with DMSO, serum-deprived medium (Med-FCS), or 60 µg/mL SiNP for 2 h before fixation and staining with either primary antibodies against FoxO1 /3a or Cy3 secondary antibody. Image processing with the Axio vision software (Zeiss) included background removal fluorescence intensity adaptation. Therefore, the image settings were fixed onto the positive control Menadione for each image. The scale bar indicates 50 µm.

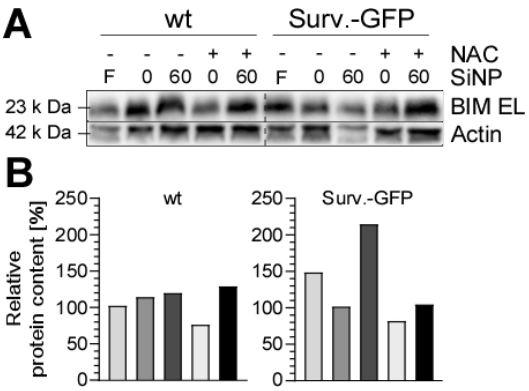

Supplementary Figure 15. Quantification of BIM EL protein level relative to housekeeping gene Actin. A) BIM EL protein expression was determined through immunoblot analysis (Figure 32). B) BIM EL protein expression quantified via ImageJ software and analyzed with GraphPad Prism software. BIM EL band intensities normalized to the corresponding actin band.

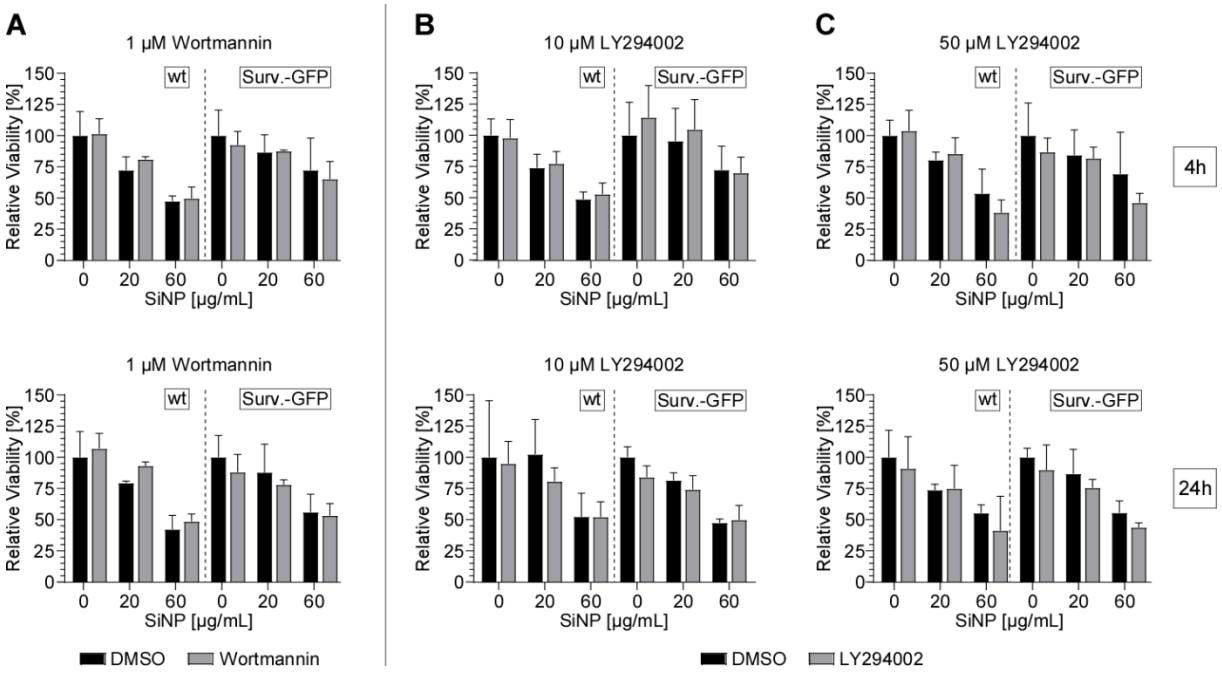

Supplementary Figure 16. Impact of PI3K inhibitor Wortmannin and LY294002 onto SiNP toxicity. The inhibitor Wortmannin (A) and LY294002 (B, C) were pre-incubated for 2 h in the serum-containing medium before cells were treated with SiNP in a serum-deprived medium for 4 h or 24 h. An experiment was exercised three times in triplicates. Statistical analysis was performed via the Anova two-way test, but no significant differences were found when DMSO-treated controls were compared to Wortmannin or LY294002-treated cells.

6.5 SUPPLEMENTARY TABLES

Supplementary Table 1. Amorphous silica nanoparticles of type AmSil20 characterized by TEM and Dynamic light scattering analysis (DLS) in water, PBS, or cell culture medium determining the Zeta potential, nanoparticle size, size distribution, and shape according to (Breder-Bonk et al., 2023).

	SiNP		**Milli-Q-water**	**PBS**	**RPMI 1640**
R_{TEM}. [nm]	15.7 ± 1.9	Zeta potential.[mV]	-51	-18	-20
NP conc. stock solution. [p/mL]	5.72 1016	Rh. [nm]	16.4	18.4	17.7
SiO_2 conc. stock solution. [mg/mL]	575	μ^2	0.12	0.08	0.07

7 OWN PUBLICATION

Breder-Bonk, C., Docter, D., Barz, M., Strieth, S., Knauer, S. K., Gul, D., & Stauber, R. H. (2023). The Apoptosis Inhibitor Protein Survivin Is a Critical Cytoprotective Resistor against Silica-Based Nanotoxicity. *Nanomaterials (Basel)*, *13*(18). https://doi.org/10.3390/nano13182546

nanomaterials

MDPI

Article

The Apoptosis Inhibitor Protein Survivin Is a Critical Cytoprotective Resistor against Silica-Based Nanotoxicity

Christina Breder-Bonk [1,*], Dominic Docter [1], Matthias Barz [2,3], Sebastian Strieth [4], Shirley K. Knauer [5], Désirée Gül [1,*] and Roland H. Stauber [1]

check for updates

Citation: Breder-Bonk, C.; Docter, D.; Barz, M.; Strieth, S.; Knauer, S.K.; Gül, D.; Stauber, R.H. The Apoptosis Inhibitor Protein Survivin Is a Critical Cytoprotective Resistor against Silica-Based Nanotoxicity. *Nanomaterials* **2023**, *13*, 2546. https://doi.org/10.3390/nano13182546 Academic Editor: Saura Sahu

Received: 21 August 2023
Revised: 8 September 2023
Accepted: 9 September 2023
Published: 12 September 2023

[1] Molecular and Cellular Oncology, University Medical Center Mainz, Langenbeckstrasse 1, 55101 Mainz, Germany; docter@uni-mainz.de (D.D.); rstauber@uni-mainz.de (R.H.S.)

[2] Leiden Academic Center for Drug Research (LACDR), Leiden University, Einsteinweg 55, 2333 CC Leiden, The Netherlands; barz@uni-mainz.de

[3] Department of Dermatology, University Medical Center of the Johannes Gutenberg University Mainz, Langenbeckstraße 1, 55131 Mainz, Germany

[4] Department of Otorhinolaryngology, University Medical Center Bonn, Venusberg-Campus 1, 53127 Bonn, Germany; sebastian.strieth@ukbonn.de

[5] Center for Medical Biotechnology (ZMB), Department of Molecular Biology II, University of Duisburg-Essen, Universitätsstrasse 5, 45141 Essen, Germany; shirley.knauer@uni-due.de

* Correspondence: chbreder@uni-mainz.de (C.B.-B.); guel@uni-mainz.de (D.G.)

Abstract: Exposure to nanoparticles is inevitable as they become widely used in industry, cosmetics, and foods. However, knowledge of their (patho)physiological effects on biological entry routes of the human body and their underlying molecular mechanisms is still fragmented. Here, we examined the molecular effects of amorphous silica nanoparticles (aSiNPs) on cell lines mimicking the alveolar-capillary barrier of the lung. After state-of-the-art characterization of the used aSiNPs and the cell model, we performed cell viability-based assays and a protein analysis to determine the aSiNP-induced cell toxicity and underlying signaling mechanisms. We revealed that aSiNPs induce apoptosis in a dose-, time-, and size-dependent manner. aSiNP-induced toxicity involves the inhibition of pro-survival pathways, such as PI3K/AKT and ERK signaling, correlating with reduced expression of the anti-apoptotic protein Survivin on the protein and transcriptional levels. Furthermore, induced Survivin overexpression mediated resistance against aSiNP-toxicity. Thus, we present the first experimental evidence suggesting Survivin as a critical cytoprotective resistor against silica-based nanotoxicity, which may also play a role in responses to other NPs. Although Survivin's relevance as a biomarker for nanotoxicity needs to be demonstrated in vivo, our data give general impetus to investigate the pharmacological modulation of Survivin's functions to attenuate the harmful effects of acute or chronic inhalative NP exposure.

Keywords: alveolar-capillary barrier; lung model; nanotoxicity; amorphous silica nanoparticles; inflammation; cytotoxic response

1. Introduction

Over the past 20 years, nanomaterials have gained tremendous importance for industry. Due to multiple beneficial properties, the produced number of nanoparticles (NPs) and NP-containing products in the cosmetic and food industries is rising every year [1]. This development has led to an increased occurrence of NPs and thus NP exposure to the human body. However, the detailed effects of NP at nano-biological interfaces are still fragmented. NPs can enter the body by passing through biological diffusion barriers such as the skin (epidermis), the gastrointestinal tract (gastrodermis), or the alveolar-capillary barrier of the lung (respiratory epithelium). These cell-based barriers serve two opposing aspects by distinguishing different particles, molecules, and substances for either passage (i.e., gas exchange at the alveolar-capillary barrier) or rejection (hazardous substances). The alveolar region lines an area of 100–140 m^2 of the lung and is therefore an attractive target for drug and gene delivery but also represents a critical point for harmful nanosized particles. Regarding the increasing use of drugs and drug carriers in the form of nanopar-

Nanomaterials **2023**, *13*, 2546. https://doi.org/10.3390/nano13182546 https://www.mdpi.com/journal/nanomaterials

ticles, it is of great importance to evaluate their interaction profile with biological barriers to determine possible treatment problems and undesired toxicity effects.

Synthetic non-metal silica (SiO_2) nanoparticles (SiNP) rank with 1.5 million tons among the most synthesized NPs used in hundreds of products, such as photovoltaic, tire compounds, or electrical and thermal insulation materials [2,3]. Furthermore, daily-use products such as cosmetics or toothpaste contain SiNP [4,5]. SiNP can be differentiated into crystalline and amorphous SiNP exhibiting different chemical as well as biological properties. Crystalline SiNP (crSiNP) possess a high reactivity responsible for several lung diseases like emphysema, silicosis, cancer, or pulmonary tuberculosis [6]. In contrast to crSiNP, the amorphous form of SiNP (aSiNP) has been considered to exhibit low toxicity [7,8]. Furthermore, the main benefits of aSiNP use combine an uncomplicated cost-saving production with the possibility for manifold surface functionalizations [9,10]. The synthesis of aSiNP can be adjusted for higher biodegradability [11]. For this reason, aSiNPs have quickly been applied in the industrial, medicinal, and other technological fields, and are a Food and Drug Administration (FDA) approved food additive [12].

However, despite their FDA approval, it has been shown that aSiNP can cause serious health implications. Several in vitro studies on nanoscale aSiNPs indicate cytotoxic and inflammatory effects and suggest that the NPs are taken up by digestion, skin absorption, and especially by inhalation [13,14]. Several types of NPs including aSiNPs possess the ability to translocate rapidly from the alveolar surface into the body [15]. Beyond these unintentional uptake routes, the active application of aSiNP as a drug or drug carrier system leads to the tremendously increasing presence of aSiNP in the blood system. The enhanced presence of aSiNP in the bloodstream is followed by a fast accumulation of aSiNP in tissue regions. The accumulation of aSiNP can cause dose-dependent cytotoxic effects and, in turn, can lead to organ injuries or at worst to organ failures [16,17].

In previous studies, it has been suggested that aSiNP can lead to cell death by inducing apoptosis in various cell lines [18–20]. The cytotoxicity of NPs could result from nanoparticle-mediated enzyme inhibition, and reactive oxygen species (ROS) production resulting in DNA and lipid modifications, but those effects are impaired by the formation of a protein corona enclosing the nanoparticle surface. However, in general, apoptosis is positively regulated by intrinsic receptor–ligand-mediated signaling processes or via mitochondrial-generated stimuli. The apoptotic cascade is negatively regulated by several pro-survival pathways that prevent the initiation of cell death [21]. One molecular actor involved in these pathways is a member of the inhibitor of apoptosis protein (IAP) family, Survivin/BIRC5 [22]. In normal cells, the Survivin protein encoded by the baculoviral IAP repeat containing 5 (BIRC5) gene is mainly expressed during the G2-M phase of the cell cycle where it regulates cytokinesis and chromosomal segregation [23]. Moreover, Survivin can counteract apoptosis by downregulating the activity of effector caspase-3 and -7, e.g., promoting resistance against radiation and other stressors [24]. Due to its prosurvival/anti-apoptotic activity, Survivin is highly expressed in most cancer tissues and is often associated with poor treatment outcomes [25]. Generally, high levels of Survivin suppressed or prevented the apoptosis initiation in malignant cells [24,26]. Furthermore, other studies showed that Survivin can act as a cytoprotective agent in non-malignant tissues such as the auditory system of the human cochlea and kidney [27,28]. In this context, Survivin is discussed as an adjusting therapeutic target to prevent apoptotic processes in injured tissue regions, as well as a crucial factor in transplantation medicine [29,30].

Regarding the lack of detailed knowledge about aSiNP-induced cell death, the objective of this study was to analyze the molecular effects of monodisperse amorphous silica nanoparticles (aSiNP) on cell models mimicking the alveolar-capillary barrier of the lung. By molecular characterization of endothelial lung cell line H441 and epithelial cell line ISO-HAS-1, we provided a model system suitable for in

vitro nanotoxicity studies. Our experimental workflow, including state-of-the-art NP characterization, in vitro/in vivo imaging (fluorescence and electron microscopy), assessment of cell viability, as well as molecular pathway analyses, allowed us to give the first evidence that the anti-apoptotic protein Survivin acts as cytoprotective resistor against nanotoxicity. An analysis of healthy human and mouse lung tissue supports the clinical relevance of our in vitro data and the introduced model system as a first step system for further research projects.

2. Materials and Methods

2.1 Nanoparticles, Antibodies (Ab), and Reagents

Aqueous dispersions of acidic colloidal silica particles were purchased (aSiNP15: NexSil20A; aSiNP125: NexSil125A, Nyacol Nano Technologies, Inc., Ashland, MA, USA; aSiNPL: LudoxTM-40 Sigma Aldrich, Munich, Germany). Ab were Polyclonal rabbit and monoclonal mouse α (anti)-survivin (NB-500-201/NB-500-205, Novus Biologicals, Littleton, CO, USA); anti-ß-Actin (A2066; Sigma Aldrich); polyclonal rabbit α-phospho-AKT (9275, Cell Signaling); monoclonal rabbit α-AKT (4691; Cell Signaling, Danvers, MA, USA); monoclonal α-E-cadherin (610182, BD Transduction Laboratories); polyclonal rabbit α-p44/42 MAPK [pErk] (Thr202/Tyr204) (9212; Cell Signaling); polyclonal rabbit α-ZO-1 (40-2200; Invitrogen, Waltham, MA, USA); polyclonal rabbit α-cleaved Caspase-3 (9661, Cell Signaling); monoclonal mouse α-TTF-1 (M3575; Dako, Glostrup, Denmark). Appropriate secondary antibodies conjugated to HRP-, Cy3, or FITC were purchased from Sigma Aldrich (Munich, Germany) and Santa Cruz Biotechnology (Heidelberg, Germany). MEK inhibitor UO126 (Cell Signaling).

2.2 Characterization of Amorphous Silica Nanoparticles (aSiNPs)

Amorphous silica nanoparticles NexSil20A (aSiNP15), NexSil125A (aSiNP125), LudoxTM-40 (aSiNPL) were acquired commercially (Sigma Aldrich, Munich, Germany). In addition to SiO_2, the used dispersion of SiNP contains Na_2O and has a pH of 10. The pristine nanoparticles without surface coating were characterized with respect to shape, size, and size distribution in dry state as well as in water-based solutions.

2.3 Transmission Electron Microscopy (TEM)

Imaging was performed using a Philips EM420 as described before [31].

2.4 Physicochemical Characterization Methods

The zeta potential was determined by the use of Zetaziser Malvern Zetasizer Nano ZS) with an appropriate device and parameter set up to examine the nanoparticle characteristics in regard to the aggregation behavior in different solutions [31]. For these measurements, particle stocks (600 mg/mL) were diluted in filtered MilliQ water (Millipore Billerica, Burlington, MA, USA) to final concentrations of 4.4 × 10^{13} NP/mL (600 µg/mL). Particle size, pH, and zeta potential were measured for all particles (Tables S1 and S2).

2.5. Endotoxin Detection in aSiNPs Dispersions

All aSiNP dispersions were analyzed for Gram-negative bacterial endotoxin contaminations by the QCL-1000® Endpoint Chromogenic LAL Assay (Lonza Verviers, S.p.r.l., Verviers, Belgium) according to the manufacturer's recommendations.

2.6. Preparation of aSiNPs for Apical Exposure

To avoid nanoparticle aggregation of commercially purchased aSiNPs (see Section 2.1), predilutions of the aSiNP dispersions were prepared in pure water (Aqua ad iniectabilia, Braun Melsungen AG, Melsungen). Due to nanoparticle aggregation in serum-containing medium, serum-free medium was used during the 4 h exposure. All dilutions were applied 1:10 in serum-free RPMI medium to the cells (10 µL NP-dispersion + 90 µL RPMI). Final concentrations of 10^{10} NP/mL (0.6 µg/mL), 10^{11} NP/mL (6 µg/mL) 10^{12} NP/mL (60 µg/mL), 10^{13} NP/mL (600 µg/mL) cover a range of non-toxic, sub-toxic and toxic concentrations and were chosen according to preliminary toxicity test performed for this project. After an exposure time of 4 h, the cells were either evaluated or washed twice with RPMI medium and cultivated for an additional 20 h period. After 4 h and 24 h recovery cell cytotoxicity was studied by various assays. In the context of the performed experiments, the additional incubation in the serum-containing medium was adjusted to the experimental requirements, described in detail in the figure captions.

2.7. Nanoparticle Uptake Studies

Cells were seeded on pre-coated coverslips (NUNC—Thermo Fisher Scientific, Dreieich, Germany) and cultivated until confluency was reached. Cells were exposed to 10^{12} NP/mL (aSiNP) in serum-deprived medium for 2 h at 37 °C. Cells were fixed in 3.7% (*v*/*v*) paraformaldehyde in PBS for 20 min at RT. Preparation for transmission electron microscopy analysis was performed as follows: Cells were fixed in 1% (*w*/*v*) osmium tetroxide (2 h, RT) and dehydrated in ethanol. Cells were passaged through propylene oxide, and then samples were embedded in agar-100 resin (PLANO, Wetzlar, Germany). Polymerization was acquired at 60 °C for 48 h. Resin block was cut into ultrathin sections using ultra microtome (Leica Microsystems, Wetzlar, Germany). Slices were placed onto copper grids for staining with 1% (*w*/*v*) uranyl acetate in alcoholic solution and lead citrate. Further analysis was performed by use of TEM technology (see Section 2.3).

2.8. Cultivation of Model Cell Lines ISO-HAS-1 and H441

Cell lines used for the applied cell model were acquired commercially from ATCC, ATCC-HTB-174, Promochem, Wesel, Germany. Cells were seeded according to their proliferation rate from confluent culture flasks into 96-well plates with 1.6×10^4 cells/well for human microvascular endothelial cell line ISO-HAS-1 and with 3.2×10^4 cells/well for human adenocarcinoma cell line H441. Cells were cultivated for 24 h (37 °C, 5% CO_2) prior to SiNP treatment in RPMI 1640 medium (Gibco, Billings, MT, USA) containing L-glutamine, 10 % FCS, and Pen/Strep (100 U/100 µg/mL). The presence or absence of mycoplasma was examined using the commercial detection kit from Venor GeM Advance (Minerva Biolabs, Berlin, Germany). Cell counting was performed via Casy Cell Counter and Analyzer TT (Innovatis, Magdeburg, Germany).

2.9. Plasmids

The eukaryotic expression constructs for GFP and Survivin–GFP-tagged versions have been reported elsewhere [32]. The pGL3-luciferase reporter construct, pGL3Surv, containing the human Survivin promoter (nucleotides: –628 to +21), has been described [33]. Generation of recombinant retroviral particles and transduction was carried out as described [34,35].

2.10. Cells Transfection and Luciferase Assay

Stable expression of Survivin–GFP in H441 was established using transfection technology and subsequent fluorescence-activated cell sorting over two rounds described elsewhere [34]. Luciferase assays were performed as specified [36]. Luciferase reporter assays were performed in three independent experiments, each including a triplicate approach.

2.11. Apoptosis and Viability Assays

Caspase-3 hydrolysis was quantified using a fluorogenic substrate and via detection of cleaved caspase-3 using immunoblot-based analysis [36]. LIVE/DEAD™ Viability/Cytotoxicity Kit (Life Technologies, Darmstadt, Germany) was performed by supplier instructions to visualize loss of membrane integrity. Imaging was performed with digital Axiocam CCD camera (Carl Zeiss, Jena, Germany). Cell viability was examined using an ATP-dependent assay (CellTiter-Glo™ Viability Assay kit, Promega, Walldorf, Germany), resulting in a colorimetric change proportional to the number of viable cells. In addition, colorimetric MTT (3-(4,5-Dimethylthiazol-2-yl)-2,5-diphenyltetrazolium bromide) assay was performed to measure the metabolic activity, which correlates with the cell viability. Metabolic active cells cause a reduction in the MTT molecule resulting in a color change from a yellow tetrazole to a purple formazan dye (Sigma-Aldrich). All data were normalized to untreated control samples for each time point and statistically analyzed as reported in each figure caption.

2.12. Origin of Human and Mouse Tissue

Healthy human lung tissue was obtained from tumor patients at the University Hospital of Frankfurt. Studies of human tissue biopsies were performed according to the requirements of the local ethics committee, and informed consent was obtained in accordance with the Declaration of Helsinki. Four-week-old female NMRI nu/nu mice (Charles River Laboratories, Sulzfeld, Germany) were used. Animals were kept at 22 ± 1 °C under a 12:12 h light–dark cycle, and fed chow and water ad lib. Experimental protocols were approved by the local Animal Care and Use Committee.

2.13. Tissue Preparation and Immunohistochemistry (IHC)

Human and murine lung tissues were fixed with formalin and embedded in paraffin (FFPE) prior to preparation for IHC as described [37]. Survivin was visualized using a polyclonal α-Survivin Ab, diluted 1:100. TTF-1 was applied with a 1:50 Ab dilution of monoclonal α-TTF-1 Ab.

2.14. Microscopy and Fluorescence Imaging of Cells

Observation, image analysis, and quantification of protein localization were performed as described [32]. Twelve-bit black and white images were captured using a digital Axiocam CCD camera (Carl Zeiss, Jena, Germany). Nuclei were stained with 1.25 µg/mL Hoechst 33,342 for 20 min (Sigma Aldrich, Munich, Germany). At least 200 fluorescent cells from three separate images were examined in three independent experiments.

2.15. Protein Extraction, Immunoblot Analysis, and Immunofluorescence

Treated cells were harvested and washed once in ice-cold PBS (1500 rpm, 4 °C, 5 min). Cells were sonicated in ice-cold modified extraction buffer to prepare lysates for immunoblot analysis [34,37]. Prior to application onto an SDS gel, lysates were diluted to similar protein concentrations and heated at 95 °C, 300 rpm for 5 min, with 6× dissociation buffer. Equal loading of lysates was controlled by detecting the housekeeping gene Actin. Immunoblotting was performed as described [36]. Detailed protocol for immunofluorescence has been described elsewhere [32,35].

2.16. Statistical Analysis

For experiments stating *p*-values, an unpaired *t*-test was performed. Unless stated otherwise, *p*-values represent data obtained from three independent experiments performed in triplicates. *p*-values < 0.05 were considered as significant (* $p < 0.05$; ** $p < 0.01$; *** $p < 0.001$, **** $p < 0.0001$). Statistical analysis and graph setup were performed using Prism9 (Graph Pad Software).

3. Results

3.1. 'Characterization of the Nano–Bio Interface I'—Nano-scaled Amorphous Silica Nanoparticles

As the physico-chemical properties of NPs are critical determinants of NP-induced biological effects, we performed state-of-the-art characterization of the aSiNPs used in our study, aSiNP15/125 (aSiNP15/aSiNP125) and LudoxTM-40 (aSiNP L), analyzing morphology and shape, surface area, zeta potential, size, and stability (Figure 1, Tables S1 and S2).

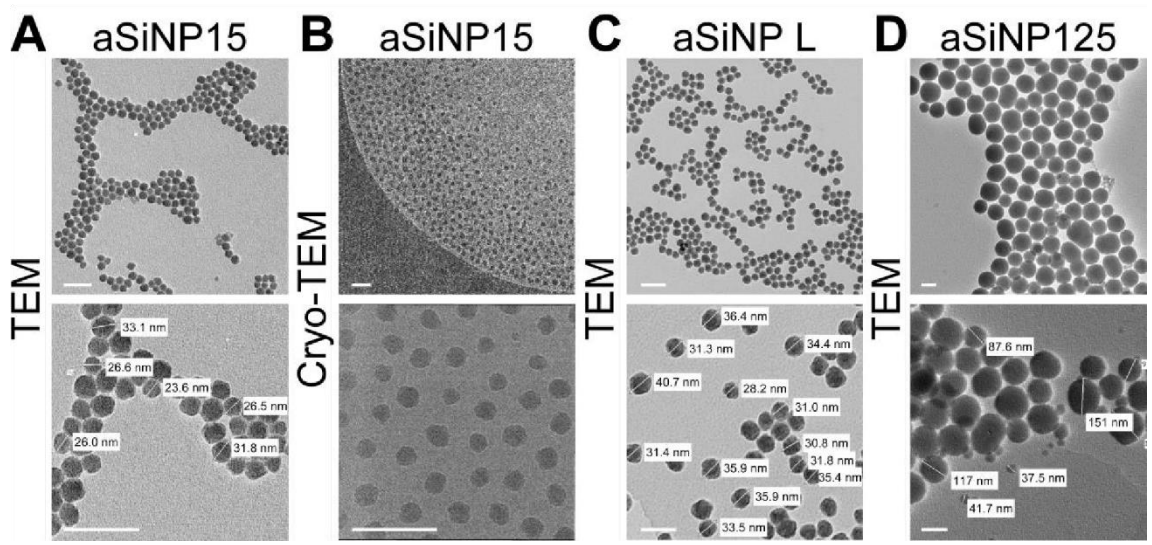

Figure 1. Characterization of the used amorphous silica NP system (aSiNP) by (Cryo-)transmission electron microscopy (TEM). Representative pictures of analyzed aSiNPs are shown in overview (upper row) and higher magnification (lower row): (**A**) aSiNP15 (TEM), (**B**) aSiNP15 (Cryo-TEM), (**C**) aSiNP L (TEM), and (**D**) aSiNP125 (TEM). Scale bars, 100 nm.

(Cryo-)transmission electron microscopy (TEM) and dynamic light scattering (DLS) measurements revealed the stable size of the used aSiNPs in a dry state as well as in solution (see Table S1). The hydrodynamic diameter remained constant, 33 nm for aSiNP15 and aSiNP L, or 125 nm for aSiNP125. Furthermore, all aSiNP retained a constant negative zeta potential in a serum-free cell culture medium, which can stabilize the suspensions via repulsive forces [38].

Importantly, since NP aggregation often precludes determining whether biological effects are triggered by individual NPs or NP aggregates ("microparticles"), time-dependent DLS measurements were performed (Table S1). Distribution curves showed no significant aggregation when analyzing aSiNP dispersions in water, or physiological solutions such as phosphate-buffered saline (PBS, 540 mM salt in total) or serum-free cell culture medium (RPMI-1640; 139 mM salt in total, Table S1). Furthermore, aSiNP15 and aSiNP L retain their nanoparticular size in water, PBS, and serum-free cell culture medium over time (Table S2). Before all experiments, the absence of endotoxin contamination in the aSiNP preparations was controlled by an enzyme-linked immunosorbent assay ELISA (see Section 2.5).

3.2. 'Characterization of the Nano–Bio Interface II'—A Biological Model to Mimic the Alveolar-Capillary Barrier of the Lung

NPs can penetrate the body by different entry routes, such as the lung by passing the alveolar-capillary barrier (Figure 2A). Industrial exhaust or particulate matter products can enrich the air with harmful (nano)particles that can inadvertently enter the epithelial cells of the lung and further into the endothelial compartments, posing potential health risks to humans [39]. Thus, the alveolar-capillary barrier is an important part of the nano–bio interface and the physical defense system. In this context, studies of potential nanotoxic effects on the alveolar-capillary barrier are mandatory. However, this is rather difficult to access in vivo. Several models have been developed to mimic human lung tissue, such as different animal models, monolayer 2D cell cultures or 3D spheroid cultures, and organoids, to circumvent the poor availability of primary human samples [40].

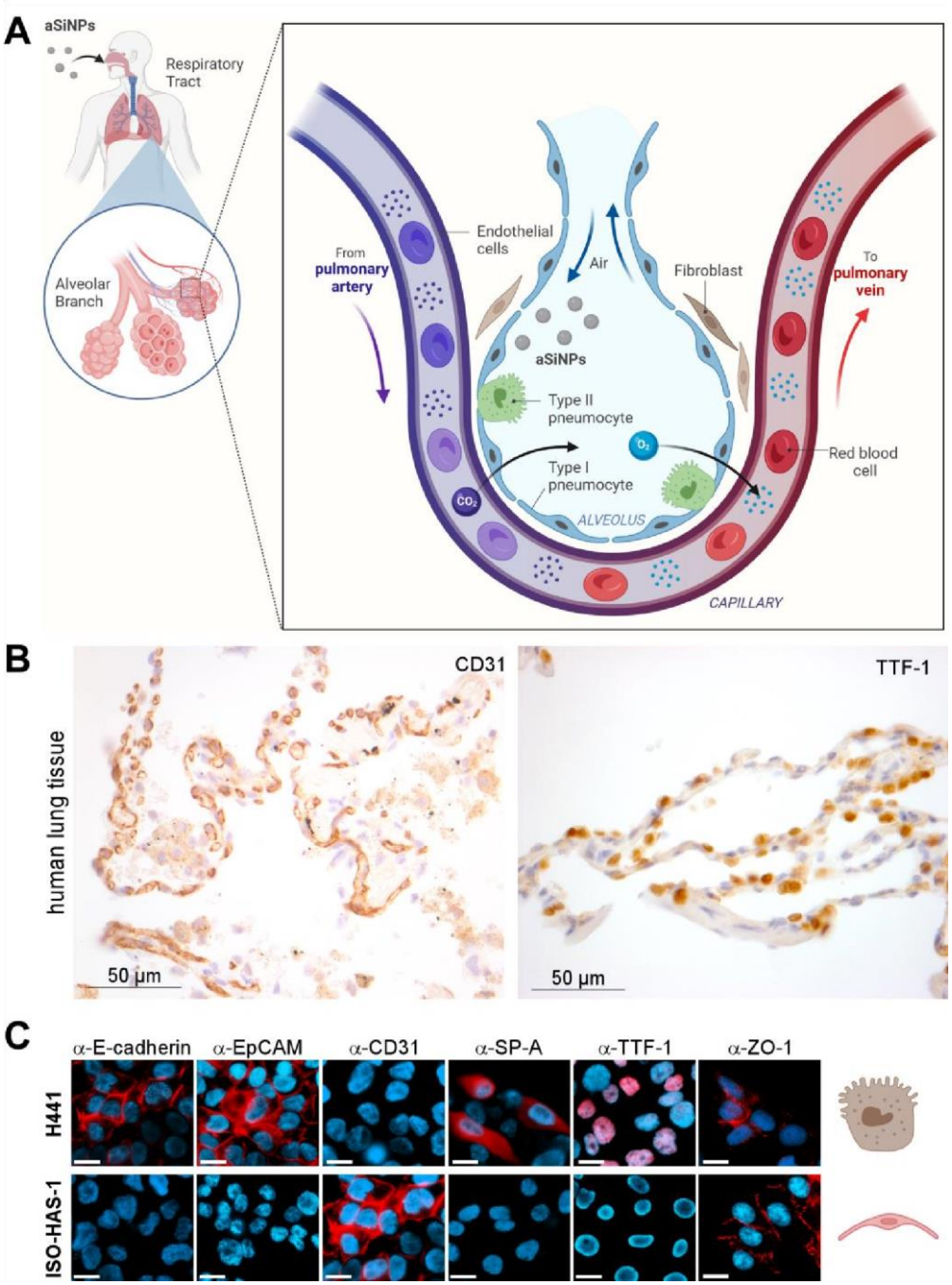

Figure 2. Biological model to mimic the alveolar-capillary barrier of the lung: (**A**) Illustration of a bronchial strain as the first protective cellular barrier against inhaled nanoparticle-containing air. (**B**) Light microscopic analysis of biomarker expression. Expression of CD31 and TTF-1 was analyzed in epithelial human lung tissue by immunohistochemistry with specific antibodies (brown). HE (hematoxylin/eosin) staining was applied to visualize tissue morphology (blue). CD31 surface marker was present

on the membrane of epithelial cells in the human lung tissue, whereas TTF-1 was prominently expressed in cell nuclei. (**C**) Marker profiling of the H441 and ISO-HAS-1 dual cell line model was carried out by fluorescence microscopy after staining with specific antibodies (α-E-cadherin, α-EpCAM, α-CD31, α-SP-A, α-TTF-1, α-ZO-1) and the nuclear stain Hoechst-33342 (blue) to evaluate the cellular differentiation state. Scale bars, 10 µm. Respective cell types are symbolized by referring to (**A**). Created with BioRender.com.

Here, we introduce a dual cell line model that should mimic the alveolar-capillary barrier in vitro [41]. It consists of a human epithelial (adenocarcinoma) lung cell line with characteristics of type II pneumocytes and Clara cells (NCI H441) and the human microvascular endothelial cell (MEC) line ISO-HAS-1, mimicking the properties of alveolar lung tissue and functioning as a representative of endothelial-blood-vessel-forming cells (Figure 2A) [31,42]. Type II pneumocytes were chosen above type I pneumocytes because they produce the surfactant protein layer protecting and maintaining the alveolar stability important for physical defense [43,44]. Although both cell lines originate from tumor tissue, their use as in vitro models for functional, healthy lung tissue has been already suggested in previous studies [45].

Our model system was characterized molecularly to prove its suitability as a model system of the lung. Therefore, immunofluorescence/histochemical staining of specific lung cell markers and general differentiation markers was utilized. First, we performed marker profiling in human lung tissue to demonstrate physiological relevance. Here, specific expression of Cluster of Differentiation 31 (CD31) in the cellular membrane of endothelial, alveolar cells (Figure 2B, left), as well as nuclear expression of the thyroid transcription factor-1 (TTF-1) in epithelial cells (Figure 2B, right), could be revealed. Next, molecular marker profiling confirmed the epithelial character of the lung cell line H441 by positive staining for E-cadherin and the epithelial cell adhesion molecule EpCAM (Figure 2C, upper panel). In contrast, the endothelial cell line ISO-HAS-1 was characterized as E-cadherin/EpCAM negative (Figure 2C, lower panel). Furthermore, ISO-HAS-1 could be distinguished from H441 by positive staining for the endothelial-specific adhesion molecule CD31. In order to further prove the suitability of our in vitro system, we showed that the lung (and thyroid)-specific transcription factor TTF-1 (thyroid transcription factor1) is specifically expressed in epithelial H441 cells, but not in endothelial ISO-HAS-1 cells (Figure 2C). Since TTF-1 is essential for the expression of lung surfactant proteins, such as Surfactant protein-A (SP-A), and is thus crucial for maintaining a healthy morphology as well as host defense mechanisms of the lung [46,47], we also analyzed our model cell lines for SP-A expression. Consistent with our findings for TTF-1, SP-A is expressed exclusively in H441 cells, whereas ISO-HAS-1 cells were characterized as TTF-1/SP-Anegative (Figure 2C). Additionally, staining of ZO-1 (Zonula occludens-1, Tight junction protein-1) was performed to visualize the presence of tight junctions, which are critical for functional and protective cell barriers [48].

In summary, we here revealed several similarities between healthy human lung tissue and our characterized two-cell model, suggesting that this (tumor-derived) system is suitable for in vitro nanotoxicity studies mimicking the alveolar-capillary barrier of the (healthy) lung.

3.3. 'Effects at the Nano–Bio Interface'—aSiNPs Induce Cell Death upon Exposure to Alveolar-Capillary Barrier Model Cells

After confirming that the used aSiNP preparations remain stable under physicochemical cell culture conditions (see Sections 2.2 and 2.4), we next investigated the effects of aSiNPs on our lung model cells H441 and ISO-HAS-1. First, to visualize cellular surface interactions and the potential uptake of aSiNP, we treated H441 cells with increasing amounts of fluorescent aSiNP (Kisker red, 50 nm, Nylon) in a serum-deprived medium (Figure 3A). Because serum proteins can cover nanoparticles with a protein corona, serumfree conditions were chosen to retain aSiNP's full hazardous potential for all experiments (see Section 2.6) [49]. Interestingly, Kisker NPs could be detected at the outer cell membrane, as well

as internalized in the cell, and the amount of interacting/internalized aSiNPs increased with the used NP dose.

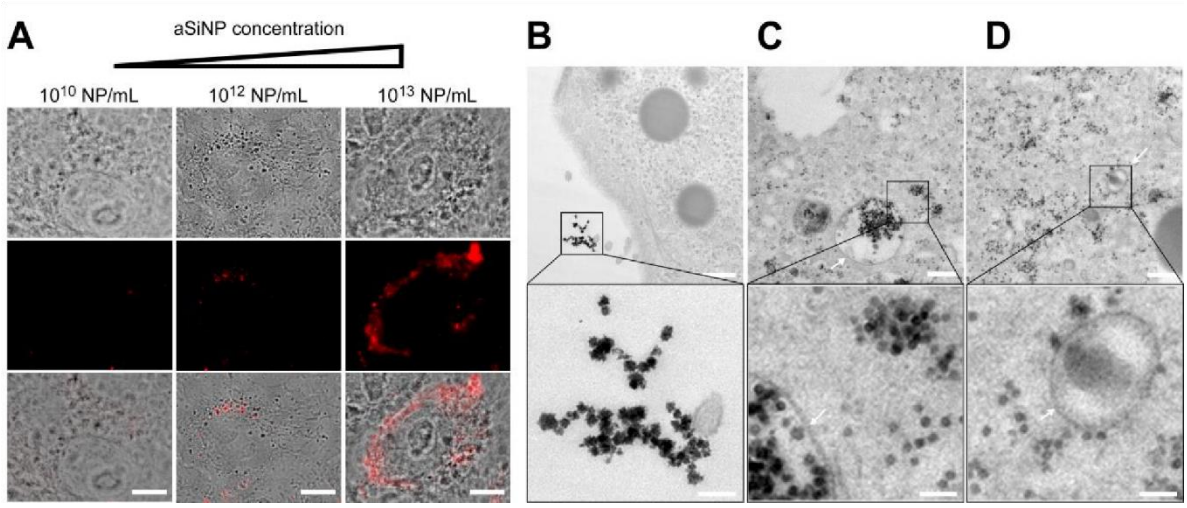

Figure 3. Interaction and internalization of aSiNPs by epithelial lung cells: (**A**) Immunofluorescence and light microscopy of H441 cells after incubation with increasing concentrations of fluorescent aSiNP (Kisker red) for 2 h in serum-deprived medium. Scale bars, 10 µm. (**B**–**D**) aSiNP15 nanoparticle uptake by H441 cells was visualized by TEM. H441 cells were treated with 10^{12} NP/mL for 2 h in serum-containing (**B**) or serum-free medium (**C**,**D**). Representative images are shown in overview (upper row), and in detail view (lower row) indicating the presence (**B**) or absence (**C**,**D**) of a protein corona around aSiNP15. Endocytic vesicles are marked by arrows. Scale bars, 500 nm (upper panel), and 100 nm (lower panel).

To obtain a more detailed picture of the aSiNP–cellular interaction, which might also allow conclusions about biological effects, confluent H441 monolayers were treated with 10^{12} aSiNP15 NP/mL (in medium, 2 h, see Section 2.7), and fixed and analyzed by transmission electron microscopy (Figure 3B). Interestingly, in the presence of serum, aSiNP15s were primarily located extracellularly. Since serum proteins can form a protein corona around nanoparticles, especially around pristine nanoparticles with a negative surface charge like the used aSiNP15 [49,50], we examined the uptake of aSiNP15 in the absence of fetal calf serum (FCS) (Figure 3C,D). Here, aSiNP15s were detectable on the cell surface, but also freely dispersed in the cytoplasm, and localized in membranebound endocytic vesicles, indicating the internalization of aSiNP15s (Figure 3C,D, arrows). Detailed examination of representative TEM images also revealed a more irregular shape and/or a darker border covering the aSiNPs incubated with serum (Figure 3B, lower panel). This NP-surrounding layer vanished in the absence of serum (Figure 3C,D, lower panel), and thus can be interpreted as protein corona covering the NPs. Similar results were obtained in ISO-HAS-1 cells and for other aSiNP types, such as aSiNP L (Figure S2). Based on these findings, subsequent aSiNP exposure experiments were conducted in a serum-free medium to prevent the binding of serum proteins to the nanoparticles, which might significantly affect their physico-chemical/biological properties.

As a next step, we performed cell viability measurements using aSiNP15 in our dual cell line model revealing dose- and time-dependent toxicity (Figure 4). Apical exposure of epithelial (H441) or endothelial (ISO-HAS-1) cell lines to 10^{13} NP/mL resulted in cell death 4 h after NP exposure, as revealed by a viability assay based on the cell membrane integrity (Figure 4A). Lower particle concentrations (10^{12} NP/mL) led to a partial loss of the membrane integrity after 24 h (Figure 4A, lower panel). However, both cell types responded similarly to aSiNP15 treatment.

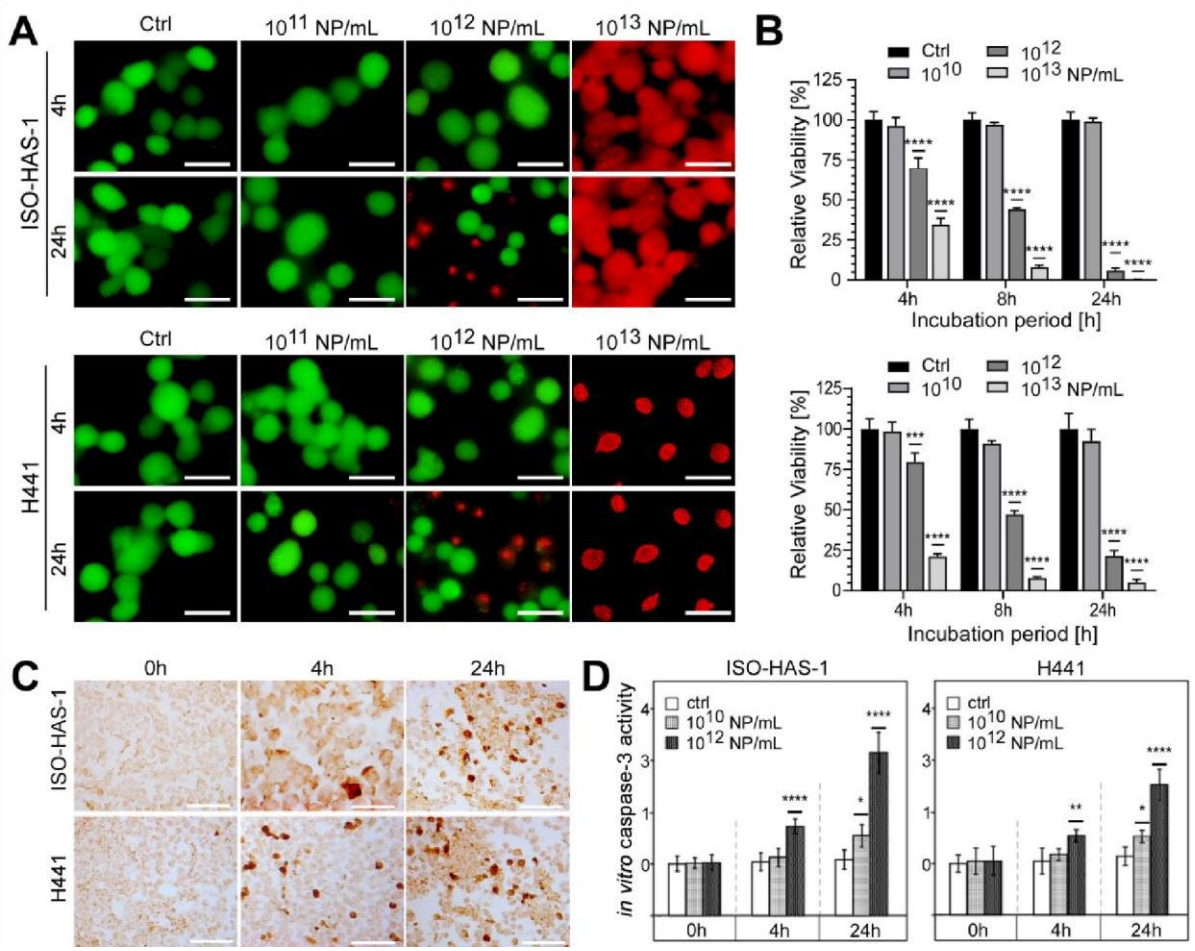

Figure 4. aSiNP15 treatment induced dose- and time-dependent toxicity on a dual alveolar-capillary barrier model. ISO-HAS-1 and H441 cells were treated with different particle concentrations in serum-free medium for 4 h; for later time points, treated cells were cultured for additional 20 h in serum-containing medium: (**A**) Live and dead staining analyzed by fluorescence microscopy. Green fluorescence marks viable cells; red fluorescence visualizes dead cells. (**B**) CellTiter-Glo™ Viability Assay. Data were normalized to untreated control samples for each time point. Unpaired *t*-test was used to compare treated cells to untreated control groups. Column, mean; bars, ±S.D. ***, $p < 0.001$, ****, $p < 0.0001$. (**C**,**D**) aSiNP15 induced apoptosis in ISO-HAS-1 and H441 cells via activation of caspase-3. (**C**) Light microscopic analysis of apoptosis marker caspase-3. Immunohistochemical staining of ISO-HAS-1 (upper panel) and H441 (lower panel) revealed expression of cleaved caspase-3 as a marker for apoptosis after 4 h of aSiNP15 treatment. Briefly, cells were treated with 10^{12} NP/mL for 4 or 24 h, fixed, stained for cleaved α-caspase-3, and visualized by light microscopy. Scale bars, 150 µm. (**D**) Quantification of in vitro caspase-3 activity confirmed time- and dose-dependent activation of apoptosis. Cleaved α-caspase-3 assay was performed with untreated and aSiNP15treated cells. Cells were incubated for 4 h and 24 h with 10^{10} or 10^{12} NP/mL as indicated. Data were normalized to untreated control samples for each time point. Unpaired *t*-test was used to compare treated cells to untreated control groups. Column, mean; bars, ±S.D. *, $p < 0.05$, **, $p < 0.01$, ****, $p < 0.0001$.

These results were confirmed by measuring the metabolic activity (ATP content) of viable cells (Figure 4B). ISO-HAS-1 as well as H441 cells revealed decreased vitality after treatment with NP concentrations above 10^{10} NP/mL. Particle concentrations of 10^{12} NP/mL showed a constant decrease in viability over the treatment period of 24 h in total, ranging from 69.6% (4 h) over 44.2% (8 h) to 5.8% (24 h) in ISO-HAS-1 cells relative to untreated controls (Figure 4B, upper panel). Comparable results were obtained for epithelial cells H441 (79.6%, 4 h; 47.2%, 8 h; 21.5%, 24 h). Higher particle concentrations (10^{13} NP/mL) increased toxicity at early time points in both cell types: viability of ISOHAS-1 cells decreased to 34.5 %, and of H441 cells to 17 % after exposure to 10^{13} NP/mL for 4 h, and declined further with treatment time (Figure 4B). Additionally, morphological changes were evaluated over the incubation period of 24 h (Figure S1). Low aSiNP15 concentrations (10^{10} NP/mL) had no impact on either ISO-HAS-

1 or H441 cells over 24 h. However, prolonged incubation with high NP concentrations (10^{13} NP/mL) led to cell damage, indicating apoptotic and/or necrotic phenotypes (Figure S1). Interestingly, whereas aSiNP L (with comparable size to aSiNP15) treatment resulted in comparable toxic effects (Figure S2), aSiNPs of a larger size (aSiNP125) resulted in significantly less apoptotic and/or necrotic cells under the same treatment conditions (Figure S3). These findings were further consolidated with uptake studies, which revealed that aSiNPs of greater size (aSiNP125) were also taken up by the cells without the induction of an apoptotic phenotype (Figure S4).

To independently prove that aSiNP15 treatment results in the induction of apoptosis, we quantified the expression of cleaved caspase-3, a major effector caspase, which is activated by cleavage during apoptosis initiation. First, immunohistochemical staining of cleaved caspase-3 in our dual cell line lung model revealed that exposure to 10^{12} NP/mL or higher concentrations triggered apoptosis after 4 h of treatment in both cell types (Figure 4C). Dose- and time-dependent induction of apoptosis was confirmed by an in vitro caspase-3 activity assay (Figure 4D). Whereas treatment with 10^{12} NP/mL likewise resulted in significant activation of caspase-3 and, thus, apoptosis induction after 4 and 24 h, lower concentrations of aSiNP15 (here 10^{10} NP/mL) just marginally activated the caspase-3 cascade after an elongated treatment period (24 h). Consistent with our previous data exposure, 10^{12} aSiNP125/mL had no comparable apoptotic effect under the same treatment conditions [49]. These data indicate that aSiNP-induced toxicity could critically depend on the particle size, besides the particle concentration.

3.4. 'Signaling at the Nano–Bio Interface'—High Concentrations of aSiNP15 Attenuate Pro-Survival Pathways

Next, our study aimed at providing insights into the underlying molecular mechanisms of aSiNP-induced cell death. Regulation of cellular survival and death involves a complex signaling network in which several phosphorylating kinases play key roles. For example, phosphatidylinositol 3-kinase (PI3K)/Akt and ERK (extracellular-signal-regulated kinases; also known as mitogen-activated protein kinases, MAPK) signaling are known pro-survival pathways in lung and endothelial cells, and their contributions to apoptosis regulation are well documented [51].

To examine if aSiNP15-induced toxicity depends on PI3K/Akt and/or ERK signaling, immunoblot analyses were performed profiling the (activation-dependent) phosphorylation of both kinases (Figure 5). Interestingly, PI3K/Akt and ERK signaling was attenuated in a dose- and time-dependent manner: whereas exposure to 10^{12} NP/mL reduced the levels of phosphorylated Akt and ERK over 6 h of treatment (Figure 5A and Figure S5), treatment with 10^{10} NP/mL did not affect phosphorylation nor the activation of either Akt or ERK signaling (Figure 5B).

To further confirm the relevance of the ERK signaling pathway for aSiNP-mediated toxicity, the MEK inhibitor UO126 was utilized to suppress ERK1/2 signaling (Figure 5C). Importantly, inhibitor treatment further increased aSiNP15-induced toxicity, likewise, in a time- and dose-dependent manner. The combination of MEK inhibition with high aSiNP15 concentrations (10^{12} NP/mL) resulted in a significant decrease in cell viability after 4 h. Interestingly, pre-treatment with the MEK inhibitor sensitized cells to aSiNP15-induced toxicity as revealed by a significant reduction in cell viability even when treated with sub-lethal aSiNP15 concentrations of 10^{10} or 10^{11} NP/mL for extended incubation times of 8 h or 24 h.

In sum, these results strongly support the hypothesis that aSiNP-induced toxicity is mediated by the attenuation of PI3K/Akt and ERK pro-survival signaling.

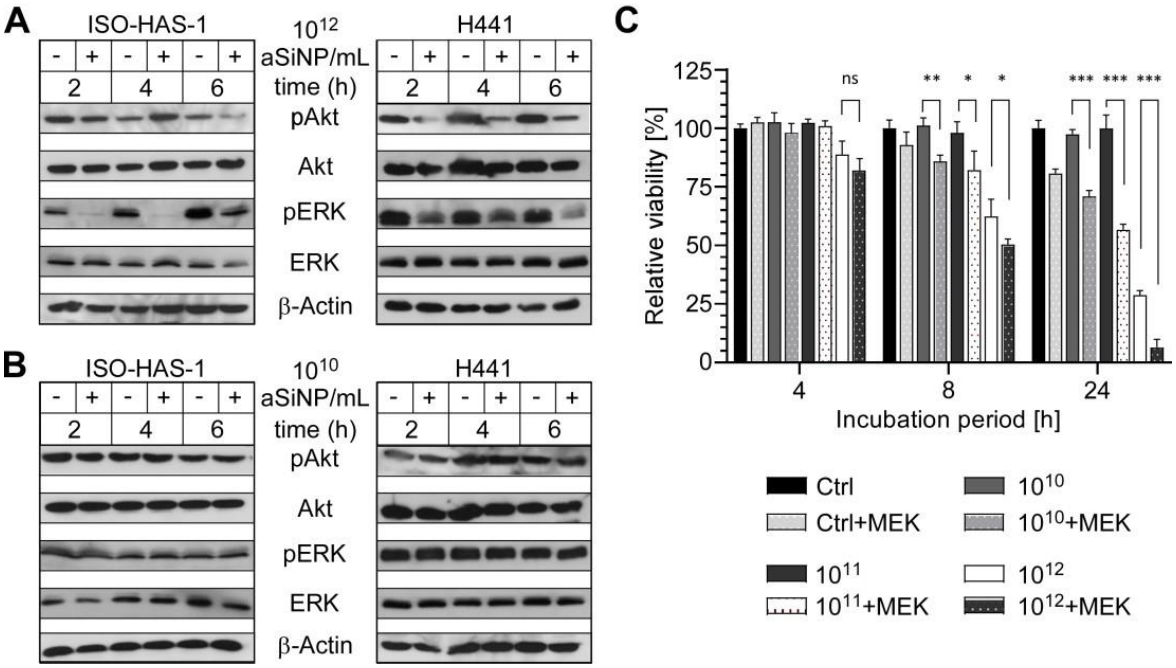

Figure 5. High concentrations of aSiNP15 attenuate PI3K/Akt and ERK signaling. (**A**,**B**) Activation of PI3K/Akt and ERK signaling pathways was analyzed by assessing the level of phosphorylated PI3K/Akt (pAkt) and ERK (pERK; Thr202/Tyr204) by immunoblot analysis. Whereas sub-toxic NP concentrations (10^{10} NP/mL) had no effect (**B**), pAkt and pERK decreased after incubation with 10^{12} NP/mL. ISO-HAS-1 and H441 were treated with 10^{12} NP/mL (**A**) or 10^{10} NP/mL (**B**) aSiNP15 (indicated by "+"), or in serum-deprived medium as control (indicated by "−") for 2 h, 4 h, and 6 h. Proteins were detected by (phosphorylation-) specific antibodies, the respective non-phosphorylated proteins, and Actin served as loading controls. (**C**) Relevance of ERK signaling was confirmed by combined MEK (mitogen-activated protein kinase kinase) inhibitor treatment. After H441 cells were pre-treated for 2 h with or without the MEK inhibitor UO126 (10 µM), treatment with 10^{10}, 10^{11}, or 10^{12} NP/mL of type aSiNP15 was conducted for 4 h, 8 h and 24 h. Cell viability was measured via an MTT assay. Data were normalized for each time point to untreated controls. (*) Unpaired *t*-test was performed to compare MEK inhibitor-treated samples to samples with similar treatment without inhibitor. Columns, mean; bars, ±S.D. *, $p < 0.05$, **, $p < 0.01$, ***, $p < 0.001$, ns, not significant.

3.5. 'Survival and Death at the Nano–Bio Interface'—aSiNP-Induced Cell Death Is Regulated by the Anti-Apoptotic Protein Survivin

Within the complex network of regulating cell death and survival, a plethora of individual molecular interactions govern the mutual influence of single proteins in diverse signaling cascades. One molecular actor involved in these pathways is a member of the inhibitor of apoptosis protein (IAP) family, Survivin/BIRC5. Interestingly, previous studies have suggested that PI3K/Akt and ERK signaling might stimulate Survivin expression, while suppression of these pathways attenuates Survivin protein levels, subsequently resulting in apoptosis induction [37,52–54].

Thus, we analyzed the expression of the anti-apoptotic protein Survivin after aSiNP15 treatment on the protein and the transcriptional level (Figure 6). Remarkably, immunoblot analysis revealed that Survivin expression decreased in ISO-HAS-1 and H441 cells treated with 10^{12} NP/mL over an incubation period of up to 6 h (Figures 6A,B and S6). Again, lower aSiNP15 concentrations (10^{10} NP/mL) did not significantly affect Survivin expression (Figure 6D,E). Interestingly, long-term incubation over 24 h revealed cell line-dependent effects concerning protein expression. Whereas high aSiNP15 concentrations (10^{12} NP/mL) led to decreased Survivin levels after 24 h in both cell lines (Figure 6C), the sublethal aSiNP dose (10^{10} NP/mL) reduced the amount of Survivin protein in H441 cells, but not in ISO-HAS-1 (Figure 6E). On the contrary, Survivin expression appeared to be increased in ISO-HAS-1 cells after 24 h of incubation with low concentrations of aSiNP15 (10^{10} NP/mL, Figure 6F).

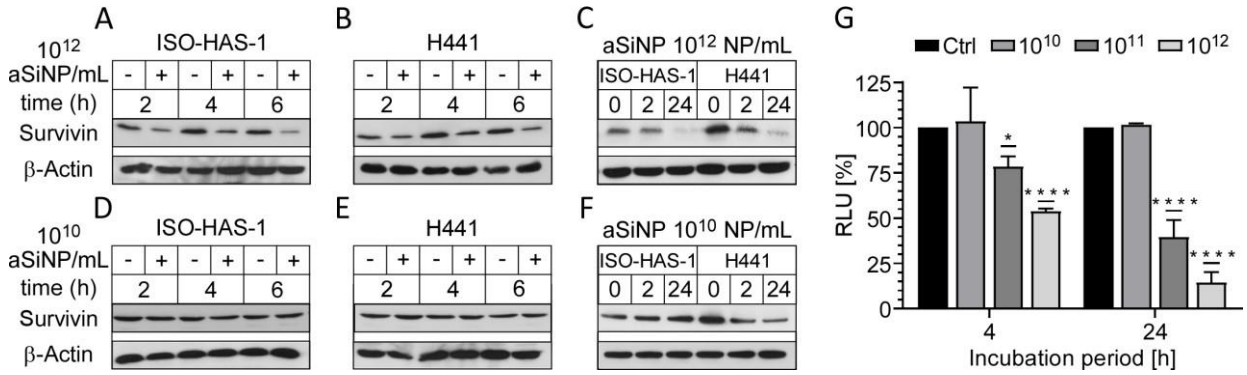

Figure 6. aSiNP-mediated toxicity was accompanied by dose-dependent downregulation of the antiapoptotic protein Survivin: (**A**–**F**) Immunoblot analysis revealed dose-dependent downregulation of Survivin in response to treatment with aSiNP15. ISO-HAS-1 and H441 cells were treated with ("+") 10^{12} NP/mL (**A**–**C**) or 10^{10} NP/mL (**D**–**F**) aSiNP15 or without particles ("−") for 0 and 2 h in serumfree medium. For incubation times longer than 4 h, serum-containing medium was added after 4 h to prevent starvation-induced cell death. Proteins were detected by specific antibodies. β-Actin served as loading control. (**G**) Suppression of the Survivin promoter was revealed by a luciferase reporter assay following aSiNP15 treatment. Briefly, H441 cells were treated with 10^{10}, 10^{11}, and 10^{12} NP/mL for 4 h in serum-free medium. Likewise, for the 24 h time point, serum-containing medium was added after 4 h. After incubation, cells were lysed, and lysates were used for quantification of luciferase activity as described [36]. Data were normalized to untreated controls, and unpaired *t*-test was performed. Columns, mean; bars, ± S.D. *, $p < 0.05$, ****, $p < 0.0001$.

To investigate whether Survivin downregulation also occurs on the transcriptional level, H441 cells were transfected with a luciferase reporter plasmid containing the Survivin promoter sequence (Figure 6G, Supplementary Figure S7). The reporter assay indeed confirmed that high particle concentrations (10^{11} and 10^{12} NP/mL) induce a significant decrease in the Survivin promoter activity after 4 h of treatment. A prolonged incubation period (24 h) further decreased Survivin transcription, while low particle concentrations (10^{10} NP/mL) had no repressive effect, which is in line with the immunoblot results (Figure 6C,F).

Importantly, to further confirm Survivin's protective role against aSiNP-induced toxicity, we analyzed whether overexpression of Survivin might be able to counteract cell death after aSiNP15 treatment (Figure 7). First, H441 cells were retrovirally transduced with the Survivin–GFP (green fluorescent protein) fusion protein or internal ribosome entry site (IRES)–GFP constructs, and selected for GFP expression. Immunofluorescence microscopy of stably expressing cells confirmed characteristic sub-cellular localization patterns of Survivin during mitosis and in interphase cells (Figure 7A). Ectopic expression and functionality of the Survivin-GFP construct was verified by fluorescence microscopy (Figure 7A). Next, cell lines were challenged with low (10^{10} NP/mL) and high doses (10^{12} NP/mL) of aSiNP15 for up to 24 h (Figure 7B–D). In comparison to the control cells (H441), Survivin-overexpressing cells (H441 Surv) showed a significant decrease in apoptosis induction (Figure 7D). Furthermore, these cells kept their healthy phenotype upon aSiNP15 treatment, while shrinking and cell detachment from the culture dish occurred in wild-type cells for the same treatment conditions (Figures 7B and S1). However, aSiNP15-induced cell death after long-term incubation could not be prevented by Survivin overexpression but was significantly decreased in comparison to wild-type cells (Figure 7C).

Taken together, our data strongly suggest that aSiNP15-induced toxicity depends, at least in part, on the regulation of the anti-apoptotic protein Survivin. Further, the results indicate that a high expression level of Survivin potentially attenuates aSiNP15induced toxicity.

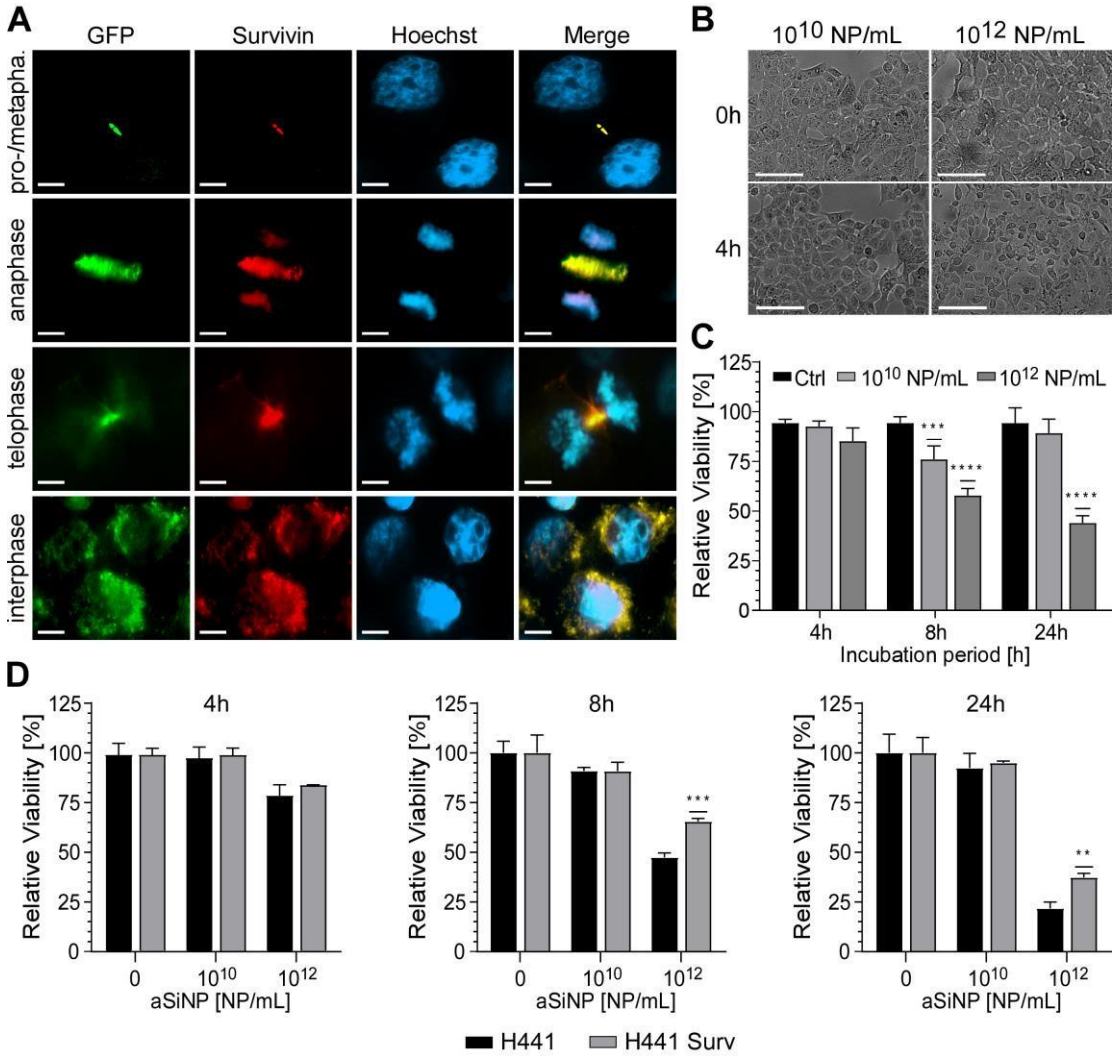

Figure 7. Overexpression of Survivin counteracts aSiNP15-induced cell death: (**A**) In stably SurvivinGFP-expressing H441 cells (H441 Surv), Survivin exhibits its characteristic localization during mitotic phases shown via immunofluorescence microscopy (as indicated). In prophase/metaphase, it localizes at chromatin sides. In anaphase, Survivin dissociates from chromatin and associates with the midzone spindle apparatus. In telophase, it localizes at the midbody, and disperses in the cytoplasm and/or in the nucleus during interphase. Scale bars, 10µm. (**B**) Morphological stability of H441 cells after treatment with different aSiNP15 concentrations at the beginning of treatment (0 h) and after 4 h aSiNP15 exposure. Cell morphology was visualized by light microscopy. Scale bars, 150 µm. (**C**) High doses of aSiNP15 induce cell death after long-term incubation. An MTT viability assay of stably expressing Survivin–GFP H441 cells was performed after 4 h, 8 h, and 24 h of aSiNP15 treatment as indicated. Data were normalized to untreated controls, and unpaired *t*-test was performed. Columns, mean; bars, ±S.D. ***, $p < 0.001$, ****, $p < 0.0001$. (**D**) CellTiter-Glo™ viability assay of H441 Surv (grey) and control cells (H441, black) was performed after 4 h, 8 h, and 24 h of aSiNP15 treatment as indicated. Data were normalized to untreated controls, and unpaired *t*-test was performed. Columns, mean; bars, ±S.D. **, $p < 0.01$, ***, $p < 0.001$.

3.6. 'Probing Physiological Relevance of the Nano–Bio Interface'—Survivin Is Expressed in Healthy Mouse and Human Lung Tissue

Since our in vitro alveolar-capillary model suggests Survivin as a cytoprotective resistor against aSiNP-induced toxicity, it is mandatory to analyze its physiological relevance in vivo. Therefore, we used an established immunohistochemistry (IHC) protocol to analyze Survivin expression in human and murine lung alveolar cells (ATII) (Figure 8A,C) [34,37]. Again, the thyroid transcription factor-1 (TTF-1) was used as a common marker for ATII-lung cells. The IHC staining visualized specific staining of Survivin consistent with TTF-1-labeled epithelial lung cells (Figure 8B,D). Tissues from different origins also differ in their staining pattern, which has to be considered for the model system, which should mimic the target

tissue: lung tissue from mouse origin revealed no TTF-1positive cell layer of epithelial cells and showed no consistency with Survivin-positive cells (Figure 8C,D), in contrast to the human lung tissue (Figure 8A,B). Of note, no IHC signal was detectable upon omission of the primary α-Survivin Ab or pre-absorption of the α-Survivin Ab with recombinant human Survivin–GFP protein, confirming staining specificity.Conclusively, our data confirm that Survivin is expressed in healthy lung tissue, and thus Survivin's cytoprotective role against aSiNP-induced toxicity is also relevant for animal-based research and its clinical transfer to human disease, but tissue differences should be considered in the experimental setup.

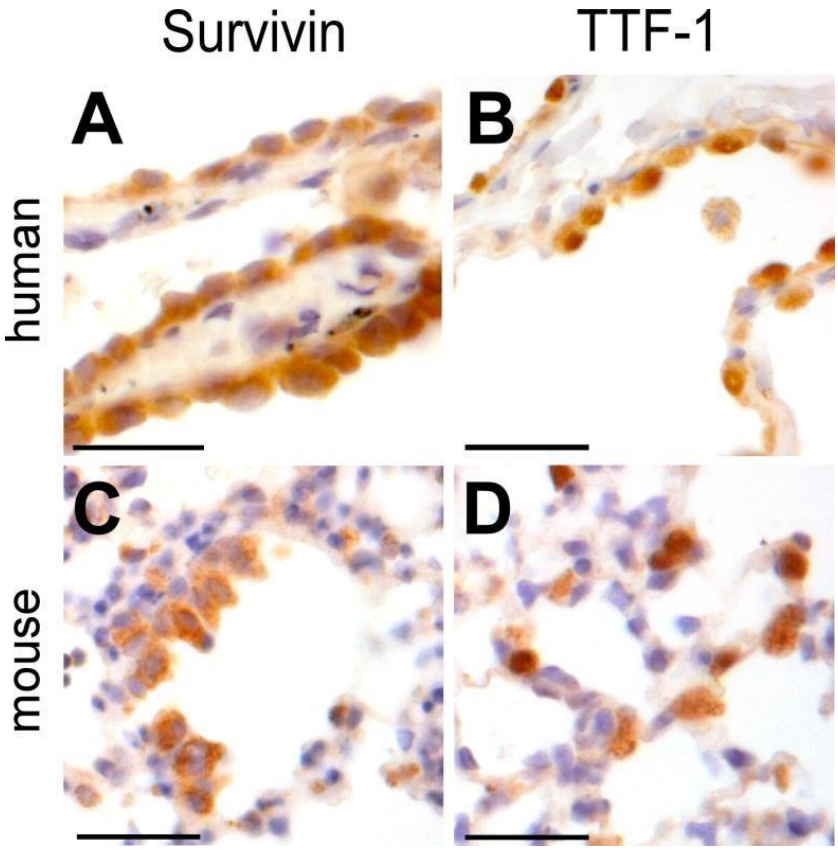

Figure 8. Survivin is physiologically expressed in epithelial cells of the human and mouse lung. Immunohistochemical staining of Survivin (**A**,**C**) and TTF-1 (**B**,**D**) in epithelial human and mouse lung tissue with specific antibodies (brown) and visualized by light microscopy. HE staining was applied to visualize lung tissue structure (blue). Survivin localized in the nuclei and cytoplasm of mouse and human epithelial lung cells (**A**,**C**), whereas TTF-1 was prominently overexpressed in the nuclei (**B**,**D**). Scale bars, 50 µM.

4. Discussion

Nanoparticles, as easy and cheap to synthesize materials, are very popular due to manifold modification opportunities. In particular, silica nanoparticles are easy to modify and are frequently used in industry, most notably in cosmetic applications, food processing, and the medical industry as part of drug formulations [3,4,10,12,55]. The growing number of nanoparticle-containing products as well as nanoparticle waste makes it necessary to monitor their possible harmful effects and simultaneously examine treatment options. In this context, the demand for suitable lung models regarding the complexity of tissue samples, ethical issues, and the experimental handling of animal models is increasing. We therefore compared specific differentiation markers of human lung tissue to those of mouse lung and cell culture models. For the first time, we showed that tissue cells of the human lung express the inhibitor of apoptosis protein, Survivin, which is critical for mitosis and proliferation [31,56–59]. Furthermore, we implemented cell culture models that reflect the necessary characteristics of lung tissue cells.

Monoculture cell line models, consisting of the human epithelial lung carcinoma cell line H441 and human microvascular endothelial cell (MEC) line ISO-HAS-1, reproduce necessary properties of differentiated lung tissue to a good extent and can, therefore, serve as good model systems for lung tissue. On a molecular level, adhesion molecules are necessary for tissue integrity and, consequently, for their functionality, like EpCAM or E-cadherin for epithelial lung tissue or CD31 for endothelium [60,61]. Consequently, the differentiation status of the epithelial cell line H441 and endothelial cell line ISO-HAS-1 was distinguished by tissue-specific differentiation markers. H441 expressed epithelial-specific markers α-E-cadherin and α-EpCAM pivotal for the generation of epithelial cell–cell contact and barrier formation, as well as lungspecific markers α-SP-A and α-TTF-1 [62–67]. The endothelial differentiation marker CD31 was expressed exclusively by the ISO-HAS-1 cell line, which proves that the two selected cell lines are highly differentiated and suitable for establishing simplified lung culture models [68].

The pro-survival stimulating properties of IAP family member Survivin could be a conceivable approach in the treatment of tissue damages, e.g., regarding the possible beneficial use of Survivin in transplants [29]. Thus, Survivin is known to increase cancer cell proliferation and resistance against chemotherapeutics and radiation [23,24,69]. It was also demonstrated that Survivin plays a key role in protecting and restoring the auditory system after ototoxic effects have led to hearing loss [28]. Several studies showed that Survivin is expressed in a broad range of non-malignant tissues and stem cells, indicating the crucial role of Survivin as a pro-survival factor in increasing resistance and proliferation [70,71]. These cytoprotective mechanisms may likewise be used against nanoparticular stress as proposed in this work.

In comparison to the corresponding mouse model, the dual lung model, based on cell lines, is well suited to reflect the specific properties of lung tissue cells and to simultaneously enable simplified and cell-specific analyses. However, type I pneumocytes, representing the majority of the lung surface tissue cells, should be considered for future research approaches on lung model systems [44]. On the basis of the used cell model, sublethal concentrations of aSiNP15 did indeed not affect the two cell lines, whereas higher particle doses resulted in morphological changes. We subsequently revealed decreasing cell viabilities over the treatment time, suggesting a time- and concentration-dependent toxicity effect. In addition, we found that a larger nanoparticle size reduced the toxicity of aSiNPs at constant material properties and concentrations, which, besides differences in their surface area, might be also attributed to a size-dependent protein corona formation [50]. However, Survivin expression was reduced by higher aSiNP15 concentrations, as well as the Survivinenhancing prosurvival factor ERK. These results indicate that the MEK/ERK/Survivin axis is part of the defense mechanism against aSiNP toxicity. Survivin expression, location, and modification are modulated by several signaling pathways. To demonstrate that aSiNP toxicity is mediated by decreasing phosphorylation of ERK1/2, we made use of an MEK inhibitor to prevent the activation of ERK1/2 by MEK-mediated phosphorylation. In contrary to previous experiments the use of non-toxic concentrations of aSiNP15 led to significantly lower viabilities in combination with the MEK inhibitor. Therefore, the cytoprotective effect of survivin might be decreased due to reduced ERK1/2 activation by the inhibition of MEK-mediated ERK phosphorylation. The data suggest that suppressed phosphorylation of ERK may contribute to decreased Survivin expression by interfering with MAPK/ERK pro-survival signaling, in turn, leading to caspase-3 activation and apoptosis.

The effect of aSiNP on cells has been discussed in numerous publications, but the mechanisms are still not clearly understood [72]. The most commonly observed effects of aSiNP exposure include the induction of apoptosis through DNA damage or mitochondria-, TNF-α-, and NO-related signaling pathways [72,73]. Mechanistically, silanol groups (SiOH) on the nanoparticle surface can interact electrostatically with the cell membrane [74]. Furthermore, their nucleophilic character can attack electrophilic carbonyl groups of proteins [75]. Since we used non-coated SiNP without the addition of any surfactant, potential unspecific effects caused by foreign ions and/or surface functionalizations should

be negligible. In addition, signaling processes are likely to be triggered by the generation of reactive oxygen species (ROS) mediated by the cleavage of strained siloxane rings [74–77]. We showed that aSiNPs accumulate in the cells with increasing particle concentrations correlating with morphological changes and augmented cell toxicity. Whether Survivin can induce ROS-clearing processes under subtoxic conditions, or if several different defense responses are addressed by Survivin, remains to be clarified.

Zhao et al. (2010) and others showed that Survivin is sufficiently induced by the PI3K/Akt/p70S6K1 pathway, thereby protecting cells from apoptotic stimuli [52,54]. Other studies described Akt/PI3K activation mediated by low NO levels as a Survivin-inducing pathway [28]. In comparison to untreated controls, the amount of phosphorylated Akt and ERK was not enhanced by non-toxic aSiNP15 concentrations in both cell types, underlining that these pathways are necessary for sustaining normal cell homeostasis [78]. Further, the PI3K/Akt pathway was less affected by aSiNP15 treatment in endothelial ISO-HAS-1 cells compared to the MEK/ERK pathway. However, H441 cells exhibited slightly less phosphorylated Akt, while ERK1/2 was highly phosphorylated after incubation with high particle concentrations, correlating with a decreasing Survivin expression.

Survivin is a common tumor marker aberrantly expressed in various cancer types [79–82]. However, overexpression of Survivin via transduction of H441 cells with a Survivin–GFP construct enhanced their resistance to aSiNP15 treatment. These data suggest that Survivin indeed serves as an active resistor against aSiNP15-mediated toxicity for non-necrotic particle concentrations. aSiNP-mediated stress signaling addresses the Ras/Raf/MEK/ERK pathways rather than the PI3K/Akt pathway in the endothelial cell line ISO-HAS-1. A crosstalk between these pathways is also conceivable, making it more complex to understand and utilize for the further development of clinical treatments [83].

5. Conclusions

Due to their wide range of applications, aSiNPs have become a constant companion in our everyday lives. Therefore, it is of tremendous importance to examine possible hazardous effects on the human system. The most common entry routes for aSiNPs are the epithelium of the skin, the gastrointestinal tract, and the alveoli of the lung. We can confirm that silica nanoparticles of the type aSiNP15 exert a concentration- and timedependent negative impact on the viability of epithelial and endothelial cells. Based on the presented data, we suggest that Survivin protects cells against aSiNP-mediated toxicity. The mechanisms behind the empirical data include the MAPK pathway by MEK activation and subsequent ERK1/2 phosphorylation leading to enhanced Survivin levels and apoptosis inhibition. To underline the relevance of our study for (patho)physiological conditions, we demonstrated that Survivin is expressed in ATII-type lung cells, as well as in healthy human and murine lung tissue. Furthermore, we propose a well-differentiated dual cell model consisting of H441 and ISO-HAS-1 cells mimicking lung tissue in a simplified and transferable way usable for high throughput experiments prior to (pre-)clinical in vivo studies on human or mouse tissue of the lung.

Supplementary Materials: The following supporting information can be downloaded at: https:// www.mdpi.com/article/10.3390/nano13182546/s1, Figure S1: ISO-HAS-1 and H441 cells were treated with different particle concentrations in serum free medium for 4h; Figure S2: Impact of aSiNP L on ISO-HAS-1 cells; Figure S3: Effect of amorphous silica nanoparticle with a diameter of 125 nm (aSiNP125); Figure S4: Interaction and internalization of aSiNPs with an increased diameter of 200 nm by epithelial lung cells. Figure S5: Quantification of protein bands detected via Western blot analysis shown in Figure 5 by using Image J software; Figure S6: Quantification of protein bands detected via Western blot analysis shown in Figure 6 by using Image J software; Figure S7: Luciferase Reporter

Assay; Table S1: Characterization of the amorphous silica nanoparticle title; Table S2: Characterization of nanoparticle stability in different aqueous solutions over time.

Author Contributions: The manuscript was written through contributions of all authors as follows: conceptualization, D.D., M.B., S.S., S.K.K., D.G. and R.H.S.; methodology, validation, and formal analysis, C.B.-B., D.D. and D.G.; data curation, C.B.-B., D.D., D.G. and R.H.S.; writing—original draft preparation, C.B.-B., D.G., S.K.K. and R.H.S.; writing—review and editing, C.B.-B.,

M.B., S.S., D.G., S.K.K. and R.H.S.; visualization, C.B.-B., D.D., D.G. and R.H.S.; resources, supervision, project administration, and funding acquisition, D.D., D.G. and R.H.S. All authors have read and agreed to the published version of the manuscript.

Funding: This work was supported by the *Deutsche Forschungsgemeinschaft* (DFG), project number DO-1910/2-1. The author C.B.B was supported by a scholarship of the Deutsche Gesellschaft für Hämatologie und Medizinische Onkologie e. V. (DGHO) and the Gesellschaft für Medizinische Innovation –Hämatologie und Onkologie mbH (GMIHO).

Acknowledgments: The authors thank Sandra Olf for her excellent technical assistance. Professor Kirkpatrick is thankfully acknowledged for technical assistance during TEM analysis.

Conflicts of Interest: The authors declare no conflict of interest.

References

1. Davies, J.C.T. PEN 13-Nanotechnology Oversight. Available online: https://www.wilsoncenter.org/publication/pen-13 - nanotechnology-oversight (accessed on 14 January 2019).
2. Liljenström, C.L.D.; Finnveden, G. Silicon-Based Nanomaterials in a Life-Cycle Perspective, Including a Case Study on SelfCleaning Coatings. 2013. Available online: https://www.researchgate.net/publication/280264076_Silicon-based_nanomaterials_ in_a_life-cycle_perspective_including_a_case_study_on_self-cleaning_coatings (accessed on 14 January 2019).
3. Vance, M.; Lawson, N.C.; Rupal, M.; Beck, P.; Burgess, J.O. Color and Gloss of Nano-Filled Resin-Modified Glass Ionomers and Resin Composites. *J. Esthet. Restor. Dent.* **2015**, *27*, 293–299. [CrossRef]
4. Croissant, J.G.; Fatieiev, Y.; Khashab, N.M. Degradability and Clearance of Silicon, Organosilica, Silsesquioxane, Silica Mixed Oxide, and Mesoporous Silica Nanoparticles. *Adv. Mater.* **2017**, *29*, 1604634. [CrossRef]
5. Dekkers, S.; Krystek, P.; Peters, R.J.; Lankveld, D.P.; Bokkers, B.G.; van Hoeven-Arentzen, P.H.; Bouwmeester, H.; Oomen, A.G. Presence and risks of nanosilica in food products. *Nanotoxicology* **2011**, *5*, 393–405. [CrossRef]
6. Leung, C.C.; Yu, I.T.; Chen, W. Silicosis. *Lancet* **2012**, *379*, 2008–2018. [CrossRef]
7. Barnes, C.A.; Elsaesser, A.; Arkusz, J.; Smok, A.; Palus, J.; Lesniak, A.; Salvati, A.; Hanrahan, J.P.; Jong, W.H.; Dziubaltowska, E.; et al. Reproducible comet assay of amorphous silica nanoparticles detects no genotoxicity. *Nano Lett.* **2008**, *8*, 3069–3074. [CrossRef]
8. Arts, J.H.; Muijser, H.; Duistermaat, E.; Junker, K.; Kuper, C.F. Five-day inhalation toxicity study of three types of synthetic amorphous silicas in Wistar rats and post-exposure evaluations for up to 3 months. *Food Chem. Toxicol.* **2007**, *45*, 1856–1867. [CrossRef]
9. Barik, T.K.; Sahu, B.; Swain, V. Nanosilica-from medicine to pest control. *Parasitol. Res.* **2008**, *103*, 253–258. [CrossRef]
10. Fadeel, B.; Garcia-Bennett, A.E. Better safe than sorry: Understanding the toxicological properties of inorganic nanoparticles manufactured for biomedical applications. *Adv. Drug Deliv. Rev.* **2010**, *62*, 362–374. [CrossRef]
11. da Cruz Schneid, A.; Albuquerque, L.J.C.; Mondo, G.B.; Ceolin, M.; Picco, A.S.; Cardoso, M.B. Colloidal stability and degradability of silica nanoparticles in biological fluids: A review. *J. Sol.-Gel Sci. Technol.* **2022**, *102*, 41–62. [CrossRef]
12. Higashisaka, Y.Y.K.; Tsutsumi, Y. Applications and Safety of Nanomaterials Used in the Food Industry. *Food Saf.* **2015**, *3*, 39–47. [CrossRef]
13. Napierska, D.; Thomassen, L.C.; Rabolli, V.; Lison, D.; Gonzalez, L.; Kirsch-Volders, M.; Martens, J.A.; Hoet, P.H. Size-dependent cytotoxicity of monodisperse silica nanoparticles in human endothelial cells. *Small* **2009**, *5*, 846–853. [CrossRef]
14. Thomassen, L.C.; Aerts, A.; Rabolli, V.; Lison, D.; Gonzalez, L.; Kirsch-Volders, M.; Napierska, D.; Hoet, P.H.; Kirschhock, C.E.; Martens, J.A. Synthesis and characterization of stable monodisperse silica nanoparticle sols for in vitro cytotoxicity testing. *Langmuir* **2010**, *26*, 328–335. [CrossRef]
15. Choi, H.S.; Ashitate, Y.; Lee, J.H.; Kim, S.H.; Matsui, A.; Insin, N.; Bawendi, M.G.; Semmler-Behnke, M.; Frangioni, J.V.; Tsuda, A. Rapid translocation of nanoparticles from the lung airspaces to the body. *Nat. Biotechnol.* **2010**, *28*, 1300–1303. [CrossRef]
16. Xie, G.; Sun, J.; Zhong, G.; Shi, L.; Zhang, D. Biodistribution and toxicity of intravenously administered silica nanoparticles in mice. *Arch. Toxicol.* **2010**, *84*, 183–190. [CrossRef]
17. Fruijtier-Polloth, C. The toxicological mode of action and the safety of synthetic amorphous silica-a nanostructured material. *Toxicology* **2012**, *294*, 61–79. [CrossRef]
18. Ahamed, M. Silica nanoparticles-induced cytotoxicity, oxidative stress and apoptosis in cultured A431 and A549 cells. *Hum. Exp. Toxicol.* **2013**, *32*, 186–195. [CrossRef]
19. Lankoff, A.; Arabski, M.; Wegierek-Ciuk, A.; Kruszewski, M.; Lisowska, H.; Banasik-Nowak, A.; Rozga-Wijas, K.; Wojewodzka, M.; Slomkowski, S. Effect of surface modification of silica nanoparticles on toxicity and cellular uptake by human peripheral blood lymphocytes in vitro. *Nanotoxicology* **2013**, *7*, 235–250. [CrossRef]

20. Yang, Y.X.; Song, Z.M.; Cheng, B.; Xiang, K.; Chen, X.X.; Liu, J.H.; Cao, A.; Wang, Y.; Liu, Y.; Wang, H. Evaluation of the toxicity of food additive silica nanoparticles on gastrointestinal cells. *J. Appl. Toxicol.* **2014**, *34*, 424–435. [CrossRef]
21. Elmore, S. Apoptosis: A review of programmed cell death. *Toxicol. Pathol.* **2007**, *35*, 495–516. [CrossRef]
22. Wheatley, S.P.; Altieri, D.C. Survivin at a glance. *J. Cell Sci.* **2019**, *132*, 223826. [CrossRef]
23. Unruhe, B.; Schroder, E.; Wunsch, D.; Knauer, S.K. An Old Flame Never Dies: Survivin in Cancer and Cellular Senescence. *Gerontology* **2016**, *62*, 173–181. [CrossRef] [PubMed]
24. Rauch, A.; Carlstedt, A.; Emmerich, C.; Mustafa, A.M.; Goder, A.; Knauer, S.K.; Linnebacher, M.; Heinzel, T.; Kramer, O.H. Survivin antagonizes chemotherapy-induced cell death of colorectal cancer cells. *Oncotarget* **2018**, *9*, 27835–27850. [CrossRef] [PubMed]
25. Li, Y.; Lu, W.; Yang, J.; Edwards, M.; Jiang, S. Survivin as a biological biomarker for diagnosis and therapy. *Expert. Opin. Biol. Ther.* **2021**, *21*, 1429–1441. [CrossRef] [PubMed]
26. Rahimmi, A.; Fathi, F.; Nikkhoo, B.; Soleimani, F.; Khademerfan, M. Over-expression of survivin could prevent the oxidative stress and toxicity of rotenone in SH-SY5Y cells. *Iran. J. Basic. Med. Sci.* **2022**, *25*, 842–849. [CrossRef] [PubMed]
27. Chen, J.; Chen, J.K.; Conway, E.M.; Harris, R.C. Survivin mediates renal proximal tubule recovery from AKI. *J. Am. Soc. Nephrol.* **2013**, *24*, 2023–2033. [CrossRef]
28. Knauer, S.K.; Heinrich, U.R.; Bier, C.; Habtemichael, N.; Docter, D.; Helling, K.; Mann, W.J.; Stauber, R.H. An otoprotective role for the apoptosis inhibitor protein survivin. *Cell Death Dis.* **2010**, *1*, e51. [CrossRef] [PubMed]
29. Assadiasl, S.; Mousavi, M.J.; Amirzargar, A. Antiapoptotic Molecule Survivin in Transplantation: Helpful or Harmful? *J. Transpl.* **2018**, *2018*, 6492034. [CrossRef]
30. Lee, B.S.; Kim, S.H.; Jin, T.; Choi, E.Y.; Oh, J.; Park, S.; Lee, S.H.; Chung, J.H.; Kang, S.M. Protective effect of survivin in Doxorubicin-induced cell death in h9c2 cardiac myocytes. *Korean Circ. J.* **2013**, *43*, 400–407. [CrossRef]
31. Kasper, J.Y.; Feiden, L.; Hermanns, M.I.; Bantz, C.; Maskos, M.; Unger, R.E.; Kirkpatrick, C.J. Pulmonary surfactant augments cytotoxicity of silica nanoparticles: Studies on an in vitro air-blood barrier model. *Beilstein J. Nanotechnol.* **2015**, *6*, 517–528. [CrossRef]
32. Knauer, S.K.; Bier, C.; Habtemichael, N.; Stauber, R.H. The Survivin-Crm1 interaction is essential for chromosomal passenger complex localization and function. *EMBO Rep.* **2006**, *7*, 1259–1265. [CrossRef]
33. Knauer, S.K.; Kramer, O.H.; Knosel, T.; Engels, K.; Rodel, F.; Kovacs, A.F.; Dietmaier, W.; Klein-Hitpass, L.; Habtemichael, N.; Schweitzer, A.; et al. Nuclear export is essential for the tumor-promoting activity of survivin. *FASEB J.* **2007**, *21*, 207–216.[CrossRef] [PubMed]
34. Fetz, V.; Bier, C.; Habtemichael, N.; Schuon, R.; Schweitzer, A.; Kunkel, M.; Engels, K.; Kovacs, A.F.; Schneider, S.; Mann, W.; et al. Inducible NO synthase confers chemoresistance in head and neck cancer by modulating survivin. *Int. J. Cancer* **2009**, *124*, 2033–2041. [CrossRef] [PubMed]
35. Kramer, O.H.; Knauer, S.K.; Zimmermann, D.; Stauber, R.H.; Heinzel, T. Histone deacetylase inhibitors and hydroxyurea modulate the cell cycle and cooperatively induce apoptosis. *Oncogene* **2008**, *27*, 732–740. [CrossRef] [PubMed]
36. Kramer, O.H.; Knauer, S.K.; Greiner, G.; Jandt, E.; Reichardt, S.; Guhrs, K.H.; Stauber, R.H.; Bohmer, F.D.; Heinzel, T. A phosphorylation-acetylation switch regulates STAT1 signaling. *Genes. Dev.* **2009**, *23*, 223–235. [CrossRef] [PubMed]
37. Engels, K.; Knauer, S.K.; Loibl, S.; Fetz, V.; Harter, P.; Schweitzer, A.; Fisseler-Eckhoff, A.; Kommoss, F.; Hanker, L.; Nekljudova, V.; et al. NO signaling confers cytoprotectivity through the survivin network in ovarian carcinomas. *Cancer Res.* **2008**, *68*, 5159–5166. [CrossRef]
38. Matter, F.L.; Laura, A. Niederberger, Markus From colloidal dispersions to aerogels: How to master nanoparticle gelation. *Nano Today* **2020**, *30*, 100827. [CrossRef]
39. Sonwani, S.; Madaan, S.; Arora, J.; Suryanarayan, S.; Rangra, D.; Mongia, N.; Vats, T.; Saxena, P. Inhalation Exposure to Atmospheric Nanoparticles and Its Associated Impacts on Human Health: A Review. *Front. Sustain. Cities* **2021**, *3*, 690444. [CrossRef]
40. Kapalczynska, M.; Kolenda, T.; Przybyla, W.; Zajaczkowska, M.; Teresiak, A.; Filas, V.; Ibbs, M.; Blizniak, R.; Luczewski, L.; Lamperska, K. 2D and 3D cell cultures—A comparison of different types of cancer cell cultures. *Arch. Med. Sci.* **2018**, *14*, 910–919.[CrossRef]
41. Hermanns, M.I.; Kasper, J.; Dubruel, P.; Pohl, C.; Uboldi, C.; Vermeersch, V.; Fuchs, S.; Unger, R.E.; Kirkpatrick, C.J. An impaired alveolar-capillary barrier in vitro: Effect of proinflammatory cytokines and consequences on nanocarrier interaction. *J. R. Soc. Interface* **2010**, *7* (Suppl. S1), S41–S54. [CrossRef]
42. Pryhuber, G.S.; Khalak, R.; Zhao, Q. Regulation of surfactant proteins A and B by TNF-alpha and phorbol ester independent of NF-kappa B. *Am. J. Physiol.* **1998**, *274*, L289–L295. [CrossRef]
43. Kasper, M.; Barth, K. Potential contribution of alveolar epithelial type I cells to pulmonary fibrosis. *Biosci. Rep.* **2017**, *37*, BSR20171301. [CrossRef] [PubMed]
44. Zhao, C.Z.; Fang, X.C.; Wang, D.; Tang, F.D.; Wang, X.D. Involvement of type II pneumocytes in the pathogenesis of chronic obstructive pulmonary disease. *Respir. Med.* **2010**, *104*, 1391–1395. [CrossRef] [PubMed]

45. Salomon, J.J.; Muchitsch, V.E.; Gausterer, J.C.; Schwagerus, E.; Huwer, H.; Daum, N.; Lehr, C.M.; Ehrhardt, C. The cell line NCl-H441 is a useful in vitro model for transport studies of human distal lung epithelial barrier. *Mol. Pharm.* **2014**, *11*, 995–1006. [CrossRef]
46. Khubchandani, K.R.; Snyder, J.M. Surfactant protein A (SP-A): The alveolus and beyond. *FASEB J.* **2001**, *15*, 59–69. [CrossRef]
47. Wert, S.E.; Dey, C.R.; Blair, P.A.; Kimura, S.; Whitsett, J.A. Increased expression of thyroid transcription factor-1 (TTF-1) in respiratory epithelial cells inhibits alveolarization and causes pulmonary inflammation. *Dev. Biol.* **2002**, *242*, 75–87. [CrossRef]
48. Kuo, W.T.; Odenwald, M.A.; Turner, J.R.; Zuo, L. Tight junction proteins occludin and ZO-1 as regulators of epithelial proliferation and survival. *Ann. N. Y. Acad. Sci.* **2022**, *1514*, 21–33. [CrossRef] [PubMed]
49. Docter, D.; Bantz, C.; Westmeier, D.; Galla, H.J.; Wang, Q.; Kirkpatrick, J.C.; Nielsen, P.; Maskos, M.; Stauber, R.H. The protein corona protects against size- and dose-dependent toxicity of amorphous silica nanoparticles. *Beilstein J. Nanotechnol.* **2014**, *5*, 1380–1392. [CrossRef]
50. Tenzer, S.; Docter, D.; Kuharev, J.; Musyanovych, A.; Fetz, V.; Hecht, R.; Schlenk, F.; Fischer, D.; Kiouptsi, K.; Reinhardt, C.; et al. Rapid formation of plasma protein corona critically affects nanoparticle pathophysiology. *Nat. Nanotechnol.* **2013**, *8*, 772–781.[CrossRef]
51. Cao, Z.; Liao, Q.; Su, M.; Huang, K.; Jin, J.; Cao, D. AKT and ERK dual inhibitors: The way forward? *Cancer Lett.* **2019**, *459*, 30–40. [CrossRef]
52. Belyanskaya, L.L.; Hopkins-Donaldson, S.; Kurtz, S.; Simoes-Wust, A.P.; Yousefi, S.; Simon, H.U.; Stahel, R.; Zangemeister-Wittke, U. Cisplatin activates Akt in small cell lung cancer cells and attenuates apoptosis by survivin upregulation. *Int. J. Cancer* **2005**, *117*, 755–763. [CrossRef]
53. Ye, Q.; Cai, W.; Zheng, Y.; Evers, B.M.; She, Q.B. ERK and AKT signaling cooperate to translationally regulate survivin expression for metastatic progression of colorectal cancer. *Oncogene* **2014**, *33*, 1828–1839. [CrossRef] [PubMed]
54. Zhao, P.; Meng, Q.; Liu, L.Z.; You, Y.P.; Liu, N.; Jiang, B.H. Regulation of survivin by PI3K/Akt/p70S6K1 pathway. *Biochem. Biophys. Res. Commun.* **2010**, *395*, 219–224. [CrossRef] [PubMed]
55. Croissant, J.G.; Fatieiev, Y.; Almalik, A.; Khashab, N.M. Mesoporous Silica and Organosilica Nanoparticles: Physical Chemistry, Biosafety, Delivery Strategies, and Biomedical Applications. *Adv. Heal. Mater.* **2018**, *7*, 1700831. [CrossRef]
56. Stahl, P.; Kollenda, S.; Sager, J.; Schmidt, L.; Schroer, M.A.; Stauber, R.H.; Epple, M.; Knauer, S.K. Tuning Nanobodies' Bioactivity: Coupling to Ultrasmall Gold Nanoparticles Allows the Intracellular Interference with Survivin. *Small* **2023**, *19*, e2300871. [CrossRef] [PubMed]
57. Wang, P.; Zhen, H.; Zhang, J.; Zhang, W.; Zhang, R.; Cheng, X.; Guo, G.; Mao, X.; Wang, J.; Zhang, X. Survivin promotes glioma angiogenesis through vascular endothelial growth factor and basic fibroblast growth factor in vitro and in vivo. *Mol. Carcinog.* **2012**, *51*, 586–595. [CrossRef] [PubMed]
58. Koike, H.; Morikawa, Y.; Sekine, Y.; Matsui, H.; Shibata, Y.; Suzuki, K. Survivin is associated with cell proliferation and has a role in 1a,25-dihydroxyvitamin D3 induced cell growth inhibition in prostate cancer. *J. Urol.* **2011**, *185*, 1497–1503. [CrossRef] [PubMed]
59. Wolanin, K.; Piwocka, K. Role of survivin in mitosis. *Postep. Biochem.* **2007**, *53*, 10–18.
60. Na, T.Y.; Schecterson, L.; Mendonsa, A.M.; Gumbiner, B.M. The functional activity of E-cadherin controls tumor cell metastasis at multiple steps. *Proc. Natl. Acad. Sci. USA* **2020**, *117*, 5931–5937. [CrossRef]
61. Liu, L.; Shi, G.P. CD31: Beyond a marker for endothelial cells. *Cardiovasc. Res.* **2012**, *94*, 3–5. [CrossRef]
62. Gao, J.; Liu, X.; Yang, F.; Liu, T.; Yan, Q.; Yang, X. By inhibiting Ras/Raf/ERK and MMP-9, knockdown of EpCAM inhibits breast cancer cell growth and metastasis. *Oncotarget* **2015**, *6*, 27187–27198. [CrossRef]
63. Huang, L.; Yang, Y.; Yang, F.; Liu, S.; Zhu, Z.; Lei, Z.; Guo, J. Functions of EpCAM in physiological processes and diseases (Review). *Int. J. Mol. Med.* **2018**, *42*, 1771–1785. [CrossRef] [PubMed]
64. Lee, Y.C.; Wu, C.T.; Chen, C.S.; Chang, Y.L. E-cadherin expression in surgically-resected non-small cell lung cancers--a clinicopathological study. *Thorac. Cardiovasc. Surg.* **2000**, *48*, 294–299. [CrossRef] [PubMed]
65. Benlhabib, H.; Mendelson, C.R. Epigenetic regulation of surfactant protein A gene (SP-A) expression in fetal lung reveals a critical role for Suv39h methyltransferases during development and hypoxia. *Mol. Cell Biol.* **2011**, *31*, 1949–1958. [CrossRef] [PubMed]
66. Sano, H.; Kuroki, Y. The lung collectins, SP-A and SP-D, modulate pulmonary innate immunity. *Mol. Immunol.* **2005**, *42*, 279–287. [CrossRef] [PubMed]
67. La Rosa, S.; Chiaravalli, A.M.; Placidi, C.; Papanikolaou, N.; Cerati, M.; Capella, C. TTF1 expression in normal lung neuroendocrine cells and related tumors: Immunohistochemical study comparing two different monoclonal antibodies. *Virchows Arch.* **2010**, *457*, 497–507. [CrossRef]
68. Pusztaszeri, M.P.; Seelentag, W.; Bosman, F.T. Immunohistochemical expression of endothelial markers CD31, CD34, von Willebrand factor, and Fli-1 in normal human tissues. *J. Histochem. Cytochem.* **2006**, *54*, 385–395. [CrossRef]
69. Vallet, C.; Aschmann, D.; Beuck, C.; Killa, M.; Meiners, A.; Mertel, M.; Ehlers, M.; Bayer, P.; Schmuck, C.; Giese, M.; et al.

Functional Disruption of the Cancer-Relevant Interaction between Survivin and Histone H3 with a Guanidiniocarbonyl Pyrrole Ligand. *Angew. Chem. Int. Ed. Engl.* **2020**, *59*, 5567–5571. [CrossRef]
70. Fukuda, S.; Pelus, L.M. Survivin, a cancer target with an emerging role in normal adult tissues. *Mol. Cancer Ther.* **2006**, *5*, 1087–1098. [CrossRef]
71. Gil-Kulik, P.; Krzyzanowski, A.; Dudzinska, E.; Karwat, J.; Chomik, P.; Swistowska, M.; Kondracka, A.; Kwasniewska, A.; Cioch, M.; Jojczuk, M.; et al. Potential Involvement of BIRC5 in Maintaining Pluripotency and Cell Differentiation of Human Stem Cells. *Oxid. Med. Cell Longev.* **2019**, *2019*, 8727925. [CrossRef]
72. Asweto, C.O.; Wu, J.; Alzain, M.A.; Hu, H.; Andrea, S.; Feng, L.; Yang, X.; Duan, J.; Sun, Z. Cellular pathways involved in silica nanoparticles induced apoptosis: A systematic review of in vitro studies. *Env. Toxicol. Pharmacol.* **2017**, *56*, 191–197. [CrossRef]
73. Kusaczuk, M.; Kretowski, R.; Naumowicz, M.; Stypulkowska, A.; Cechowska-Pasko, M. Silica nanoparticle-induced oxidative stress and mitochondrial damage is followed by activation of intrinsic apoptosis pathway in glioblastoma cells. *Int. J. Nanomed.* **2018**, *13*, 2279–2294. [CrossRef] [PubMed]
74. Al Samri, M.T.; Biradar, A.V.; Alsuwaidi, A.R.; Balhaj, G.; Al-Hammadi, S.; Shehab, S.; Al-Salam, S.; Tariq, S.; Pramathan, T.; Benedict, S.; et al. In vitro biocompatibility of calcined mesoporous silica particles and fetal blood cells. *Int. J. Nanomed.* **2012**, *7*, 3111–3121. [CrossRef]
75. Lehman, S.E.; Morris, A.S.; Mueller, P.S.; Salem, A.K.; Grassian, V.H.; Larsen, S.C. Silica Nanoparticle-Generated ROS as a Predictor of Cellular Toxicity: Mechanistic Insights and Safety by Design. *Env. Sci. Nano* **2016**, *3*, 56–66. [CrossRef] [PubMed]
76. Siegrist, S.; Kettiger, H.; Fasler-Kan, E.; Huwyler, J. Selective stimulation of the JAK/STAT signaling pathway by silica nanoparticles in human endothelial cells. *Toxicol. Vitr.* **2017**, *42*, 308–318. [CrossRef] [PubMed]
77. Zhang, H.; Dunphy, D.R.; Jiang, X.; Meng, H.; Sun, B.; Tarn, D.; Xue, M.; Wang, X.; Lin, S.; Ji, Z.; et al. Processing pathway dependence of amorphous silica nanoparticle toxicity: Colloidal vs pyrolytic. *J. Am. Chem. Soc.* **2012**, *134*, 15790–15804. [CrossRef]
78. Altomare, D.A.; Khaled, A.R. Homeostasis and the importance for a balance between AKT/mTOR activity and intracellular signaling. *Curr. Med. Chem.* **2012**, *19*, 3748–3762. [CrossRef]
79. Nitschkowski, D.; Marwitz, S.; Kotanidou, S.A.; Reck, M.; Kugler, C.; Rabe, K.F.; Ammerpohl, O.; Goldmann, T. Live and let die: Epigenetic modifications of Survivin and Regucalcin in non-small cell lung cancer tissues contribute to malignancy. *Clin. Epigenetics* **2019**, *11*, 157. [CrossRef]
80. Munscher, A.; Prochnow, S.; Gulati, A.; Sauter, G.; Lorincz, B.; Blessmann, M.; Hanken, H.; Bottcher, A.; Clauditz, T.S. Survivin expression in head and neck squamous cell carcinomas is frequent and correlates with clinical parameters and treatment outcomes. *Clin. Oral. Investig.* **2019**, *23*, 361–367. [CrossRef]
81. Zhou, J.; Guo, X.; Chen, W.; Wang, L.; Jin, Y. Targeting survivin sensitizes cervical cancer cells to radiation treatment. *Bioengineered* **2020**, *11*, 130–140. [CrossRef]
82. Knauer, S.K.; Unruhe, B.; Karczewski, S.; Hecht, R.; Fetz, V.; Bier, C.; Friedl, S.; Wollenberg, B.; Pries, R.; Habtemichael, N.; et al. Functional characterization of novel mutations affecting survivin (BIRC5)-mediated therapy resistance in head and neck cancer patients. *Hum. Mutat.* **2013**, *34*, 395–404. [CrossRef]
83. Arkun, Y. Dynamic Modeling and Analysis of the Cross-Talk between Insulin/AKT and MAPK/ERK Signaling Pathways. *PLoS ONE* **2016**, *11*, e0149684. [CrossRef] [PubMed]

8 DANKSAGUNG

Diese Arbeit war in vielerlei Hinsicht sehr herausfordernd und ohne die Unterstützung von allen Seiten wäre daraus auch nichts geworden. Für diese Unterstützung möchte ich euch danken!

An dieser Stelle möchte ich mich bei meinem Doktorvater Prof. Dr. Roland Stauber bedanken, der mir die Möglichkeit gegeben hat diese Arbeit aufzunehmen, das Thema unter konstruktiver Kritik weiterzuentwickeln und nach Freistellung und Elternzeit auch fortzuführen und abzuschließen. Für die unkomplizierte Rückkehr danke ich dir sehr!

Prof. Dr. Bernhard Lieb danke ich für seine herzliche und positive Betreuung als Zweitgutachter, sowie für die Arbeit, die mit der Korrektur und Bewertung meiner Dissertation einhergeht.

Ein großes Dankeschön geht an alle meinen derzeitigen und ehemaligen lieben Kolleginnen, bei denen ich mir immer einen guten Rat einholen konnte, sei es bezüglich meiner Arbeit im Labor, oder privater Natur, oder dass ich mir meinen experimentellen Frust einfach von der Seele reden konnte.
Vielen Dank and dieser Stelle an Dr. Desirée Gül und Madita Wandrey, durch deren Korrekturen sich die Qualität der Arbeit deutlich verbessert hat.

Es war schön in den ganzen herausfordernden Jahren, speziell die Jahre mit Kind, so großartige und kluge Menschen um mich herum zu haben.

Vielen Dank auch an alle meine Freunde, die mich mit viel Humor und Witz und ihrer Freundschaft aufgepäppelt haben und Urse, die die erste Version meiner Arbeit durchlesen und korrigieren durfte.

Vor allem danke ich meiner kleinen Tochter, die mich angetrieben hat, effizient und schnell zu arbeiten, damit ich wieder mehr mit ihr spielen kann. Diesbezüglich richtet sich mein großer Dank an alle Betreuenden, vor allem an die Omas und Opas, die bei jeder Gelegenheit geholfen haben. Ohne euch wäre die Arbeit jetzt noch nicht fertig. Nicht zuallerletzt danke ich Marco, dass er mir als Freund, Ehemann und Partner uneingeschränkt den Rücken freigehalten hat und mich darin bestärkt hat alles zu schaffen.

9 EIDESSTATTLICHE ERKLÄRUNG

Hiermit versichere ich, dass die vorliegende Arbeit selbstständig verfasst worden ist, dass keine anderen Quellen und Hilfsmittel als die angegebenen benutzt worden sind und dass die Stellen der Arbeit, die anderen Werken – auch elektronischen Medien – dem Wortlaut oder Sinn nach entnommen wurden unter Angabe der Quelle als Entlehnung kenntlich gemacht worden sind. Ich habe weder die vorgelegte Arbeit noch Teile davon als Prüfungsarbeit für eine staatliche oder andere wissenschaftliche Prüfung oder bei einer anderen Fakultät oder einem anderen Fachbereich als Dissertation eingereicht.

_____

(Datum, Ort, Unterschrift)

10 CURRICULUM VITAE

Persönliche Daten

Name	Christina Breder-Bonk
Geburtsname	Breder
Geburtsdatum/-ort	Saryagatsch/ Kasachstan
Staatsangehörigkeit	Deutsch
Anschrift	Thomas-Jefferson-Str. 5, 55122 Mainz

Akademischer Werdegang

2018-jetzt	**Promotionsstudium** im Fachbereich Biologie Johannes Gutenberg-Universität Mainz Prof. Dr. Roland H. Stauber AG Molekulare und zelluläre Onkologie, Universitätsmedizin Mainz
2014-2017	**Master of Science, Universität Bielefeld** M. Sc. Molekulare Biotechnologie Gesamtnote: 1,8
2011-2014	**Bachelor of Science, Johannes Gutenberg-Universität, Mainz** B. Sc. Molekulare Biologie Gesamtnote: 1,8
2010-2011	**Johannes Gutenberg-Universität, Mainz** Besuch von Kursen des Studiengangs B. Sc. Biomedizinische Chemie
2007-2010	**Wiedtal-Gymnasium Neustadt/Wied** Allgemeine Hochschulreife. Note: 1,7
2001-2007	**Realschule Neustadt/Wied** Sekundarabschluss I. Note: 1,5

Erfahrungen

2018-2023	**Wissenschaftlich Mitarbeiterin** an der Universitätsmedizin der Johannes-Gutenberg-Universität Mainz, AG Molekulare und zelluläre Onkologie
2017-2018	**Wissenschaftliche Mitarbeiterin** in der Physiologischen Chemie der Johannes-Gutenberg-Universität, Mainz
2015	**Hilfswissenschaftlerin**, Arbeitsgruppe Zellkulturtechnik der Universität Bielefeld
2013-2014	**Studentische Mitarbeiterin**, Patentagentur IMG Innovations-Management GmbH, Zweigstelle Mainz